PONTIFICIA UNIVERSIDAD CATOLICA DE CHILE

SCHOOL OF ENGINEERING

THERMOECONOMIC ASSESSMENT AND MULTI-OBJECTIVE OPTIMIZATION OF A CONCENTRATING SOLAR POWER + PHOTOVOLTAIC + MULTI-EFFECT DISTILLATION PLANT.

CARLOS ENRIQUE MATA TORRES

Thesis submitted to the Office of Graduate Studies in partial fulfillment of the requirements for the Degree of Doctor in Engineering Sciences

Advisor:

RODRIGO ESCOBAR

Santiago de Chile, January 2021

PONTIFICIA UNIVERSIDAD CATOLICA DE CHILE
SCHOOL OF ENGINEERING

THERMOECONOMIC ASSESSMENT AND MULTI-OBJECTIVE OPTIMIZATION OF A CONCENTRATING SOLAR POWER + PHOTOVOLTAIC + MULTI-EFFECT DISTILLATION PLANT

CARLOS ENRIQUE MATA TORRES

Members of the Committee:

RODRIGO ESCOBAR

JOSÉ MIGUEL CARDEMIL

FRANCISCO SUÁREZ

DIEGO ALARCÓN

PATRICIA PALENZUELA

JUAN DE DIOS ORTÚZAR

Thesis submitted to the Office of Graduate Studies in partial fulfillment of the requirements for the Degree Doctor in Engineering Sciences

Santiago of Chile, January, 2021

A mi padres, Carlos e Iris,
y mi querida Familia,
gracias por todo.

Dream big, believe in your dreams,
and live the life you have imagined.

ACKNOWLEDGEMENTS

This journey called Ph.D., in which I have been for more than 4 years, it has been very challenging and inspiring. I only can be grateful for such wonderful period of life that have been possible thanks to all the people around me. First of all, I want to give my sincere gratitude to my supervisor Dr. Rodrigo Escobar for giving me the opportunity with his trust and friendship, and for advising me with his feedback and contributions during these years. I also want to show special gratitude to Dr. Jose Miguel Cardemil, who has been an important figure throughout my Ph.D., giving me his advice and help.

During these years, I had the opportunity to do part of my research in two international internships, which have made huge contributions. I especially want to express thanks to the Plataforma Solar de Almeria for receiving me for 7 months in the city of Almeria. I had the privilege of working with Dr. Diego Alarcón and Dr. Patricia Palenzuela from the Solar Desalination Unit, who hugely support me with their advice and supervision in my research, and I sincerely appreciate their great human quality. I also want to thank Dr. Andrea Cipollina and his entire team at the Universita degli Studi di Palermo, for welcoming me into their team, show me their Italian and Sicilian culture, and giving me their advice that contributed to my research.

I want to acknowledge the scholarships used during the Ph.D., firstly the scholarship from the Vicerectoría de Investigación of Pontificia Universidad Católica de Chile, and then the scholarship from the Agencia Nacional de Investigación y Desarrollo, number PFCHA / Doctorado Nacional 2018/21181537.

It is also important to acknowledge the Pontificia Universidad Catolica de Chile an all their staff, that welcomed me to do my Ph.D. I also want to thank the support and their love for science of the people and friends from the Grupo Solar UC and Fraunhofer Chile Research-CSET. Special mention to Adriana, Yeliz, Redlich, Armando, Carlos F., Carlos V., Gonzalo

Q., Kerstin, Felipe D., Fernando A., Javier A., Cristian, Alan, Paulo, Gonzalo R., Alicia, among others.

This path would not have been the same without the experiences and friendships that I now have in several corners of the world. My time in Santiago, Almería and Palermo have been very special, where I have known great friends who made me feel like family. To mention a few are: David F., Kenneth, Daniela, Catalina M., David P., Noel, Rocio, Jorge G., Heidi, Aurelio, Marina, Sergio, Curro, Nacho, Monica, Diego and Javier.

Last but not least, I want to thank the unconditional support of my family, my parents Carlos and Iris, my sister Carla, my aunt Margaret and my grandparents. They have all been my role models and are the reason for who I am today. They have seen me shine from a distance, seeing how I fulfill each of my dreams and goals, and how I make them prouder every day. Finally, I dedicate a special dedication to Adriana Zurita, who has been my partner and companion along this path. She has given me her support and love from the beginning. Thank you very much for making me feel at home, for the patience and the happy moments. Finally, we can say "We did it."

CONTENTS

Pag.

LIST OF TABLES

Pág.

LIST OF FIGURES

Pag.

NOMENCLATURE

Acronyms

ACC	Air Cooled Condenser
BPE	Boiling Point Evaporation
CAPEX	Capital expenditure
CFWH	Closed Feed-Water Heater
CPH	Combined Power and Heat
CSP	Concentrating Solar Power
D	Desalination
DNI	Direct Normal Irradiation
DIST	Distribution
EES	Engineering Equation solver
ERD	Energy recovery device
EWS	Escondida Water Supply
GA	Genetic Algorithm
GHI	Global Horizontal Irradiation
GOR	Gain Output Ratio
HTF	Heat Transfer Fluid
HX	Heat exchanger
LCOE	Levelized Cost of Electricity
LCOW	Levelized Cost of Water
LINMAP	Linear Programming Technique for Multidimensional Analysis of Preference
MED	Multi-Effect Distillation
MENA	Middle East and North Africa
MS	Molten salts
NEA	Non-Equilibrium Allowance
NRMSD	Normalized Root-Mean-Square Deviation

NSGA-II	Non-Dominated Sorted Genetic Algorithm
OPEX	Operating expenses
P/R	Pumping and recovery
PB	Power Block
POA	Plane of the array
Pout 1	First power output profile
Pout 2	Second power output profile
PV	Photovoltaic
PV_dum	Dumped energy from the PV plant
p	
PX	Pressure exchanger
RC	Rankine cycle
RO	Reverse Osmosis
RT	Recovery turbine
SGS	Steam Generation System
SM	Solar Multiple
TES	Thermal Energy Storage
TMY	Typical Meteorological year
TRNSYS	Transient System Simulation Program
TTD	Terminal Temperature Difference
UAE	United Arab Emirates
WAVE	Water Application Value Engine

Variables

[A]	Incident matrix
a_{ch}	Chemical exergy, kW
A_f	Amortization factor, dimensionless
A_m	Membrane area, m^2
b_i	Brine stream

b_{mix1}	Mixed brine stream
b_{mix2}	Brine output stream of the recovery system
cd_i	Condensate distillate stream
c_{ex}	Unit exergy cost, dimensionless
CF	Capacity factor
C_i	Exergy cost, kW
$\dot{C}_{i,t}$	Thermoeconomic cost, $
$c_{i,t}$	Unit thermoeconomic cost, $/MWh or $/m^3
D	Diffusivity, m^2/s
Dia	Diameter, m
D_h	Hydraulic diameter, m
dsh_i	Desuperheater distillate stream
$[Ex_i]$	Exergetic cost vector, kW
$Elec$	Net electricity production, MWh
f	Factor, dimensionless
f_i	Feed-water stream, dimensionless
f_f	Fouling factor, dimensionless
$f_{fric,i}$	Fricction factor, dimensionless
$f_{O\&M}$	Operation and maintenance factor, dimensionless
f_{rh}	Ratio of the investment cost of the reheater from the investment cost of the boiler, dimensionless
$J_{w,i}$	Water flux, l/m^{2}h
g	Gravity constant, m/s^2
h	Enthalpy, kJ/kg
ht	Height, m
i	Discount rate, dimensionless
k_i	Mass transfer coefficient, m/s
K_s	Salt permeability coefficient, l/m^{2}h bar
K_w	Water permeability coefficient, l/m^{2}h

L	Length, m
L_{pipe}	Length of the pipe, m
$\dot{m}$	Mass flow rate, kg/s
n	Plant lifetime, y
N	Number, dimensionless
$N_{effects}$	Number of effects, dimensionless
$O_{time,k}$	Annual operation time, h
P	Power, kW
Par_CSP	Parasitic consumption from the CSP, MWh
Par_PB	Parasitic consumption from the Power Block, MWh
$Pnet$	Net output power, kWh
Pr_i	Pressure, bar
Q	Heat, kW
$q_{j,i}$	Volumetric mass flow rate, m^3/h
Re	Reynolds number, dimensionless
s	Entropy, kJ/(kg K)
s_{cw}	Seawater cooling water stream
s_{in_1}	Seawater input stream of the pumping system
s_{in_2}	Seawater input stream of the MED condenser
s_i	Salinity, g_{salt}/kg_{water}
Sc_i	Schmidt number, dimensionless
$Suf_{e\&w}$	Electric and Water Sufficiency, dimensionless
st_{in}	Steam input stream from the turbine exhaust
st_{out}	Condensate output stream
T	Temperature, °C
TCE	Thermoeconomic cost of Electricity, $/MWh
TCI	Total Cost of Investment, $
TCW	Thermoeconomic cost of Water, $/m^3$
U	Overall heat transfer coefficient, $kW/(K\ m^2)$

UA	Heat exchanger thermal capacity, kW/K
v	Fluid velocity, m/s
vd_i	Vapor distillate stream
w	Water or salt mass fraction of the seawater, dimensionless
$\dot{X}_{cv}$	Exergy change within the control volume, kW
$\dot{X}_{dest}$	Destroyed exergy rate, kW
$\dot{X}_i$	Exergy rate, kW
$\dot{X}_{in}$	Input exergy rate to the system, kW
$\dot{X}_{products}$	Products exergy rate, kW
$X_{p,i}$	Salinity, kg_{salt}/kg_{water}
$\dot{X}_{waste}$	Waste exergy rate, kW
W	Desalination plant capacity, m^3/day
$Water_{i,t}$	Net water production, m^3
$\dot{X}_{i,t}$	Exergy rate, kW
Z_k^{Capex}	Total capital cost (CAPEX), $
Z_k^{Opex}	Annual operational and maintenance cost, $
$\dot{Z}_{k,t}$	Purchase cost rate, $/h

Greek Symbols

η	Efficiency, dimensionless
μ	Chemical potential, kJ/kg or dynamic viscosity, kg/m s
π_i	Osmotic pressure, bar
ρ_i	Density, kg/m^3
ψ	Physical exergy kJ/kg

Subscripts and superscripts

amb	Ambiental
br	Brine

boi	Boiler
booster	Booster pump
ch	Chemical
cond	Condenser
csw	Cooling seawater
CV	Control volume
cw	Cold side of the condenser
dea	Deaerator
dea_wate r	Deaerator water output
el	Electric
ex	Exergetic
f	Feed
gen	Generator
hel	Heliostats
hot_PB	From the hot tank to the power block
hp_1	High pressure pump
in	Inlet
inHTF	Inlet Heat Transfer Fluid
k	k-th stream or component
MED	Multi-Effect Distillation
MED_i	MED effect electric consumption
MED_t	MED plant and P/R system required power
nom	Nominal
o	Reference condition
O&M	Operational and maintenance
out	outlet
outHTF	Outlet heat transfer fluid
ph	Physical

pre_tre	Pre-treatment
px	Pressure exchanger
p_MED	Seawater pumping system power
p_sea	Seawater pumping
PB_ther mal	Power block thermal
PV	Photovoltaic
rec	Receiver
rec_total	Receiver total
ref	Heliostats reflective total area
rh	Reheat
s	Steam
sg	Steam generator
st	Steam turbine
t	Time of the simulation
TES	Thermal Energy Storage
TES_col d	TES cold tank
TES_hot	TES hot tank
ttd	Terminal temperature difference
tur_MED	Recovery system turbine power
z	Thermoeconomic
w	Water
II_law	Second law
*	Average

PONTIFICIA UNIVERSIDAD CATOLICA DE CHILE
ESCUELA DE INGENIERIA

EVALUACIÓN TERMOECONÓMICA Y OPTIMIZACIÓN MULTI-OBJETIVO DE UNA PLANTA DE CONCENTRACIÓN SOLAR DE POTENCIA + FOTOVOLTAICA + DESTILACIÓN POR MULTI-EFECTO

Tesis enviada a la Dirección de Postgrado en cumplimiento parcial de los requisitos para el grado de Doctor en Ciencias de la Ingeniería.

CARLOS ENRIQUE MATA TORRES

RESUMEN

Esta tesis presenta una evaluación y optimización de una planta de energía solar híbrida integrada con una planta desaladora. El objetivo principal es desarrollar una metodología que permita modelar una planta de Concentración Solar de Potencia + Fotovoltaica + Destilación por Multi-Efecto (CSP+PV+MED) para suministrar energía eléctrica y agua, y optimizar el dimensionamiento en función de variables termoeconómicos, con el fin de estudiar los aspectos sinérgicos que dicha integración produce. Esta tesis se presenta en un formato de cuatro artículos. El trabajo tiene como objetivos: evaluar el desempeño de la planta y la formación del costo de los productos bajo diferentes condiciones, identificar el impacto del dimensionamiento y las condiciones operativas en los costos, determinar la configuración y la ubicación más competitivas y realizar una comparación con respecto a la integración con una ósmosis inversa (CSP+PV+RO) para definir la factibilidad del concepto hibrido y la competitividad frente a alternativas tradicionales de suministro eléctrico y de agua.

La metodología se estable como un procedimiento que comprende cuatro fases. Primero, el modelado y la simulación de la planta CSP+PV+MED se realizan con datos horarios, incluyendo la operación de carga parcial de los componentes y la integración entre todos los sistemas. La simulación considera varios factores para evaluar el rendimiento anual de la planta, entre los cuales está la variabilidad de la irradiación solar, el dimensionamiento de los componentes, las diferentes condiciones de operación y los parámetros de la ubicación. Segundo, se lleva a cabo un análisis termoeconómico, que consiste en calcular los costos de cada flujo de la planta en función del costo de los sistemas, el flujo exergético, la exergía destruida y la exergía desechada, con el fin de determinar la distribución de los costos de los sistemas en los productos. A partir de este análisis se obtienen las funciones objetivo: Costo Termoeconómico de Electricidad (TCE), Costo Termoeconómico de Agua (TCW) y Suficiencia Eléctrica y de Agua ($Suf_{e\&w}$). Tercero, se realiza una optimización multiobjetivo del dimensionamiento utilizando un algoritmo genético. El objetivo es determinar las

soluciones óptimas que conforman la frontera de Pareto, las cuales minimizan el TCE y TCW y maximizan $Suf_{e\&w}$. Por último, se realiza un proceso de post-análisis, en cual se analizan los resultados de la optimización para múltiples condiciones de estudio, donde se incluye un análisis comparativo con respecto a la integración CSP+PV+RO.

Los resultados del estudio revelan que el costo de los componentes tiene la mayor influencia en la formación del costo de los productos, mientras que la operación en carga parcial puede afectar significativamente los costos de electricidad y agua. En cuanto al dimensionamiento de la planta, se demuestra que la integración con una planta PV permite disminuir tanto el TCE como el TCW. Sin embargo, el análisis sobre los tamaños de la planta PV y la planta CSP+MED presentan resultados contradictorios entre sí, donde el mínimo TCE se obtiene para una planta PV grande y una planta CSP pequeña con una planta MED pequeña, y el mínimo TCW se obtiene para una planta PV pequeña y una planta CSP sobredimensionada con una planta MED grande. Para la optimización multiobjetivo, se evidencia que maximizar la producción es un factor relevante, ya que puede dar una visión más amplia sobre cuál es el mejor dimensionamiento. La solución óptima obtenida consiste en una planta PV mediana (PV=40-70 MW_e) y una planta CSP grande (SM=3-3.6 y TES=14-18 h) con 6 a 8 unidades MED.

Con respecto a la comparación de plantas CSP+PV+MED y CSP+PV+RO, la planta CSP+PV+MED logra obtener TCE competitivos, pero con un TCW 18-30% más alto en comparación con RO. La principal razón de la diferencia es el costo de energía que proviene del sistema CSP. Sin embargo, se pueden alcanzar costos competitivos con una reducción del 30% del CAPEX de los sistemas CSP y MED. En cuanto a la ubicación de la planta, la irradiación solar tiene el efecto más significativo en los costos, donde las ubicaciones ideales deberían tener una DNI superior a 2500 kWh/m^2-año. La distancia con respecto al mar incide en los costos de agua, considerando que una ubicación a más de 60 km de la costa no presenta costos competitivos. La altitud sobre el nivel del mar tiene un impacto moderado sobre 500 m, cambiando principalmente la asignación de costos. Sin embargo, su efecto es considerablemente menor que los otros dos factores. Finalmente, se presentan mapas de TCE y TCW con respecto a las variables de ubicación de la planta que se pueden utilizar como herramienta para el análisis preliminar de costos de una planta CSP+PV+MED.

Por lo tanto, esta tesis presenta una extensa metodología que contribuye a la investigación de plantas de energía solar y desalación. Los hallazgos dan una idea clara de la viabilidad económica de estas plantas y las mejoras necesarias para lograr costos competitivos.

Miembros de la Comisión de Tesis Doctoral:

Ph.D. Rodrigo A. Escobar
Ph.D. José Miguel Cardemil Iglesias
Ph.D. Francisco Suárez
Ph.D. Diego César Alarcón Padilla
Ph.D. Patricia Palenzuela
Ph.D. Juan de Dios Ortúzar

Santiago, Enero, 2021

PONTIFICIA UNIVERSIDAD CATOLICA DE CHILE
ESCUELA DE INGENIERIA

THERMOECONOMIC ASSESSMENT AND MULTI-OBJECTIVE OPTIMIZATION OF A CONCENTRATING SOLAR POWER + PHOTOVOLTAIC + MULTI-EFFECT DISTILLATION PLANT.

Thesis submitted to the Office of Graduate Studies in partial fulfillment of the requirements for the Degree of Doctor in Engineering Sciences by

CARLOS ENRIQUE MATA TORRES

RESUMEN

This thesis presents an assessment and optimization of a hybrid solar power plant integrated with desalination plants. The principal objective is to develop a methodology that allows modeling a Concentrating Solar Power + Photovoltaic + Multi-Effect Distillation plant (CSP+PV+MED) to supply electricity and water, and to optimize the design configuration in terms of thermoeconomic and productivity objectives, to study the synergetic aspects that produce this integration. This dissertation is presented in a format of four appended papers. The research aims to: evaluate the plant performance and the products cost formation under different operational and plant location conditions, identify the impact of the sizing and operating conditions in the cost of the products, determine the most competitive configuration and location parameters, and perform a comparison with respect to a Reverse Osmosis integration (CSP+PV+RO) to define the cost-benefit feasibility of the hybrid concept and the competitiveness against traditional alternatives of electricity and water supply.

The methodology process comprehends four phases. Firstly, the CSP+PV+MED plant's modeling and simulation are performed with hourly data, including the components part-load operation and the integrations between all systems. The simulation considers the solar irradiation variability, the sizing of the components, different operation conditions, and the location parameters in order to assess the plant's annual performance accurately. Secondly, an extensive thermoeconomic analysis on an hourly basis is carried out. This analysis computes each stream's cost based on the systems' cost, the exergy flow, the destroyed exergy, and the waste exergies, defining the system cost allocation into the products (electricity and water). From this analysis, the objective functions are obtained: Thermoeconomic Cost of Electricity (TCE), Thermoeconomic Cost of Water (TCW), and Electric and Water Sufficiency ($Suf_{e\&w}$). Thirdly, a multi-objective optimization of the design configuration is performed using a genetic algorithm. The goal is to determine the optimal solutions that make up the Pareto-frontier, which minimizes the TCE and TCW and maximizes $Suf_{e\&w}$. Lastly, a post-analysis process was carried out. The optimization results

are analyzed for different conditions, where a comparative analysis with respect to the CSP+PV+RO integration is included.

The results of the study reveal that the components cost has the most significant influence on the product cost formation, while the part-load operation could significantly impact the TCE and TCW. In terms of the plant sizing, it is demonstrated that PV plant integration allows lowering both TCE and TCW. However, the PV plant and the CSP+MED plant sizing has contradictory roles regarding the costs. The minimum TCE is obtained for a large PV plant and an undersized CSP plant with a small MED, and the minimum TCW is obtained for a small PV plant and an oversized CSP plant with a large MED plant. For the multi-objective optimization, it is evidenced that maximizing the production is a relevant factor, giving a more in-depth insight into what is the best design configuration. The optimal solution consists of a medium PV plant (PV=40-70 MW_e) and a large CSP plant (SM=3-3.6 and TES=14-18 h) with 6 to 8 MED units.

Concerning the CSP+PV+MED and CSP+PV+RO plant comparison, the CSP+PV+MED achieve competitive TCE but 18-30% higher TCW compared to RO. The main reason of the difference is the energy cost that comes from the CSP system. However, competitive costs can be achieved with a 30% CAPEX reduction of the CSP and MED system. Regarding the plant location, the solar irradiation has the most significant effect on the TCE and TCW, indicating that the ideal place should have DNI higher than 2500 kWh/m^2-yr. The distance with respect to the sea affects considerably the TCW, where location at more than 60 km from the coast should not be considered. The altitude above the sea level has a moderately impact over 500 m, mainly changing the cost allocation. However, its impact is considerably lower than the other two factors. Finally, the results present TCE and TCW maps regarding the plant location variables that can be used as a tool for a preliminary feasibility analysis of a CSP+PV+MED plant.

Therefore, this thesis exhibits an extensive methodology to assess a CSP+PV+MED plant that contributes to the field of solar power plants and desalination integration. The findings presented herein give a clear insight into these plants' cost-benefit feasibility and the improvements required to achieve competitive costs.

Members of the Doctoral Thesis Committee:

Ph.D. Rodrigo A. Escobar	Ph.D. Diego César Alarcón Padilla
Ph.D. José Miguel Cardemil Iglesias	Ph.D. Patricia Palenzuela
Ph.D. Francisco Suárez	Ph.D. Juan de Dios Ortúzar

Santiago, January 2021

LIST OF PAPERS

This dissertation is based on a compilation of four papers: two Q1 journal papers as the principal author and two journal paper submissions. The papers constitute the core of this thesis and are presented in "List of Papers". Additionally, other publications in journals and conferences were published during this work. These papers are gathered in "Other research articles", although they are not directly discussed in this thesis.

List of Papers

I. **Mata-Torres, C.**, Zurita, A., Cardemil, J. M., & Escobar, R. A. (2019). Exergy cost and thermoeconomic analysis of a Rankine Cycle + Multi-Effect Distillation plant considering time-varying conditions. *Energy Conversion and Management*, *192*, 114–132. https://doi.org/10.1016/j.enconman.2019.04.023

II. **Mata-Torres, C.**, Palenzuela, P., Zurita, A., Cardemil, J. M., Alarcón-Padilla, D.-C., & Escobar, R. A. (2020). Annual thermoeconomic analysis of a Concentrating Solar Power + Photovoltaic + Multi-Effect Distillation plant in northern Chile. *Energy Conversion and Management*, *213*(June). https://doi.org/10.1016/j.enconman.2020.112852

III. **Mata-Torres, C.**, Palenzuela, P., Zurita, A., Cardemil, J. M., Alarcón-Padilla, D.-C., & Escobar, R. A. Comparative analysis between hybrid Concentrating Solar Power + Photovoltaic plant integrated with Multi-Effect Distillation and Reverse Osmosis Desalination plant. (Submitted to *Desalination*)

IV. **Mata-Torres, C.**, Palenzuela, P., Zurita, A, Cardemil, J. M., Alarcón-Padilla, D.-C., & Escobar, R. A. Multi-Objective optimization of a Concentrating Solar Power + Photovoltaic + Multi-Effect Distillation plant: understanding the impact of the solar irradiation and the plant location. (Submitted to *Energy Conversion and Management*)

Other research articles

Journal publications:

i. **Mata-Torres, C.**, Escobar, R. A., Cardemil, J. M., Simsek, Y., & Matute, J. A. (2017). Solar polygeneration for electricity production and desalination: Case studies in Venezuela and northern Chile. *Renewable Energy*, *101*, 387–398. https://doi.org/10.1016/j.renene.2016.08.068

ii. Valenzuela, C., **Mata-Torres, C.**, Cardemil, J. M., & Escobar, R. A. (2017). CSP + PV hybrid solar plants for power and water cogeneration in northern Chile. *Solar Energy*, *157*(August), 713–726. https://doi.org/10.1016/j.solener.2017.08.081

iii. Ramírez-Sagner, G., **Mata-Torres, C.**, Pino, A., & Escobar, R. A. (2017). Economic Feasibility of Residential and Commercial PV Technology: the Chilean Case. *Renewable Energy*, *111*(July 2016), 332–343. https://doi.org/10.1016/j.renene.2017.04.011

iv. Simsek, Y., **Mata-Torres, C.**, Guzmán, A. M., Cardemil, J. M., & Escobar, R. (2018). Sensitivity and effectiveness analysis of incentives for concentrated solar power projects in Chile. *Renewable Energy*, *129*(214), 224. https://doi.org/10.1016/j.renene.2018.06.012

v. Zurita, A., Castillejo-Cuberos, A., García, M., **Mata-Torres, C.**, Simsek, Y., García, R., … Escobar, R. A. (2018). State of the art and future prospects for solar PV development in Chile. *Renewable & Sustainable Energy Reviews*, *92*(September), 701–727. https://doi.org/10.1016/j.rser.2018.04.096

vi. Zurita, A., **Mata-Torres, C.**, Valenzuela, C., Felbol, C., Cardemil, J. M., Guzmán, A. M., & Escobar, R. A. (2018). Techno-economic evaluation of a hybrid CSP + PV plant integrated with thermal energy storage and a large-scale battery energy storage system for base generation. *Solar Energy*, *173*(August), 1262–1277. https://doi.org/10.1016/j.solener.2018.08.061

vii. Zurita, A., **Mata-Torres, C.**, Cardemil, J. M., & Escobar, R. A. (2020). Assessment of time resolution impact on the modeling of a hybrid CSP-PV plant: A case of study in Chile. *Solar Energy*, *202*(February), 553–570. https://doi.org/10.1016/j.solener.2020.03.100

viii. Zurita, A., **Mata-Torres, C.**, Cardemil, J. M., Guédez, R. & Escobar, R. A. (2020). Multi-Objective Optimal Design of Solar Power Plants with Storage Systems according to Dispatch Strategy. (Summitted to *Energy*)

Conference papers and presentations:

i. **Mata-Torres, C.**, Escobar, R. A., & Cardemil, J. M. (2018). Techno-Economic Analysis of CSP+MED+PV Plant: Electricity and Water Production for Mining Industry in Northern Chile. In *AIP Conference Proceedings* (Vol. 2033, p. 180007), *SolarPACES 2017, Santiago, Chile*. https://doi.org/10.1063/1.5067179

ii. **Mata-Torres, C.**, Zurita, A., Cardemil, J. M., & Escobar, R. A. (2018). Exergy cost analysis of a CSP-Rankine Cycle coupled with a MED plant considering time-varying conditions and part-load operation. In *Proceedings of the 31st International Conference on Efficiency, Cost, Optimization, Simulation and Environmental Impact of Energy Systems, ECOS 2018, Guimaraes, Portugal*.

iii. **Mata-Torres, C.**, Zurita, A., Cardemil, J. M., & Escobar, R. A. (2018). Cost Allocation Analysis of a CSP+MED Plant Considering Time-Varying Conditions. *SolarPACES 2018, Casablanca, Morocco.*

iv. **Mata-Torres, C.**, Zurita, A., Cardemil, J. M., & Escobar, R. A. (2019). Thermoeconomic Analysis of a CSP+PV+MED Plant in Chile: Assessing the Impact of the PV Plant Integration. In *Proceedings of the 32nd International Conference on Efficiency, Cost, Optimization, Simulation and Environmental Impact of Energy Systems, ECOS 2019, Wroclaw, Poland*.

v. **Mata-Torres, C.**, Zurita A., Palenzuela, P., Alarcón-Padilla, D.-C., Escobar, R. A. (2019). Assessment of a Concentrating Solar Power Plant Coupled to a Multi-Effect Distillation with an Air-Cooled Condenser. *SolarPACES 2019, Daegu, South Korea.*

vi. **Mata-Torres, C.**, Escobar R. A. (2019). Performance Comparison Between a CSP+PV+MED and CSP+PV+RO Plant in Northern Chile. *ISES Solar World Congress 2019, Santiago, Chile.*

1. INTRODUCTION

1.1 Content

Worldwide water consumption has increased in the last years, especially in water-stressed regions, where the physical water scarcity is often a seasonal phenomenon rather than a chronic one (UNESCO & UN-Water, 2020). Northern Chile is one of those regions where the water supply mainly comes from continental and groundwater reservoirs, with the largest fraction of the demand required by the mining industry. Specifically, the Antofagasta region presents the highest water consumption rates for copper mining with more than 11 m^3/s (Comision Chilena del Cobre, 2015). Mining activities in this area focus on copper production by the concentration method, which is a water-intensive process. To solve the actual and future water supply, the mining industry has started to evaluate and build projects to use freshwater from desalination plants in their processes (Comision Chilena del Cobre, 2016a). Evidence of this is the presence of 11 desalination projects currently in operation and several more under environmental assessment. Among the desalination projects, the *Escondida Water Supply* (EWS) stands out, consisting of a Reverse Osmosis (RO) plant with a pumping system used to produce 2500 L/s of industrial quality water. There is also the *Spence Growth Project* that is currently in a planning phase with a production estimation of 800 L/s and a 155 km water transportation system. The water consumption projection in copper mining is estimated to reach 24 m^3/s by 2030, of which the desalinated water could reach 11 m^3/s (Comision Chilena del Cobre, 2019b). This increase focuses on the Antofagasta region (70%), the Tarapacá region (14%), and the Atacama region (13%) (Comision Chilena del Cobre, 2016b). Therefore, a scenario where the seawater desalination would become a relevant resource in the coming years in Northern Chile is observed.

Regarding the electric situation in Chile, the total installed capacity has increased to 24,640 MW_e by June 2020. From this capacity, the solar Photovoltaic (PV) technology has been considerably rising its participation share in the last years (Comision Nacional de Energía, 2020; Zurita, Castillejo-Cuberos, et al., 2018), reaching an installed capacity of 3104 MW_e

(13% of the national capacity). The solar PV generation also achieved 8% and 9% of the total national generation in 2019 and 2020, respectively. Thus, solar electricity has become relevant in the national electric system, attracting investors' interest due to the very high solar irradiation levels. Simultaneously, the attention by the Concentrating Solar Power (CSP) technology has also increased since it can provide reliable and dispatchable energy, including the ability for baseload generation. For instance, the Cerro Dominador project located in the Antofagasta region represents the first CSP plant in Latin America with a capacity of 110MW_e, and it is currently in the final construction phase, expected to end its commissioning and start its operation at the first semester of 2021.

Moreover, the Chilean government has an energy policy agenda establishing as a goal that 70% or more of the electric generation must come from renewable energy sources by 2050 (Ministerio de Energía, 2014). It has also been established a decarbonization plan for the electric sector by 2040 (Comisión Nacional de Energía, 2020). These measures indicate that variable renewable energy will soon become the principal generation source in Chile, mostly driven by solar energy. The main reason for the interest in solar energy in Chile is the high solar irradiation levels throughout the year. The northern regions of the country, where the Atacama Desert is located, present total yearly Direct Normal Irradiation (DNI) levels above 3500 kWh/m^2. These irradiation levels occur due to a combination of meteorological and geographical conditions, which include an extremely arid climate, low humidity levels, very high altitudes, and high clearness-indexes throughout the year (Escobar et al., 2015; Zurita, Castillejo-Cuberos, et al., 2018).

In summary, it is expected that further development of water desalination and solar energy projects in Northern Chile will likely occur during the next few years. The analysis of concept schemes that integrate the solar generation with desalination plants are relevant for the region since it would allow the sustainable development and supply of both resources, electricity and water. Specifically, the integration between a Concentrated Solar Power (CSP) plant and a Multi-Effect Distillation (MED) system has been widely studied in the literature showing the great potential of implementation in arid regions with high availability of solar radiation (Aboelmaaref et al., 2020a; Leiva-Illanes, Escobar, Cardemil, & Alarcón-

Padilla, 2017, 2018; Mohammadi, Saghafifar, Ellingwood, & Powell, 2019). However, some market barriers have been identified for their commercial deployment. Among them, the high capital cost of the system (mainly related to the CSP plant), the complex integration between the technologies, and the conservative market approach from the energy and desalination industry (Alhaj & Al-Ghamdi, 2019; Mohammadi et al., 2019; Omar, Nashed, Li, Leslie, & Taylor, 2020a) can be highlighted as the main barriers. The integration of a PV plant to a CSP+MED could enhance the plant's productivity taking advantage of the low PV cost, although the plant could be able to operate in different modes depending on the PV sizing (Valenzuela, Mata-Torres, Cardemil, & Escobar, 2017). A relevant downside of the CSP+MED plant is the misalignment of the optimal location between the power and the desalination plants since they must be co-located (Alhaj & Al-Ghamdi, 2019). Thus, the techno-economic analyses should consider the site's relevant factors such as the direct normal irradiation (DNI) levels, the water salinity, and the distance from shore (Mohammadi et al., 2019; Qasim, Badrelzaman, Darwish, Darwish, & Hidal, 2019).

This situation evidences the need to evaluate the actual performance of the CSP+PV+MED plant integration under high radiation conditions such as those present in northern Chile and other desertic areas. The cogeneration of electricity and water with a reliable system can contribute to the sector's sustainable development. Still, it is required to conduct an in-depth analysis to understand the plant's operation and thermoeconomic performance. The sizing of the CSP+PV+MED plant and the meteorological and geographical parameters also have a relevant impact on the plant’s performance. In order to analyze the competitiveness of the CSP+PV+MED concept in high solar radiation locations, this dissertation focuses on developing a methodology to assess and optimize the performance and costs of the plant, intending to determine the most suitable configurations and parameters for several locations. In this way, this dissertation gives a comprehensive insight into this concept's feasibility, showing the research paths that could be followed to improve the plant's performance.

1.2 Objectives

The present research work's main objective is to develop a methodology that allows modeling a Concentrating Solar Power + Photovoltaic + Multi-Effect Distillation (CSP+PV+MED) plant to supply electricity and water and optimizing the design configuration in terms of thermoeconomic and productivity objectives. The aim is to assess the plant performance, and the products cost under different meteorological and geographical conditions, to determine the most competitive configuration and location parameters, and to perform a comparison with respect to a Reverse Osmosis plant integration (CSP+PV+RO).

To reach this general objective, the following specific objectives were defined:

i) To develop the physical model of a CSP+PV+MED plant considering the operation at part-load conditions of the sub-systems, to evaluate the annual plant performance carrying out simulations that consider the hourly solar resource variability and the transient operation.

ii) To perform a thermoeconomic analysis of the plant performance to determine the actual cost allocation into the products and the plant's cost formation process.

iii) To carry out a multi-objective optimization of the plant in terms of three objective functions: minimize the Thermoeconomic Cost of Electricity (TCE) and Thermoeconomic Cost of Water (TCW) and maximize the Electric and Water Sufficiency ($Suf_{e\&w}$).

iv) To determine the impact of the plant design configuration, the solar irradiation, and the geographical conditions of the plant location (distance from the coast and altitude of the plant location) on the plant performance and the products cost formation.

v) To perform a comparison between the CSP+PV+MED plant and the CSP+PV+RO plant under different demand location scenarios to determine the MED integration competitiveness.

1.3 Hypothesis

This research's hypothesis is based on the possibility of finding out how the cost formation process throughout the plant affects the final electricity and water cost and determining the optimal configuration of the CSP+PV+MED plant under different scenarios. Conforming to this, the next hypotheses are raised:

i) The thermoeconomic analysis used as a tool to allocate the plant cost allows us to accurately determine the electricity and water costs of a CSP+PV+MED plant, considering the transient operation.

ii) The multi-objective optimization approach is a suitable method to determine the Pareto-frontier and analyze the optimum solutions in a cogeneration plant with two products, electricity, and water.

iii) The plant solar irradiation and geographical conditions, and the demand location determine the best technologies selection and the optimum sizing to produce electricity and water most competitively.

iv) The inland plant locations with a higher solar resource would have a better yield and lower cost than the coastal locations, compensating the seawater's transport to plant location.

v) Under the current conditions, the CSP+PV+MED requires improvement on the MED efficiency or a cost reduction to achieve competitive water costs compared to the CSP+PV+RO.

1.4 Methodology

The methodology developed in this work aims to perform a thermoeconomic analysis and a multi-objective optimization of the CSP+PV+MED and CSP+PV+RO plant. Figure 1-1 depicts a detailed flow chart of the methodology, where the scientific publications dealing with each section are presented in white circles. The methodology was performed using Transient System Simulation Software (TRNSYS), Engineering Equation Solver (EES), and MATLAB, shown in brackets for the different analyses.

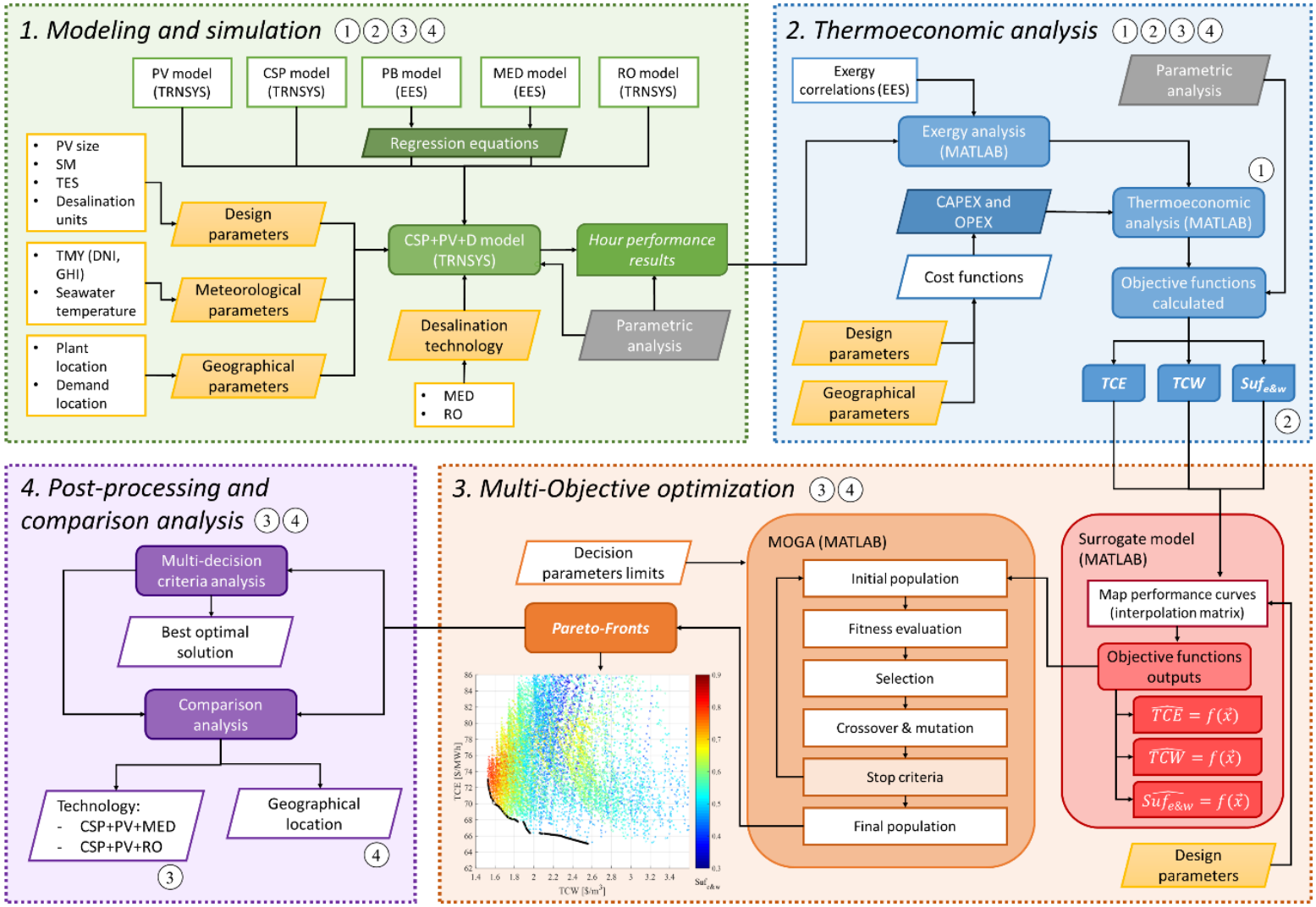

Figure 1-1: Methodology flow chart.

In general, the process includes four phases, which were developed throughout the scientific articles from the main body of this dissertation:

i) Modeling and simulation of the system that integrates the plant.
ii) Thermoeconomic analysis of the plant.
iii) Multi-objective optimization of the plant.
iv) Post-processing and comparison analysis.

The first phase comprehends the physical modeling of the plant. The model comprises four main systems: the PV plant, the CSP plant based on a central receiver system, the PB system, the MED plant. Additionally, a RO plant was added to analyze the performance of the CSP+PV+RO plant. Figure 1-2 shows the layout of the CSP+PV+MED plant modeled in this work. The model was developed in TRNSYS (Transient System Simulation Tool), a graphical-based software used to simulate complex thermal and electrical system considering the dynamic and transient behavior. The model was made in a single TRNSYS deck (unique file) to allow the interaction between all systems and components. The design parameters, the meteorological data, and the geographical parameters were considered as input files of the model. The system models were computed using different components (TRNSYS types) developed from myself or adapted from the TRNSYS library or previous research studies. The model of the CSP and PV systems are described in Chapter 3. The PB and the MED model were developed using EES, in which the thermodynamic performance and the energy and heat transfer balance are assessed. The integration into the TRNSYS environment was carried out using multi-variable polynomial regressions. In Chapter 2 are described the models, while the TRNSYS integration is detailed in Chapter 3. Finally, the RO model is described in Chapter 4. The plant simulation was performed for a Typical Meteorological Year (TMY) with hourly data. Several operational assumptions and control procedures were considered, including the plant's operation mode and the startup and shut down procedures of the components (Chapter 3 and Chapter 4). The model's output is the thermodynamic operation of the plant accounting for the solar irradiation, molten salts, steam, seawater, freshwater, brine temperatures, mass flow rates, and the electric flows of each component in hourly resolution.

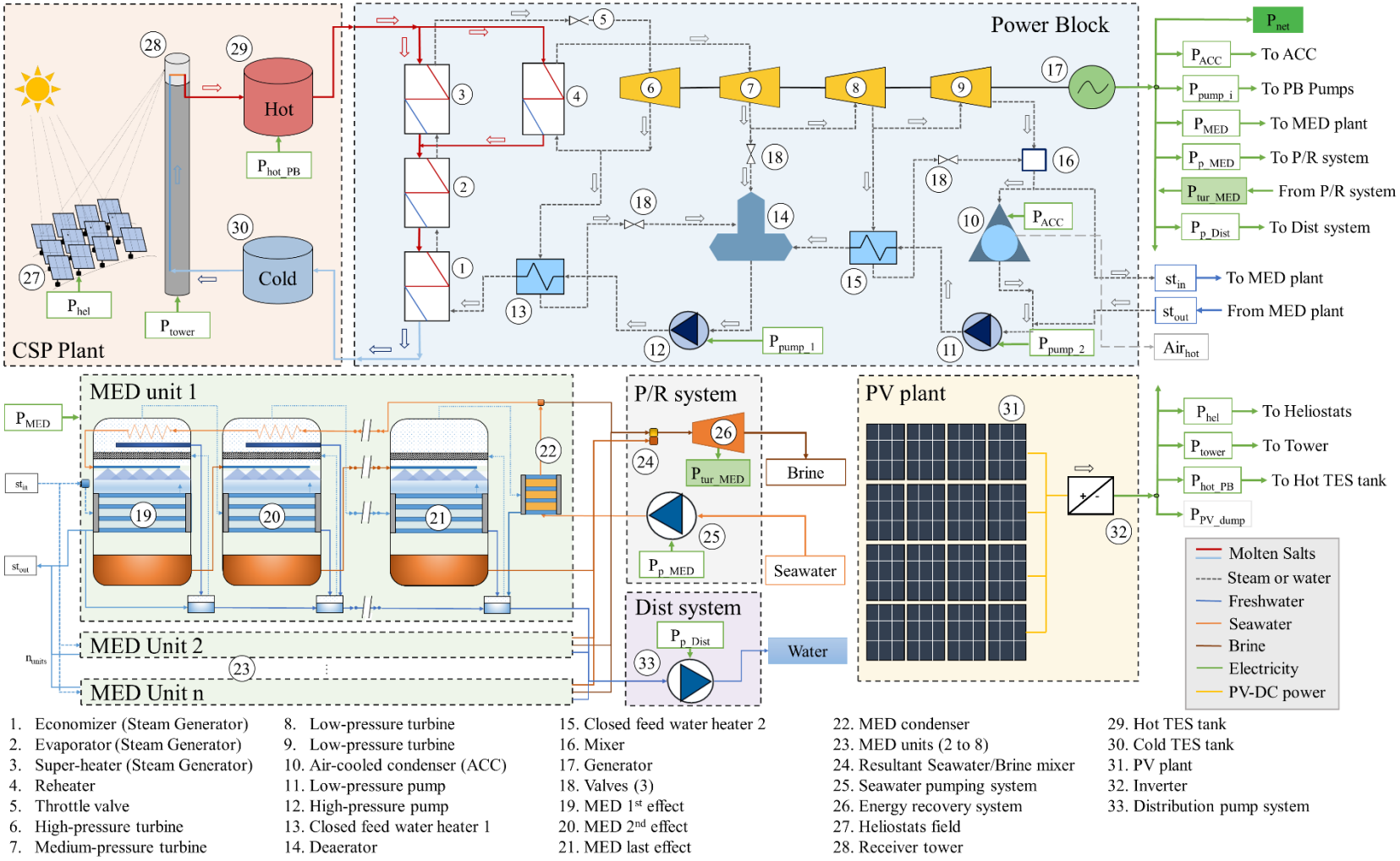

1. Economizer (Steam Generator)
2. Evaporator (Steam Generator)
3. Super-heater (Steam Generator)
4. Reheater
5. Throttle valve
6. High-pressure turbine
7. Medium-pressure turbine
8. Low-pressure turbine
9. Low-pressure turbine
10. Air-cooled condenser (ACC)
11. Low-pressure pump
12. High-pressure pump
13. Closed feed water heater 1
14. Deaerator
15. Closed feed water heater 2
16. Mixer
17. Generator
18. Valves (3)
19. MED 1st effect
20. MED 2nd effect
21. MED last effect
22. MED condenser
23. MED units (2 to 8)
24. Resultant Seawater/Brine mixer
25. Seawater pumping system
26. Energy recovery system
27. Heliostats field
28. Receiver tower
29. Hot TES tank
30. Cold TES tank
31. PV plant
32. Inverter
33. Distribution pump system

Figure 1-2: Layout of the CSP+PV+MED plant.

The second phase consists of the thermoeconomic analysis, which merges the thermodynamic assessment based on exergy analysis and the economic analysis providing useful information about the cost formation process. The thermoeconomic analysis computes each stream's cost based on the costs of the systems, the exergy flow, the destroyed exergy, and the waste exergies. The thermoeconomic cost is calculated by a linear equation system solved by a matrix computation composed of cost balance and auxiliary equations. From this analysis, the objective functions are obtained: TCE, TCW, and $Suf_{e\&w}$. The analysis was performed in MATLAB using: the hourly thermodynamic results from the model simulation, the exergy correlations for the molten salts, steam, and seawater properties from EES and the literature, and the Capital Expenditures (CAPEX) and the annual Operation and Maintenance (OPEX) costs of the plant. The methodology is based on the well-known Specific Exergy Costing (SPECO) method (Lazzaretto & Tsatsaronis, 2006). The description is extended in Chapters 2 and Chapter 3.

The third phase entails the multi-objective optimization of the plant using a Genetic Algorithm (MOGA). The optimization was developed in MATLAB to obtain the set of optimal solutions (Pareto-Frontier) in terms of the design parameters. Three objective functions were considered: minimize the TCE and TCW to get the trade-off between both costs and maximize the $Suf_{e\&w}$ to evaluate the plant productivity concerning the products' cost. Moreover, to avoid the high computational time of several simulations of the physical system that would imply a MOGA, a surrogate model to approximate the TRNSYS simulation and the thermoeconomic analysis was created. The methodology is widely described in Chapter 4.

The last phase consists of the post-processing and comparison analysis carried out for the different scenarios evaluated. A decision-making criteria analysis was performed using the LINMAP method (Linear Programming Technique for Multidimensional Analysis of Preference) in order to select an optimum solution among the Pareto-front and analyze its cost formation. A comparison between the CSP+PV+MED and CSP+PV+RO plant is performed considering different plant and demand locations described in Chapter 4. A

specific analysis of the impact of the solar irradiation and the geographical conditions of the plant location is carried out to determine their real influence and relevance (described in Chapter 5).

1.5 Contents and research contribution

1.5.1 Contents

The present work is organized into six chapters, following the paper compilation format. The first chapter presents the introduction and a summary of the contents and research contributions. Chapters 2, 3, 4, and 5, show the study developed in this dissertation, associated with the journal papers I, II, III, and IV, respectively. Finally, Chapter 6 presents the conclusions of the dissertation. Each article constitutes independent research that is concatenated with the previous one. They contain the state of the art, literature review, methodology, results, and conclusions of this research. In this way, each chapter is an autonomous section and can be read without the strict need for reading the rest of the chapters. However, it is inevitable to have some redundant contents between the different chapters, especially in the introduction and methodology sections.

The content of each chapter is indicated as follows:

- In Chapter 2, a complex exergy cost formation and thermoeconomic analysis applied to a Rankine Cycle (RC) fed by molten salts and coupled to a MED plant (RC+MED) are performed. The study aims to evaluate the destroyed exergy distribution and the allocation of the fuel and plant costs into the products. Also, it identifies the impact of the system design and operating conditions on the exergy and thermoeconomic costs of the electricity and water. Therefore, this work represents the first step on the CSP+PV+MED analysis, where the focus is on assessing the two more complex plant systems: the RC and MED integration. The study considers transient conditions such as the variation of the ambient temperature and the plant part-load operation. Also, a sensitivity analysis varying the MED plant capacity and the plant's location with

respect to the sea level is carried out. Thus, the detailed model developed allows us to accurately assess the actual exergy and thermoeconomic cost of the RC+MED plant's final products under the different conditions and configurations.

- In Chapter 3, detailed annual performance and thermoeconomic analysis of a Concentrated Solar Power plant coupled to a Photovoltaic and a Multi-Effect Distillation plants (CSP+PV+MED) are performed. The aim was to assess the impact of the PV integration into the CSP+MED plant and to evaluate the sizing of the plant in terms of the design parameters (PV plant size, solar multiple, Thermal Energy Storage capacity, and numbers of MED units) that allow achieving the lowest thermoeconomic electric and water costs (TCE and TCW). For this purpose, the performance and the cost formation process have been analyzed, including the variable and intermittent operation of the CSP and the PV plant and the nominal and part-load operation of the power block and MED plant. The analysis has been carried out by applying an extensive methodology based on an hourly simulation of the plant and a thermoeconomic analysis that calculates the systems' cost allocation into the products (electricity and water). Therefore, the detailed thermoeconomic analysis presented herein allows assessing a CSP+PV+MED plant's actual production costs considering the annual operation for a specific location, providing important insights about the plant's sizing.
- In Chapter 4, a multi-objective optimization of a CSP+PV+MED plant and a CSP+PV plant integrated with a Reverse Osmosis (RO) plan is carried out to perform a thermoeconomic comparison between both plants. The aim is to assess the performance and cost differences between RO and MED integration into a CSP+PV plant under different scenarios, which will result in relevant information about the potential of these cogeneration plants. A multi-objective optimization procedure of the plants (CSP+PV+MED and CSP+PV+RO) has been performed to determine the optimum sizing that reduces the cost and maximizes the production (electricity and water) in terms of the design parameters. The analysis is conducted for three locations with different demands (coast, mountain, and valley) and different plant sites to study the effect of the solar irradiation and the geographical conditions

(distance and altitude of the locations). Therefore, this work allows determining the influence of systems performance, the systems costs, and the location conditions to determine the competitiveness of the CSP+PV+MED plant and identify the principal research paths required to improve its overall performance.

- In Chapter 5, a multi-objective optimization of the CSP+PV+MED plant is performed to analyze the effect of the solar irradiation, the distance from the coast, and the plant location's altitude. The aim is to assess the plant's performance and product costs under different conditions to determine the conditions necessary to maximize the plant's competitiveness when required to select the ideal location. The study considers four TMY with DNI varying from 2000-3500 kWh/m^2-yr, six distance of plant from the sea (from 5 to 100 km), and six plants altitudes (from 20 to 1000 m.a.s.l.). Each variable's impact is assessed, and the combined effect of the variables is performed, resulting in costs maps of electricity and water. The analysis could be extrapolated to a different location in order to provide insights about the actual cost of this plant.

1.5.2 Results

This section summarizes the results of the main results from the appended papers presented in Chapters 2, 3, 4, and 5. These results are presented as follow:

In Chapter 2 (Paper I), a Rankine Cycle coupled to a Multi-Effect Distillation (RC+MED) plant is studied to analyze the exergy destruction, the exergy cost formation, and the thermoeconomic cost of the final products: electricity and freshwater. Figure 1-3 presents a summary of the chapter results. In this case, it evaluates the two most complex plant systems to assess their allocation of costs. For this purpose, a detailed RC+MED model was performed, considering a high-disaggregation level, in which the solar molten salts drive the RC. The analysis was carried out varying the part-load operation conditions, the ambient temperature, the MED plant size, and the location plant’s altitude. Finally, a detailed analysis

of an operational day for the RC+MED considering two power output profiles was carried out.

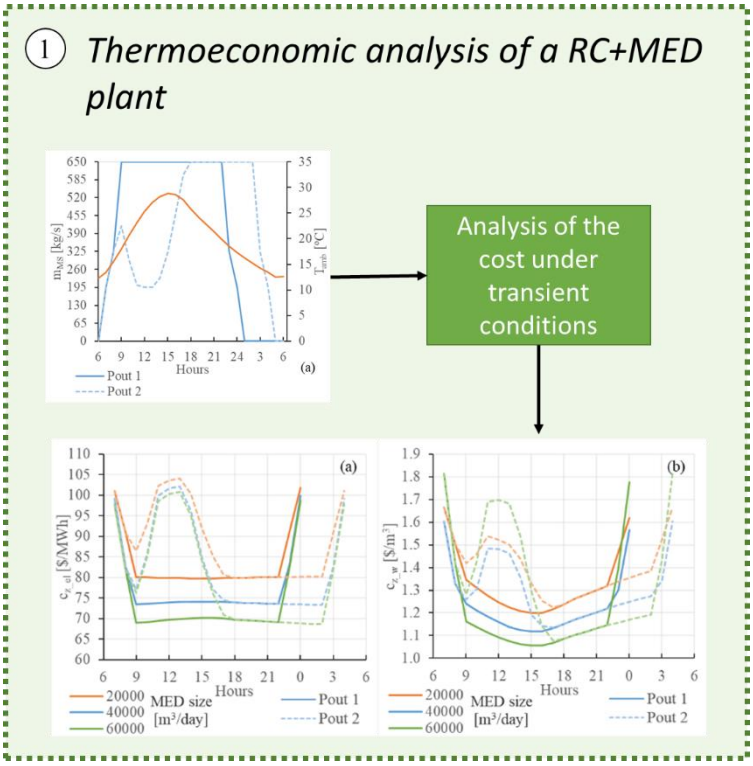

Figure 1-3: Graphical resume of the first journal paper results.

From the results, it can be highlighted that:

- The MED coupling to the RC increases the destroyed exergy on the dissipative components of the plant (the MED and the ACC) compared to a stand-alone RC, reducing the overall exergy efficiency of the plant by 10%. This is caused because of the rise of the condensing pressure. Additionally, it was found that the MED plant is the second component with the highest contribution to the plant destroyed exergy.
- The exergetic cost analysis considers the allocation of the destroyed and wastes exergy on the products. The part-load operation is the most relevant factor, and the temperature has a significant impact only on the water cost. In the thermoeconomic cost analysis, the cost of the components has a higher impact than the destroyed and waste exergy effects, obtaining that the part-load operation is the main factor that affects both costs and the ambient temperature slightly effect only in the water cost.

- More extensive MED plants configuration (over 50,000 m^3/day, which represents between the 80-100% of the maximum capacity) presents the lowest exergy and thermoeconomic costs of electricity and water. In contrast, the location altitude influences the water cost, so locations near the coast (low altitude) could achieve lower water costs.
- The thermoeconomic cost of electricity is mainly composed of 86% by fuel cost (the molten salts from a CSP plant) and 14% by the RC cost. In comparison, the thermoeconomic cost of water is roughly composed 58% by the fuel cost, 6% by the RC cost, and 36% by the MED plant and P/R system cost. This evidences that a high cost of the fuel is allocated to the water; hence it must be considered in the following analyses.
- Considering an operational day of the RC+MED, the operation at the part-load conditions during the day could increase the water production since the MED plant can increase the hours of operation. Still, the exergy and thermoeconomic cost of water could be moderately higher.

Chapter 3 (paper II) presents the evaluation of a CSP plant of 100 MW_e integrated with a PV and MED plant. A detailed thermoeconomic analysis was carried out to assess the impact of the PV integration into the CSP+MED plant. Figure 1-4 presents a summary of the chapter results. It was integrated the CSP and PV model with the power block and MED models from the previous work. A seawater pumping system and a brine recovery system (P/R system) were also considered. The thermoeconomic analysis was implemented, extending the research developed in Chapter 2, which considers the solar radiation and meteorological data variation in the plant's operation. The sizing of the plant in terms of the design parameters (PV plant size, solar multiple, Thermal Energy Storage capacity, and numbers of MED units) is evaluated through a unidimensional sensitivity analysis, showing the impact on the performance and the thermoeconomic electric and water costs (TCE and TCW). Finally, a multivariable parametric study is conducted, where different optimum configurations that minimize the TCE and TCW are analyzed.

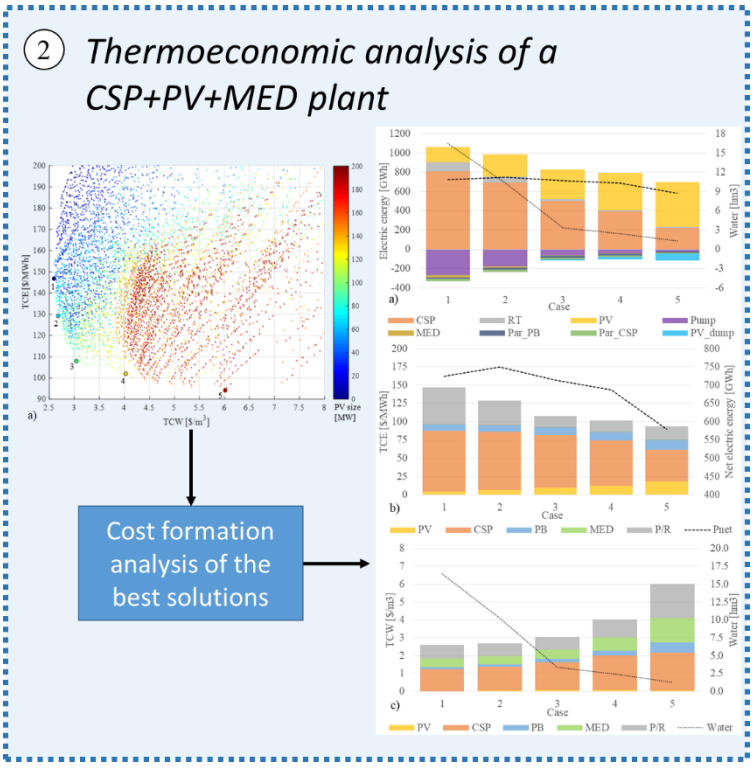

Figure 1-4: Graphical resume of the second journal paper results.

The main results can be summarized as follow:

- The principal impact of the PV integration to the CSP+MED plant is that it increases the net output electricity of the whole plant. However, its integration could increase or decrease the water production depending on the PV and the CSP plant size. If the PB and MED system are able to work at the part-load operation during the daylight hours, the water production could be increased. But, if the PV output is greater than the plant's nameplate capacity and the PB and MED system are shut down, the water production is significantly reduced.
- In terms of the thermoeconomic results, the TCE is significantly reduced with the PV integration. However, the TCW is mostly related to the water production, so the impact on TCW will depend on the MED plant's operational hours.
- The sizing of the PV and CSP plant present a contradictory role between the TCE and TCW. Large PV plants (150 MW) with small or medium CSP plants are required to achieve lower TCE, while large CSP plants with small PV plants (50 MW) are

needed to obtain lower TCW. The number of MED units has an important role in the plant cost, due to it influences the plant operation and P/R system cost. The lower TCW is obtained with medium or high MED units, achieving a water capacity factor of over 85%.

- From the multivariable parametric analysis, a Pareto-frontier between the TCE and TCW is obtained, evidencing a solution space where both costs can be reduced. Moreover, the water production changes dramatically across the Pareto-front, obtaining the higher values for the sizing that reduces the TCW.

Chapter 4 (paper III) presents a thermoeconomic comparison between the MED and RO processes integrated with a hybrid CSP+PV plant. Figure 1-5 shows a summary of the chapter results.

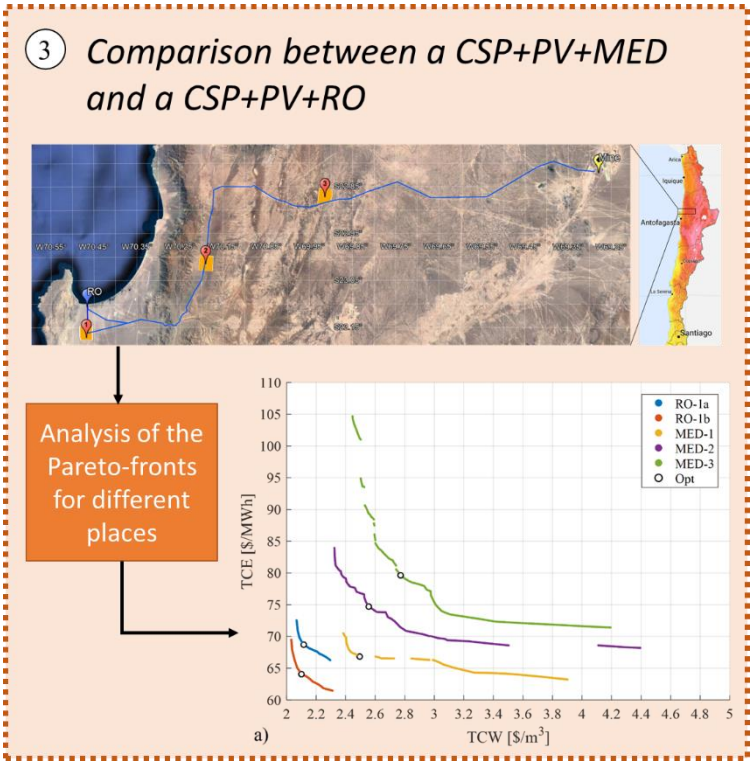

Figure 1-5: Graphical resume of the third journal paper results.

The analysis includes a multi-objective optimization based on GA in terms of the design parameters (PV plant size, solar multiple, Thermal Energy Storage capacity, and numbers of MED units) and considering three objective functions (TCE, TCW, and $Suf_{e\&w}$). The aim to assess the optimum sizing of the plant and its corresponding product cost formation. In that way, the thermoeconomic methodology from Chapter 3 was used as input for optimization. The study considers three locations for the demand: a coastal city (Antofagasta), an inland mountain (Atacama Mine), and an inland city in a valley (Copiapó), and different locations regarding the distance from the sea for the solar power plants. Additionally, a sensitivity analysis of the CSP, PB, MED, and pipeline costs was carried out. The main results can be summarized as follow:

- The CSP+PV+RO plant obtained the most competitive trade-off of TCE and TCW for all the cases evaluated. In contrast, the CSP+PV+MED plant showed a competitive TCE, while the TCW was more than 15% higher than the RO integration. The main reason for the difference is the energy cost (CSP, PV, and PB systems) to produce water, principally allocated by the heat that drives the MED plant.
- The sizing optimization of the CSP+PV+MED should include the plant's productivity as an objective function since different configurations could achieve similar TCE and TCW but with significant differences in terms of electric and water production. In the analysis, the configurations that achieve values over 70% $Suf_{e\&w}$ consist of a medium PV plant (PV=50 MW_e) and a large/oversized CSP plant (SM=3 and TES=14h) integrated with 7 or 8 MED units. In this way, low TCW with high $Suf_{e\&w}$ could be achieved in detriment of slightly higher TCE.
- The CSP+PV+MED analysis in different locations, trying to take advantage of the better solar resource in detriment of transport seawater to the plant location, resulted in that it is better to produce the water near the coast and then transport it. Nevertheless, there are some specific conditions at inland locations that can have a more competitive cost. These conditions consist of plant locations at 60 km or less from the coast and DNI 25% than the levels from the coast (respect to 2500 kWh/m^2-yr). Locations with 10 to 20% better DNI but respect to 3000 kWh/m^2-yr do not have

significant performance improvement, so it is not beneficial to locate the plant at inland locations.

- The cost sensitivity analysis puts in evidence that the priority must be to decrease the CSP specific cost to make the CSP+PV+MED plant competitive. In contrast, the MED cost could have considerable relevance to lowering the TCW. A combined reduction of the CSP, PB, and MED cost by 30% could obtain cost-competitive against the RO integration.

Chapter 5 (Paper IV) presents a multi-objective optimization of the CSP+PV+MED plant to analyze the impact of the solar irradiation, the distance from the coast, and the altitude of the plant location. The aim is to determine the effect of the conditions into the performance and define the ideal location characteristics to obtain a specific TCE or TCW. The thermodynamic and optimization methodology of Chapter 4 was used to obtain Pareto-fronts and optimum solutions. Figure 1-6 presents a summary of the chapter results.

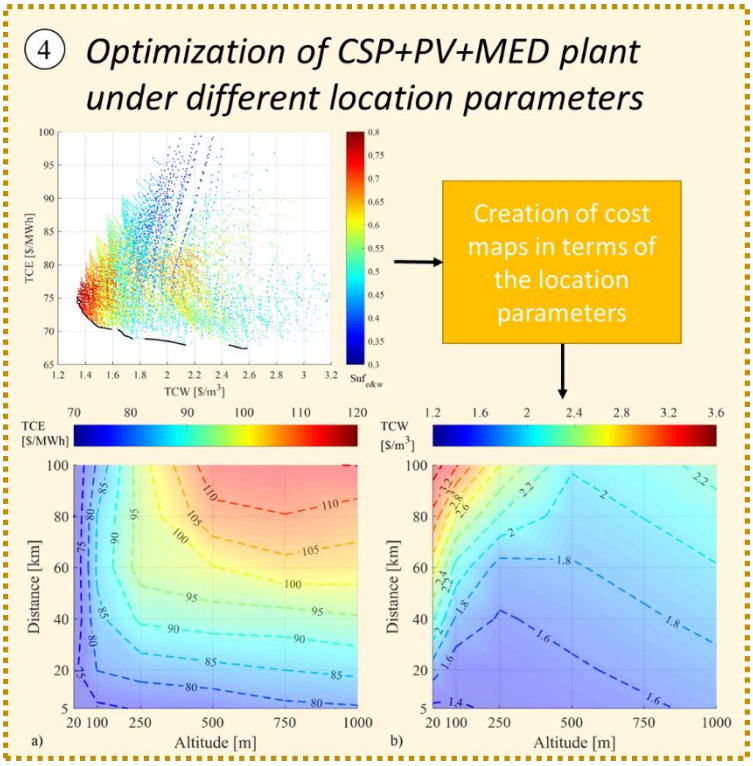

Figure 1-6: Graphical resume of the fourth journal paper results.

The main result can be summarized as follow:

- The solar irradiation is the variable that has the major effect on the TCE and TCW, reducing the costs as the DNI is higher. However, its effect is not linear. The higher the solar radiation, the smaller the cost reduction. For irradiation levels under 2500 kWh/m^2-yr, the increase in both costs are significant, so possible locations with these DNI levels are not recommended.
- The distance from the coast is the second most important variable that impacts the plant costs because it is related to the investment cost of the pipeline. It principally affects the TCW, while the TCE is affected if the brine pipeline's head losses are lower than the altitude. Over 60 km distance from the coast, the cost of the conveyance system becomes significant. Thus, locations under this threshold should have better conditions.
- The altitude has a lower impact on the costs because it only changes the plant's electric balance. The higher the altitude, the larger would be the electric parasitic consumption of the conveyance system. Moreover, depending if the brine pipeline's can recover energy, part of its cost is allocated into the TCE. Thus, it is better to have a higher solar irradiation and lower distance to the coast instead of a lower altitude in terms of the plant cost.
- Maps of the TCE and TCW in terms of the condition’s variables are obtained. These maps can be used as a tool to define the cost feasibility of the CSP+PV+MED plant for different worldwide locations. They illustrate the location conditions required to obtain a specific cost or the possible cost that would have the plant with certain conditions.

1.5.3 Contributions

The major contributions of this dissertation are the following. The detailed contributions are extended in each of the chapters corresponding to the published and summited journal articles:

- A physical model to simulate and evaluate a CSP+PV+MED plant is carried out. The detailed model developed allows us to accurately assess the complex thermal plant's performance, including the integration of the different systems in hourly resolution. The model integrates variables that have not been often evaluated in the literature, for instance:
    - The location of the plant and demand respect to the sea (distance and altitude).
    - The conveyance system and their respective power consumption to transport the seawater, brine, and freshwater.
    - The seawater temperature variation.
    - The part-load operation of the MED plant.
    - The startup and shutdown procedure of the MED plant.
    - The operational assumption of the PV coupling with a CSP+MED plant.
    - The operational assumption of the RO plant integration to a CSP+PV plant.
- An exhaustive thermoeconomic analysis in hourly resolution is developed, permitting to accurately assess the cost allocation of plant systems into the products: electricity and water. The methodology considers the effects of:
    - The variation of the solar irradiation and meteorological conditions.
    - The non-design operation and transient conditions of the systems (CSP, PB, MED, and RO systems).
    - The irreversibilities of the plant components.
    - The thermoeconomic analysis of the TES tanks in transient conditions.
    - The consideration of the chemical and potential exergy of the seawater, freshwater, and brine flows.
    - The cost of the system's components.

- A multi-objective optimization methodology is developed to optimize the sizing of the CSP+PV+MED plant in terms of the product costs and plant productivity (TCE, TCE, and $Suf_{e\&w}$). The optimum solutions are evaluated to define which solution could be the most suitable.
- In general, a design and optimization tool for the CSP+PV+MED plant is developed, which can be used as a case-by-case to determine these plants' feasibility in other regions with a similar scenario of water electricity demand.
- The performance and cost differences between RO and MED integration into CSP+PV under different situations are assessed. The CSP+PV+MED competitiveness in terms of costs and productivity is determined, and the possible technological and cost improvement are presented.
- The impact of the sizing parameters (PV plant size, solar multiple, Thermal Energy Storage capacity, and numbers of MED units) and the plant location conditions (DNI, distance, and altitude with respect to the sea) on the plant performance and the cost of electricity and water are determined. Cost maps of the CSP+PV+MED plant are presented as a tool to illustrate the location conditions required to obtain the best costs.

1.5.4 Perspectives of future works

Based on the analysis performed and the results presented in this dissertation, further research in the CSP+PV+D plant is suggested as future work:

- In terms of the cost feasibility of the CSP+PV+MED, the energy cost is the main contributor to the TCW, which is significantly influenced by heat cost that drives the MED plant. This evidences that is required to lowering the heating cost in order to obtain competitive TCW. Concept plants where the heat is provided by low or medium-temperature solar thermal systems (parabolic-trough, linear Fresnel, or flat collectors) and consider integrating directly from the solar field could be possible options since the temperature required by the MED plant is under 100°C. An

extended analysis of these possible concepts should be developed to determine if they can effectively reduce water costs.

- Another important factor to improve the CSP+PV+MED plants' cost feasibility is enhancing the MED plant's performance. A re-design of the MED plant-focused to increase the GOR could produce more water with the same heat and cost allocation. This could be made by increasing the number of effects, raising the top brine temperature, or decreasing the last effect temperature. Integration of nanofiltration pretreatment, absorption/adsorption system at the condenser, and thermal vapor compressor could enhance performance. Additionally, the hybridization of the MED with a RO plant could boost productivity at a low cost adding. However, these concepts should be analyzed considering the power block's impact and the plant's overall performance.
- Another point that should be analyzed is to adapt the MED design to reduce the seawater flow rate or integrate other brine disposal methods to eliminate the need to return the brine to the sea. This will impact the pipeline's specific cost and the conveyance system's overall cost for inland locations. The coupling of an Air-Cooled condenser to the MED plant could reduce the extra seawater requirement. Similarly, brine disposal processes that can extract a sub-product from the brine, like evaporation ponds and zero liquid discharge, should be evaluated. Moreover, these concepts have to be analyzed to assess their technical viability and impact on cost formation.
- The work presented herein is focused on Chilean conditions. It is proposed to extend the analysis to other locations with different conditions in the MENA (the Middle East North Africa) region, Mediterranean Europe, and Australia. These locations have different topographic characteristics, seawater temperature and salinity, and DNI levels that could change the plant performance.

1.5.5 Study limitations

This study has some limitations due to the nature of the research methods applied, the time and resource constraints:

- The study has been carried out considering the seawater salinity corresponding to Chilean locations (35 g_{salt}/kg_{water}), which is lower than other potential places in the Mediterranean and Persian Gulf (37-42 g_{salt}/kg_{water}). The seawater salinity can modify the MED and RO plant's design and yield, resulting in different performance and cost competitiveness of these technologies.
- A flat electric and water production profiles for the demand was considered. Estimate different demand profiles of electricity or water in terms of the moment of the day or the season could influence in defining the plant operation mode in a particular moment to prioritize the production of one product rather than the other. Also, the weighting between both productivities in the objective function could be affected by these factors.
- The simulation was performed using TMY with an hourly resolution. However, a higher time resolution (15-30 min) may lead to more accurate analysis since it will be considered part of the sub-hourly variability of the solar irradiation.

2. EXERGY COST AND THERMOECONOMIC ANALYSIS OF A RANKINE CYCLE + MULTI-EFFECT DISTILLATION PLANT CONSIDERING TIME VARYING CONDITIONS

2.1 Introduction

Freshwater is considered a renewable resource, but climate change has led to a growing water scarcity, which is particularly evident in arid regions (IRENA & IEA-ETSAP, 2012). This situation has encouraged a growing interest in desalination technologies increasing their global installed capacity in the last years (Mokhtari, Sepahvand, & Fasihfar, 2016; Shenvi, Isloor, & Ismail, 2015). Reverse Osmosis (RO) dominates the market accounting for almost 65% of the installed capacity, whereas the different thermal desalination technologies cover the remaining capacity (Abdelkareem, El Haj Assad, Sayed, & Soudan, 2018). In particular, the main issue of thermal desalination plants is their high-energy consumption (Al-Karaghouli & Kazmerski, 2013), therefore, research has been focused on improving their design, energy efficiency and operation (Carballo et al., 2018; Elsayed, Mesalhy, Mohammed, & Chow, 2018; Gabriel, Linke, & El-Halwagi, 2015; Shakib, Amidpour, & Aghanajafi, 2012), and evaluating the integration of thermal desalination in dual purpose or cogeneration plants to produce electricity and water (Iaquaniello, Salladini, Mari, Mabrouk, & Fath, 2014; Khoshgoftar Manesh, Ghalami, Amidpour, & Hamedi, 2013; Uche, Serra, & Valero, 2001). In cogeneration plants, the high-grade heat given by the fuel is transformed into electrical power, and the residual low-grade heat is used by the thermal desalination process to produce water. Moreover, most of the desalination plants are located in arid regions with high availability of solar radiation, which enables the possibility to drive water desalination processes and cogeneration plants using solar energy. These processes have received large attention from the scientific community during recent years since solar desalination offers a sustainable means of renewable energy utilization at low operational costs (Al-Karaghouli & Kazmerski, 2013).

Recent literature shows several studies focusing on the analysis and optimization of the integration between Concentrating Solar Power (CSP) plants and Multi-Effect Distillation (MED) systems (Blanco, Palenzuela, Alarcón-Padilla, Zaragoza, & Ibarra, 2013; Casimiro et al., 2014; Mata-Torres, Escobar, Cardemil, Simsek, & Matute, 2017; Palenzuela, Alarcón-Padilla, & Zaragoza, 2015b; Palenzuela, Zaragoza, & Alarcón-Padilla, 2015; Valenzuela et al., 2017). These studies evidence the high potential of implementation of these systems, based on their energy and techno-economic performance. In addition, these studies have shown that the integration can be even more favorable than the integration with RO, depending on the plant location, environmental conditions, among other local features. Palenzuela et al. (Palenzuela, Alarcón-Padilla, et al., 2015b; Palenzuela, Zaragoza, et al., 2015) results showed that the CSP+MED plant presents a higher energy efficiency (around 2%) than the CSP+RO when the exhaust steam leaves the turbine at high temperatures (more than 55°C) due to the use of air-cooled condenser, and also when the seawater presents high salinity (42 g_{salt}/kg_{water}), which increases the RO unit electric consumption. Nonetheless, the overall products costs of the CSP+RO plant were lower or similar. Mata-Torres et al. (Mata-Torres et al., 2017) carried out a simulation of a CSP+MED plant with fossil back-up considering a seawater pumping system to the plant's location. Results of this work showed the existence of optimum size of the MED plant that minimizes the Levelized Cost of Water (LCOW). Lastly, Valenzuela et al. (Valenzuela et al., 2017) performed a study of a CSP+MED plant integrated with a photovoltaic (PV) plant, where the CSP system works as a back-up of the PV system, obtaining two different configurations that minimize the Levelized Cost of Electricity (LCOE) and LCOW and identifying a domain of solutions that allows minimizing both costs.

In these studies, it has been observed that during the assessment of a CSP+MED plant is common for CSP and MED plants costs to be allocated into LCOE and LCOW, separately; which means that the CSP cost only affects the LCOE, while the MED cost is allocated to the LCOW. The only exception is a fraction of the CSP plant cost that is allocated to the LCOW as a function of the electricity consumption of the MED plant and the seawater pumping system. In this way, the internal interactions between the systems are not accounted for the cost distribution (such as the use of the exhaust steam of the turbines to drive the

MED plant). For instance, different methods have been studied in the literature to obtain the cost allocation in cogeneration plants. Wang and Lior (Wang & Lior, 2007) performed an evaluation of several methodologies to carry out a fuel allocation cost of a gas turbine plant coupled to a thermal vapor-compression MED (MED+TVC) plant. Results show that the exergy cost formation methodology, which is based on a comprehensive analysis of exergy destruction, allow computing the cost allocation with high detailed information. Leiva-Illanes et al. (Leiva-Illanes et al., 2018) presented a comparison between the levelized cost and the thermoeconomic methods to assess the product cost of a solar polygeneration plant, obtaining that the thermoeconomic method constitutes a more rational cost allocation method, which is recommended for a precise analysis of a multi-purpose plant.

These studies indicate that the cost allocation method based on exergy flows and cost distribution (exergy cost and thermoeconomic analysis) are suggested to evaluate in detail the formation cost within a plant with different products. In this way, these methods have been implemented by (Askari, Ameri, & Calise, 2018; Kouta, Al-Sulaiman, Atif, & Marshad, 2016; Leiva-Illanes et al., 2017; Ortega-Delgado, Garcia-Rodriguez, & Alarcón-Padilla, 2016; Wellmann, Meyer-Kahlen, & Morosuk, 2017) to assess the performance of solar power plants integrated with desalination technologies, determining the best design or operating conditions of the systems. Ortega-Delgado et al. (Ortega-Delgado, Garcia-Rodriguez, et al., 2016) carried out a comparison between thermal desalination and RO technologies integrated to a CSP plant performing a sensitivity analysis varying the costs of the solar field, the MED, the RO, the discount rate and the capacity factor. With this methodology, they obtained that the RO scheme produces water at a lower cost than thermal desalination. Leiva-Illanes et al. (Leiva-Illanes et al., 2017) performed a thermoeconomic analysis of a solar polygeneration plant, obtaining that the criterion to optimize the plant design should be to minimize the total thermoeconomic cost, and the best configuration obtained considered the MED plant replacing the condenser.

Furthermore, the above approaches use the cost allocation analysis at low disaggregation level, which simplifies the number of streams evaluated. However, this approach does not represent the cost formation of each stream of the plant in detail. The use of medium or high

disaggregation levels (i.e. performing the analysis for each component of the system) could give an in-depth analysis of the cost formation process of each stream that allows assessing a more accurate cost allocation. For example, Piacentino (Piacentino, 2015) performed a detailed thermoeconomic analysis of a MED+TVC plant, in which the seawater, freshwater, and brine exergy flows were split into their chemical and thermal fraction and the exergy efficiency was calculated at the sub-component level to acquire an in-depth understanding of the whole formation process and the destroyed exergy distribution. Results indicated a water cost variation throughout the plant, where the contributions of the last effects were higher. Also, Catrini et al. (Catrini, Cipollina, Micale, Piacentino, & Tamburini, 2017) performed a thermoeconomic analysis for a combined heat and power steam cycle integrated with a MED+TVC plant, obtaining that the water unit cost is significantly higher in comparison to the electricity cost, due to higher exergy destruction involved in the production process of the water. Moreover, it is performed a parametric analysis in function of the turbine extraction pressure and the number of MED units to understand their effect on both product costs. Leiva-Illanes et al. (Leiva-Illanes et al., 2019) carried out a exergy cost analysis of a solar polygeneration plant to analyze the exergy cost formation of the products and determine the key equipment which design could be improved, resulting that the solar collectors, the evaporator and the productive sub-systems (MED, refrigeration and process heat plant) are the key components that contribute to the products formation cost.

In summary, the cost allocation method considers the cost and the processes involved in the production of each stream of the plant, but a detailed analysis requires to perform the analysis at the component level. In that context, to the best of authors' knowledge, there is no study in the literature performing a detailed exergy cost and thermoeconomic analysis of a CSP+MED plant, considering a high disaggregation level. Moreover, the thermoeconomic analyses of cogeneration plants have been performed at nominal conditions, but, considering that a CSP+MED plant operates using solar radiation as the main energy source, its operating conditions are highly variable due to the nature of the availability of solar radiation. These variations enforce the power cycle of the CSP plant and the MED plant to operate at part-load conditions during several periods of the day, which induces additional complexity to

the exergy analysis and the fuel cost allocation. Besides, the ambient temperature also varies during the day, changing the exergy and cost allocation of the waste stream.

In this study, it is presented a detailed exergy cost formation and thermoeconomic analyses applied to a Rankine Cycle (RC) fed by solar molten salts (MS), and coupled to a MED plant (RC+MED). The aim is to assess the distribution of exergy destructions, exergetic cost formation and the thermoeconomic cost of the final products. The study considers transient conditions such as the variation of the ambient temperature and the plant part-load operation due to variations on the MS mass flow rate. Moreover, a sensitivity analysis varying the MED plant capacity and the location of the plant respect to the sea level, as well as, the analysis of an operational day of the RC+MED plant considering two power output profiles were carried out. The analyses presented herein take into account parasitic exergy losses that have not been commonly considered in the literature, for instance: the exergy and cost expenses by the pumping system from the sea to the MED plant location, and the electricity consumed by the MED plant and the RC condenser. Additionally, the model includes the possibility of using the exergy associated to the energy potential of the brine to produce useful work. Therefore, the detailed model developed allows to accurately assess the actual exergy and thermoeconomic cost of the final products of the RC+MED plant, under the different conditions and configurations.

2.2 System description

The RC+MED plant analyzed herein consist of a steam RC coupled with a MED plant in parallel with the condenser of the power cycle. The RC is fed by solar molten salts since it constitutes the typical heat transfer fluid (HTF) employed in Central Receiver CSP plants. The MED plant uses a fraction of the exhaust turbine steam to provide heat to the desalination process, and the condenser dissipates the heat of the remaining flow. Also, a seawater pumping system from the sea to the plant location, and an energy recovery system of the resultant brine that is returned to the sea (P/R System) were considered. The electric consumption of the MED plant, the seawater pumping system, and the condenser were included. In Figure 2-1 is presented a detailed scheme of the RC+MED plant.

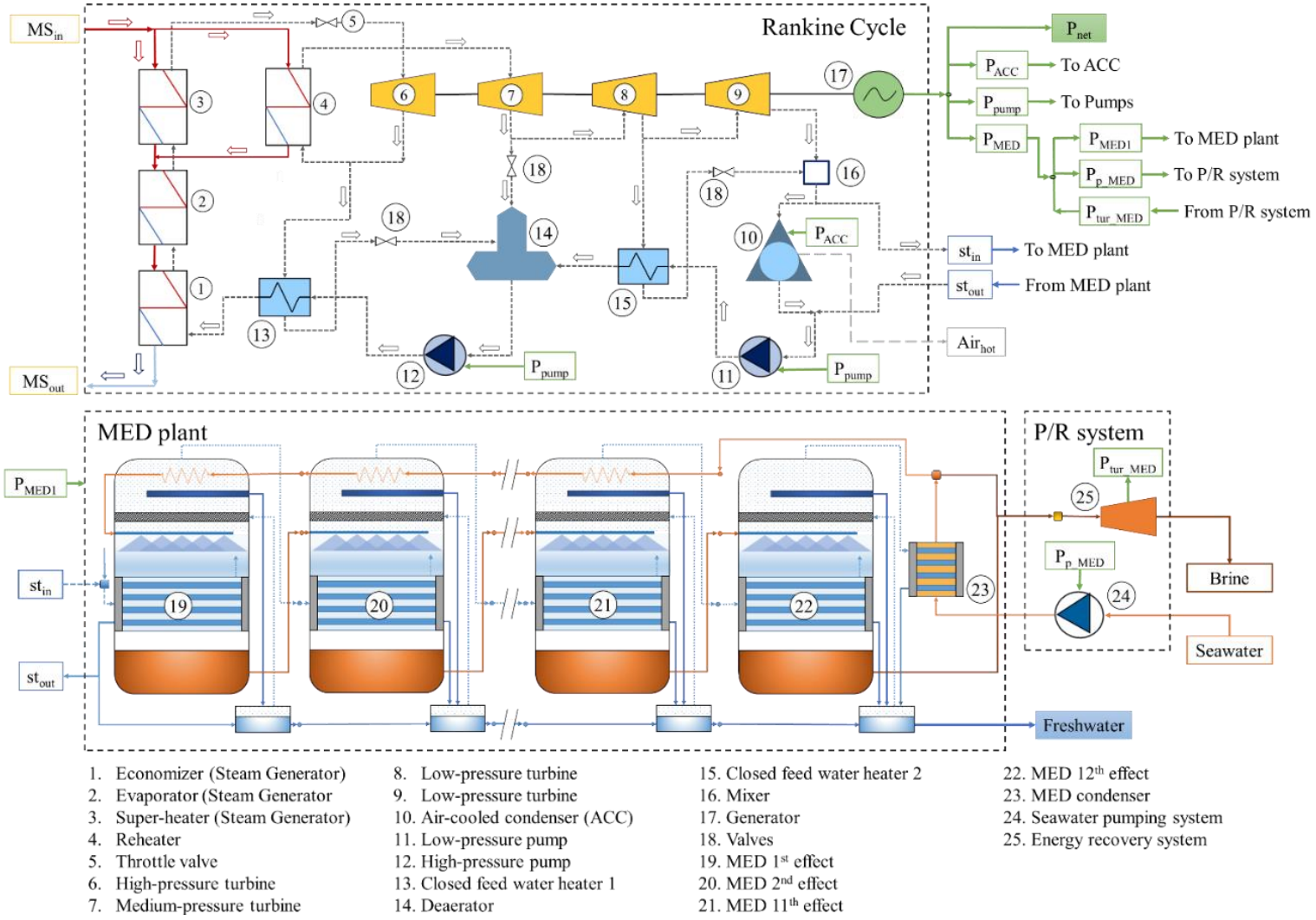

1. Economizer (Steam Generator)
2. Evaporator (Steam Generator
3. Super-heater (Steam Generator)
4. Reheater
5. Throttle valve
6. High-pressure turbine
7. Medium-pressure turbine
8. Low-pressure turbine
9. Low-pressure turbine
10. Air-cooled condenser (ACC)
11. Low-pressure pump
12. High-pressure pump
13. Closed feed water heater 1
14. Deaerator
15. Closed feed water heater 2
16. Mixer
17. Generator
18. Valves
19. MED 1st effect
20. MED 2nd effect
21. MED 11th effect
22. MED 12th effect
23. MED condenser
24. Seawater pumping system
25. Energy recovery system

Figure 2-1: The RC+MED detail plant scheme

Moreover, in Figure 2-2 shows where is located the RC+MED plant respect to the sea, considering that the P/R system is located at the coast, and the seawater and the resultant brine are transported into the pumping and discharge pipes.

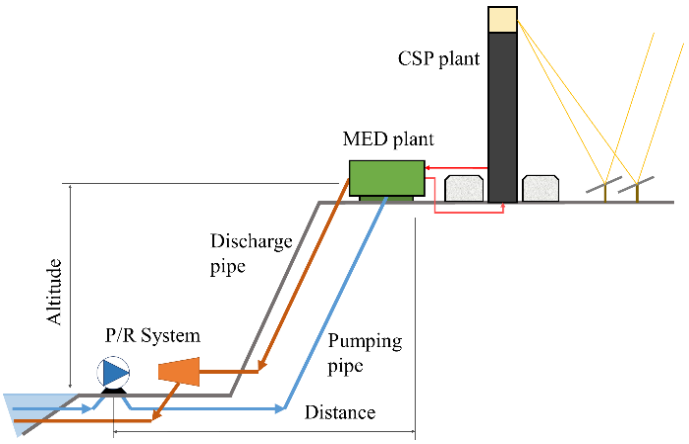

Figure 2-2: The RC+MED plant location respect to the sea

2.2.1 Rankine Cycle

The Rankine Cycle consists of a 100 MW plant powered by a molten salt (MS) mixture (60% $NaNO_3$ and 40% KNO_3) as HTF. This RC is the typical power cycle that is coupled to a CSP plant, which design temperature of the MS is usually set to 565°C. Specifically, the RC modeled herein considers re-heating, a throttling valve to control the part-load operation, three regeneration heat feeders (two closed feed-water heaters –CFWH– and an open feed-water heater or deaerator), and an Air-Cooled Condenser (ACC). For the design conditions of the stand-alone RC, the condensing pressure is defined as the saturation pressure at 25°C higher than the ambient temperature (Patnode, 2006). However, when considering the MED plant coupling in parallel to the ACC, the condensing pressure of the RC+MED plant is assumed as 31.2 kPa, in order to ensure a saturation temperature of 70°C. That temperature is required to enable the MED plant (Mata-Torres et al., 2017). Moreover, for the design conditions, it is considered a pinch point difference of 15°C and 20°C in the steam output of the superheater and the reheater respectively, and 30°C in the water stream input of the evaporator. The CFWH considered a design terminal temperature difference (TTD) of 5°C,

and the deaerator a fixed pressure of 170 kPa. Lastly, the input condensate stream of both RC pumps is defined as to have a 1°C of subcooling.

The RC model considers part-load operation using the constant pressure control, that keeps the same working pressure in the boiler and the part-load operation by using throttle valves. The part-load operation is limited to 30% of the design MS mass flow rate, which was considered to lower operation point that the steam turbines can work. The evaporators, super-heater, re-heater, and CFWH consider a design exchanger transfer conductance-area product (UA), while the effective UA is calculated by the correlation presented by Patnode (Patnode, 2006). Turbines' part-load operation was modeled with the Stodola's cone law, and the isentropic efficiency of the turbine variation was calculated according to the correlation proposed by Patnode (Patnode, 2006). Finally, at part-load operation, the MED plant is firstly powered, and the ACC is activated only when a remaining steam flow exists.

2.2.2 MED plant

The MED plant model consists of a forward-feed plant of 12 effects and 11 pre-heaters. This plant incorporates a condenser in the final effect to condensate the vapor distillate produced and heating the input seawater. The developed model is based on the models described by Palenzuela et al. (Palenzuela, Alarcón-Padilla, & Zaragoza, 2015a) and Ortega-Delgado et al. (Ortega-Delgado, García-Rodríguez, & Alarcón-Padilla, 2017; Ortega-Delgado, Palenzuela, & Alarcón Padilla, 2016). These models describe in detail the thermodynamic performance of a MED plant, considering the flash evaporation of the brine in each effect, and the flash evaporation of the distillate in the flash boxes. Also, the thermal losses as the Boiling Point Elevation (BPE) and the Non-Equilibrium Allowance (NEA) were calculated following the equation presented in (El-Dessouky & Ettouney, 2002; Ortega-Delgado, et al., 2017), and pressure losses were considered decreasing 0.2°C the temperature of the vapor distillate between the effects. The model considers that the freshwater produced is free of salt, and the resultant brine of the last effect has a maximum salinity of 72 g_{salt}/kg_{water}. Moreover, the model incorporates the assessment of the operation of the MED at part-load or non-design conditions. For this, firstly, the effects, preheaters, and condenser heat

exchanger areas were calculated for the design conditions, and then, there are fixed for the calculation of the plant operation. The overall heat transfer coefficients (U) were calculated using the correlation proposed by El-Dessouky and Ettouney (El-Dessouky & Ettouney, 2002). In addition, a de-superheater was considered before the first effect, aiming to reduce the temperature of the steam inlet to the saturation temperature. That de-superheater considers the utilization of the freshwater obtained in the last effect of the MED plant, to remove the heat. Finally, the influence of the non-condensable gases was not considered in this model, since its effect is insignificant.

2.2.3 Seawater pumping and brine energy recovery system (P/R system)

The seawater pumping system model considers a simple piping scheme and a pump, in which the seawater is pumped to the RC+MED plant location. The model calculates the piping losses and the hydraulic power required by the pump by the Darcy-Weisbach equations and energy balance. Then, the electric power requirement is calculated considering a fixed pump efficiency. On the other hand, the brine energy recovery system rescues the potential energy of the resultant waste at the MED plant. Indeed, the MED plant has two main waste streams: the brine of the last effect and the excess seawater that is used in the MED plant condenser (cooling seawater). These streams are mixed and returned to the sea through this system. The energy recovery device consists of a hydraulic turbine which produces work to reduce the total electric requirement from the pumping system. As well as the pumping system, the piping losses are calculated and the hydraulic head at the final of the pipeline is determined. Then, the work is calculated considering the turbine efficiency.

2.3 Methodology

The RC+MED plant analysis was performed by coupling two computational tools: Engineering Equation Solver (EES) software to assess the thermodynamic and exergy performance of the RC, the MED plant and the pumping and recovery system (P/R system); and MATLAB R2016b to carry out the exergetic cost and thermoeconomic analyses. This section describes the analysis performed and the computational process.

2.3.1 Energy analysis

The RC+MED plant performance was analyzed using EES in two different decks. The RC model assesses the thermodynamic states of all the streams and the components in the RC, considering mass and energy balance equations in steady-state conditions, as well as heat transfer equations for the heat exchangers. The model first calculates the thermodynamic performance at design conditions, determining the design UA. Then, the thermodynamic performance at operating conditions is estimated considering the temperature and mass flow rate of the MS, and the ambient temperature as inputs. All model's calculations are carried out considering steady-state conditions.

The MED plant model describes the thermodynamic performance of all the streams for each effect of the MED plant and the performance of the P/R system. The disaggregation level of the MED model considers for each effect: the main heat exchanger, the feed water preheater, the distillate flash box, and the condensate water mixer. The mass and energy balance and the heat transfer equations are applied for each one of these subcomponents of the effect. Further information about the mathematical model can be found in Ortega-Delgado et al. (Ortega-Delgado, García-Rodríguez, et al., 2017), which shows the equations considered in detail for each one of subcomponents. Moreover, the MED plant electric consumption is calculated in terms of the freshwater production, considering a value of 1.5 kWh_e/m^3 (Cipollina, Micale, & Rizzuti, 2009) which takes into account the use of water and vacuum pumps.

Regarding the P/R system, the head losses are calculated using the Darcy-Weisbach equation. The friction factor is calculated in terms of the length, diameter and relative roughness of the pipe, and the kinematic viscosity of the fluid. Then, the total head at the pump and at the recovery system are calculated by applying an energy balance. The electric consumption of the pump and the turbine work are calculated computing their respective efficiencies. It is worth to mention that other piping losses are not considered. In the first instance, the MED model is used to calculate design parameters in terms of the MED plant

capacity, the location's altitude and the distance from the sea. At this point, the heat exchange areas of each effect, preheaters and the condenser are calculated. Then, the performance of the MED plant is obtained, considering the steam mass flow rate and the enthalpy of the turbine exhaust steam, the ambient temperature, the seawater flow rate and its salinity as inputs.

Table 2-1 presents the design parameters considered in the modeling of the RC, MED and P/R systems. These parameters include the nominal temperature and mass flow rate of the MS, the ambient temperature, the salinity and temperature of the input seawater.

2.3.2 Exergy analysis

A preliminary exergy analysis was carried out to calculate the exergy flow of all the streams considered in the RC+MED plant. The exergy is a property which defines the maximum useful work that could be obtained from a system or stream at a specified state in comparison to a reference state. In an exergy analysis, it is useful to decompose the exergy flow into their physical and chemical exergy. The physical exergy represents the maximum amount of work that can be obtained from a system as its pressure and temperature are changed to the reference state. In contrast, the chemical exergy is related to the difference in the chemical potential of the substance that changes its chemical composition or concentration compared to the reference state (Bejan, Tsatsaronis, & Moran, 1995; Dinçer & Rosen, 2012). The exergy analysis in this work was carried out in EES, using the software library and literature reference for specific streams.

In this analysis, the physical exergy was calculated for all the RC streams (molten salts and water steam) and the MED plant streams (seawater, water, and brine). The physical exergy is denoted by ψ, and it is defined as:

$$\psi = (h - h_o) - T_o(s - s_o) + gz + \frac{V^2}{2} \quad (2.1)$$

Table 2-1. Design parameters of the RC, MED plant and P/R system

	Unit	Value
Nominal MS mass flow	kg/s	650
Nominal MS input temperature	ºC	565
Nominal MS output temperature	ºC	295
Evaporator UA	kW/K	2098.55
Super-heater UA	kW/K	1439.28
Re-heater UA	kW/K	720.38
CFWH 1 UA	kW/K	1359.50
CFWH 2 UA	kW/K	484.74
Superheated steam pressure	kPa	10000
Steam extraction pressure 1 (CFWH 1)	kPa	2200
Steam extraction pressure 2 (Deaerator)	kPa	600
Steam extraction pressure 3 (CFWH 2)	kPa	70
High-pressure turbine efficiency	-	0.90
Low-pressure turbine efficiency	-	0.86
Pump efficiency	-	0.85
Input seawater temperature	ºC	20
Cooling seawater stream temperature	°C	35
Brine temperature at last effect	ºC	40
Salinity of seawater	g/kg	32
Brine exhaust salinity	g/kg	72
Gain Output Ratio (Nominal conditions)	-	9.64
Pump and turbine efficiency (P/R system)	-	0.8

where h and s are the enthalpy and entropy of the stream at a given state, respectively; while h_o, s_o and T_o are the properties at the reference state. The other two terms are the potential and kinetic energy that consider the gravity constant (g), altitude (z) and the fluid velocity (V). For this analysis, the kinetic energy was not considered, and the potential energy was only considered for the MED plant streams, associated to the seawater, the freshwater and the brine, because they are the only streams that present a significant altitude variation. Moreover, the enthalpy and entropy of the seawater, freshwater and brine were calculated using the correlation proposed by Sharqawy et al. (Sharqawy, Lienhard V, & Zubair, 2011a). Then, the physical exergy rate ($\dot{X}_{ph}$) is given by (Dinçer & Rosen, 2012):

$$\dot{X}_{ph} = \dot{m}\psi \tag{2.2}$$

where $\dot{m}$ is the mass flow rate of the stream. In the analysis of the MED plant, it is required to calculate the chemical exergy of the streams related to the seawater, the freshwater or the brine. This exergy was considered separately from the physical exergy. For the reference state, it was established a salinity of 32 g_{salt}/kg_{water} and a seawater temperature of 20ºC. The chemical exergy of a flow stream is denoted by a_{ch}, and it is determined by (Sharqawy, Lienhard V, et al., 2011a; Sharqawy, Zubair, & Lienhard, 2011):

$$a_{ch} = \sum_{i=1}^{n} w_i(\mu_i^* - \mu_i^0) \tag{2.3}$$

where w_i is the water or salt mass fraction (dimensionless) of the seawater, the brine or the water, which is in terms of the salinity of the stream, and μ_i is the chemical potential of the water or the salts in seawater in kJ/kg that are determined by differentiating the total Gibbs energy function with respect to the composition (Sharqawy, Lienhard V, et al., 2011a). The chemical potential is calculated by different correlations proposed by Sharqawy et al. (Sharqawy, Zubair, et al., 2011). The μ_i^* is calculated with the stream salinity and the reference temperature, while the μ_i^0 is calculated with the seawater reference salinity and temperature. It is worth to mention that for the present analysis; the chemical exergy is only expressed in terms of the salinity of the stream. So, given the salinity reference, the freshwater chemical exergy (considered free of salt) can be defined as 2.35 kJ/kg. Then, the chemical exergy rate ($\dot{X}_a$) is given by:

$$\dot{X}_a = \dot{m} a_{ch} \tag{2.4}$$

When an exergy balance of a system, component or subcomponent is performed, it can be identified the lost work potential caused by the irreversibilities or exergy destructions. The irreversibilities can be explained by friction, chemical reactions, heat transfer, among other processes, which always generate entropy and destroy exergy. Thus, the exergy balance of a control volume is expressed as (Dinçer & Rosen, 2012):

$$\sum_{in} \dot{X}_{ph} - \sum_{out} \dot{X}_{ph} + \sum_{in} \dot{X}_a - \sum_{out} \dot{X}_a - \dot{X}_{dest} = \frac{d\dot{X}_{CV}}{dt} \tag{2.5}$$

where $\dot{X}_{dest}$ is the exergy destruction rate, and $\dot{X}_{CV}$ is the exergy change within the control volume. When steady-state is considered, the exergy change rate is neglected. In this way, the exergy destruction can be calculated for each component of the RC+MED plant. For the present analysis, the exergy balance was applied to all the components of the RC+MED (47 components), with each effect of the MED plant considered as a component. Additionally, the net electricity and the freshwater chemical exergy were considered as products of the plant. Indeed, the freshwater physical exergy was considered a waste of the MED plant, since to the main purpose of the plant is to produce a quantity of freshwater, which is related to the amount of chemical exergy obtained.

Finally, two definitions for the exergetic efficiency were considered to evaluate the efficiency of the plant. The first one is commonly known as the second law efficiency (η_{II_law}), which measure how efficient is the plant compared to an ideal plant, considering the input exergy to the system ($\dot{X}_{in}$) and the total exergy destruction throughout the plant, and the latter is commonly denominates exergetic efficiency (η_{ex}), which compares the exergy of the products with the exergy input (Dinçer & Rosen, 2012).

$$\eta_{II\_law} = 1 - \frac{\sum \dot{X}_{dest}}{\sum \dot{X}_{in}} \tag{2.6}$$

$$\eta_{ex} = 1 - \frac{\sum \dot{X}_{dest} + \sum \dot{X}_{waste}}{\sum \dot{X}_{in}} = \frac{\sum \dot{X}_{products}}{\sum \dot{X}_{in}} \tag{2.7}$$

2.3.3 Exergetic cost analysis

The exergetic cost analysis allows assessing the process of cost formation of the products from an exergy point of view. This analysis permits to identify how the exergy destructions and the exergy of waste flows are allocated to the final products. Through this analysis is possible to determine the amount of resources required to generate a specific product. The analysis was performed by MATLAB, using the numeric values of physical and chemical exergies obtained from the procedure implemented in EES. The analysis consists of a linear equation system given by,

$$[A] \times [C_i] = [Ex_i] \tag{2.8}$$

where the matrix [A], known as the incident matrix, summarizes the flow connections between each component of the plant, and the exergy cost (C_i) considers the consumption of exergy to produce a given flow and depends on the conditions and the processes employed to produce it. Hence, the exergy cost vector ($[C_i]$) is the one to be evaluated, and the exergetic cost vector ($[Ex_i]$) is the solution, that only takes the fuel exergy values for the respective auxiliary equation (Gómez-Hernández, González-Gómez, Briongos, & Santana, 2018; Leiva-Illanes et al., 2017). This system can be solved by using matrix algebra (Bejan et al., 1995; Dinçer & Rosen, 2012; Tsatsaronis, 1993). The equation system is represented by the exergy cost (C_i) balance equation for each component as:

$$\sum C_{in} - \sum C_{out} = 0 \tag{2.9}$$

where the inputs are the resources from other components or the environment (known as fuel), and the outputs are the products that could be considered as resources for other components or for the environment (known as final products). For each component, according to its own process, the fuel is partially transformed into products and destroyed by the irreversibilities, therefore, the cost of the irreversibilities is allocated to the products. Consequently, the exergy cost of a given stream is related to the exergy rate ($\dot{X}_i$) through the unit exergy cost (c_{ex_i}) by:

$$C_i = c_{ex\_i}\dot{X}_i \tag{2.10}$$

There are more than one input and output for some components, which implies that there would be more streams than components. In such cases, it is required to use auxiliary equations. These equations correlate or match the unit exergy cost of different streams to complete the equation system. Furthermore, the matrix is determined by the exergy analysis, which depends exclusively on the physical scheme of the plant and the thermodynamic analysis. In this study, the RC+MED plant presents 148 streams and 47 components. Thus, several auxiliary equations were considered. These equations were separated into three main groups: RC equations, MED plant equations, and P/R system equations. More details about the auxiliary equations are described in APPENDIX A1. Finally, the exergetic cost vector only considers the fuel exergy of the hot MS mass flow rate and the physical exergy of the seawater from the sea.

2.3.4 Thermoeconomic analysis

The thermoeconomic analysis combines the thermodynamics evaluation based on the exergy analysis and the economic analysis providing useful information of the cost-effective design or operation of a system that could not be achieved by conventional energy and economic analyses. The aim is to assess the monetary value of each stream of the system. Thus, the thermoeconomic cost represents the monetary value of the resources allocated in a specific stream. This methodology allows allocating the economic cost of plant components to the products based on the exergy analysis, the exergy destruction and the waste exergies. The analysis consists of a linear equation system similar to the one presented in Section 3.3:

$$\left[\dot{A}\right] \times \left[\dot{C}_\iota\right] = \left[\dot{Z}_i\right] \tag{2.11}$$

where the matrix $\left[\dot{A}\right]$ summarize the thermoeconomic cost balance and has the same structure than the incidence matrix described in the previous section, which only depends on the physical system scheme. The cost vector ($\left[\dot{C}_\iota\right]$) is the one to be determined and the thermoeconomic vector ($\left[\dot{Z}_i\right]$) includes the $\dot{Z}_i$ factor per component and the unit thermoeconomic cost of the fuels, which is determined by an economic analysis. Hence, the equation system is composed by the thermoeconomic cost ($\dot{C}_i$) balance equation for each component given by:

$$\sum \dot{C}_{in} - \sum \dot{C}_{out} + \dot{Z}_i = 0 \quad (2.12)$$

where the purchase cost rate of the component ($\dot{Z}_i$) is included. Thus, the thermoeconomic cost rate ($\dot{C}_i$) considers the cost formation process to produce a given flow, which depends on the exergy performance and the cost of the components employed. Lastly, the cost rate is related with the exergy rate through the unit thermoeconomic cost (c_{z_i}), and is defined as follows (Bejan et al., 1995; Dinçer & Rosen, 2012):

$$\dot{C}_i = c_{z\_i}\dot{X}_i \quad (2.13)$$

Furthermore, the auxiliary equations were the same applied for the exergetic cost analysis, changing only two of them: the unit thermoeconomic cost of the seawater is null, and the unit thermoeconomic cost of the hot MS was fixed.

The thermoeconomic vector was calculated performing an economic analysis, where the total cost of investment (*TCI*) for each of the components was computed considering cost correlations available in the literature (Adibhatla & Kaushik, 2017; Ameri, Ahmadi, & Hamidi, 2009; Piacentino, 2015; Xiong, Zhao, Zhang, Zheng, & Luh, 2012). The cost function details are described in APPENDIX A5. Then, the purchase cost rate of each component is obtained by the following expression in $/h:

$$\dot{Z}_i = \frac{A_f + f_{O\&M}}{O_{time,i}} TCI_i \quad (2.14)$$

where the $f_{O\&M}$ is the operation and maintenance factor that was set to 5%, $O_{time,i}$ is the annual operating time of the component in hours and the A_f is the amortization factor of the investment cost expressed as,

$$A_f = \frac{i(1+i)^n}{(1+i)^n - 1} \quad (2.15)$$

where i is the discount rate, and n is the plant technical lifetime. The selected values were 5% and 30 years (Zurita, Mata-Torres, et al., 2018). For this analysis, it was considered that all RC, MED plant and P/R system components have an availability of 80% during the year, while the ACC has an availability of 70%.

Regarding the MS unit cost, which is assumed as the fuel for the RC+MED plant, it was considered that are delivered by a CSP plant. Furthermore, it was considered an installation cost of 5$/W for the CSP plant and the TCI of 500 MM$. These values are a conservative cost of a CSP plant considering the recent literature (Lilliestam & Pitz-Paal, 2018). Thus, the purchase cost rate was obtained, and the unit thermoeconomic cost of the MS stream was calculated considering the net exergy input (the difference between the exergy input of the hot MS stream and the exergy output of the cold MS stream) at nominal conditions. The MS unit thermoeconomic cost obtained was 42.87$/MWh, and it was remained fixed for the parametric analysis. Finally, as mentioned before, the final products of this analysis are the net electricity of the plant and freshwater chemical exergy. The units of their unit thermoeconomic cost were reported in $/MWh and $/m^3.

2.3.5 Computational procedure

A computational procedure was carried out, which consist of 5 sections that allow determining the plant's exergy balance and the thermoeconomic costs. Figure 2-3 presents a flow diagram of this process, where each section is:

1. MED plant design using EES: the design configuration of the MED plant and the P/R system (HX areas of the effects, preheaters and the final condenser, diameter of the pipeline, design capacity of the pumping and recovery system) was calculated. Outputs of this section are the HX areas of the MED plant and the maximum design flow that the MED plant can take from the turbine exhaust stream.
2. RC model operation using EES: the design and operation of the RC were modeled. The exergy for each stream was evaluated according to the thermodynamic and the exergy performance. The output of this section is the steam mass flow rate, the enthalpy of the stream that feeds the MED plant, and the exergy vector of the RC cycle.
3. MED plant operation using EES: the operation of the MED plant and P/R system was calculated obtaining all the stream exergies for both systems.
4. Economic analysis: the cost rates of the different components are calculated considering several cost functions.

5. Exergetic cost and thermoeconomic analysis using MATLAB: the exergetic cost and the thermoeconomic analysis is carried out to finally determine the exergy and unit exergy and thermoeconomic costs.

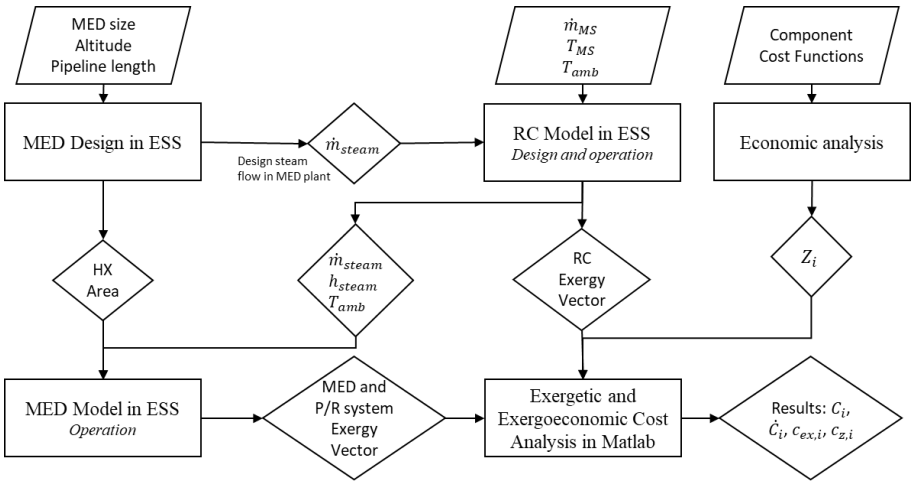

Figure 2-3: Flow diagram of the computational process.

2.4 Results and discussion

The analysis of the RC+MED plant was carried out varying the MS mass flow rate (part-load operation) and the ambient temperature to assess the exergy destruction distribution, the exergetic cost formation and the thermoeconomic cost of the final products. Also, the MED plant size and the plant's altitude and distance from the sea location was evaluated. The design conditions were defined as: a MS mass flow rate of 650 kg/s (which represent the full-load operation of the plant), a MS hot temperature of 565ºC, an ambient temperature of 25ºC, a MED plant size of 40,000 m^3/day, a location's altitude of 100 m and a distance from the sea of 20 km. The parametric analyses were performed varying one design conditions, keeping the other constant.

2.4.1 Exergy performance results

The exergy analysis was performed under design conditions, which are summarized in Table 2-2, showing the inputs and outputs considered in the exergy analysis for a standalone RC

and a RC+MED fed by MS. Results indicate that the RC+MED plant produces 13.56 MW less of electricity than the standalone RC, due to the increase of the turbine exhaust pressure, the electric consumption of the MED plant and the seawater pumping system. In fact, 33% of this reduction is caused by the MED plant and seawater pumping total consumption, and the other 67% is a result of increasing the turbine's exhaust pressure. On the other hand, the chemical exergy of the freshwater has a very low value compared to the other product flow, considering that it is used a significant amount of exergy to be produced. The operation of the MED plant presents a high exergy destruction rate, and the waste streams exergy are higher than the final product: the freshwater chemical exergy. However, this chemical exergy is equivalent to 1654.9 m^3/h freshwater production, which is a relevant production to be considered, thus, the freshwater production is associated with a high-exergy destruction process. In this way, coupling the MED plant implies an increase on the turbine's exhaust stream exergy, which results in higher exergy destruction in the dissipative components after the turbine (the MED plant and the ACC). In terms of efficiency, the RC+MED is not more efficient than a standalone RC since the η_{II_law} and η_{ex} of the RC+MED are 9.8% and 13.3% lower than the values obtained with the standalone RC, respectively. These findings are in agreement with results reported by Leiva-Illanes et al. (Leiva-Illanes et al., 2018), and Mata-Torres et al. (Mata-Torres, Zurita, Cardemil, & Escobar, 2018), in which the coupling of the MED plant decreases the exergy efficiency.

Figure 2-4 shows the exergy destruction distribution on the main components of the RC+MED plant and the wasted exergy distribution. The main exergy destruction occurs in the steam generator where the high-temperature steam is produced. However, the dissipative components combined (the MED plant and the ACC) presents the second highest exergy destruction contribution, reaching 31% of the total. Thus, the condensing pressure of the dissipative components is the main factor that affects their exergy destruction, besides the fact that the MED plant allows recovering a small part as freshwater chemical exergy. The P/R system has a small contribution to the total exergy destruction; however, its influence can be more relevant varying the location of the plant with respect to the coast. On the other hand, the MED plant waste streams accounted for 76.6% of the total wasted exergy, half of that comes from the brine thermal and chemical exergy, whereas the other half comes from

the freshwater thermal and potential exergy. Indeed, freshwater and brine output streams are obtained approximately at 40ºC, which is not useful for other production processes.

Table 2-2: Comparison between a RC and a RC+MED fed by molten salts.

	Unit	RC	RC+MED
Nominal MS mass flow	kg/s	650	650
MS exergy input	MW	155.13	155.13
Seawater exergy input	MW	-	0.33
Net electricity	MW	100.00	86.44
Water (chemical exergy)	MW	-	1.08
Destroyed exergy	MW	52.03	64.78
Wasted exergy	MW	2.41	3.17
η_{II_law}	%	66.46%	59.94%
η_{ex}	%	64.90%	56.30%

The exergy performance of the plant was evaluated considering a parametric analysis under part-load operation (varying the MS mass flow rate from 195 to 650 kg/s, which represents 30% to 100% of the capacity) and varying the ambient temperature (from 0 to 40°C). Figure 2-5 shows the total exergy destruction, the destroyed exergy distribution and efficiencies for both parametric analyses.

Under part-load operation (Figure 2-5.a), exergy efficiencies (η_{II_law} and η_{ex}) decrease not linearly as the MS mass flow rate is reduced, achieving values 15% and 20% lower than at full-load operation, respectively. This evidences that fewer exergy outputs are produced at part-load operation, and the off-design operation of the RC+MED plant increases the destroyed exergy rate, even when the total exergy destruction tends to decrease. Also, the contribution of each component to the total destroyed exergy changes as the MS mass flow rate is lower. The main change occurs on the throttle valve, which its contribution raises to 15% at the lowest MS mass flow rate. This is caused by the input pressure reduction at the high-pressure turbine that is calculated using the Stodola's relation. On the other hand, the

contribution of the MED plant and the P/R system increases until the RC operates at 70% of its capacity. At this point, the ACC is activated. Therefore, under a part-load operation between 70-100%, the ACC destroyed exergy increases while the MED plant and the P/R system destroyed exergy remains stable.

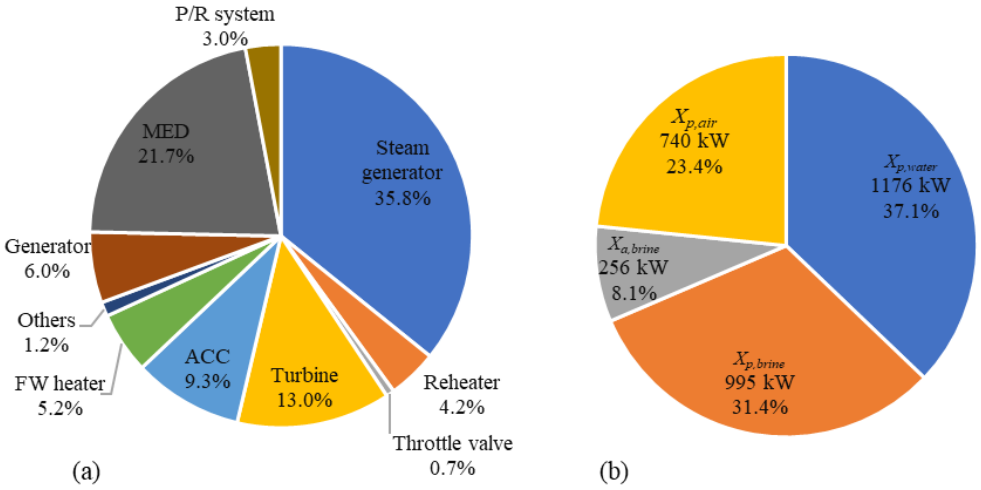

Figure 2-4: (a) Distribution of the destroyed exergy per component, and (b) Distribution of the wasted exergy for the RC+MED plant.

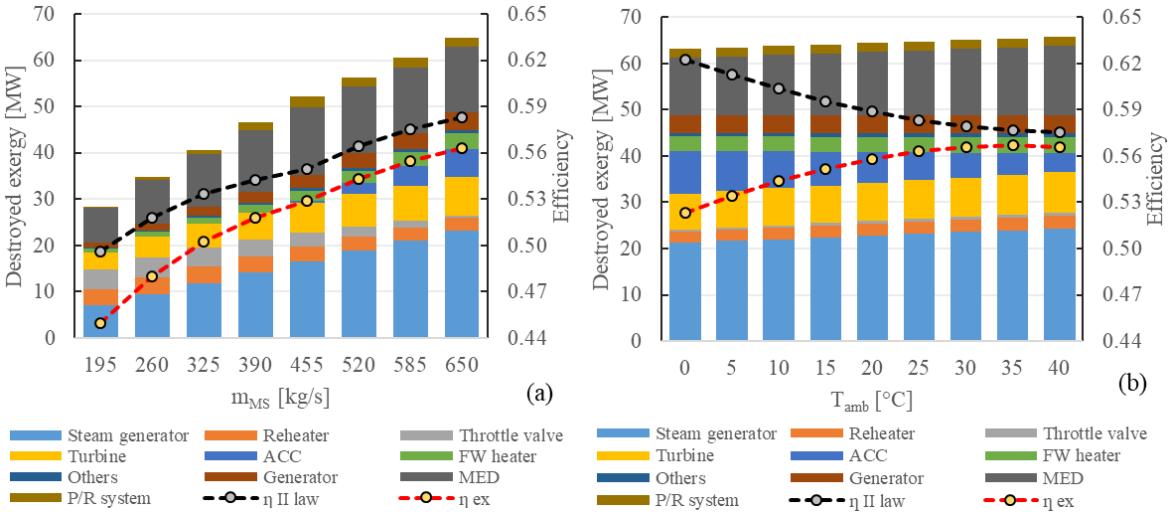

Figure 2-5: Destroyed exergy and efficiency for:(a) part-load operation and (b) ambient temperature variation.

When the ambient temperature varies (Figure 2-5.b), η_{II_law} decreases at higher temperatures, while the η_{ex} increases. This difference on the behavior presented by the efficiencies is produced as the η_{II_law} only considers the total exergy destruction of plant, while the η_{ex} also considers the wasted exergy, which decreases for higher temperatures due to the ambient temperature is closer to the temperature of waste streams. Thus, for lower ambient temperatures, the exergy waste increases considerably resulting in a decrease of the η_{ex}. Moreover, the η_{II_law} varies between 62% and 58%, while the η_{ex} varies from 52% to 57%. Also, the destroyed exergy slightly increases with the rise of the ambient temperature, but the exergy destruction contribution remains almost stable for all components. The most relevant differences are observed in the ACC and MED plant's contributions, increasing the ACC contribution as the ambient temperature is lower, while the MED plant contribution decreases. This happens because the heat transfer in the ACC, between the steam and the air, is produced with a larger temperature difference at lower ambient temperatures increasing the entropy of the process. Finally, the steam generator and the turbines have a slight increase in the destroyed exergy contribution for higher temperatures. In a previous study by the authors (Mata-Torres, Zurita, et al., 2018), it were found the same tendency in the exergy efficiency and destroyed exergy distribution of the plant, so it is evidenced that steam generators and dissipative components are the more relevant to evaluate its design and operation. Furthermore, the results presented by Kouta et al. (Kouta et al., 2016) and Elsafi (Elsafi, 2015) agree with these findings related to the relevance of the dissipative components. It is important to notice that the thermodynamic performance and the exergy products of the RC+MED plant is constant for all the temperatures (only changing the air mass flow rate at ACC), yet, the physical exergies change with the temperature variation.

2.4.2 Exergetic cost results

The exergetic cost analysis was performed considering a parametric variation on the MS mass flow rate and the ambient temperature of the RC+MED plant. The products considered in the analysis were the net electricity and the freshwater chemical exergy. Also, as a point of reference, the exergy cost analysis of a standalone RC was considered, considering the

net electricity as the only product. The exergy cost and unit exergy cost for both parametric analyses are presented in Figure 2-6.

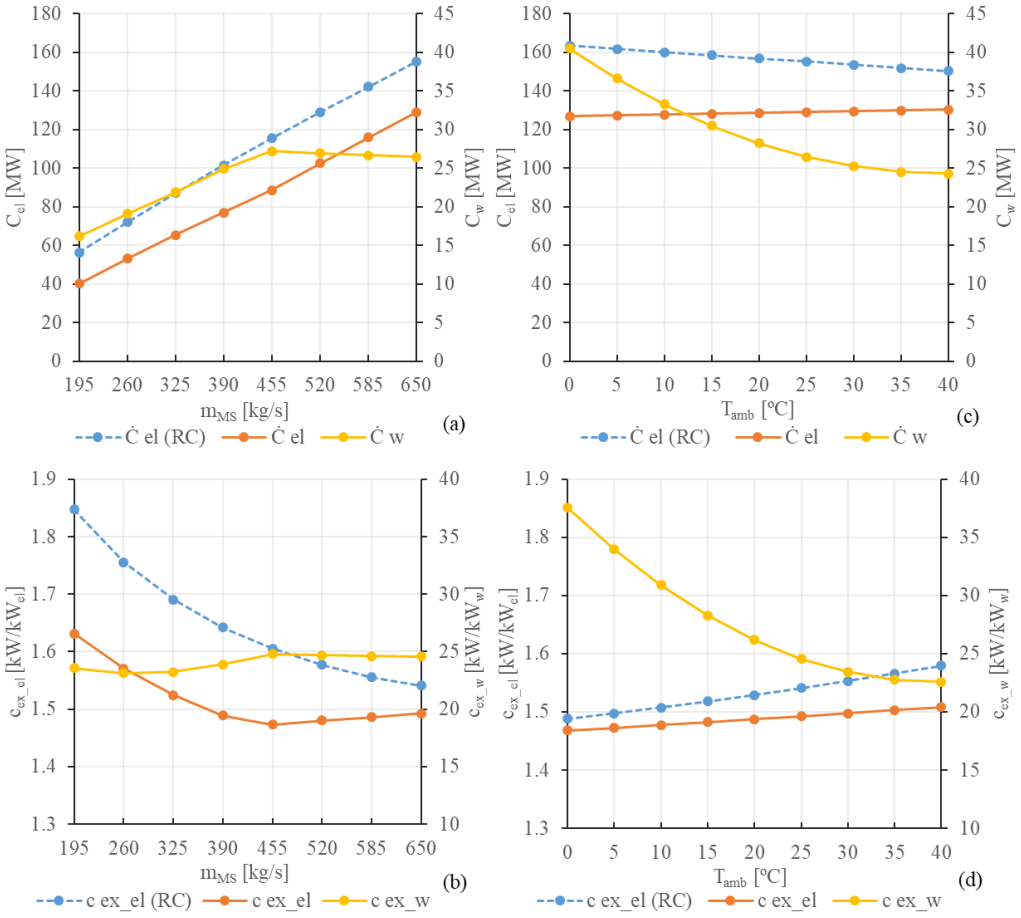

Figure 2-6: Exergy cost and unit exergy cost of the electricity and water for (a-b) part load operation and (c-d) ambient temperature variation.

Figure 2-6.a shows that the electricity exergy cost (C_{el})linearly increases as the MS mass flow rate rises, while the water exergy cost (C_w) increases until the MS mass flow rate rises to 455 kg/s and then it remains stable. In contrast, the unit exergy cost results show that the electric unit exergy cost (c_{ex_el}) gradually decreases with the rise of the MS mass flow rate, but from 455 kg/s, remains almost stable (Figure 2-6.b). The water unit exergy cost (c_{ex_w}) presents a similar behavior, however, from 195 kg/s to 455 kg/s it has a smaller variation than the c_{ex_el} decreasing its value. Moreover, the largest variation exhibited by the c_{ex_el} in

comparison to the full-load operation is about 9%, while for the c_{ex_w} is only 5%. These results expose that the destroyed exergy from the throttle valve under part-load operation is allocated in the c_{ex_el}, while the c_{ex_w} has a lower destroyed exergy allocation decreasing its unit cost formation. Thus, the part load operation has a more significant influence on c_{ex_el} than c_{ex_w}. Moreover, in Mata-Torres et al. (Mata-Torres, Zurita, et al., 2018), it was obtained that the exergy cost fraction of the water increases with a lower MS mass flow rate. This tendency is observed in Figure 2-6.a, where the variation of the C_{el} is sharper (ranging from more than 80 MW) than the C_w, which varies only 10 MW.

Regarding the ambient temperature variations, the exergetic cost analysis (Figure 2-6.c) shows that the C_{el} presents a similar numeric value for all temperatures, while the C_w presents a non-linear variation, achieving higher values as the temperature is reduced. The unit exergy cost analysis (Figure 2-6.d) shows that the c_{ex_el} slightly increases at higher temperatures, while the c_{ex_w} increases with a non-linear trend for lower temperatures. In this case, the largest variation of c_{ex_el} in comparison to the design conditions is about 3%, while for the c_{ex_w} is 67%. This high variation of the c_{ex_w} is attributed to the rise of the exergy waste at lower temperatures, which exergy costs are allocated to the water, and the c_{ex_el} slightly variation is for the increase of steam generator and turbines destroyed exergy contribution. These results indicate that the c_{ex_w} is highly dependent on the ambient temperature. Furthermore, the results are reinforced by the findings reported in (Mata-Torres, Zurita, et al., 2018), where the exergy cost fraction of the water decreases for higher temperatures, meaning the most of the exergy costs are allocated to the electricity for higher temperatures, decreasing both C_w and c_{ex_w}. However, the variation in the C_{el} is small, so the variation is of the c_{ex_el} almost insignificant. Moreover, the C_{el} and the c_{ex_el} from the RC+MED were lower than both exergy cost and unit exergy cost of electricity of the stand-alone RC, which evidences that the water production allocates a significant part of the destroyed exergy and the wasted exergy cost, decreasing the electricity cost allocation.

2.4.3 Thermoeconomic analysis

The thermoeconomic analysis was performed considering a similar parametric analysis than the previous one. Results of both thermoeconomic and unit thermoeconomic costs are presented in Figure 2-7. For this analysis, as mentioned in section 3.4, the MS unit thermoeconomic cost was calculated under design conditions, obtaining a cost of 42.87 USD/MWh$_t$. This value was fixed for the purpose of the parametric analyses.

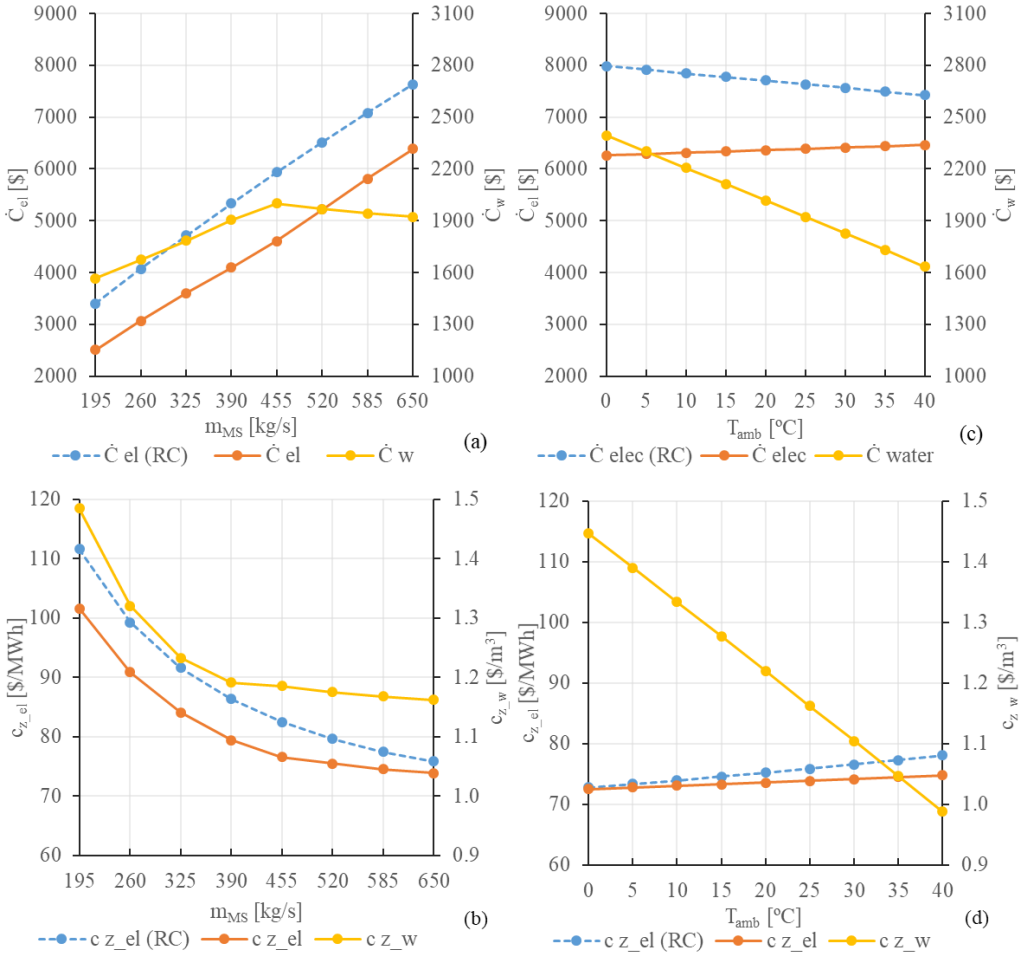

Figure 2-7: Thermoeconomic cost and unit thermoeconomic cost of the electricity and water for (a-b) part load operation and (c-d) ambient temperature variation.

Under part-load operation, the thermoeconomic costs (Figure 2-7.a) show that both electricity and water costs ($\dot{C}_{el}$ and $\dot{C}_w$) have a similar behavior than the exergy costs, where

the $\dot{C}_{el}$ is higher as the MS mass flow rate rises, and the $\dot{C}_{w}$ increases until 455 kg/s and then slightly decreases until the full-load operation. Figure 2-7.b illustrates that both: electric and water unit thermoeconomic costs (c_{z_el} and c_{z_w}) gradually decrease with the rise of the MS mass flow rate. The largest variation of the c_{z_el} with respect to the full-load operation was 38%, while the c_{z_w} shows a maximum variation of 28%. The increases in both unit cost at part-load operation are related to the products exergy decreasing while the components cost rate remains equal. However, these results evidence that the c_{z_w} is influenced by the c_{z_el}, due to the electric consumption of the MED plant and pumping system. Therefore, both unit costs are highly influenced by the part-load operation.

For the ambient temperature variation, the thermoeconomic analysis (Figure 2-7.c) shows that the $\dot{C}_{el}$ has a small variation, while the $\dot{C}_{w}$ increases at lower temperatures. The results about the unit thermoeconomic cost (Figure 2-7.d) shows that the c_{z_el} slightly increases at higher temperatures, while the c_{z_w} linearly rises at lower temperatures. Furthermore, the c_{z_el} shows a maximum variation of 3%, while for the c_{z_w} is about 46%. In this case, the products exergy and the component cost rate remain equal, so the costs variation are assigned by the destroyed and waste exergy flows. The increase of the c_{z_el} is associated with the steam generator and the turbines destroyed exergy contribution, but its effect is negligible, while the tendency observed for the c_{z_w} is similar to the c_{ex_w}, which is affected by the increase on the waste exergy from the MED plant at lower temperatures that is completely allocated to the water cost. Thus, it can be established that the c_{z_w} is dependent on the ambient temperature. Additionally, both $\dot{C}_{el}$ and c_{z_el} of the RC+MED were lower than the $\dot{C}_{el}$ and c_{z_el} presented by the standalone RC, concluding that the MED plant coupling to a RC implies that a significant part of plant costs and the destroyed and waste exergies costs are allocated to the water, not only increasing its cost but also lowering the electricity cost.

2.4.4 MED plant sizing and location altitude impact

When analyzing an RC+MED plant, there are two variables that can significantly influence the exergetic cost and the thermoeconomic analyses: the MED plant size and the plant location's altitude. The MED plant size can be between 0 (no MED plant) and its maximum

capacity, which occurs when the condenser is fully replaced. The advantages of implementing a large MED plant is the increase of freshwater production, but, the electricity consumption from the MED plant and the pumping system will also increase as well as the plant may operate more time at partial load conditions. A smaller MED plant may operate more time at nominal conditions decreasing its specific electricity consumption, but the RC will require a larger condenser. Moreover, the location's altitude can strongly influence the electric consumption of the seawater pumping system, decreasing the net electricity, but allowing to obtain freshwater at a certain altitude where it may not be available. In this section is presented the same parametric analysis of the previous section, but also varying the MED plant size and the plant location's altitude. The analysis considered an RC+MED plant with a maximum MED plant size of 60,000 m^3/day. Thus, six MED plant size was evaluated, from 10,000 m^3/day to 60,000 m^3/day. Also, four altitude levels were evaluated, considering also a different distance from the sea (100 m above the sea level and 20 km from the coast for the base case, and 200 m and 30 km, 500 m and 50 km and 1000 m and 100 km for the other cases respectively, selected from previous calculation). Moreover, it is important to consider that the piping losses due to the distance only accounts 10% of the total in all cases, thus the altitude is the main driver that affects the seawater pumping consumption.

2.4.4.1 Exergetic cost analysis results

Figure 2-8 presents the unit exergy cost of electricity and water for different MED plant sizes, at 100 m of altitude. In Figure 2-8.a and Figure 2-8.b it is presented the c_{ex_el} for different MS mass flow rates and ambient temperatures. Results show that the lowest values of c_{ex_el} at full-load operation are found for larger MED plant capacities (more than 50,000 m^3/day). Moreover, as the MS mass flow rate decreases, the c_{ex_el} of large MED pants is more sensitive to variations than smaller MED plant sizes. On the other hand, the c_{ex_el} of large MED plants slightly increases as the temperature rises, while the c_{ex_el} of smaller MED plant sizes (between 10,000 and 20,000 m^3/day) decreases at higher temperatures, yet, the effect of the temperature on the c_{ex_el} is not significant. From these results, it was obtained that larger MED plants imply the use of a smaller condenser, decreasing the destroyed exergy

in this component. Hence, the c_{ex_el} has a lower allocation of the destroyed exergy of the plant.

Figure 2-8.c and Figure 2-8.d shows the results for the c_{ex_w} considering the same parametric analysis. These results indicate that the lowest c_{ex_w} is found also for the largest MED plant (60,000 m^3/day). Moreover, for smaller sizes, the c_{ex_w} increases as the MS mass flow rate is reduced. This situation occurs due to smaller MED plant sizes require larger condensers, which present higher exergy destruction increasing the turbine's exhaust steam and the electricity cost used to operate the MED plant. Conversely, the c_{ex_w} of large MED plant sizes does not change under part-load operation. This happens because of a combination of several effects. Firstly, the part-load operation of the MED plant reduces its destroyed exergy rate and the cooling seawater flow, which also decreases the electric power required to operate the P/R system. However, the specific thermal exergy of the waste streams increases. Thus, the effect of increasing the c_{ex_el} and the specific thermal exergy of the waste streams is compensated by decreasing the electricity consumption of the MED plant and the P/R system. In contrast, for every MED plant size, the c_{ex_w} increases as the ambient temperature is lower, but the c_{ex_w} of larger MED plants is less sensitive to temperature variations than the c_{ex_w} of smaller MED plants. Moreover, the increase of the c_{ex_w} by the ambient temperature is directly related to the increase of the waste exergies allocated to the water. Therefore, results indicate that the largest MED plant sizes achieve the lowest c_{ex_el} and c_{ex_w} under all the conditions evaluated.

The unit exergy costs were also evaluated for different plant location's altitudes, considering a fixed MED plant size of 40,000 m^3/day. These results are presented in Figure 2-10. The main results indicate that the c_{ex_el} is not affected by the altitude since the RC operation remains equal for all altitudes. Conversely, Figure 2-10.a and Figure 2-10.b show that the c_{ex_w} significantly increases with the altitude. At part-load operation (Figure 2-10.a), it is observed a slightly increase of the c_{ex_w} from 650 to 455 kg/s (70-100% of part-load operation). In this point, the 40,000 m^3/day MED plant achieves its maximum capacity and the ACC starts to operate or is turn off. So, the cost increase is related to the reduction of the ACC destroyed exergy and the increase of the turbine's exhaust steam flow cost. Then, for

lower MS mass flow rate (under 455 kg/s), it is observed a significant decrease in the c_{ex_w}. As was mentioned before, the part-load operation of the MED plant decreases the seawater steam flow lowering the electric requirements of the P/R system. This effect became more relevant for higher altitudes, decreasing the c_{ex_w}. In addition, the c_{ex_w} increases due to the ambient temperature reduction at all altitudes (Figure 2-10.b), which is related to the increase in the waste exergies. Therefore, the plant location's altitude has a strong impact on the c_{ex_w}, and the operation conditions (MS mass flow rate and ambient temperature) have a significant influence at higher altitudes.

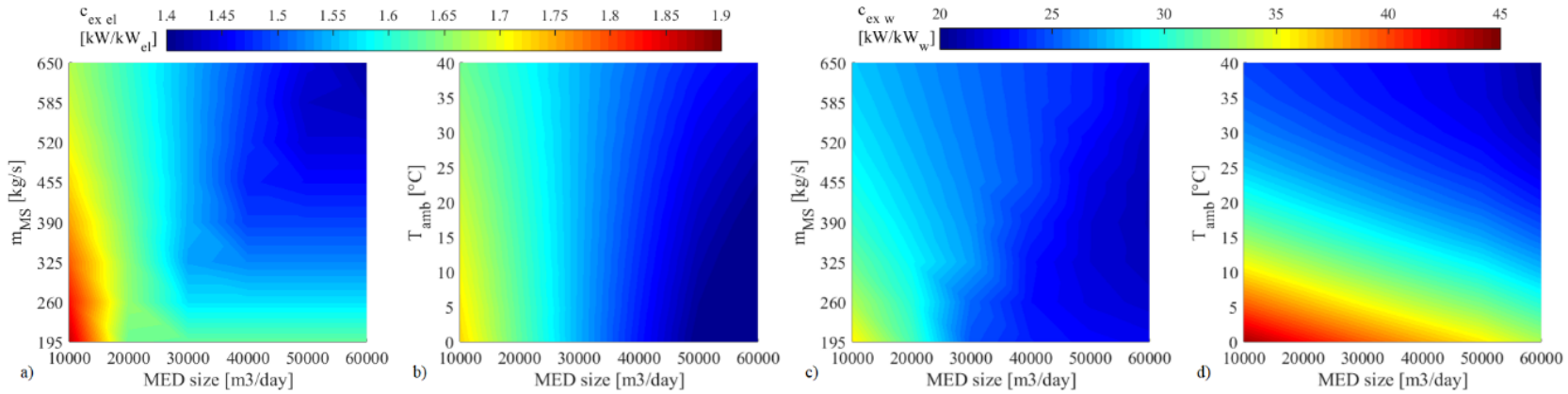

Figure 2-8: Unit exergy cost of electricity and water for different MED sizes plant at 100 m of altitude

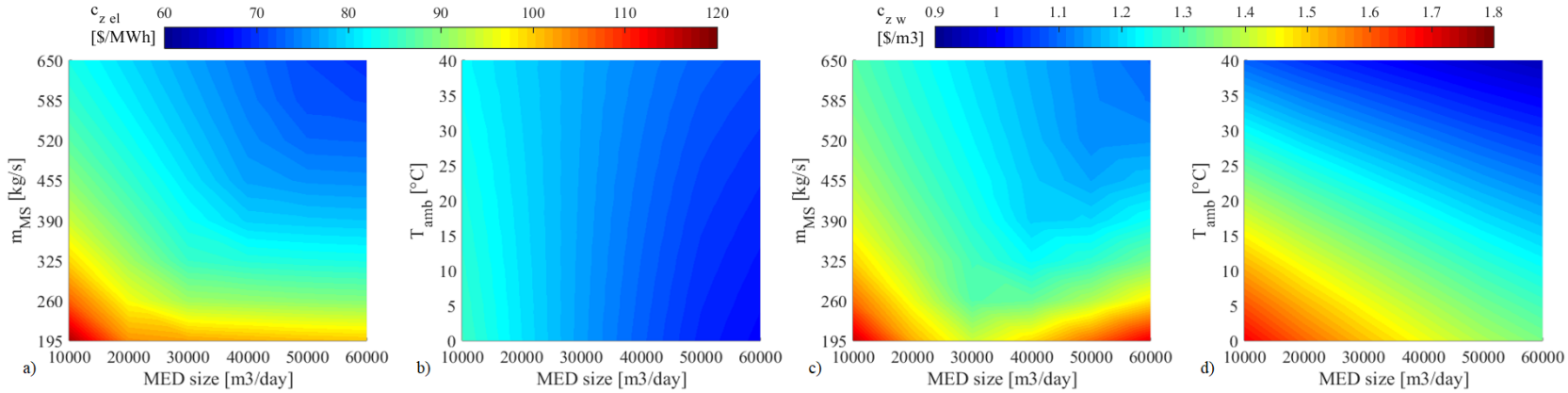

Figure 2-9: Unit thermoeconomic cost of electricity and water for different MED sizes plant at 100 m of altitude

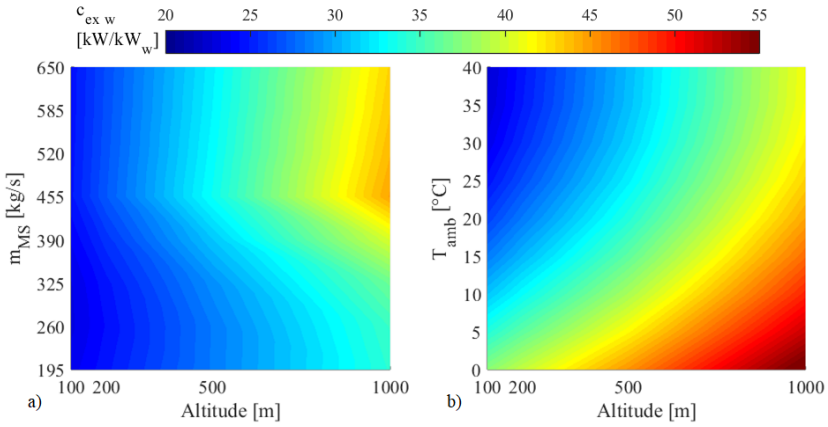

Figure 2-10: Unit exergy cost of water for different plant location's altitudes with a MED plant of 40000 m^3/day.

2.4.4.2 Thermoeconomic cost analysis results

The results of the unit thermoeconomic cost for different MED plant sizes are presented in Figure 2-9. Figure 2-9.a and Figure 2-9.b show the variation of the c_{z_el} under the same parametric analysis, where the results indicate that the lowest values of the c_{z_el} are related to the largest MED sizes (more than 40,000 m^3/day). At larger capacities, the c_{z_el} presents a similar variation at part-load operation and it is more sensitive than at smaller capacities. Hence, for large MED plant sizes, the exergy destroyed by the throttle valve is mostly allocated to the electricity affecting the c_{z_el}, while for small MED plant sizes the condenser destroys less specific exergy, which compensates the throttle valve exergy destruction. In contrast, it is observed that the c_{z_el} presents the same behavior than the one observed for the unit exergy cost when the ambient temperature varies (Figure 2-8.b), showing an almost negligible effect. Thus, the main variations on the c_{z_el} are observed in part-load operation.

Figure 2-9.c shows that the lowest c_{z_w} is found for the largest MED plant size (60,000 m^3/day) at full-load operation. However, for large MED plants, the c_{z_w} strongly increases at part-load operation, while medium MED sizes (30,000 m^3/day) present the lowest variation. This behavior is affected by several factors. For large MED plant, the freshwater production decreases at part-load operation, while the plant cost rate remains equal and the associated electricity cost of the pumping consumption increases. These two last factors have a greater

impact on the c_{z_w}, hence its value increases strongly. For medium MED plants, the part-load operation of the MED plant starts at 325-455 kg/s of MS mass flow rate, so, up to 50% part-load, the main contributors of the c_{z_w} increase are the electricity and the turbine's exhaust steam costs rise. In contrast, below 50% part-load, the c_{z_w} increase is explained mainly by the freshwater production decreasing, while the plant cost rate remains equal. However, these factors have a lower impact on the c_{z_w} in comparison to large MED plant sizes, which results in a smaller variation. Finally, for small MED plants, the freshwater production does not vary at part-load operation because the maximum MED capacity is achieved at 15-30% part-load operation. Thus, the main contributors of the increase on the c_{z_w} are the electricity and the turbine's exhaust steam costs (higher for these MED sizes), resulting in a similar behavior between the c_{z_w} and the c_{z_el}.

In contrast, the variation on the ambient temperature (Figure 10.d) shows that the c_{z_w} increases as the ambient temperature lower, for all the scales analyzed, where the most significant variations are observed at small sizes. This variation on the c_{z_w} is related to the MED plant waste exergies. Therefore, the results from this thermoeconomic analysis indicate that the largest MED plants achieve the lowest c_{z_el} and c_{z_w}, but, if the plant operates several hours at part-load, the lowest c_{z_w} would be obtained for medium MED sizes (30,000 – 40,000 m^3/day).

Lastly, the results of the unit thermoeconomic cost for different plant location's altitudes are presented in Figure 2-11. Similar to the exergetic cost analysis, it was obtained that the c_{z_el} is not affected by the altitude of the plant, since the RC operation and the gross electricity productions remain equal. Figure 2-11.a and Figure 2-11.b show that the c_{z_w} increases significantly with the altitude. Moreover, the c_{z_w} is less sensitive to variations at higher altitudes under part-load operation. It is observed an inflection point at 455 kg/s of MS mass flow rate (70% of part-load operation), denoted as the flow when the ACC is activated for a 40,000 m^3/day MED plant size. As depicted in the exergetic cost analysis, from 650 to 455 kg/s it is observed a slight increase of the c_{z_w}, due to the rise of both: the turbine's exhaust steam and the electricity cost. However, for lower MS mass flow rates (under 455 kg/s), it is observed a different behavior. From 455 to 325 kg/s (50-70% of part-load operation), the

c_{z_w} tends to decrease, and then, from 325 to 195 kg/s (30-50 of part-load operation), it sharply increases. In this region, there are three main effects that contribute to such behavior. First, the electricity consumption of the P/R system decreases due to the lowering of the seawater cooling flow rate. Second, the c_{z_el} increases up to 100 $/MWh at lowest part-load operation, which strongly impacts the c_{z_w} due to the MED plant and pumping consumption. And lastly, the cost rate of the MED plant remains equal at the part-load operation while the freshwater production decreases, increasing c_{z_w}. Hence, from 455 to 325 kg/s, the first effect is more relevant, but, for lower MS mass flow rates, the other two effects become more relevant.

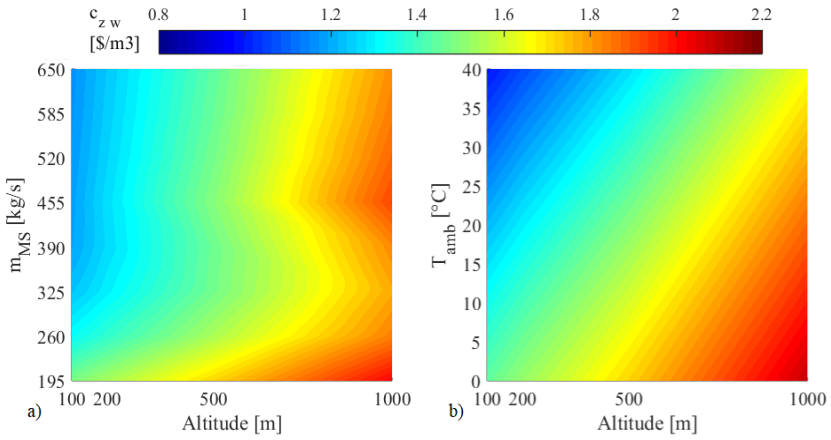

Figure 2-11: Unit thermoeconomic cost of water for different plant location's altitudes with a MED plant of 40000 m^3/day.

These results demonstrate that the plant cost rates have a major impact on the c_{z_w} than the destroyed exergy. Conversely, Figure 2-11.b also indicates that the c_{z_w} increases as the ambient temperature are lower for all the altitudes, and it is equally sensitive for the highest elevations. This increase is related to the MED plant waste exergies that increases for lower temperatures. Finally, it is established that the altitude has a strong impact on the c_{z_w}, however, several factors affect the c_{z_w} at part-load operation, which is more relevant at higher altitude.

The thermoeconomic analysis has shown that the c_{z_w} tends to be influenced by the c_{z_el}. This is due to a significant part of the c_{z_w} comes from the MS and RC components cost. Table 2-3 shows the composition of the c_{z_el} and the c_{z_w} from the MS, the RC, and the MED plant and P/R system cost, for three different MS mass flow rates, ambient temperatures, MED plant sizes, and altitudes. In this analysis, the base case is the design configuration (650 kg/s, 25ºC, 40,000 m^3/day and 100 m), changing one design variable and remaining constant the other. It is observed that the c_{z_el} is mainly composed 86% by the MS cost and 14% by the RC cost (which only changes for part-load operation), while the c_{z_w} is roughly composed 36% by the MED plant cost, 58% by the MS cost and 6% by the RC cost. This composition changes significantly at part-load operation, different ambient temperatures, and location's altitudes.

Table 2-3: Composition of the electricity and water thermoeconomic cost from the MS, RC and MED plant costs.

	Variable	c_{z_el} [$/MWh]	$c_{z\_el\_MS}$ [%]	$c_{z\_el\_RC}$ [%]	$c_{z\_el\_MED}$ [%]	c_{z_w} [$/m^3]	$c_{z\_w\_MS}$ [%]	$c_{z\_w\_RC}$ [%]	$c_{z\_w\_MED}$ [%]
m_{MS} [kg/s]	260	90.88	74.1%	25.9%	0.0%	1.32	48.4%	10.4%	41.2%
	455	76.62	82.4%	17.6%	0.0%	1.19	57.6%	7.9%	34.5%
	650	73.88	86.6%	13.4%	0.0%	1.16	58.2%	5.9%	35.8%
T_{amb} [°C]	10	73.03	86.7%	13.3%	0.0%	1.33	62.8%	6.0%	31.2%
	25	73.88	86.6%	13.4%	0.0%	1.16	58.2%	5.9%	35.8%
	40	74.78	86.5%	13.5%	0.0%	0.99	52.0%	5.8%	42.2%
MED size [m^3/day]	20000	79.89	86.3%	13.7%	0.0%	1.25	58.9%	6.5%	34.6%
	40000	73.88	86.6%	13.4%	0.0%	1.16	58.2%	5.9%	35.8%
	60000	69.70	86.9%	13.1%	0.0%	1.01	55.8%	5.2%	39.0%
Altitude [m]	100	73.88	86.6%	13.4%	0.0%	1.16	58.2%	5.9%	35.8%
	500	73.88	86.6%	13.4%	0.0%	1.44	62.1%	7.1%	30.8%
	1000	73.88	86.6%	13.4%	0.0%	1.82	65.6%	8.2%	26.2%

2.4.5 Operational day performance

To integrate all the parametric analysis performed, an analysis of one operational day of the RC+MED considering the design conditions of the plant. Two power output profiles were considered, with different operation modes of an RC+MED plant coupled to a CSP plant. The first one (Pout 1) is the typical profile observed in a CSP plant, considering the ramping up and down of the plant. The second one (Pout 2) is a profile in which the CSP plant works in parallel with a PV plant, forced to operate at part-load during the day and to store more energy in the thermal energy storage enhancing the production at non-solar hours. This profile has been used by Starke et al. (Starke, Cardemil, Escobar, & Colle, 2016), Valenzuela et al. (Valenzuela et al., 2017) and Zurita et al. (Zurita, Mata-Torres, et al., 2018), when analyzing hybrid CSP+PV plants. Figure 2-12.a shows the two profiles in function of the MS mass flow rate and ambient temperature throughout the day.

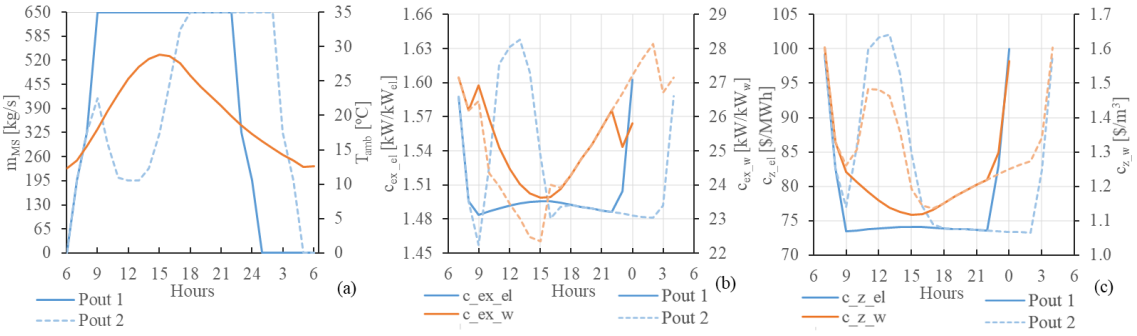

Figure 2-12: (a) Layout of one operational day with two MS mass flow rate input, (b) unit exergy cost of electricity and water, and (c) unit thermoeconomic cost of electricity and water for one day of operation.

Figure 2-12.b and Figure 2-12.c show the results for unit exergy cost and unit thermoeconomic cost for both output profiles, respectively. In Figure 2-12.b, the c_{ex_el} presented by the Pout 1 profile remains constant during the day with a small variation, while the c_{ex_w} presents an important variation during the day, because of the temperature variation. Moreover, the c_{ex_el} developed by the Pout 2 profile presents a large increase due to the part-load operation, while the c_{ex_w} has a relevant decrease during the part-load operation.

Moreover, in Mata-Torres et al. (Mata-Torres, Zurita, et al., 2018) it is shown a similar result, were the c_{ex_w} has an important variation, however, the main driver that changes its cost is the ambient temperature. In Figure 2-12.c, the c_{z_el} remains stable throughout the day for the Pout 1 profile, while c_{z_w} has a moderate variation due to temperature variations. Besides that, the c_{z_el} observed for the Pout 2 presents a large increase of more than 25 $/MWh, while the c_{z_w} presents a significant increase at part-load operation. These results reinforce the analysis carried out in the previous section, showing that, in the exergetic cost analysis, the c_{ex_el} depends mainly on the part-load operation, while the c_{ex_w} highly depends on the ambient temperature. In contrast, in the thermoeconomic analysis, the c_{z_el} and the c_{z_w} are strongly influenced by the part-load operation, while the c_{z_w} depends moderately on the temperature.

Furthermore, the MED plant size and the altitude can impact on the performance cost during the day. Figure 2-13 shows the unit exergy cost results for one operational day considering three MED plants sizes and altitudes. In Figure 2-13.a and Figure 2-13.c is shown that the c_{ex_el} decreases as the MED plant size are larger, yet, it does not change with the altitude variation. For the Pout 2 profile, the large MED plant sizes present a higher increase on the c_{ex_el} at part-load operation, compared to small MED plants. In Figure 2-13.b and Figure 2-13.d it is shown that the Pout 1 profile has a variation on c_{ex_w} at the different MED plant sizes and altitudes during the day, which is related to the temperature variation. However, for the Pout 2 profile, different effects in c_{ex_w} are observed at part-load operation, on which it can be highlighted that the 40,000 m^3/day MED plant size and the higher altitudes cases present the largest decrease. In this case, it is noted that the c_{ex_el} is mainly influenced by the part-load operation, and the impact is higher for large MED plants, while the ambient temperature has a moderate influence on the c_{ex_w}. Yet, the impact of part-load operation becomes more relevant than the ambient temperature for small MED plants and higher altitudes.

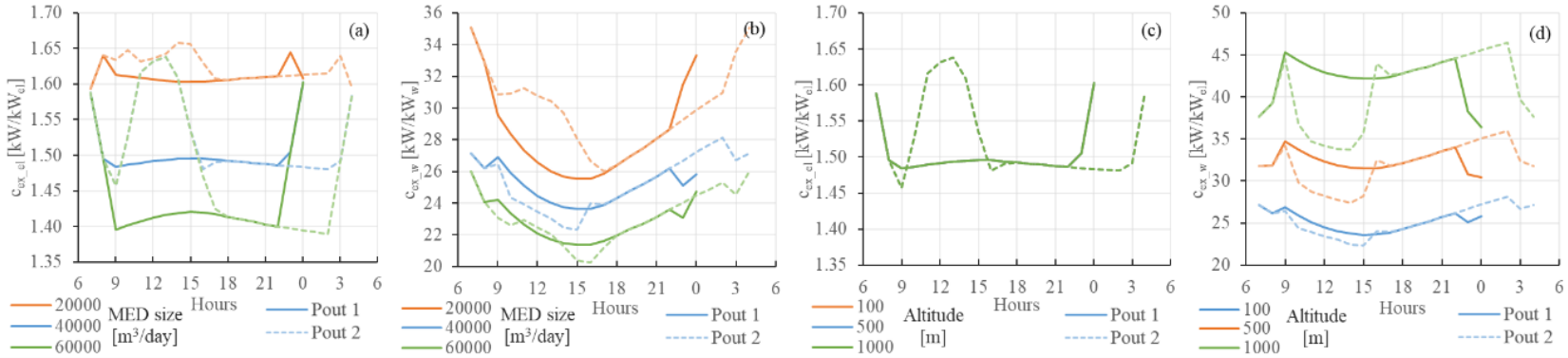

Figure 2-13: Unit exergy cost of electricity (a, c) and water (b, d) for one operational day varying the MED plant size and the plant location's altitude.

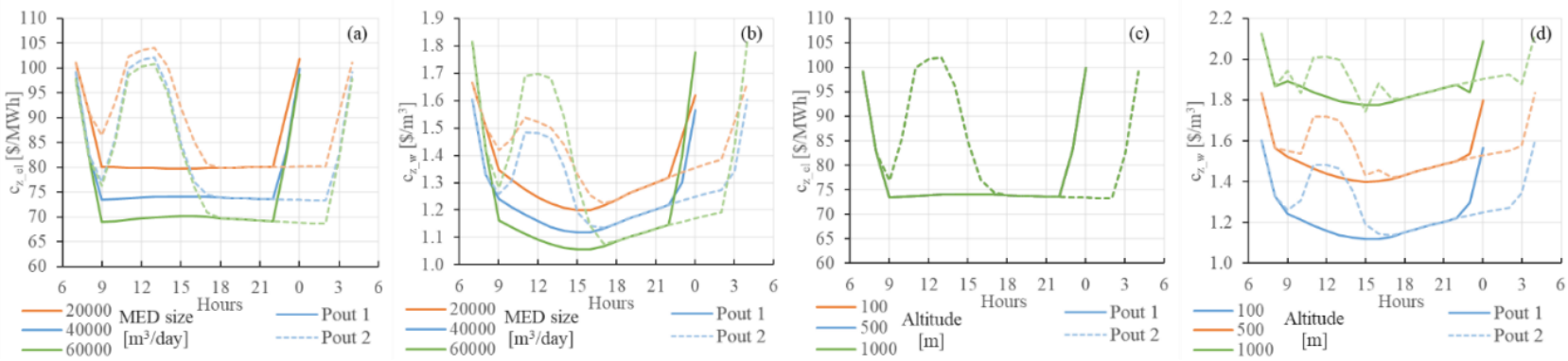

Figure 2-14: Unit thermoeconomic cost of electricity (a, c) and water (b, d) for one operational day for different MED plant sizes and height of the plant.

Figure 2-14 shows the unit thermoeconomic cost results for one operational day considering three MED plants sizes and altitudes. In Figure 2-14.a and Figure 2-14.c, the c_{z_el} decreases as the MED plant size is larger, but it does not change with the altitude variation. Moreover, for the Pout 2 profile, the largest MED plant sizes present the largest increase in the c_{z_el} at part-load operation. In Figure 2-14.b and Figure 2-14.d, the c_{z_w} also decreases for large MED plant sizes and it increases at higher altitudes, but, the c_{z_w} in all cases has a moderate variation due to the ambient temperature. For the Pout 2 profile, the largest MED plant size presents the largest increase of the c_{z_w} at part-load operation, while at higher altitudes it is less sensitive. Thus, the c_{z_el} is strongly influenced by the part-load operation, while the c_{z_w} is mainly affected by the part-load operation, having a higher impact for larger MED plants and at lower altitudes. The ambient temperature has a minor impact being less sensitive at higher altitudes.

The exergetic cost and thermoeconomic analysis results have shown that the part-load operation during the day implies a variation on the unit cost. The daily production, the daily unit exergy cost (c^*_{ex}), daily thermoeconomic cost (c^*_z) of electricity and water of each one of the cases were calculated and summarized in Table 2-4. Such results show that the net electricity production for the Pout 2 profile decreases compared to the operation mode described by the Pout 1 profile, while the water production increases. However, the c^*_{ex} and c^*_z observed under the Pout 1 operation mode are lower than the cost for the Pout 2 profile, in almost all the cases reported. The only exception was for the altitude of 500 m and 1000 m, where $c^*_{ex\_w}$ for the Pout 2 profile is lower than the cost observed for Pout 1 profile. It can be concluded that the operation at part-load of the RC+MED plant for some hours during the day may provide more water production but at a moderate higher unit exergy and thermoeconomic cost. Also, results illustrate that the largest MED plant size achieves the lowest c^*_{ex} and c^*_z, which indicate that it constitutes the best configuration. Finally, it is shown throughout all the analyses, that the effect of the altitude is allocated to the water, but for a higher altitude, the differences between $c^*_{z\_w}$ for the Pout 1 and the Pout 2 profile are smaller; thus, it is less sensitive to part-load operation from the thermoeconomic point of view.

Table 2-4: Daily production, daily unit exergy and thermoeconomic cost of the electricity and water.

			Electricity [MWh]	Water [m^3]	$c^*_{ex\_el}$ [kW/kW_{el}]	$c^*_{ex\_w}$ [kW/kW_w]	$c^*_{z\_el}$ [$/MWh]	$c^*_{z\_w}$ [$/$m^3$]
MED size [m^3/day]	Pout1	20,000	1357	15069	1.61	28.43	81.34	1.33
		40,000	1342	28159	1.50	25.03	75.33	1.21
		60,000	1335	38486	1.42	22.67	71.46	1.17
	Pout2	20,000	1300	18707	1.62	30.02	84.56	1.41
		40,000	1291	32057	1.50	25.41	78.35	1.28
		60,000	1288	40272	1.45	23.14	75.15	1.28
Altitude [m]	Pout1	100	1342	28159	1.50	25.03	75.33	1.21
		500	1252	28159	1.50	32.42	75.31	1.49
		1000	1130	28159	1.50	42.36	75.28	1.85
	Pout2	100	1291	32057	1.50	25.41	78.35	1.28
		500	1196	32057	1.50	32.27	78.30	1.55
		1000	1070	32057	1.50	41.40	78.25	1.89

2.5 Conclusions

A Rankine Cycle coupled to a Multi-Effect Distillation (RC+MED) plant was studied to analyze the exergy cost formation, the exergy destruction and the thermoeconomic cost of the final products: electricity and freshwater. For this purpose, a detailed RC+MED model was performed, considering a high-disaggregation level, in which the solar molten salts drive the RC. The analysis was performed varying the molten salts mass flow rate, allowing to assess the performance in part-load operation, the ambient temperature, the MED plant size, and the location plant's altitude. Finally, a detailed analysis of an operational day for the RC+MED considering two power output profiles (where one was the typical profile observed in a CSP plant, and the other was a profile in which the CSP plant works in parallel with a PV plant) was carried out. Those analyses allowed to identify the impact of these operational conditions on the exergy performance, as well as the exergy and thermoeconomic costs of the final products.

Results for the exergy performance show that coupling the MED plant to the RC increases the exergy destruction on the dissipative components of the plant (the MED and the ACC), and it reduces the exergetic efficiency of the system. Additionally, it was found that the MED plant is the second component with the highest contribution to the exergy destruction of the plant, reaching 21.7% of the total; while the chemical exergy of the freshwater has a small value compared to other outputs. The parametric analyses indicate that the throttle valve increases its destroyed exergy contribution under the plant part-load operation, and the wasted exergy rises as the ambient temperature is lower.

The exergetic cost analysis showed that the part-load operation has a more significant influence in the exergy cost of electricity than on the cost of water, while the latter is highly dependent on the ambient temperature since it increases its value at lower temperatures. This behavior evidences that the exergy destroyed by the throttle valve is mainly allocated to the electricity, while the increase in exergy waste is allocated to the freshwater produced. In contrast, the results from the thermoeconomic analysis evidenced that both unit costs are highly influenced by the part-load operation, while the effect of the ambient temperature on

the unit thermoeconomic cost of electricity is almost negligible but is moderately significant on the cost of water. This reflects that the electric consumption by the MED and the P/R system becomes more relevant in the cost formation process of the cost of water.

Regarding the parametric analysis of the MED plant size and the plant location's altitude, the exergetic cost analysis showed that the largest MED plant sizes (above 50,000 m^3/day) achieve the lowest unit exergy cost of electricity and water under all the conditions evaluated. Moreover, results indicate that the variation of the plant location's altitude has a strong impact on unit exergy cost of water increasing its value with the altitude, in which the operational conditions (molten salts mass flow rate and ambient temperature) have a more significant influence at higher altitudes. The thermoeconomic cost results showed that the largest MED plant sizes achieved the lowest unit thermoeconomic cost of electricity and water. However, the lowest water cost could be obtained for medium MED plant sizes (30,000 – 40,000 m^3/day) if the plant operates several hours at part-load conditions. In addition, it was found that the altitude has a strong impact on the unit thermoeconomic cost of water, increasing its value for higher location due to the pumping energy requirements. Lastly, it was determined that the unit thermoeconomic cost of electricity is mainly composed by the molten salts cost (86%) and by the RC cost (14%), while the unit thermoeconomic cost of water is roughly composed by the molten salts cost (58%), by the RC cost (6%) and by the MED plant and P/R system cost (36%).

The analysis of the operational day of the RC+MED indicates that unit exergy cost of electricity mainly depends on the part-load operation, being more sensitive to increase with large MED plant sizes; while the unit exergy cost of water is moderately influenced by the ambient temperature. In contrast, the unit thermoeconomic results showed that both, electricity and water costs, are strongly influenced by the part-load operation, in which the unit electricity cost present higher effect for large MED plant sizes and lower altitudes, while the unit water cost is moderate dependent on the temperature, being less sensitive at higher altitudes. Lastly, the analysis showed that the part-load operation of the RC+MED plant during the day may provide more water production, but at moderate higher exergy and thermoeconomic cost.

The result of this work demonstrated that the exergetic cost analysis considers the allocation of the destroyed and waste exergy on the products, in which the results show that the part-load operation is the most relevant factor and the temperature has an important impact only in the water cost. Whereas, in the thermoeconomic cost analysis, the cost of the components has a higher impact than the destroyed and waste exergy effects, obtaining that the part-load operation is the main factor that affects both costs, and the ambient temperature has a slight effect only in the water cost. Hence, the operation of these plants should be conceived as full-load most of the time. Moreover, larger MED plants configuration (between the 80-100% of the maximum capacity) present the lowest exergy and thermoeconomic costs of electric and water. However, these configurations could present a technical challenge at part-load operation because the MED plant has to ensure the cooling requirements by the RC. In contrast, the location altitude does not impact the electricity cost, but it has a high influence in the water cost, so locations near of the cost (low altitude) could achieve lower water costs. Nevertheless, these locations may present lower direct normal irradiation resource that would decrease the energy available for the power cycle in a CSP plant. Therefore, in further works, it is recommended to include CSP components and the solar resource variability of the location in the analyses, which would allow to assess the cost formation of the products from the sun exergy and to evaluate other solar technologies integration such as the hybridization into a CSP+PV concept.

3. ANNUAL THERMOECONOMIC ANALYSIS OF A CONCENTRATED SOLAR POWER + PHOTOVOLTAIC + MULTI-EFFECT DISTILLATION PLANT IN NORTHERN CHILE

3.1 Introduction

A growing interest in desalination technologies has been evidenced in the last years in response to a rising demand and water shortage worldwide, which has led to an increase of the global installed capacity of this type of technologies (Ahmed, Hashaikeh, & Hilal, 2019; Shenvi et al., 2015). Within the desalination market, Reverse Osmosis (RO) is the dominating technology with more than 67% of worldwide installed capacity, followed by thermal desalination (Ahmed et al., 2019; Mayor, 2019; Shahzad, Burhan, Ang, & Choon Ng, 2017). The growing freshwater demand has also led to an increase in the energy demand and consumption rate of fossil fuels since desalination systems are processes with high energy intensity that are associated with conventional thermoelectric power plants. Therefore, future development of desalination plants using sustainable energy sources is being considered as an opportunity, where renewables energies represent one of the most relevant solutions (Al-Karaghouli & Kazmerski, 2013).

Northern Chile has become a case study because it is one of the aridest regions worldwide, and it also constitutes the area where the most relevant mining facilities of the country are located. Water supply in this region is mainly obtained from aquafers that have been overexploited over the last years, leading mining industries to start looking for new sources of freshwater, such as desalination plants (Sola et al., 2019). In this way, water for mining coming from desalination has been progressively increasing in the course of the last years, and it is expected to be triplicated by 2029 (Comision Chilena del Cobre, 2018, 2019a). Besides this, most of the demand spots are located inland between 1000 and 4000 meters above the sea level, which makes the water conveyance (pipeline cost and pumping) an essential aspect of these systems (Herrera-León, Lucay, Cisternas, & Kraslawski, 2019).

Water cost in Chile ranges from 1.4 to 5.5 $/m^3$, where water conveyance represents approximately 40-90% of the total cost (Concha, Castro, & Vergara, 2016). On the other hand, northern Chile is endowed with one of the highest levels of solar irradiation in the world due to a combination of meteorological and geographical conditions, reaching Direct Normal Irradiation (DNI) levels up to 3500 kWh/m^2-yr (Escobar et al., 2015; Zurita, Castillejo-Cuberos, et al., 2018). Thus, the integration of Concentrating Solar Power and Desalination (CSP+D) systems have been proposed as case studies in this region due to its possible potential.

The Concentrating Solar Power (CSP) plants constitute a natural partner for thermal desalination (Mayor, 2019), with the potential of reducing environmental impact and solving the freshwater supply issue in remote areas, however, the integration of CSP+D plants has not been demonstrated in a commercial project yet (Alhaj & Al-Ghamdi, 2019). Among the vast literature on this topic, Mohammadi et al. (Mohammadi et al., 2019) presented a detailed and extensive review of the state-of-the-art of CSP+D systems focused on only freshwater and cogenerating plants (electricity and freshwater), in which the potential of these systems is described, highlighting the integration with Multi-Effect Distillation (MED) systems. However, it is also recognized that the main commercial barriers for these systems are the solar field cost, the integration strategy, and the conservative behavior of the desalination market (Alhaj & Al-Ghamdi, 2019; Shahzad et al., 2017).

Regarding CSP+MED systems, several studies have been conducted assessing their performance (Moser, Trieb, & Fichter, 2013; Ortega-Delgado, Garcia-Rodriguez, et al., 2016; Palenzuela, Alarcón-Padilla, et al., 2015b; Palenzuela, Zaragoza, et al., 2015), and the results have shown that CSP+MED could be competitive against RO under specific conditions of the location. In this context, Sharan et al. (Sharan, Neises, Mctigue, & Turchi, 2019) analyzed a CSP+MED concept in which a supercritical CO_2 power cycle was integrated to a MED plant and the evaluation was conducted in six coastal locations, obtaining competitive and even lower water costs than a RO plant. Additionally, some authors have performed analyses considering the effect of the distance from the sea and the altitude of the location (Hoffmann & Dall, 2018; Mata-Torres et al., 2017), demonstrating

that the seawater pumping system represents a significant contribution to the water cost. Therefore, the study of such systems should consider the impact of geographical conditions such as DNI levels, location's altitude and distance from the coast, as well as the water salinity.

Another concept that has been studied is the hybridization of a CSP with a Photovoltaic (PV) plant, which combines the benefit of the low cost of a PV plant, with the flexible dispatchability of a CSP plant to increase its capacity factor. Thus, several optimal configurations that allow integrating the production of both plants have been identified by different authors (Starke, Cardemil, Escobar, & Colle, 2018; Zurita, Mata-Torres, et al., 2018). However, the hybridization of a CSP+MED plant with a PV system presents different outcomes. According to Valenzuela et al. (Valenzuela et al., 2017), the hybridization allows reducing the electricity and the water costs but enforces the CSP+MED plant to operate at part-load several hours throughout the year.

These studies have mainly performed economic analyses based on energy, known as levelized cost methodology, which allows determining the cost of the products of a system. Nonetheless, the thermoeconomic method is a more accurate option to analyze complex cogeneration plants that would enable obtaining an appropriate assessment of the cost of the products, i.e. electricity and water, as it integrates an exergy analysis with an economic analysis (Kouta et al., 2016; Leiva-Illanes et al., 2018). In the literature, several authors have evaluated the thermoeconomic cost of a combined power and heat (CPH) plant or CSP plant integrated with MED plant for electricity and water production (Catrini et al., 2017; Leiva-Illanes et al., 2017; Wellmann et al., 2017), identifying that the best design recommendation is to use lower steam extraction pressure and replacing the condenser by a MED plant. However, it is also essential to reduce the investment cost of the system for achieving economic viability.

These thermoeconomic analyses are focused on the plant's design and configuration, but the integration of a PV plant to a CSP+MED implies that the plant would operate at different off-design conditions, and the variability of the solar irradiation must be considered. In

addition to that, the location of the plant with respect to the sea level, as well as of the pumping system costs, must be assessed because they can drastically change the yield and the cost of the products. In a previous study developed by the authors (Mata-Torres, Zurita, Cardemil, & Escobar, 2019a), a thermoeconomic analysis of a Rankine Cycle integrated to a MED plant was performed, evaluating the impact of the part-load operation, ambient temperature, MED plant size, and location's altitude on its performance. The results showed that the component costs have a higher impact on the product costs than the destroyed and waste exergy, pointing out that the part-load operation significantly impacts both costs. Larger MED plants achieved the lowest cost of electricity and water, while the locations' altitude increased the cost of the water significantly. This analysis exposes the impact of operational conditions on the performance of the plant, but it is required to include the CSP components operation and cost, and the solar irradiation variability, to properly assess their impact on the product costs formation. Lastly, Mata-Torres et al. (Mata-Torres, Zurita, Cardemil, & Escobar, 2019b) performed an analysis of a CSP+PV+MED plant evidencing that PV integration mainly increases the electricity output and moderately increases the water production while the thermoeconomic costs of the products decrease, especially the electricity cost. However, this analysis considers only one scenario in which the cost of the P/R system was not considered. Thus, there is a lack of information on assessing the actual impact of the integration of the PV plant to a CSP+MED, and how these systems can work in a cogeneration scheme, as well as determining the size of the system that deliver the lower costs.

This study presents the annual performance and thermoeconomic analysis of a CSP+PV+MED plant located in northern Chile. The goal is to assess the benefits and drawbacks of the integration of a PV plant into the CSP+MED plant. For this purpose, the performance and the process of cost formation on this system integration have been analyzed. The analysis has been carried out by applying an extensive methodology based on an hourly simulation of the plant and an hourly thermoeconomic analysis that allows calculating the daily, monthly, and annual costs. The cost allocation of the systems to the products (electricity and water) has also been assessed considering the hourly variation of the irradiation data and their effect on the operation of the plant. A unidimensional analysis

in terms of the design parameters of the plant (size of the PV plant, solar multiple, Thermal Energy Storage capacity, and the number of MED units) has been carried out in order to analyze the impact of these parameters on the plant performance and products costs. Finally, a multivariable parametric analysis varying the design parameters of the plant was carried out to find the configuration that allows obtaining the lowest costs of electricity and water. Therefore, the detailed thermoeconomic analysis presented herein allows assessing the actual production costs of a CSP+PV+MED plant considering the annual operation for a specific location and exposes the impact of the design parameters on the operation costs of the plant.

3.2 System description

The system consists of a MED unit integrated to a CSP+PV plant, in a schemed called as CSP+PV+MED plant. Figure 3-1 shows the layout of the plant with further details of the components, systems, and subsystems considered. As observed in the figure, the MED unit is coupled with the power block of the CSP plant in parallel to the condenser. Also, a seawater pumping system to feed the MED plant, and a system that recovers the potential energy of the resultant brine disposal returned to the sea (P/R system) is considered. The plant operates delivering a net power output of 100 MW_e to the grid. In order to fulfill this objective, the PV plant has been established as the priority to deliver the electric power to the grid, and the CSP plant works as a backup (Starke et al., 2016; Valenzuela et al., 2017; Zurita, Mata-Torres, et al., 2018). This operation strategy would allow storing thermal energy in the Thermal Energy Storage (TES) system to be used in periods of low irradiation that, in turn, would increase the net output power of the whole plant. Notice that the parasitic consumption of the plant (from the solar tower, the power block, the MED plant, and the seawater pumping system) is also included in the electric power balance.

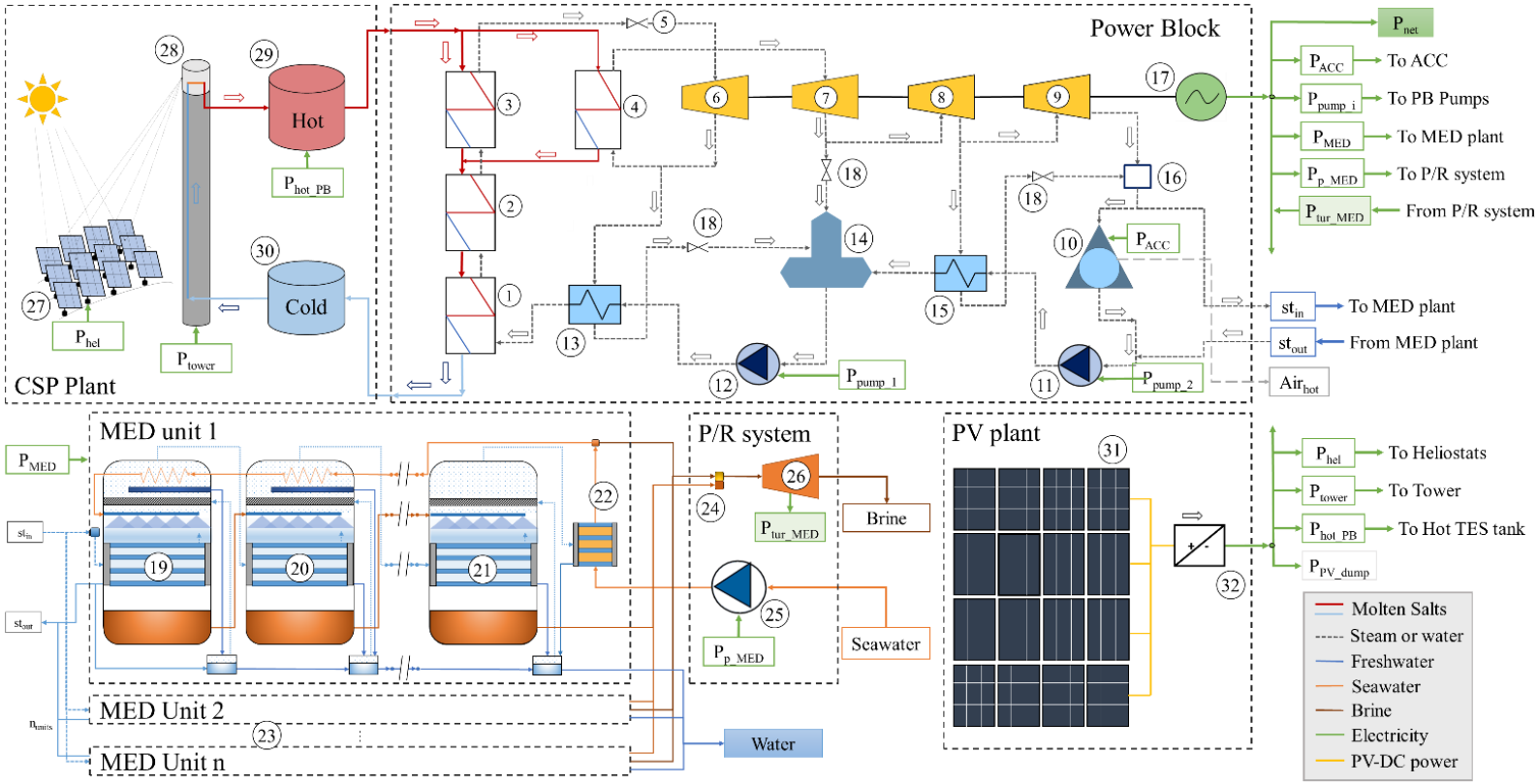

1. Economizer (Steam Generator)
2. Evaporator (Steam Generator)
3. Super-heater (Steam Generator)
4. Reheater
5. Throttle valve
6. High-pressure turbine
7. Medium-pressure turbine
8. Low-pressure turbine
9. Low-pressure turbine
10. Air-cooled condenser (ACC)
11. Low-pressure pump
12. High-pressure pump
13. Closed feed water heater 1
14. Deaerator
15. Closed feed water heater 2
16. Mixer
17. Generator
18. Valves (3)
19. MED 1st effect
20. MED 2nd effect
21. MED last effect
22. MED condenser
23. MED units (2 to 8)
24. Resultant Seawater/Brine mixer
25. Seawater pumping system
26. Energy recovery system
27. Heliostats field
28. Receiver tower
29. Hot TES tank
30. Cold TES tank
31. PV plant
32. Inverter

Figure 3-1: Scheme of the CSP+PV+MED plant proposed.

3.2.1 CSP plant

The CSP plant consists of a central receiver tower plant with a two-tank direct TES system, and a steam power block with a gross output power of 110 MW_e. The plant uses a molten salt mixture (60% $NaNO_3$ and 40% KNO_3) as heat transfer fluid (HTF) and storage media. The central receiver consists of a cylindrical receiver that heats the HTF up to 565 °C (Turchi & Heath, 2013). Then, the molten salts are stored in the hot tank. As required the hot salts flow through the Steam Generation System (SGS) delivering heat to a power block that produces electricity in a steam turbine. The cold molten salts are stored in the cold tank around 300 °C. The solar field is composed of heliostats with an area of 144 $m^{2,}$ having a reflectivity of 95% (Blair et al., 2014). The power block consists of a steam Rankine Cycle, which considers a high-pressure turbine stage, a low-pressure turbine stage with three extractions, two Close Feed-Water Heaters (CFWH), a deaerator, a reheater and an Air Cooled-Condenser (ACC). The steam can be condensed by a MED plant coupled at the turbine exhaust steam outlet, in parallel to the ACC. In this configuration, the turbine back pressure is set to the saturation temperature of the MED plant inlet steam.

3.2.2 PV plant

The PV plant consists of a modular PV plant with one-axis tracking and inverters of 1 MW_e. The PV plant size is scalable with the number of inverters and is connected in parallel with the power block. In this way, the PV plant and the power block work in synergy to deliver a baseload capacity.

3.2.3 MED plant and P/R system

The MED plant consists of several units of 10,000 m^3/day capacity each, with a forward-feed plant configuration of 14 effects and 13 pre-heaters. The design parameters of the MED unit are as follows: the steam enters at the first effect at 70 °C, the seawater inlet temperature is 20 °C, and the salinity is 35 g_{salt}/kg_{water}. The temperature of the last effect is 34°C, while the brine output salinity is 63 g_{salt}/kg_{water}. With these parameters, each unit requires a steam

mass flow rate of 11.45 kg/s or 25.9 MW_{th} of thermal energy to reach the nominal operating conditions. Considering that the maximum exhaust steam mass flow rate of the power block is 88 kg/s at nominal conditions, the maximum number of units of the MED plant would be 8. Moreover, if another salinity is considered due to being in another location, the MED plant design parameters (number of effects and steam mass flow rate) and performance would change. Finally, the P/R system considers two pipelines, one for the seawater pumped and another for the brine disposal. In addition, it is considered a seawater pumping station, and a hydraulic turbine.

3.3 Model development

The simulation model for the CSP+PV+MED plant was developed in Transient System Simulation Program (TRNSYS) software, which was also used to run the simulations with the aim of determining the performance of each system, subsystem, and components of the plant. The model was developed in a single TRNSYS deck that integrates the electric power balance between the different components of the plant, as well as the startup and shut down of these components. Most of the TRNSYS types were developed by the authors in previous works (Mata-Torres et al., 2019a; Zurita, Mata-Torres, et al., 2018). The simulations were performed for a Typical Meteorological Year (TMY) with data on an hourly basis.

3.3.1 CSP and PV plant

The CSP plant model is composed of the heliostats, the central receiver, and the thermal storage tank types (Mata-Torres et al., 2017; Valenzuela et al., 2017; Zurita, Mata-Torres, et al., 2018). The TRNSYS Type that describes the heliostats field was developed based on Type 394 from the STEC (Solar Thermal Electric Components) library (Schwarzbözl, Eiden, Pitz-Paal, Zentrum, & Scott, 2006), which establishes a heliostats field efficiency in function of the solar altitude and azimuth to calculate the incident power on the receiver. This model considers a power consumption of the heliostats, a daily soling rate, and a cleaning period of 0.055 kW_e, 0.5%, and 20 days, respectively (National Renewable Energy Laboratory, 2018; Zurita, Mata-Torres, et al., 2018).

The central receiver type is a simplified model of a cylindrical receiver composed by tubes. The model calculates the HTF mass flow rate at a defined outlet temperature in terms of the incident radiation, the thermal losses, and the input HTF temperature. The thermal losses are constituted by the natural and forced convection losses and the radiation losses, which depends on the wind velocity, the ambient and sky temperatures, the central receiver and tower dimensions, and receiver superficial temperature. Also, the model considers the electric power consumption of the HTF tower pumps according to the HTF mass flow rate flowing through the receiver. The design of the receiver and of the heliostats solar field were calculated in terms of the solar multiple (SM - rate between the solar field thermal power and the thermal power of the power block at the nominal point) using SAM from NREL (Blair et al., 2014; National Renewable Energy Laboratory, 2018). Moreover, the central receiver integrates a control procedure that delimits its operation by four parameters controls:

- Energy required to start up the tower operation, set to 25% of the nominal thermal energy for 1 hour.
- Minimum thermal power to initiate the startup, set to 20% of the nominal power,
- Minimum thermal power to operate the receiver in normal conditions, set to 25% of the nominal thermal power.
- Maximum thermal power operation defined at 110% of the nominal power.

The TES system was modeled considering two storage tanks with variable volume (Type 39 from TRNSYS library), one for the hot HTF tank, and another for the cold HTF tank. A control system was integrated into the TES model, in which the HTF mass flow rate that goes to the power block was restricted in terms of the hot tank volume in order to decrease the number of the power block start-ups, allowing the power block operation for at least two hours (Zurita, Mata-Torres, et al., 2018). The electric power consumption related to the power block HTF pumps was also considered in this model.

Lastly, the PV plant was simulated using the Type 190 of TRNSYS, which includes the inverter efficiency curve and determines the electrical performance of the PV array. The size of the array was set to 1 MW_e (20 modules in series and 178 strings in parallel) and was scaled up to the PV plant size in terms of the number of inverters. In this analysis, it was considered a one-axis tracking to maximize the yearly yield of the plant, and an average soiling rate of 10%.

3.3.2 Power Block

The power block model, used in a previous work by the authors (Mata-Torres et al., 2019a), was developed in Engineering Equation Solver (EES) software to calculate the performance of the power block operating at nominal and off-design conditions. The model allows determining the design parameters of the power block, such as the overall heat transfer coefficients (UA) of the evaporator, the superheater, the reheater, and the CFWHs. The same design parameters that were used in Mata-Torres et al. (Mata-Torres et al., 2019a) were considered for this study. These parameters are used as inputs for the off-design model in EES to calculate the yield of the power block. The off-design model considers a constant pressure control during part-load operation, establishing a minimum of 30% for part-load operation. The variation of the steam mass flow rate in the heat exchangers to calculate the effective UA under part-load operation (equation presented in (Patnode, 2006)) and the change of efficiency and the pressures of the steam turbines by the Stodola's ellipse law were also considered.

The integration of the power block model into the TRNSYS environment was carried out by the use of a multi-variable polynomial regression in order to reduce the computational time significantly. The inputs of the polynomial regression were: the temperature of the HTF leaving the hot tank (T_{inHTF}), the HTF mass flow rate ($\dot{m}_{inHTF}$) and the condensing temperature (T_s). Notice that the condensing temperature (that is, in turn, the steam temperature at the inlet of the MED first effect) is established by the part-load operation of the MED unit (see Section 3.3). The outputs of the regression were: the net power output from the turbine-generator (W_{net}), the turbine exhaust mass flow rate ($\dot{m}_{cond}$), the turbine

exhaust enthalpy (h_s) and the temperature of the HTF returning to the cold tank (T_{outHTF}). The polynomial regression was obtained by performing a parametric analysis with the power block model implemented in EES, considering 11.000 operation points in a range of T_{inHTF} between 550 and 565 °C (range established according to preliminary simulations), $\dot{m}_{inHTF}$ between 200 and 700 kg/s (corresponding to off-design from 30% to 105%), and T_s between 56 and 74 °C (range established according to preliminary simulations). Once the results from the parametric analysis are determined, the tool MultiPolyRegress in MATLAB software is used to fit a polynomial regression, considering a second-degree polynomial. Finally, this regression is implemented in a TRNSYS type to estimate the yield of the power block. The Normalized Root-Mean-Square Deviation (NRMSD) of the regression model outputs was 0.25% for the W_{net}, 0.01% for the $\dot{m}_{cond}$, 0.62% for the h_s, and 0.43% for the T_{outHTF}, which proves its good accuracy. The polynomial multi-variable regression together with the coefficients used for each of the output is shown in APPENDIX A2.

3.3.3 MED plant and P/R system

The MED unit model was implemented in EES and is based on the model proposed by Ortega-Delgado et al. (Ortega-Delgado, García-Rodríguez, et al., 2017; Ortega-Delgado, Palenzuela, et al., 2016) and Palenzuela et al. (Palenzuela, Alarcón-Padilla, et al., 2015a; Palenzuela, Hassan, Zaragoza, & Alarcón-Padilla, 2014), already used by the authors in (Mata-Torres et al., 2019a). The model evaluates the thermodynamic performance of the MED unit by applying mass and energy balances. To model the integration of the MED unit with the rest of the plant in TRNSYS, a multi-variable polynomial regression was developed from the results delivered by the model in EES. This model was first used to determine the design condition for a 10.000 m^3/day unit, where the effects, preheaters, and the final condenser areas were calculated. Then, the part-load operation was evaluated in terms of the available thermal load in the power block and the seawater temperature considering that it changes throughout the year. The inputs of the polynomial regression were the inlet seawater temperature (T_{sw}), the enthalpy (h_s) and the mass flow rate ($\dot{m}_s$) of the turbine's exhaust steam. Also, the temperature of the last effect of the MED unit and the output brine concentration were kept constant at their nominal values. The outputs from the polynomial

regression are: the freshwater mass flow rate ($\dot{m}_{water}$), the feed seawater mass flow rate ($\dot{m}_f$), the cooling seawater mass flow rate ($\dot{m}_{csw}$), the steam temperature at the inlet of the first effect (T_s), the freshwater outlet temperature (T_{water}), the brine outlet temperature (T_{br}), and the outlet temperature of seawater at the last condenser (T_{csw}). It is important to highlight that the variation of T_s in off-design conditions is due to the decrease on the temperature difference between effects when the steam mass flow rate decreases. The regressions and their coefficients are listed in APPENDIX A3.

The polynomial regression was developed by performing a parametric analysis using the MED model in EES, considering 567 operational points ranging the thermal load between 40 and 100% (which represents the variation of the inlet steam mass flow rate from 4.58 kg/s to 11.45 kg/s), the inlet steam enthalpy between 2550 to 2950 kJ/kg, and the seawater temperature between 15 to 23°C. The regression coefficients for the seven outputs were obtained using the regression tool in MATLAB. The variation of the freshwater mass flow rate ($\dot{m}_{water}$), the total seawater mass flow rate ($\dot{m}_{in}$ - sum of the feed and cooling seawater mass flow rates), and the steam temperature at the first effect inlet (T_s), in terms of the thermal load and the seawater temperature are shown in Figure 3-2.

It is observed that the freshwater mass flow rate (Figure 3-2.a) and the steam saturation temperature at the inlet of the first effect (Figure 3-2.c) increase significantly with the thermal load, changing from 67 to 115 kg/s; and from 60 to 70 °C, respectively. However, the variation of the seawater temperature has a negligible effect on such two variables. Regarding the total seawater mass flow rate (Figure 3-2.b), it is observed that it increases dramatically with the rise of the seawater temperature at all thermal loads, showing a change from 370 kg/s to 850 kg/s at 100% of thermal load. It is worth noting that the variation of the steam temperature at the first effect inlet with the thermal load (in a range of 10 °C) would have an impact on the turbine exhaust pressure and on the power produced by the power block. Likewise, the increase of the total seawater mass flow rate with the seawater temperature would lead to additional seawater pumping requirements for the MED cooling purposes, affecting the plant's energy consumption.

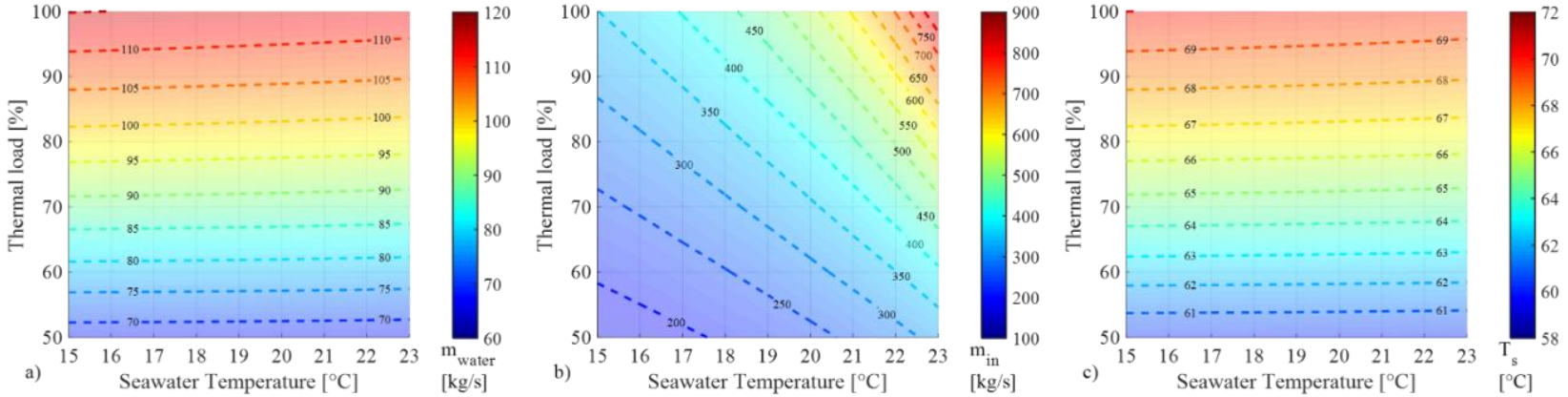

Figure 3-2: (a) Freshwater mass flow rate, (b) total seawater mass flow rate, and (c) steam temperature at the inlet of the first effect variation at different thermal loads and seawater temperature.

The Normalized Root-Mean-Square Deviation (NRMSD) has been used to evaluate the fit of the regression model for the seven outputs. The NRSMD results are depicted in Table 3-1, showing that the errors are below 1% with the highest value related to the cooling seawater mass flow rate. Therefore, the regression model developed in this work shows good accuracy and concordance with the ESS model, with the advantage of reducing significantly the computational time for the simulation.

Table 3-1: NRMSD of the outputs of the MED unit model.

Variable	NRMSD
Freshwater mass flow rate ($\dot{m}_{water}$)	0.16%
Feed seawater mass flow rate ($\dot{m}_{f}$)	0.16%
Cooling seawater mass flow rate ($\dot{m}_{csw}$)	0.71%
Steam temperature at the inlet of the first effect (T_{s})	0.25%
Freshwater outlet temperature (T_{water})	0.35%
Brine outlet temperature (T_{br})	0.00%
Cooling seawater temperature (T_{csw})	0.55%

The regression model of the MED unit was implemented in a new TRNSYS Type and integrated into the CSP+PV plant model. For this purpose, some assumptions and control procedures that limit the MED operation were considered, as follows:

- All MED units operate at the same thermal load, which means that the steam mass flow rate that goes to the MED plant is equally divided between the MED units. Likewise, the freshwater mass flow rate obtained from the MED unit is multiplied by the number of units.
- The maximum thermal load of the MED plant is defined in terms of the number of units and the steam mass flow rate of one unit at the design point (11.45 kg/s).
- When the MED plant is under operation, it is powered first, and then, the remaining steam is condensed in the ACC.
- A minimum thermal load of 70% is needed for the starting-up the MED unit in order to account the energy requirements for the start-up in the simulations.

- When the thermal load decreases below 50%, the units are turned off, and the ACC is activated for condensing all the turbine exhaust steam.
- The inlet steam saturation temperature obtained by the operation of the MED plant sets the condensing temperature of the power block, which varies between 60 to 70 °C according to Figure 3-2.c. Moreover, when the MED plant is turned off, the condensing temperature of the power block is fixed to 60 C.
- The MED unit considers the specific electric consumption of 1.5 kWh/m^3 (Palenzuela, Alarcón-Padilla, et al., 2015b).

The total seawater mass flow rate pumped to the MED plant ($\dot{m}_f + \dot{m}_{csw}$), and the resultant brine mass flow rate that is returned to the sea ($\dot{m}_{csw} + \dot{m}_{br}$), were used for the evaluation of the P/R system. The assessment consists on calculating the head losses for the intake and discharge pipelines, and the power consumption of the seawater pumps and the brine recovery energy from the hydraulic turbine, considering an efficiency of 80%. The pipelines diameter was calculated as a function of the total seawater mass flow rate of the MED plant at nominal conditions and the maximum allowable inner tube velocity, which was defined at 2.5 m/s to avoid corrosion (Herrera-León et al., 2019). The head losses of both systems were computed using the Darcy-Weisbach equation. The friction factor was calculated in terms of the length, diameter, and the relative roughness of the pipeline, and the kinematic viscosity of the fluid. All the electrical consumptions are considered as part of the electric power balance of the plant for each time step of the simulation.

3.4 Thermoeconomic model

The thermoeconomic analysis is a methodology that merges the thermodynamic assessment based on the exergy and the economic analysis providing valuable information about the cost formation of the products in a cogeneration plant. The analysis was performed using a combination of procedures in EES and MATLAB softwares and using the information obtained from the thermodynamic modeling of the plant on an hourly basis. The

methodology is based on a well-known process (Lazzaretto & Tsatsaronis, 2006) that was extended on a previous work by the authors (Mata-Torres et al., 2019a).

3.4.1 Exergy analysis

The exergy analysis was applied to each energy and mass flow in the plant, considering the solar energy, molten salts, steam, seawater, freshwater, and brine streams. The analysis was performed considering a medium-disaggregation level of the systems, focusing on the power block system (Mata-Torres et al., 2019a). In detail, there were considered 88 exergy flows between the solar radiation, molten salts, steam, seawater, freshwater and brine streams, and 30 components (4 for the CSP plant, 20 for the power block, 1 for the MED plants, 3 for the P/R system, and 2 for the PV plant, presented in Figure 3-1). Regarding the solar radiation, the exergy was computed considering the Petela's approach (Petela, 1964), using the Direct Normal Irradiation (DNI) for the heliostats and receiver components, and the Irradiation on Plane of the Array (POA) for the PV plant. Likewise, the physical exergy was calculated for the rest of the streams, while the chemical exergy was considered only for the flows related to the seawater, freshwater, and brine since in those streams the change on the salinity requires such treatment (Dinçer & Rosen, 2012; Piacentino, 2015). The physical exergy was denoted by ψ, and it is defined as:

$$\psi = (h - h_0) - T_0(s - s_0) + gz \tag{3.1}$$

where h and s are the enthalpy and entropy of the stream at a given state, properties with the subscript "0" are at the reference state, g is the gravity, and z is the altitude. Potential exergy was only considered for the streams related to the MED plant and P/R system because they have a considerable change of altitude. The EES library was used for assessing the thermophysical properties of molten salts and steam, while properties of the seawater, freshwater, and brine were calculated by the correlation defined by Sharqawy et al. (Sharqawy, Lienhard V, et al., 2011a). The chemical exergy (a_{ch}) is defined by the salinity using the approach of the chemical potential and the mass fraction, as follows:

$$a_{ch} = \sum_{i=1}^{n} w_i(\mu_i{}^* - \mu_i{}^0) \tag{3.2}$$

where w_i is the water or salt mass fraction (dimensionless), and μ_i is the chemical potential of the water or the salt in seawater in kJ/kg. The chemical potential of the seawater is calculated by correlations set in detail by Sharqawy et al. (Sharqawy, Zubair, et al., 2011), where the μ_i^* is chemical potential at the stream salinity and the reference temperature, while the μ_i^0 is calculated considering the seawater reference salinity and temperature.

3.4.2 Thermoeconomic analysis

The thermoeconomic analysis is a methodology that computes the cost of each stream based on the costs of the systems, the exergy flow, the destroyed exergy, and the waste exergies. The thermoeconomic cost ($\dot{C}_{k,t}$) is calculated by a linear equation system solved by a matrix computation, which is composed of cost balance and auxiliary equations. The cost balance equation is given by:

$$\sum \dot{C}_{in,t} + \dot{Z}_{k,t} = \sum \dot{C}_{out,t} \tag{3.3}$$

where $\dot{Z}_{k,t}$ is a cost rate of the component, evaluated at the time step. Some auxiliary equations are required to complete the matrix and achieve a unique solution. These auxiliary equations relate the unit thermoeconomic cost ($c_{k,t}$) of different steams or with the unit cost of the fuel or the wastes, following the fuel-product principles (Lazzaretto & Tsatsaronis, 2006). The $c_{k,t}$ is obtained from the relation between the thermoeconomic cost and the exergy rate ($\dot{X}_{k,t}$) as (Bejan et al., 1995):

$$\dot{C}_{k,t} = c_{k,t}\dot{X}_{k,t} \tag{3.4}$$

The set of auxiliary equations implemented in this work follows the approach presented in (Mata-Torres et al., 2019a). However, the disaggregation level of the MED plant was simplified to only one device. Moreover, the present study includes a thermoeconomic analysis of the CSP and PV plant. Specifically, the hot and cold TES tanks present a dynamic behavior that consists of a volume and temperature variation of the molten salts (Ma, Morozyuk, Liu, Yan, & Liu, 2019). Thus, a variation of the cost balance equation was proposed (Eq. 3.5), including the term of cost accumulation rate ($\Delta\dot{C}_{CV,i,t}$) (Dinçer & Rosen, 2012), which is related to the exergy accumulation term that is usually eliminated. The cost

accumulation rate of the component can be separated as the cost stored at the beginning of the time step ($\dot{C}_{initial,i,t}$) and the cost stored at the final of the time step ($\dot{C}_{final,i,t}$).

$$\dot{C}_{in,k,t} - \dot{C}_{out,k,t} + \dot{Z}_{k,t} = \Delta\dot{C}_{CV,k,t} = \left(\dot{C}_{final,k,t} - \dot{C}_{initial,k,t}\right) \quad (3.5)$$

Both terms are related to the exergy stored by the molten salts (defined by the temperature in the tank) and the tank´s volume at the time step. Thus, to complement the auxiliary equations, the following were proposed for each tank:

$$c_{final,k,t} = c_{out,k,t} \quad (3.6)$$

$$c_{initial,k,t} = c_{final,k,t-1} \quad (3.7)$$

The thermodynamic analysis was performed for every time step of the simulation (8760 hours), in which the hot and cold TES tanks transfer the cost accumulated through each time step. Moreover, the streams considered as the products of the plant were the net electricity output and the freshwater chemical exergy flow (Catrini et al., 2017; Mata-Torres et al., 2019a). Their unit costs were defined as Thermoeconomic Cost of Electricity (TCE) in \$/MWh and the Thermoeconomic Cost of Water (TCW) in \$/m^3. Finally, the daily, monthly and annual cost were computed from the results of the hourly cost rates by the following expression, where $Elec_{i,t}$ is the net electricity production in MWh, $Water_{i,t}$ is the water production in m^3 and T is the number of hours:

$$TCE = \frac{\sum_{t=1}^{T} \dot{C}_{el,t}}{\sum_{t=1}^{T} Elec_t} \quad (3.8)$$

$$TCW = \frac{\sum_{t=1}^{T} \dot{C}_{w,t}}{\sum_{t=1}^{T} Water_t} \quad (3.9)$$

3.4.3 Economic analysis

The economic analysis comprises the cost evaluation of the components to obtain the cost rates, which is obtained by the following expression in \$/h:

$$\dot{Z}_{i,t} = \frac{A_f + f_{O\&M}}{O_{time,i}} Z_i \quad (3.10)$$

where $f_{O\&M}$ is the operation and maintenance factor that was set to 5%, $O_{time,i}$ is the annual operating time of the component in hours and the A_f is the amortization factor that depends on the interest rate and the plant's technical lifetime (Mata-Torres et al., 2019a). The total capital investment (Z_i) of the components or system considered were calculated, considering several cost correlations in the literature (Adibhatla & Kaushik, 2017; Aly, Bernardos, Fernandez-Peruchena, Solvang Jensen, & Pedersen, 2019; Ameri et al., 2009; Dieckmann et al., 2017; Fu, Feldman, & Margolis, 2018; Herrera-León et al., 2019; Jorgenson, Mehos, & Denholm, 2016; Piacentino, 2015; Xiong et al., 2012). Likewise, the pipeline cost was updated with information reported in previous works adapted to particular conditions in Chile (Herrera-León et al., 2019; Hoffmann & Dall, 2018; Shahabi, McHugh, Anda, & Ho, 2015). The Z functions are presented in detail in APPENDIX A5. Finally, the annual operating time was computed from the performance of the plant, counting the number of hours that work at year each component.

3.5 Results and discussion

The study of the CSP+PV+MED plant was performed considering the meteorological conditions at Crucero located in northern Chile (Lat. −22.24° S and Lon. −69.51°), which presents a large number of days with high DNI levels throughout the year with a DNI total of 3389 kWh/m^2-yr (Escobar et al., 2015). Figure 3-3 shows the yearly DNI profile, wherein February presents several cloudy days due to a local phenomenon in northern Chile known as the Altiplanic Winter. This phenomenon consists of moist air that comes from Bolivia that brings unsettled weather and occasional rain. This location is at 1000 meters above sea level and 100 km away from the coast, which was considered for the P/R system design and operation. The seawater temperature data was obtained for Antofagasta from (Global Sea Temperature, 2019), where the monthly profile was extracted, varying between 15.0 and 20.8 C.

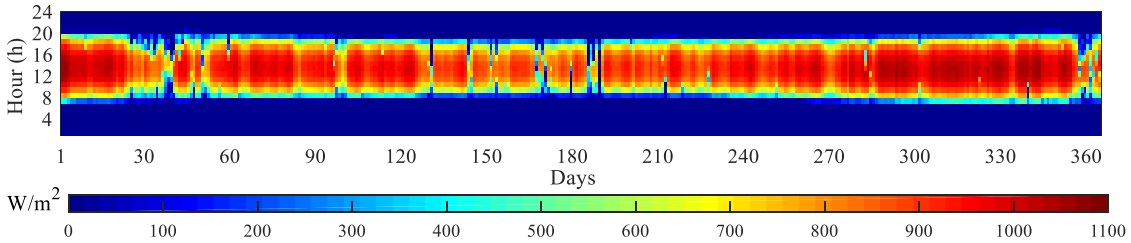

Figure 3-3: DNI profile for the location at Crucero, Chile.

In this section, the annual performance and thermoeconomic analysis of the CSP+PV+MED plant are presented, considering a configuration of 100 MW_e for the PV plant, a SM of 2.4, 12 hours of TES, and four units for the MED plant. A comparison analysis was performed between the plant with and without the PV system, in order to understand the impact of the PV integration on the performance and the thermoeconomic indicators of the whole plant. A unidimensional sensitivity analysis is also presented, varying each one of the design parameters, showing the impact on the performance and the cost of the products. Finally, a multivariable parametric analysis is shown, where different optimum configurations that minimize both the thermoeconomic electric and water costs are analyzed.

3.5.1 Annual performance

Figure 3-4 shows the hourly performance of the CSP+MED plant for two days in summer (from 8^{th} to 9^{h} of January) and in winter (from 20^{th} to 21^{th} of July), in which the gross power production of the CSP plant (CSP) and the recovery turbine (RT) production, as well as, the power consumption of the seawater pumping system (Pump), the MED plant (MED), the parasitic of the power block (Par_PB) and the parasitic of the CSP (Par_CSP) are presented. It is observed that the CSP power is at full load during the day, and the water production (Water) is near to the nominal condition for summer and winter days, only varying the operating hours per day (approximately 22 hours in summer and 15 hours in winter). It is worth to mention that in summer, the power consumption of the seawater pumping system (Pump) reaches 43 MW_e, while during the winter it decreases to 21 MW_e, mainly because of the seawater temperature variation that reduces the inlet seawater mass flow rate. Thus,

the power balance of the plant changes, obtaining a higher net output power (Pnet) during the winter months, but with lower operating hours.

In contrast, Figure 3-5 shows the hourly performance of the CSP+MED system integrated with the PV plant, in which the gross power production of the PV plant (PV) and the dumped power in the PV plant (PV_dump) are also presented. In summer, it is observed that the power produced by the PV plant is around 80-95 MW, which forces the power block of the CSP plant to work at minimum part-load operation in order to complement the net output power to 100 MW_e. In this case, the MED plant works at part-load (around 60% thermal load), decreasing the power consumption of the seawater pumping system. Moreover, around noon, the PV plant reaches its maximum power output, and the electric power balance exceeds the nominal net output power, so part of the power from the PV plant is dumped. Also, the CSP parasitic consumption (Par_CSP) decreases because the TES system is charged, which forces to dump the energy excess from the CSP plant. At night, the power block and the MED plant operates at full load, with a net output power of 78 MW.

Conversely, in winter, the power production of the PV plant is about 70 MW, and the power block of the CSP plant complements to 100 MW_e, but the TES system is not completely charged during the daylight hours. Thus, the energy stored in the TES is not enough to operate during all-night, turning off the CSP and the MED plant between 4 to 6 am. Additionally, the MED plant is off during the daylight hours because the available steam is 60% of the nominal thermal load, and the plant needs 70% for the start-up process. Thus, the MED plant mainly works at between 10 and 12 hours during the night. The main differences in the plant performance are that in summer the power block and the MED plant works 24 hours, while in winter both systems are shut down, decreasing the daily water production.

Figure 3-6 and Figure 3-7 show the daily electric energy balance and the water production of the CSP+MED and CSP+PV+MED plants, respectively. In Figure 3-6, it is observed significant variability in the total daily electric energy produced by the CSP plant and the net output electricity throughout the year (Pnet), which depends on the daily DNI. Likewise,

the water production (Water) follows the power output of the CSP plant, evidencing that the MED plant operation depends on the power block operating hours. Moreover, it is shown a variation on the energy for seawater pumping (Pump) due to the changes in the seawater temperature and the daily operational hours of the MED plant.

For the case of the PV integration (Figure 3-7), it is observed that the daily electric energy from the CSP plant is limited around 1500 MWh/day due to the combination with the PV plant. Moreover, the net output electricity remains stable during the year, having some variations for the cloudy days. Regarding the water production, it is detected two levels of daily water production, one at 35 dam^3/day and the other at 20 dam^3/day. The difference between the two levels is mainly due to the daily operational hours of the MED plant. During the days presenting high water production, the whole plant performed similarly to a summer day, in which the CSP plant and the MED plant worked 24 hours. On the other hand, in the days with low water production, the plant performed similarly to a winter day in which the MED plant worked approximately 12 hours during the night. These differences also affect the seawater pumping consumption and energy balances of the plant, leading to significant changes in the PV dumped energy.

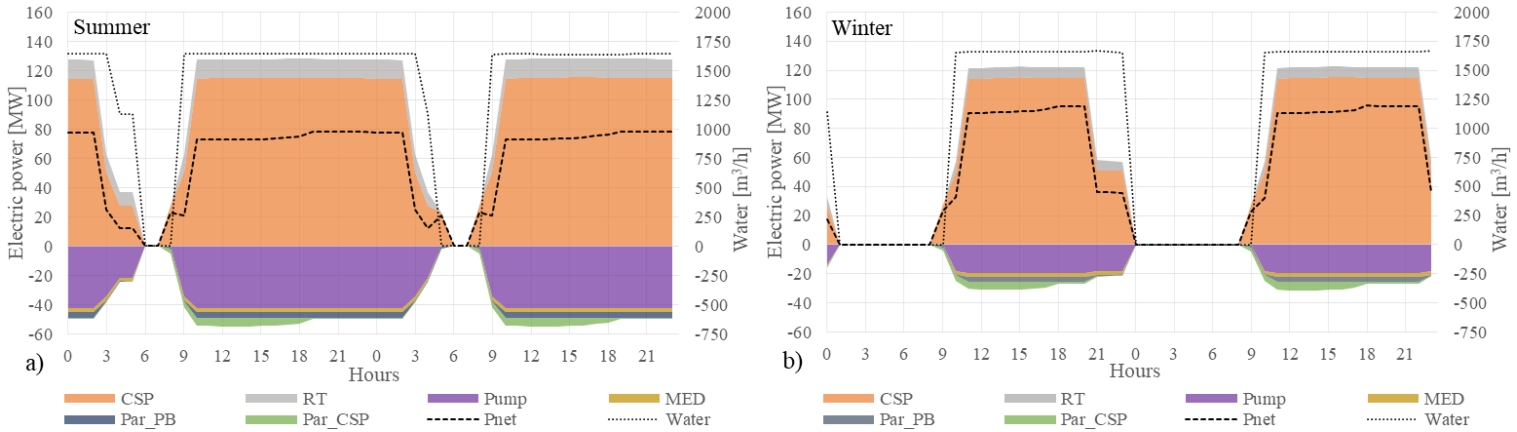

Figure 3-4: Electric power balance and water production of the CSP+MED plant for three days in (a) summer (January 8-9th) and (b) winter (July 20-21th).

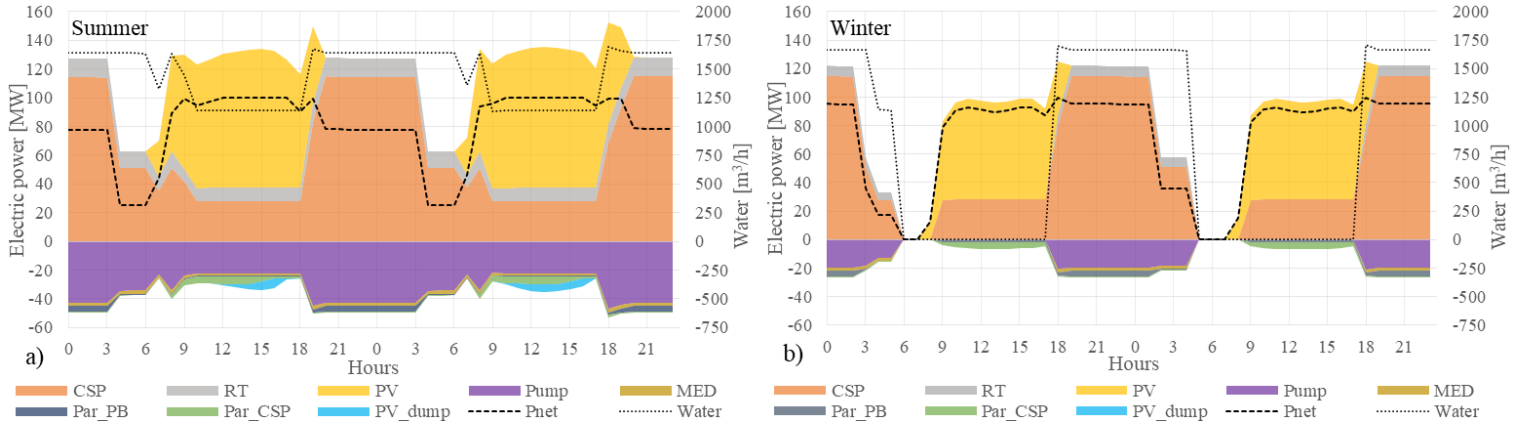

Figure 3-5: Electric power balance and water production of the CSP+PV+MED plant for three days in (a) summer (January 8-9th) and (b) winter (July 20-21th).

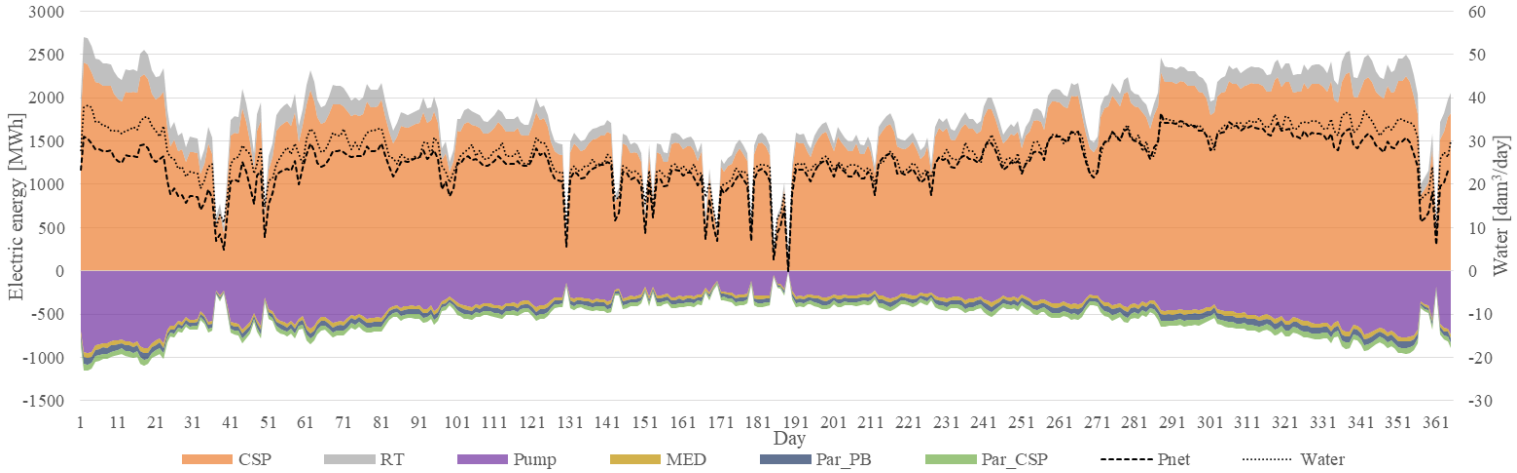

Figure 3-6: Daily electric energy balance and water production of the CSP+MED plant.

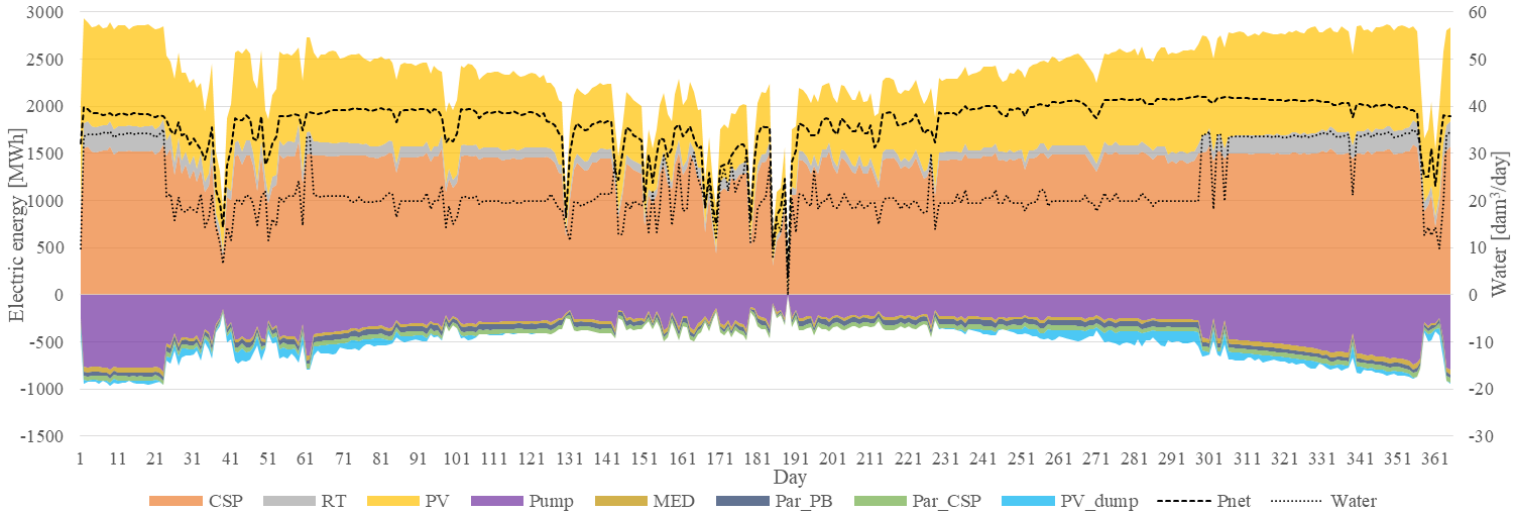

Figure 3-7: Daily electric energy balance and water production of the CSP+PV+MED plant.

Regarding the annual electricity balance and water production of the whole plant, Table 3-2 shows that the integration of the PV plant increases 30% of the total electric production and almost 48% of the net electricity production, compared to the CSP+MED plant. In addition to that, the CSP plant decreases its annual electric output due to the fact that it operates in a secondary role, increasing the solar energy dumped in the CSP solar field, and showing more part-load operation hours of the power block. The total parasitics consumption (Pump, MED, ACC, Par_PB and Par_CSP consumption) and the water production also decrease 10% and 17%, respectively, due to the fact that the CSP and MED plants reduce their annual hours of operation. In terms of the capacity factor (CF - ratio between the yearly power/water production and the maximum power/water production at nominal capacity), the CSP+MED plant achieves a power capacity factor of 51% and a water capacity factor of 68%, while the CSP+PV+MED plant obtained a power capacity factor of 76%, with a water capacity factor of 57%.

Table 3-2: CSP+PV+MED plant annual electricity distribution and water production.

Electricity production		CSP+MED		CSP+PV+MED	
CSP	[GWh]	605.6	91.4%	501.0	58.3%
PV	[GWh]	0.0	0.0%	310.5	36.1%
RT	[GWh]	57.1	8.6%	48.3	5.6%
Total	[GWh]	662.7	100.0%	859.8	100.0%
Electricity distribution					
Net	[GWh]	450.7	68.0%	668.3	77.7%
Pump	[GWh]	159.6	24.1%	131.9	15.3%
MED	[GWh]	15.0	2.3%	12.4	1.4%
Par_PB	[GWh]	18.8	2.8%	17.0	2.0%
Par_CSP	[GWh]	18.5	2.8%	16.1	1.9%
Dumped	[GWh]	0.0	0.0%	14.2	1.6%
Freshwater production					
Water production	[hm^3]	9.95		8.27	

The PV plant integration allows storing more energy in the TES system during the daylight hours, increasing the net output electricity of the plant significantly and, in a first instance, the operational hours of the power block and the MED plant. However, these last two systems operate more hours at part-load under this configuration, causing an increase of the dumped energy of the CSP solar field and a decrease of the available CSP thermal energy in the annual balance, reducing the operational hours of the MED plant; and thus, the total water production. These results are in concordance with the results previously presented by (Valenzuela et al., 2017).

3.5.2 Thermoeconomic results

Daily TCE and TCW of the CSP+PV+MED plant are shown in Figure 3-8 and Figure 3-9, which illustrate the contribution of the five main systems of the plant (the PV plant, the CSP plant, the power block - PB, the MED plant, and P/R system). In Figure 3-8, it is observed that the TCE presents an important contribution from the CSP plant and the P/R system, which are the two most expensive systems of the plant. Furthermore, the TCE shows a profile marked by two cost levels with some peaks that are related to cloudy days. The two cost levels are around 120 $/MWh and 160 $/MWh, and they are associated with the two levels of daily water production during the year. The main difference between these levels lies in the fact that the contribution of the P/R system increases significantly when the water production rises to 35 hm^3/day, meaning that the P/R system works for more hours and allocates more cost to the electricity produced. Besides that, it is observed that the cost contribution of the PV plant is small despite the amount of energy that is produced by this system, and the cost contribution of the MED plant to the TCE is almost negligible. Finally, the cost contribution of the CSP plant to the TCE presents small variations, mainly decreasing for the summer months and moderately increasing for winter days.

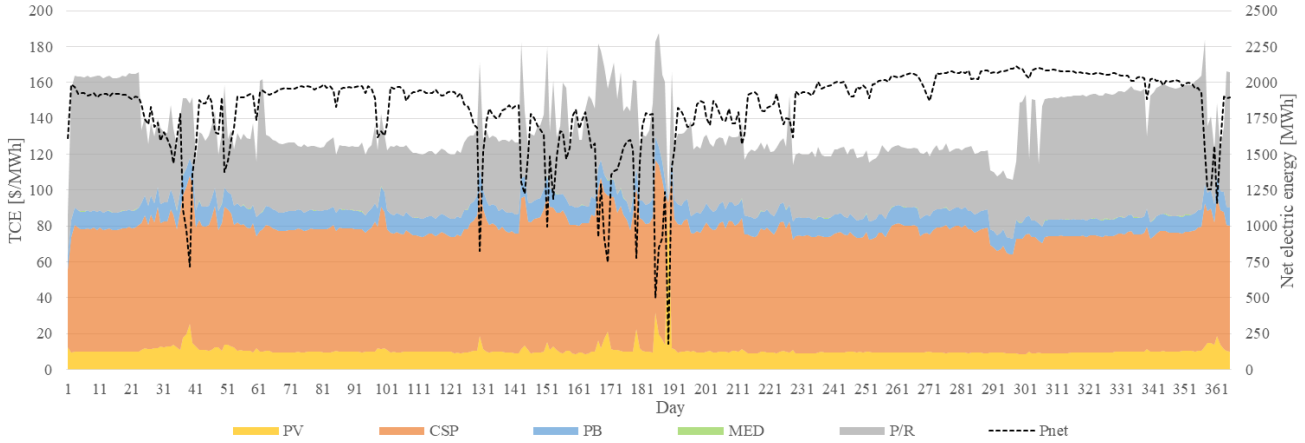

Figure 3-8: Daily TCE considering the allocation of the PV, CSP, PB, MED, and P/R systems cost for a CSP+PV+MED plant configuration.

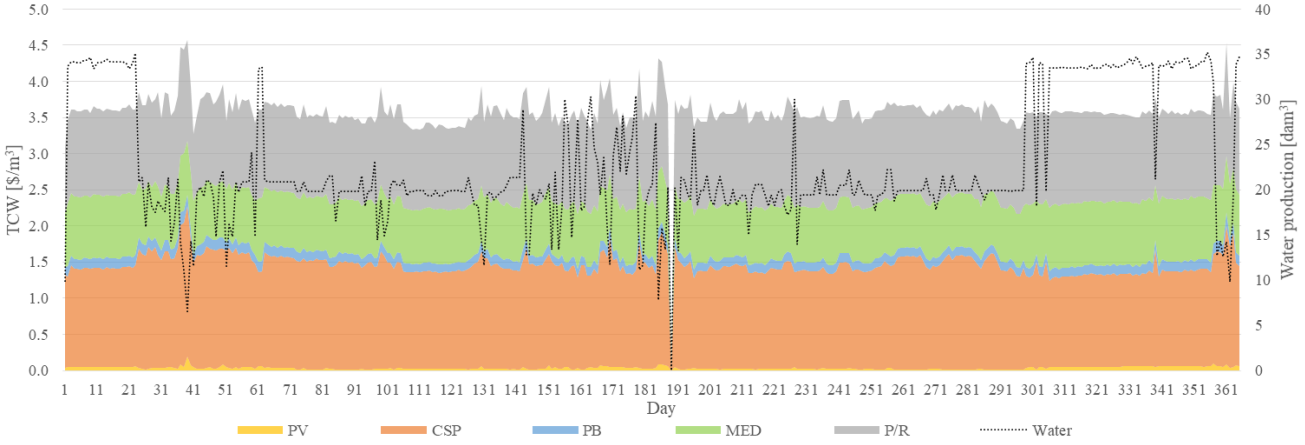

Figure 3-9: Daily TCW considering the allocation of the PV, CSP, PB, MED, and P/R systems cost for a CSP+PV+MED plant configuration.

In contrast, Figure 3-9 shows that the daily TCW presents a stable cost throughout the year, with some slight variations. The most significant change is attributable to the CSP contribution, which varies in the same form than observed for the TCE. Moreover, it is evidenced that the contribution of the MED plant and the P/R system are practically the same for each day. It is important to highlight that the TCW is not affected by the variation of the power consumption by the seawater pumping system during the year (see Figure 3-7). Finally, the cost contribution of the PV plant and the power block to the TCW are small or negligible.

Figure 3-10 show the monthly TCE and TCW obtained for the CSP+PV+MED plant, indicating that the TCE variation is mainly influenced by the CSP contribution, which moderately increases during the cloudy months (February, May, June, and July), and by the P/R system cost that is in terms of the water production. Meanwhile, the TCW presents only a small variation of the CSP cost contribution, also evidencing that it is not related to water production.

Table 3-3 shows the distribution of the total costs of the plant's main systems to the electricity and water costs in MM$ for the CSP+MED and CSP+PV+MED plants. In this way, the percentages represent the share of the total cost that is allocated to the electricity and water cost for each system. In addition that, it is evidenced that the cost contribution of the CSP plant and of the P/R system costs (which are the more expensive systems) are allocated to the electricity with 80% and 75% respectively for both cases. The distribution of the P/R system occurred because approximately 25% of the seawater pumped to the plant location is transformed into freshwater, allocating this fraction of the cost to the water. The total cost of the power block is also mainly allocated to the electricity with more than 80% for both cases; similarly, the PV plant total cost is mainly allocated to the electricity (96%), while the MED total cost is almost wholly allocated to the water (99%). Hence, the operation and performance of the plant with the PV integration have a minor impact on the allocation of the electricity and water costs. Nevertheless, it worth to mention that the P/R system cost is composed of 95% of the cost of the two pipelines, which is associated with the length of the pipeline required. Therefore, the location of the plant with respect to the sea has a crucial

role in the P/R system cost and the contribution of this system to the cost of the products, which can lead to lower costs if that distance is reduced.

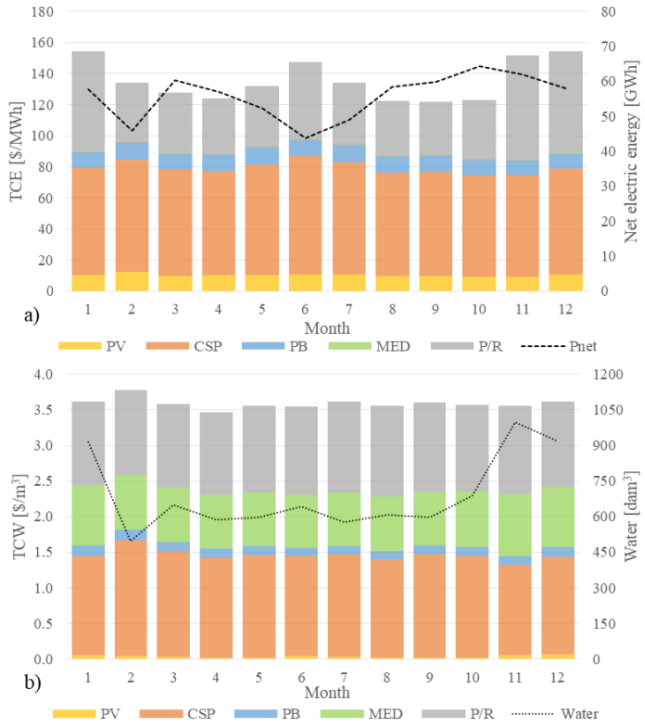

Figure 3-10: Monthly (a) TCE and (b) TCW considering the allocation of the PV, CSP, PB, MED, and P/R systems costs of the CSP+PV+MED plant.

The contribution of the cost of the main systems to the annual TCE and TCW for both plants is shown in Table 3-4. From the results, it is observed that the PV integration allows decreasing the TCE by 25%, while the TCW increases by 11%. Thus, the PV system integration main advantage is that the net output of electricity is increased, considering only a slight increase in the plant cost, which finally reduces the TCE dramatically. On the other hand, the CSP and MED plant operation are affected by the PV integration, which, in this case, reduces the water production. In contrast, the water maintains a similar cost allocation, so the TCW finally increases. Furthermore, the CSP+PV+MED plant could also improve the performance of the CSP and MED plant with smaller sizes of the PV plant, increasing the water production, which would result in a benefit on the TCW regarding the cost increase.

Table 3-3: Distribution of the PV, CSP, PB, MED, and P/R total costs to the electricity and the water costs in MM$ of the CSP+MED plant and CSP+PV+MED plant.

		Cost	PV	CSP	PB	MED	P/R	Total
CSP+MED	Total Cost	MM $	0	501.26	67.69	56.90	354.96	980.81
	Annualized cost	MM $	0	57.64	7.79	6.61	40.84	112.88
	Electricity	MM $	0	44.63	6.29	0.05	29.89	80.85
		%	0.0%	77.4%	80.7%	0.8%	73.2%	71.6%
	Water	MM $	0	13.02	1.50	6.56	10.95	32.03
		%	0.0%	22.6%	19.3%	99.2%	26.8%	28.4%
CSP+PV+MED	Total Cost	MM $	61.83	501.26	67.67	56.90	355.82	1043.48
	Annualized cost	MM $	7.11	57.60	7.79	6.61	40.94	120.05
	Electricity	MM $	6.82	45.92	6.72	0.05	30.87	90.37
		%	95.8%	79.7%	86.3%	0.8%	75.4%	75.3%
	Water	MM $	0.30	11.68	1.07	6.56	10.06	29.67
		%	4.2%	20.3%	13.7%	99.2%	24.6%	24.7%

Table 3-4: Contribution of the PV, CSP, PB, MED, and P/R systems costs to the annual TCE and TCW of the CSP+MED plant and CSP+PV+MED plant.

		Cost	PV	CSP	PB	MED	P/R	Total
CSP+MED	Electricity	$/MWh	0	99.00	13.94	0.12	66.31	179.38
		%	0.0%	55.2%	7.8%	0.1%	37.0%	100.0%
	Water	$/m^3	0	1.31	0.15	0.66	1.10	3.22
		%	0.0%	40.6%	4.7%	20.5%	34.2%	100.0%
CSP+PV +MED	Electricity	$/MWh	10.20	68.71	10.06	0.07	46.20	135.24
		%	7.5%	50.8%	7.4%	0.1%	34.2%	100.0%
	Water	$/m^3	0.04	1.41	0.13	0.79	1.22	3.59
		%	1.0%	39.4%	3.6%	22.1%	33.9%	100.0%

3.5.3 Sensitivity analysis

The operation and performance of the plant are affected by the configuration in terms of PV plant size, the CSP plant size (solar multiple and TES hours), and the number of MED units. According to the selected configuration, the operation and costs distribution would be different, which would change the annual TCE and TCW. Thus, a unidimensional analysis of the CSP+PV+MED plant has been firstly carried out, aiming to determine the impact of the selected configuration on the performance and costs. Secondly, a multivariable parametric study has been performed to find out which configurations would allow decreasing both the TCE and TCW.

3.5.3.1 CSP+PV+MED plant unidimensional analysis

The unidimensional analysis was carried out considering the base case exposed in section 5.1. Figure 3-11 presents the annual energy balance of the plant and the water production, varying the PV size, the solar multiple (SM), the TES hours, and MED units.

In Figure 3-11a, it is observed that the net output electricity increases as the PV plant size is larger, showing that the PV dumped energy increases considerably from 125 MW onwards. In contrast, the electricity production by the CSP plant and the water production decreases from 75 MW up to 150 MW PV size, in which the power block and the MED plant operation hours are mainly limited to the night. Conversely, it is observed that the water production reaches a maximum for a PV size of 50 MW. For this size, the power block operates at more than 50% of the part-load, which allows the operation of the MED plant. Also, more energy is stored in the TES system during the day, which enlarges the operation hours of the MED plant. In Figure 3-11.b and 11.c, it is observed that the electricity production of the CSP plant is increased for larger SM and TES hours, which in turn leads to a rise in water production.

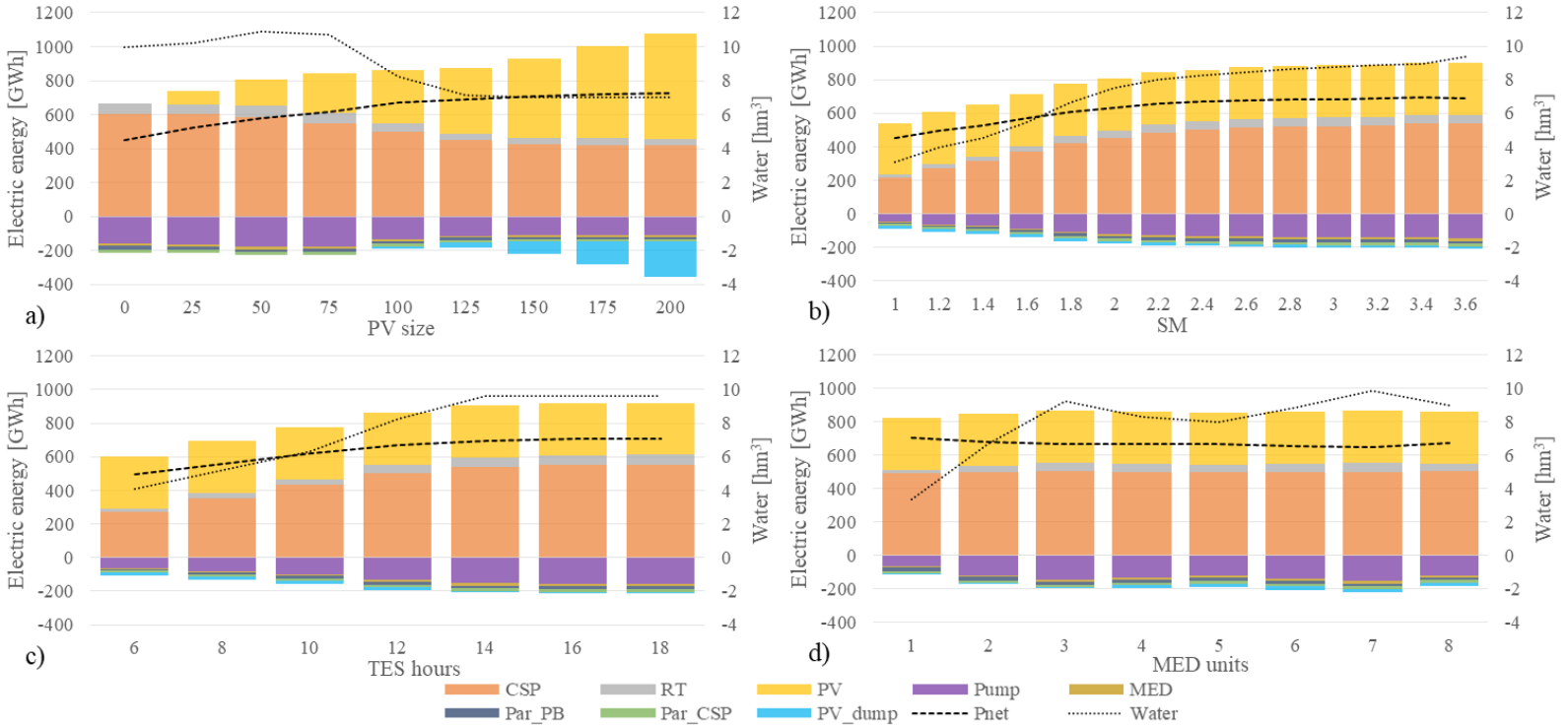

Figure 3-11: Annual electric energy distribution and water production in a unidimensional parametric analysis varying: (a) PV size, (b) SM, (c) TES hours, and (d) MED units, considering a base case configuration with 100 MW of PV, 12h of TES, a SM of 2.4 and 4 MED units.

Figure 3-11.d shows that the net electricity output remains stable with changes in the number of MED units. In contrast, water production presents an increase when the number of units varies from 1 to 3, and it remains in similar output as the number of units is increased above those values. This effect can be explained by the water capacity factor, which is represented in Figure 3-12 for a different number of units, alongside the water production. Capacity factor of around 90% is achieved for a number of units between 1 and 3; however, above three units, it starts to decrease dramatically. For a lower number of units, the thermal energy required by the MED plant decreases, so the power block can provide enough thermal energy even at minimum part-load, increasing the operational hours of the MED plant. From four units onwards, the MED plant starts to operate more hours in winter mode, decreasing its capacity factor. For the maximum number of units, the MED plant works practically only at the night hours, and the capacity factor is the minimum one.

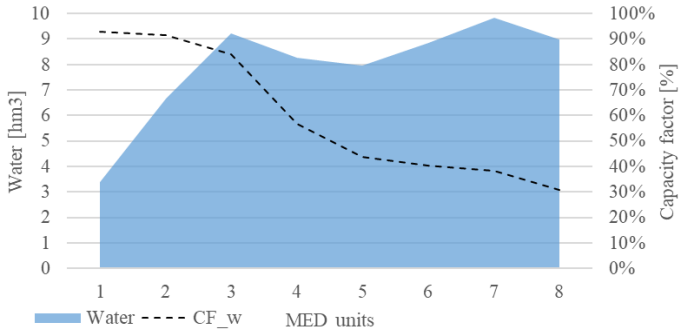

Figure 3-12: Water production and water capacity factor for the different MED units.

In terms of the cost results, Figure 3-13 presents the contribution of the main systems to the TCE and TCW for the unidimensional analysis. In first instance, Figure 3-13.a and Figure 3-13.b show that the PV sizing has a relevant impact on the TCE and TCW. In Figure 3-13.a it is observed that the TCE decreases, and the PV cost contribution increases for larger PV sizes, obtaining a minimum TCE at a PV size of 150 MW, where the PV dumped energy is compensated by the low costs of the PV plant. In contrast, in Figure 3-13.b it is observed that TCW inversely varies to the water production, obtaining a minimum TCW at 50 MW PV size, in which the water production is maximized. This occurs because the PV sizing affects the CSP and MED operation hours despite the fact the PV cost contribution is

negligible. Therefore, the PV sizing presents a contradictory role between the TCE and TCW.

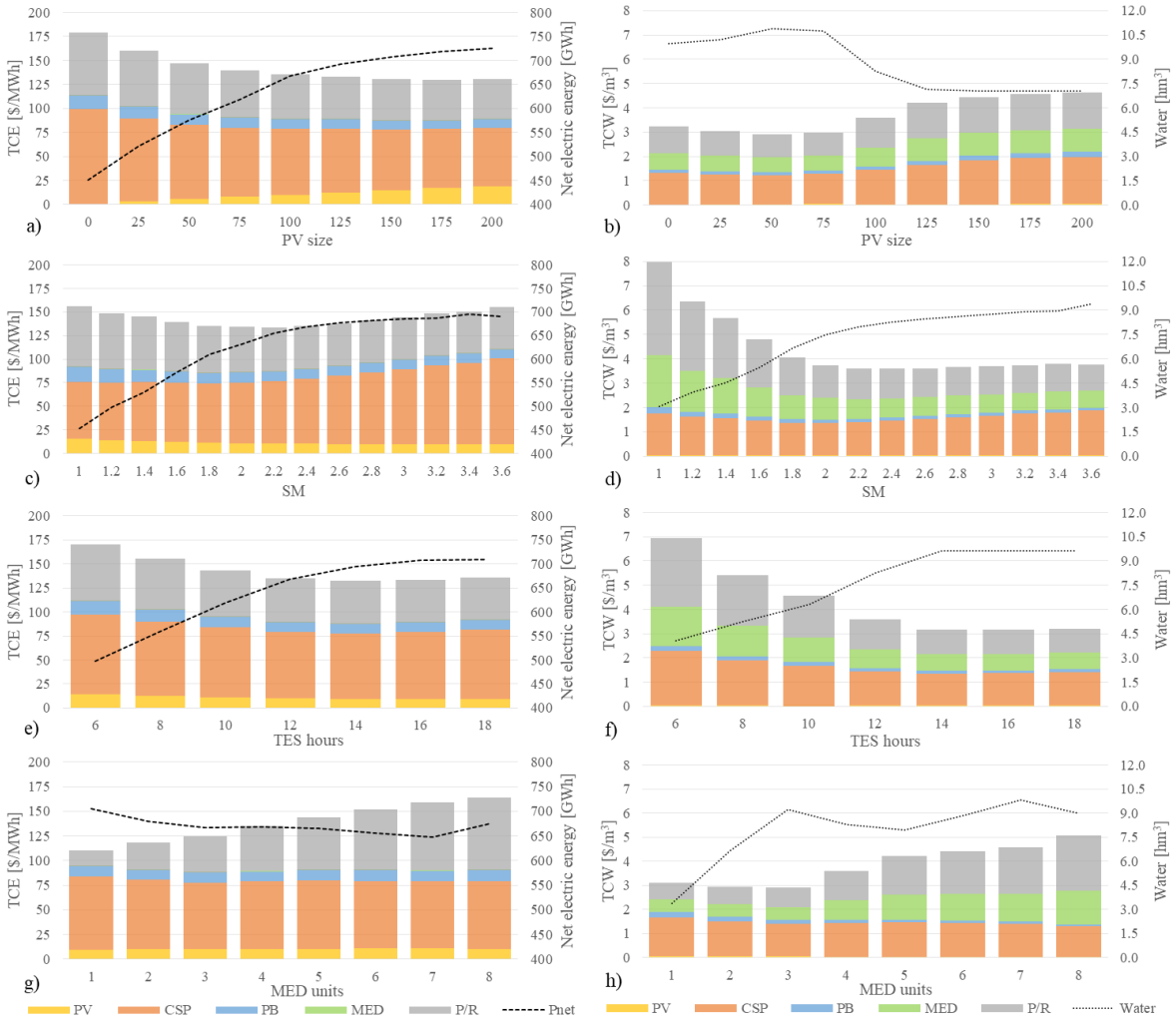

Figure 3-13: Annual contribution of the PV, CSP, PB, MED and P/R systems costs in the TCE (a, c, e, g) and TCW (b, d, f, h) at the unidimensional parametric analysis varying: (a, b) PV size, (c, d) SM, (e, f)TES hours, and (g, h) MED units, considering a base case configuration of 100 MW of PV, 12 h of TES, 2.4 of SM and 4 MED units.

In the case of the CSP plant size, it is observed that the TCE reaches a minimum for a SM of 2.2 and 14 hours of TES (Figure 3-13.c and Figure 3-13.e), compensating the high CSP cost with the electricity production. In contrast, Figure 3-13.d and Figure 3-13.f show that the TCW tends to be lower as SM and TES hours are higher, and vice versa as SM and TES

hours are lower and the water production decreases. In addition, the CSP cost contribution varies moderately for high SM and TES hours, evidencing the existence of a tradeoff between the increase of the CSP cost, the solar dumping in the solar field in summer months, and the increase of water production throughout the year. Following this, there is an optimum configuration of the CSP plant to achieve a minimum TCE. However, it is required an oversized CSP plant to increase the water production, achieving the minimum TCW.

Regarding the MED units, it is observed that the minimum TCE is found for 1 unit (Figure 3-13.g), for which the contribution of the P/R system is the lowest. However, for a higher number of units, the contribution of the P/R system significantly increases, also causing a rise in the TCE. Conversely, it was found a minimum TCW for 3 MED units (Figure 3-13.h), whereas the TCW gradually increases with a higher number of units. Therefore, the lowest TCW would be found for a configuration that allows the MED plant to have a capacity factor over 85%. This configuration could be achieved with a combination of small PV plants and a large CSP solar field, but the number of MED units also has an essential role since it can change their performance according to the operation mode of the plant (summer or winter mode).

3.5.3.2 Multivariable parametric analysis

The parametric analysis was performed considering four configuration parameters of the plant (PV size, SM, TES hours, and MED units) within the range and the steps described in Table 3-5. The analysis considered 7056 configurations in total. Figure 3-14 presents the results of TCE versus TCW clustered by the PV size and the MED units.

In Figure 3-14.a, it is observed that the configurations with lower PV size (under 50 MW) achieve the lowest TCW; however, it presents TCE higher than 130 $/MWh, while with the PV size increasing, the scattered points are moved to lower TCE and higher TCWs. Moreover, it is observed a frontier where the lowest TCW (around 4 $/m^3) for a PV size above 125 MW is located. For these PV sizes, the power cycle is shut down during the day, limiting the operational hours of the MED plant. On the contrary, in Figure 3-14.b, it is

observed that the lowest TCEs are found for one MED unit. For higher MED units, the scattered points present higher TCEs with lower TCWs, showing that the cost of the P/R system is significant for the electricity cost.

Table 3-5: Parametric multivariable parameters

Parameters	Unit	Range	Step
PV size	[MW]	0-200	25
SM	[-]	1-3.6	0.2
TES hours	[h]	6-18	2
MED units	[-]	1-8	1

Moreover, it is evident the existence of a Pareto frontier between the objective functions, the TCE and the TCW. Throughout this frontier, it is observed that the PV size gradually increases, while the MED units go from 1 for the lowest TCE to 5 for the lowest TCW. Furthermore, the configurations on the Pareto front are the results of a complex balance between the performance of the plant (electricity production, water production, PV dumped energy and solar field dumping) and the cost and thermoeconomic analysis (mainly the PV cost, CSP and P/R system cost). In Figure 3-14.a, five points were selected along the frontier to analyze the different configurations considering both TCE and TCW. The detail of each case configuration is described in Table 3-6.

The results described in Table 3-6 indicate that the configuration that gives the minimum TCW (case 1) is a combination of a small PV plant with an oversized CSP plant and a large MED plant (5 units), while the configuration with the minimum TCE (case 5) is a combination of a large PV plant with an undersized CSP plant and only one MED unit. Cases 2, 3, and 4 are between the two formers configurations mentioned and show that the tendency of the PV plant size is just the opposite to the trend of the CSP+MED plant size.

Table 3-6: Configuration and energy and thermoeconomic parameters of the five optimum configurations selected.

Case	PV [MW]	SM [-]	TES [h]	MED [units]	Electricity [GWh]	Water [hm^3]	CF_{el} [%]	CF_w [%]	C_{el} [MM $]	C_w [MM $]	TCE [$/MWh]	TCW [$/$m^3$]
1	50	3.4	16	5	723.88	16.48	82.63	90.31	106.18	42.84	146.68	2.60
2	75	3	16	3	749.74	10.29	85.59	93.99	96.78	27.58	129.08	2.68
3	100	2.2	14	1	714.33	3.36	81.54	92.12	77.00	10.25	107.80	3.05
4	125	1.8	12	1	686.98	2.40	78.42	65.82	69.97	9.69	101.85	4.03
5	150	1	8	1	578.99	1.29	66.09	35.26	54.45	7.75	94.04	6.02

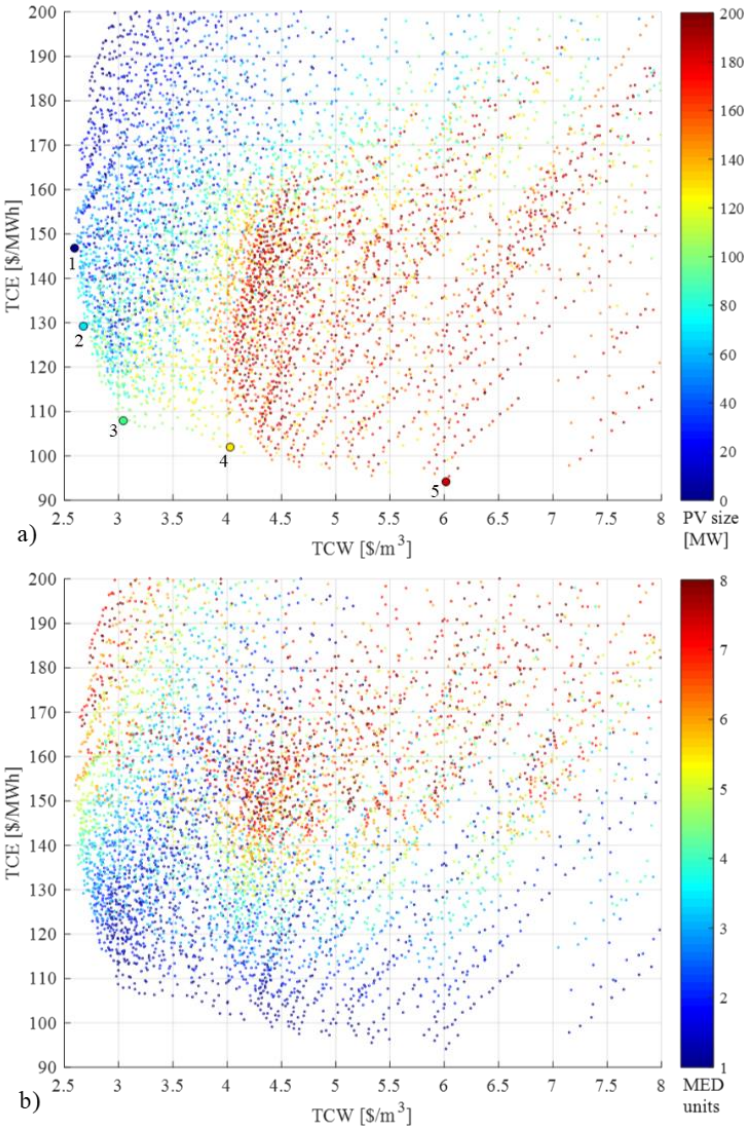

Figure 3-14: TCW versus TCE of the CSP+PV+MED plant for different PV plant size (a) and the number of MED units (b). Circle marks represent five optimum configurations.

Finally, Figure 3-15 shows the energy balance, the water production, and the TCE and TCW for each case. It is observed a noticeable difference in the distribution of the electricity generation between the cases analyzed (Figure 3-15.a). The case 1 presents a significant contribution from the CSP plant generation to the annual energy, also with a large parasitic consumption, while the case 5 has the main contribution of electric production from the PV plant, with a negligible parasitic consumption and a small amount of dumped energy. In terms of costs, it is observed that the TCE (Figure 3-15.b) is influenced by the P/R system

cost that has a higher contribution to the electricity cost if the water capacity factor and the number of the MED units are higher (case 1). Likewise, the TCW (Figure 3-15.c) is mainly affected by the lower water capacity factors, which increases the cost rate of the MED and P/R system components (case 5), thus raising the water cost.

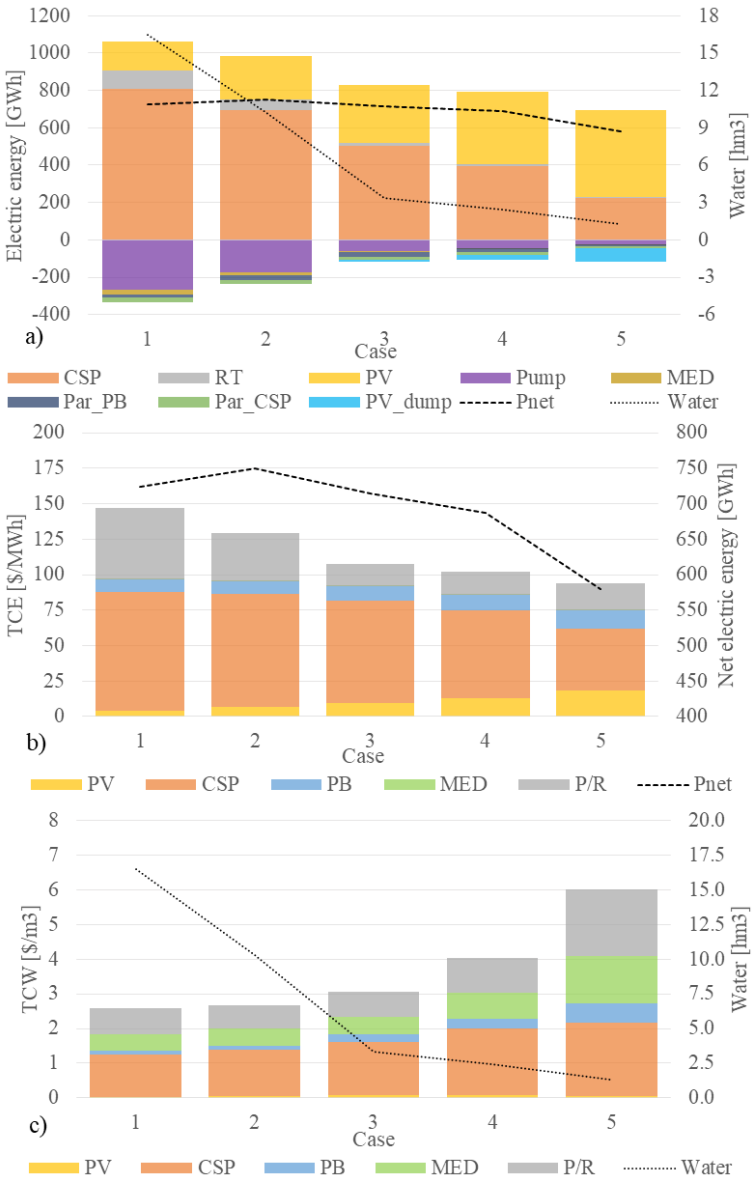

Figure 3-15: (a) Annual energy balance and water production, (b) TCE, and (c) TCW with cost compositions for the 5 cases selected.

The results summarized in Table 3-6 also indicates that the power and water capacity factors tend to increase from case 5 to 3, while the number of MED units remains constant in 1 unit. However, from case 3 to 1, the capacity factors remain stable even though the MED units increase, which also raises the MED plant capacity; and therefore, the water production. Finally, it is evidenced that the PV plant integration allows to increase the production of electricity and to decrease the costs of the products, but depending on the PV plant size, it can benefit or hinder the operation of the CSP+MED system, and by consequence the water production. Furthermore, it was obtained a significant difference in the water production between all the cases, going from 1.3 to 16.5 hm^3, while the net electricity output varies between 579 to 724 GWh, which indicates that the demand requirements could play an important role in defining an adequate configuration.

3.6 Conclusion

The operation and performance of a CSP plant of 100 MW_e integrated with a PV and a MED plant have been assessed. A detailed thermoeconomic analysis has also been performed to analyze the distribution of the costs of the components in the products: electricity and water. The analysis was carried out considering an hourly simulation of the plant to take into account the irradiation and meteorological data variation and their effect on the operation of the plant. Main conclusions are presented as follows:

- The performance results indicate that PV integration to the CSP+MED plant mainly increases the net output electricity of the whole plant. Yet, as the secondary effect, it increases or decreases the water production depending on the PV and the CSP plant size. Moreover, two operation modes of the plant were identified for the PV integration: the summer mode, in which the CSP plant and MED plant work continuously 24 hours with some of them at part-load, and the winter mode, where the CSP plant is turned off during the day, and the MED plant works fewer hours, reducing the daily water production.
- The thermoeconomic results show that the TCE is significantly reduced with the integration of the PV plant to the CSP+MED plant. However, the effect in the TCW is mostly related to water production, since the water presents almost the same cost

allocation. Therefore, the impact of the PV integration on the TCW will finally depend on the operational hours of the MED plant.

- Regarding the results of the unidimensional analysis, it was obtained a minimum TCE for a large PV plant (150 MW), where the PV dumping is compensated by the low PV cost, and a minimum TCW for a small PV plant (50 MW), where the water production is maximized. Moreover, the minimum TCE was found for optimum configurations with medium or small CSP plants, while the minimum TCW was obtained for large CSP plant sizes with high SM and TES hours. Therefore, the PV and the CSP plant size present contradictory roles between the TCE and TCW. Furthermore, the numbers of MED units have an important role since it influences the plant operation and the P/R system cost. In this way, the minimum TCE is achieved with the minimum number of MED units, while the lower TCW can be reached with medium or high number of MED units with PV-CSP configurations that achieve a water capacity factors over 85%.
- The multivariable parametric analysis shows a Pareto frontier between the TCE and the TCW that evidences a solution space where both costs can be reduced. It was found that the best configuration in terms of minimum TCW is a combination of a small PV plant with an oversized CSP plant and a large MED plant (5 units), while the best configuration in terms of minimum TCE is a combination of a large PV plant with an undersized CSP plant and only one MED unit.
- The results have demonstrated the impact of the PV integration with a CSP+MED plant, using a methodology that allows assessing the actual allocation of the system costs into the products. These systems have a high complexity level; so, the methodology presented herein contributes to a proper assessment, considering several design parameters and independent variables related to the location. Beyond that, the analysis can be used as a design tool on a case-by-case basis.
- The plant location has shown to be a relevant factor due to the pumping consumption and the P/R system cost (second-highest system cost that is mainly composed of the two pipeline costs). However, locations closer to the coast may present lower radiations levels, which directly affects the PV and CSP production. These variables

would change the thermoeconomic results and the configuration that would achieve the lowest TCE and TCW. However, the trade-off found in the Pareto frontier between the PV size, and CSP and MED size would be maintained. Therefore, further studies should analyze the impact of the altitude and distance from the coast versus the solar radiation of different locations in the thermoeconomic analysis of these systems.

4. COMPARATIVE ANALYSIS BETWEEN HYBRID CONCENTRATING SOLAR POWER + PHOTOVOLTAIC PLANT INTEGRATED WITH MULTI-EFFECT DISTILLATION AND REVERSE OSMOSIS DESALINATION PLANT

4.1 Introduction

In recent years, desalination processes have become one of the most important options to achieve a reliable water supply in vulnerable or water-stressed regions (Nassrullah, Anis, Hashaikeh, & Hilal, 2020). An example of this is the worldwide desalination operating capacity that is around 95 million m^3/day, growing with an annual rate of 7% in the last ten years (Eke, Yusuf, Giwa, & Sodiq, 2020). The reverse osmosis (RO) process dominates this market, accounting for 69% of the produced water volume (Abdelkareem et al., 2018; Jones, Qadir, van Vliet, Smakhtin, & Kang, 2019), mainly because of its continuous specific energy consumption reduction. In contrast, thermal desalination has around a 25% share of the installed capacity but still has room to get competitive costs in the next few years if certain technological improvements are implemented. The integration of thermal desalination into dual-purpose solar power plants is one of the leading research topics in the last years (Mohammadi et al., 2019; Nassrullah et al., 2020; Omar et al., 2020a; Shahzad et al., 2017).

Several studies and reviews have shown the potential of the Concentrating Solar Power (CSP) with Multi-Effect Distillation (CSP+MED) concept (Aboelmaaref et al., 2020a; Mohammadi et al., 2019). However, some market barriers have been identified for its commercial deployment. Among them, it can be highlighted the high capital cost of the system (mainly related to the CSP plant), the technology integration development to reduce the specific energy requirements, and the conservative market approach from the desalination industry (Alhaj & Al-Ghamdi, 2019; Mohammadi et al., 2019; Omar et al., 2020a). Also, a critical drawback of the CSP+MED plant is the misalignment of the optimal

location between the power and desalination plants since they must be co-located (Alhaj & Al-Ghamdi, 2019). Thus, techno-economic analyses should consider relevant factors of the site, such as the direct normal irradiation (DNI) levels, the water salinity, and the distance from the shore of the plant (Mohammadi et al., 2019).

Several studies about the integration of MED and RO into CSP plants have been performed, proving that the CSP+MED system can be competitive in some specific conditions. Laissaoui et al. (Laissaoui, Palenzuela, Sharaf Eldean, Nehari, & Alarcón-Padilla, 2018) conducted a techno-economic comparative analysis of a RO plant integrated into either a CSP or a PV plant in Algeria, obtaining that the best integration was with a CSP plant that includes 14h of thermal storage, resulting in a water cost of 0.85 $/m^3. Palenzuela et al. (Palenzuela, Alarcón-Padilla, et al., 2015b; Palenzuela, Zaragoza, et al., 2015; Palenzuela, Zaragoza, Alarcón-Padilla, & Blanco, 2013) studied the performance of CSP+MED and CSP+RO plants at different geographical locations (South of Europe and MENA regions), considering the differences in salinity and solar irradiation as the only geographical parameter. They concluded that the geographical location has a relevant role, placing the CSP+MED system in a better position than CSP+RO in the case of high salinity locations. Casimiro et al. (Casimiro et al., 2013) modeled a CSP+MED plant and compared its performance to other conventional condenser schemes in San Diego, USA, where the plant was located close to the coast (600 m). The results showed that the proposed scheme could be feasible due to the electric production is reduced only by 5%. Olwig et al. (Olwig et al., 2012) performed a techno-economic analysis of a CSP+MED and CSP+RO plant in Israel and Jordan, assuming that the CSP is located near the coast (<5 km). The study considered the solar irradiation, seawater salinity, and its temperature profile as geographical parameters, and a feed-in tariff for the electricity in the techno-economic analysis is taken into account, so the water cost strongly depended on the price of electricity. Sharan et al. (Sharan et al., 2019) assessed the performance of a CSP+MED plant using a supercritical CO_2 Brayton power cycle, in which the MED plant is integrated into the power cycle through two heat exchangers. Six coastal sites were analyzed only considering the solar irradiation as the geographical parameter difference, obtaining competitive water costs in some cases compared to the RO configuration, with values between 1.1 $/m^3 and 1.5 $/m^3. Hoffmann

and Dall (Hoffmann & Dall, 2018) performed a techno-economic study of a CSP+MED plant in Namibia, considering only one site located 50 km inland. The results showed that the seawater pumping is a primary contributor to the water cost, and the MED plant integration is not cost-competitive compared with a RO plant located at the coast, obtaining water cost 0.7 $\$/m^3$ higher.

The authors of the present article have already worked in techno and thermoeconomic analysis of CSP+PV+MED plants (Mata-Torres, Escobar, & Cardemil, 2018; Mata-Torres et al., 2017, 2020, 2019a; Valenzuela et al., 2017), with only the seawater conveyance considered as a geographical parameter. Concretely, in the study (Mata-Torres et al., 2017), a techno-economic analysis is carried out for a CSP+MED plant with Parabolic Trough Collectors, considering only one location in Chile and Venezuela. Later, Valenzuela et al. (Valenzuela et al., 2017) perform a techno-economic analysis of a CSP+PV+MED plant in northern Chile, focusing on the operational synergy between the hybrid PV+CSP plant and MED plant. However, the conveyance and geographical parameters were not considered. After that, in (Mata-Torres, Escobar, et al., 2018), an analysis of a CSP+PV+MED is carried out, where is considered the conveyance system. The study uses a techno-economic analysis approach, where only the electricity used as the parasitic consumption was allocated to the water cost. Following that, in (Mata-Torres et al., 2019a), a thermoeconomic analysis is introduced focused only on a Rankine Cycle integrated into a MED plant, assessing the impact of the part-load operation, ambient temperature, and plant location altitude for determining the cost allocation to the electricity and water. Lastly, in the study (Mata-Torres et al., 2020), an annual thermoeconomic analysis of a CSP+PV+MED plant for a location at 100 km inland was performed, showing the impact of the PV integration, concluding that the pipelines and seawater pumping cost were relevant factors that increased both plant costs by more than 25%.

From the previous literature review, it can be seen that the variables associated with the plant location are not usually taken into account in the CSP and desalination (CSP+D) assessment studies. Some studies have considered one of these parameters (distance from the coast, altitude, different DNI levels), but none have studied the possible effect of several

parameters together considering different locations respect to the coast for a specific site demand. The impact of these variables could be relevant in the performance of the plant since additional electricity consumption must be considered in the power balance that is linked with significant capital expenditure, affecting the final cost of the plant's products. Also, various plant locations would have different costs, being the inland locations those ones that could obtain higher electricity and water prices because of the seawater conveyance. However, these locations could benefit from the higher DNI levels to increase the productivity. In order to compare the plant performance at different locations, the water demand location (industry or urban) and the respective distribution system should be considered to transport the produced water. In addition, it is crucial to carry out the CSP+PV+MED assessment with a thermoeconomic method since it is an option that allows determining the cost allocation of the products, i.e., electricity and water. Also, as the plant configuration has a crucial role in the performance, an optimization of the sizing parameters can give an insight about the ideal configuration that would have the most competitive cost. Finally, several works have already been published showing the difference between the MED and RO integration as well as the cost comparison in different scenarios (Hoffmann & Dall, 2018; Olwig et al., 2012; Omar et al., 2020a; Palenzuela, Alarcón-Padilla, et al., 2015b; Sharan et al., 2019). However, it is still necessary to understand how the cost allocation under different geographical parameters is, which are the influence of these parameters on the performance and the cost formation, which is the optimal sizing of the plant, and how much the cost breach between the technologies is. The answer to all these questions will allow defining the optimal sizing and the strategic location of a CSP+PV+MED plant and the required improvements to make this concept competitive versus the CSP+PV+RO.

This work intends to fill these literature gaps presenting a thermoeconomic comparison between MED and RO processes when they are integrated into a hybrid CSP+PV plant to produce electricity and water. The aim is to assess the performance and cost differences between RO and MED integration into a CSP+PV plant under different situations, which will result in relevant information about the potential of these cogeneration schemes. It has been carried out by assessing the differences in the cost formation process and analyzing the technical and economic impact over the product costs for both technologies. The study

considers different meteorological (irradiation) and geographical (distance and altitude of the plant and demand locations) conditions. For that, different plant locations and three demand locations in Chile where the water is delivered have been considered: a coastal city, an inland mine (high altitude), and an inland city (average altitude). A multi-objective optimization procedure of the plants (CSP+PV+MED and CSP+PV+RO) has been performed to determine the optimum sizing that allow reducing the cost and maximizing the production (water and electricity) in terms of the design parameters (the size of the PV plant, solar multiple, thermal energy storage capacity, and the number of MED/RO units). Finally, a cost sensibility analysis of the CSP+PV+MED plant has been carried out in order to analyze the cost reduction effects and obtain the best combination that allows making the CSP+PV+MED plant competitive versus the CSP+PV+RO plant.

4.2 System description

The systems considered are shown in Figure 4-1: a MED unit integrated into a hybrid CSP+PV plant (CSP+PV+MED system) and a RO unit integrated into a hybrid CSP+PV plant (CSP+PV+RO system), both delivering a net power output of 100 MW_e, not including the auxiliary and parasitic power consumption of the plants.

The CSP plant consists of a central receiver solar tower with a two-tank molten salt direct thermal energy storage (TES) system. The heliostat solar field configuration and the receiver geometry are determined in terms of the Solar Multiple (SM - the ratio between the thermal power provided by the solar field and the thermal power required from the power block at the nominal design point). The power block (PB) consists of a Rankine cycle with a high-pressure and a low-pressure turbine (a condensing turbine is included as it provides the lowest electrical penalty), a reheater, an air-cooled condenser (ACC), and three extractions (two of them going to Close Feed-Water heaters – CFWH – and one to a deaerator). The ACC is selected due to the limited availability of water at the CSP plant location. The PV plant consists of a modular 1 MW_e plant, which is scalable accordingly to the number of inverters, with silicon mono-crystalline modules and a one-axis tracking system. The latter is connected in parallel to work in synergy to fulfill all the parasitic consumption and

delivering a baseload capacity. Table 4-1 shows the design and nominal parameters of these systems. More details can be found in (Mata-Torres et al., 2020, 2019a).

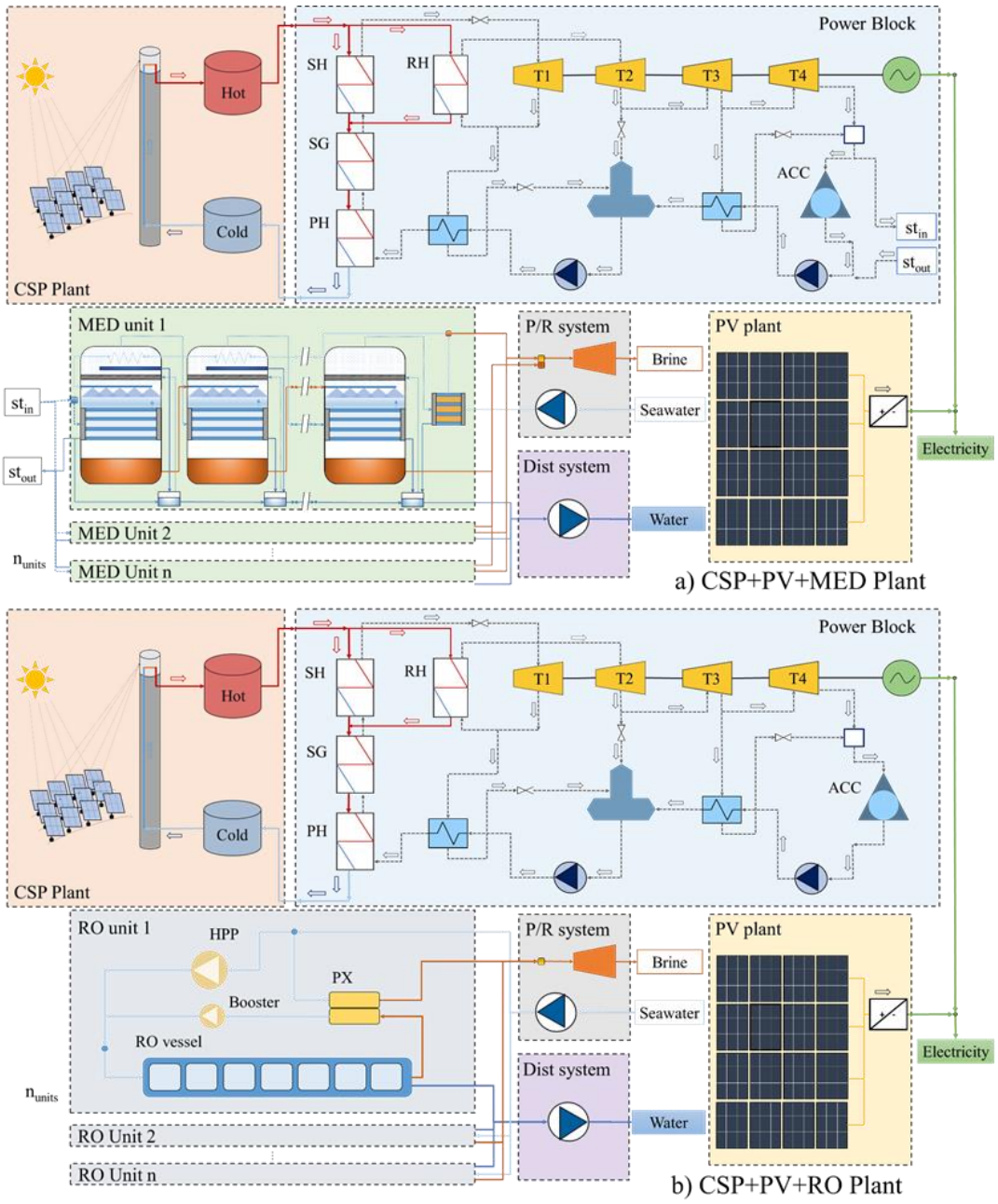

Figure 4-1: Diagram of the CSP+PV+MED (a) and the CSP+PV+RO plant (b) [22], where the specific components are: steam turbine (Ti), air-cooled condenser (ACC), superheater (SH), steam generator (SG), economizer or preheater (PH), reheater (RH), high-pressure pump (HPP), pressure exchanger (PX) and booster pump (Booster).

Table 4-1: Design and nominal parameters of the CSP, Power Block, and PV systems.

Parameter	Unit	Value
CSP plant		
Heliostat area	m^2	144
Reflectivity	%	95
Average soiling rate	%	10
Heliostat electric consumption	kW_e	0.055
Working fluid		Molten salt
Maximum HTF temperature	°C	565
Cold HTF temperature	°C	290
Power block		
Gross capacity	MW_e	110
Maximum pressure	bar	100
PV plant		
PV panel power	W	330
Modules in series	-	20
Number of strings	-	178
Inverter power	MW_e	1
Average soiling rate	%	10
Tracking system		1-axis

The MED plant is a forward-feed modular unit with a nominal capacity of 10,000 m^3/day, 14 effects, and 13 pre-heaters. The system can be scalable up to 8 units, a condition for which all the exhaust heat from the turbine is completely used. Conversely, the RO plant consists of a modular unit of 10,000 m^3/day, composed of several pressure vessels in parallel containing a determined number of membrane elements in series. The system can be scaled-up to 8 units in order to be comparable to the MED plant. The plant scheme considers a RO train, which is powered by a high-pressure pump. An energy recovery device (ERD) based on isobaric pressure exchangers (PX) and a booster pump are considered to recover the high-pressure energy from the brine. The design features and nominal parameters of these systems are presented in

Table 4-2. The integration of the desalination plant into the hybrid CSP+PV plant is established as follows:

- CSP+PV+MED: the MED plant uses the back turbine steam from the power block as the heat input, and it is connected in parallel with the ACC. The MED plant is firstly powered, and the remaining steam is condensed in the ACC. Additionally, the power consumption of the MED plant is directly taken from the CSP+PV plant. According to several studies, the MED coupling at the power cycle condenser has shown that it is the best integration option in the CSP+MED plant (Catrini et al., 2017; Leiva-Illanes et al., 2017, 2019; Palenzuela, Alarcón-Padilla, et al., 2015b).
- CSP+PV+RO: the RO integration is by its connection to the electric power generated by the hybrid CSP+PV plant. In this case, the ACC absorbs the full cooling requirement of the power block.

A pumping and recovery system (P/R system) between the sea and the desalination plant is also considered. It consists of a seawater pump and the pipeline required to transport the seawater to the desalination plant, and a disposal pipeline to return the brine. Depending on the head losses of the disposal pipeline and the altitude of the desalination plant location, it would require either a pump to transport the brine or a turbine to recover part of the potential energy of the brine. Finally, a distribution system (DIST system) to transport the water from the desalination plant to the demand location is considered, which consists of a pump station and a distribution pipeline.

Table 4-2: Design and operational parameters for the MED, RO, P/R, and DIST systems.

Parameter	Unit	Value
MED plant		
Unit capacity	m^3/day	10,000
Steam saturation temperature	°C	70
Seawater temperature	°C	20
Last effect temperature	°C	34
Seawater salinity	g/kg	35
Brine maximum salinity	g/kg	63
Nominal Gain Output Ratio (GOR)	-	10.11
Electric consumption	kWh/m^3	1.5
RO plant		
Membrane type		SW30HRLE-440
Number of Stages	-	1
Number of elements per vessel	-	7
Number of vessels per stage	-	80
Fouling factor	-	0.85
Pump efficiency	%	80
ERD Efficiency	%	95
Vessel flow rate	m^3/h	15
Seawater salinity	g/kg	35
Operating pump pressure	bar	63
Pressure loss before first element	bar	0.31
Seawater pumping pressure	bar	5
Pre-treatment pressure loss	bar	4
Piping pressure losses	bar	2
Control pressure losses	bar	1
P/R system and DIST system		
Pump efficiency	%	80
Recovery turbine efficiency	%	80

4.3 System modeling and simulation

The modeling and simulation of each case study were performed in Transient System Simulation (TRNSYS) software. The model was developed in a single TRNSYS deck to enable the integration of the different systems, and the quasi-dynamic simulations were carried out considering a Typical Meteorological Year (TMY) with an hourly resolution. Full detail of the models were presented in previous works of the authors (Mata-Torres et al., 2020, 2019a). In this section, a summary of the model of each component is described.

4.3.1 CSP+PV model

In the case of the CSP model, the heliostat field considers the efficiency in terms of sun altitude and azimuth, heliostat reflectivity, and soiling rate to calculate the incident power on the receiver. For the central receiver, a simplified model of a cylindrical receiver composed of tubes has been used. It calculates the flow rate of the heat transfer fluid (HTF) for a defined outlet temperature, considering the incident radiation, thermal losses, and the inlet HTF temperature. The TES system was modeled considering variable volume for the Hot and Cold tanks. The power block is modeled by a multi-variable regression that assesses the performance of the Rankine cycle operation at nominal and off-design conditions that is integrated to a TRNSYS type to perform faster simulations. For that, a parametric analysis of a power block model developed in Engineering Equation Solver (EES) was performed in terms of the HTF inlet flow rate and temperature together with the power block's condensing temperature. The model considers the variation of the heat transfer coefficients of the heat exchangers and the efficiency and pressures of both steam turbines under part-load operation. In the case of the PV plant, it was modeled considering a one-axis tracking system with a north-south orientation, using Type 190 of TRNSYS to assess the yield. All the mentioned models were used by the authors in a previous work (Mata-Torres et al., 2020), where a detail of the assumptions and control procedures of their operation can be found.

4.3.2 MED model

The model of the MED unit consists of a multi-variable polynomial regression that was obtained from the off-design assessment of a model already developed in EES, reported by the authors in (Mata-Torres et al., 2020). This EES model is based on the MED model proposed by Ortega-Delgado et al. (Ortega-Delgado, García-Rodríguez, et al., 2017) and evaluates the thermal performance of a 10,000 m^3/day MED through mass, energy, and heat transfer balances of all effects, preheaters, and end condenser. The design parameters in terms of the design conditions are firstly calculated. Then, a parametric analysis of the MED model unit at part-load operating conditions: thermal load between 40 and 100% (respect to the nominal steam mass flow rate), inlet steam enthalpy between 2550 and 2950 kJ/kg, and the seawater temperature between 10 and 30°C, is carried out to obtain a performance map of the plant. Finally, the regression model was computed with these data to be implemented in a TRNSYS type and integrated into the whole plant model. The model used in (Mata-Torres et al., 2020) was upgraded in this study by considering a variation of the last effect temperature with respect to the design condition (34 °C) by 1 °C for every 5 °C change on the seawater temperature with respect to the reference temperature (20°C). It allows accounting the variation of the MED plant last effect temperature with the seawater temperature variation during the year. This change has originated new coefficients that are presented in the APPENDIX A3.

For the integration of the MED unit, the assumptions and control procedures regarding the operation are explained in detail in (Mata-Torres et al., 2020). Besides that, for the TRNSYS quasi-dynamic simulation of the MED plant operation, a warm and a cold startup time were considered in the model, consisting in time delays in which the MED plant is powered to reach nominal operation temperatures, consuming thermal energy without producing water. The cold startup considers starting the MED plant from zero, assuming 3 hours for the startup (information obtained by discussions with MED plant operators). Whereas the warm startup consists in maintaining the vacuum in each of the effects, so the time to reach nominal or operational conditions to produce water is significantly lower (1 hour). It is considered that

the MED plant requires a warm startup if the plant has been stopped for less than 16 hours, and a cold startup in the opposite case.

4.3.3 RO model

The RO model is based on the one developed by (La Cerva et al., 2019), which considers the performance of pressure vessels in parallel with several membrane elements in series. It consists of an iterative process that takes the membrane properties and the inlet operational conditions (water salinity and temperature, pump pressure, feed flowrate). The model also considers the average concentration and pressure in each element of the vessel to simulate the water and salt fluxes. Furthermore, the variation of the pressure and the viscosity throughout the membrane elements, as well as the concentration polarization effect and the temperature correction factor, are considered. The seawater pressure losses are calculated using a friction factor typical for overlapped spacers, and the pressure drops in the permeate channel are neglected. The different feed seawater, permeate, and brine flow rates are calculated by multiplying the number of RO units.

On the other hand, the electric consumption of the RO plant is computed considering the performance of the RO pumps and PX. Specifically, the high-pressure pump increases the pressure of a fraction of the feed seawater. The other fraction (equal to the brine flowrate) increases its pressure by a PX, which recovers the remnant pressure of the brine, and then a booster pump raises it to the operating pressure. Additionally, the electric consumption of the intake, pretreatment, piping, and control losses are considered. The model was validated against the commercial software WAVE (Water Application Value Engine) (DuPont, 2020b). The RO model and validation are presented in APPENDIX A4.

The operational parameters of the RO model were selected considering the operating limits of the membrane (SW30HRLE-440) (Pohl, Kaltschmitt, & Holländer, 2009) and the design guidelines reported by the membrane manufacturer (DuPont, 2020a). Hence, a new TRNSYS type was developed for the RO model. The integration of the RO plant into the hybrid CSP+PV plant was carried out, connecting the RO plant electrically and allowing its

operation when the power generation of the hybrid plant is twice the nominal electric consumption of the RO process (equivalent to 3.1 kWh/m^3). When the RO plant is started, the water produced during the first hour is discarded. This is considered because the startup process requires some time to reach the nominal operation according to the manufacturer's recommendations.

4.3.4 P/R and DIST systems

The modeling process of these systems consists of calculating the head losses at the intake, discharge, and distribution pipelines and the overall height difference (potential energy) to determine the power consumption of the pumps and the electric power delivered by the recovery system (hydraulic turbine). The pipelines (intake, discharge, and distribution) geometry was defined by the length and the diameter. The length is determined by the distance between the coast, the desalination plant, and the demand site (Distance 1 and Distance 2 detailed in section 5), while the diameter was calculated in terms of the nominal flow rates and considering a maximum inner velocity of 2 m/s. In the case of the P/R system, both pipelines diameter (intake and disposal pipeline) were calculated in terms of the feed seawater mass flow rate. In the DIST system case, the distribution pipeline diameter was determined in terms of the produced water mass flow rate. Moreover, the mass flow rates depend on the number of MED/RO units, which increases the pipeline diameters as higher is the number of units evaluated.

The model computes the head losses using the Darcy-Weisbach equation by the evaluation of the friction factors in terms of the pipeline geometry together with the fluid properties (viscosity and density) and velocity for each time step. After that, it is calculated the power requirement by the pump or recovery system, respectively, considering the height difference. Finally, the electric consumptions and/or production were computed considering the efficiencies reported in

Table 4-2 and integrated into the electric power balance of the whole plant.

4.4 Methodology

In this section, the methodology used for the multi-objective optimization of the design configuration of the cogeneration plant is described. Among the different multi-objective optimization techniques, the genetic algorithm (GA) method has been used because it leads to an accurate assessment of the whole Pareto front (Chiandussi, Codegone, Ferrero, & Varesio, 2012). The GA consists of an evolutionary algorithm based on biological evolution principles, where a population of individuals is stochastically iterated to seek the Pareto-solutions (Collette & Siarry, 2003). Its main drawback is that it requires a large number of iterations, taking a considerable computational effort. This method has been widely used in similar optimization studies, where complex multi-variable energy systems with different technology combinations are optimized to produce various products (electricity, water, heat, cooling) (Ahmadi, Dincer, & Rosen, 2014; Ameri & Jorjani, 2016; Boyaghchi & Safari, 2017; Oyekale, Petrollese, & Cau, 2019; Sadri, Ameri, & Haghighi Khoshkhoo, 2017; Spyrou & Anagnostopoulos, 2010).

The complete methodology process includes four phases: firstly, the plant model (detailed in Section 3) is simulated in TRNSYS for a parametric analysis to obtain its annual performance in terms of the sizing parameters. Then, a thermoeconomic analysis (based on exergy and economic analyses) is performed in MATLAB in order to assess the value of the objective functions. Following this, a surrogate model (model that approximates the objective function results) of the TRNSYS simulation and thermoeconomic analysis in terms of the sizing parameters is implemented. After that, a multi-objective optimization using a genetic algorithm (GA) is performed considering two-objective and three-objective functions. The addition of the surrogate model approach allows decreasing drastically the computational time related to a GA and the complex thermal system simulations (Starke et al., 2018). Finally, a post-processing of the results, including a decision-making process, is performed using the Linear Programming Technique for Multidimensional Analysis of Preference method (LINMAP). Specifically, TRNSYS was used to integrate the whole

model and assess the annual performance in a transient simulation. EES was used to develop specific thermodynamic models (PB and MED plant) and compute the exergy analysis. MATLAB was used to perform the thermoeconomic analysis, the PB and MED regression models (with the EES output), the surrogate model, and the optimization.

4.4.1 Thermoeconomic analysis

The thermoeconomic analysis combines the thermodynamic and exergy assessment of the plant performance with the economic analysis, resulting in the cost formation process of the products. This analysis was performed in MATLAB using the results from the plant simulations. A low and medium-disaggregation level (the MED, RO, and P/R system were analyzed as a black box and the PV and CSP system by two or four components) was considered except the power block, in which a high-disaggregation level was established in order to accurately assess the cost formation of the electricity and the steam (Mata-Torres et al., 2019a). There were considered 100 exergy flows between the systems and its 43 components (4 for the CSP tower corresponding to the solar field, the tower receiver and two TES tanks, 20 for the power block, 2 for the PV plant, 1 for the MED plant, 1 for the RO plant, 2 for the P/R system, 1 for the DIST system, and 12 complimentary components). The modeling approach is described in detail on previous works developed by the authors (Mata-Torres et al., 2020, 2019a).

First, an exergy analysis was carried out for each energy and mass stream in the plant on an hourly basis: solar radiation, molten salts, steam, seawater, water, and brine streams. The physical exergy, which depends on the thermodynamic properties, was computed for all the streams. The potential exergy was included for those streams that present a considerable altitude change (seawater, water, and brine). Furthermore, the chemical exergy was considered only for the water and the brine streams. The waste exergy streams of the MED plant were included in the analysis.

Then, the thermoeconomic analysis was performed based on the method proposed in (Bejan et al., 1995; Lazzaretto & Tsatsaronis, 2006). In this method, the cost of each stream is

affected by the components' cost, exergy flows, destroyed exergy and wasted exergies. The method consists of a linear equation system that is composed of cost balances and auxiliary equations, which is solved by matrix computation. The cost balance associates the input and output thermoeconomic cost ($\dot{C}_{i,t}$) with the component cost rate ($\dot{Z}_{k,t}$) (eq. 4.1). Additionally, auxiliary equations are required to complete the equation system. These equations relate the unit thermoeconomic cost ($c_{i,t}$) of different streams according to fuel-product principles. The $c_{i,t}$ is obtained from the relation between the thermoeconomic cost and the exergy rate ($\dot{X}_{i,t}$) (eq. 4.2). The streams considered as the product of the plant are the net electricity output and the chemical exergy of the water at the demand location. Also, the destroyed exergy in MED/RO plant is considered, and the cost of residues/waste (brine and thermal exergy of water) is allocated to the components responsible for producing them, assigning the cost to the chemical exergy of water (product) (Mata-Torres et al., 2019a; Piacentino, 2015).

$$\sum \dot{C}_{in,t} + \dot{Z}_{k,t} = \sum \dot{C}_{out,t} \tag{4.1}$$

$$\dot{C}_{i,t} = c_{i,t}\dot{X}_{i,t} \tag{4.2}$$

Finally, the economic analysis was carried out to calculate the component cost rates ($\dot{Z}_{k,t}$) (Eq. 4.3). The total capital cost (${Z_k}^{Capex}$) and the annual operational and maintenance cost (${Z_k}^{Opex}$) are computed for each component in terms of the size and plant operation throughout the year (presented in APPENDIX A5).The amortization factor is considered with an interest rate of 5% and 30 years lifetime, and the annual operating time ($O_{time,k}$) is computed from the annual performance, taking into account the number of hours that each component works in the year.

$$\dot{Z}_{k,t} = \frac{A_f {Z_k}^{Capex} + {Z_k}^{Opex}}{O_{time,k}} \tag{4.3}$$

4.4.2 Objective functions

The optimization of the cogeneration plants' sizing aims to find the configuration that results in the lower cost of both products and higher electricity and water productivity. Therefore,

the optimization of the CSP+PV+MED and the CSP+PV+RO plants consider three key performance indicators as objective functions: the Thermoeconomic Cost of Electricity (TCE), the Thermoeconomic Cost of Water (TCW), and the Electric and Water Sufficiency ($Suf_{e\&w}$), which represents the annual production respect to the maximum possible production of both electricity and water. The parameters that determine the sizing of the cogeneration plants were the size of the PV plant, the SM of the solar field, the TES capacity in hours, and the number of desalination units (MED or RO units). The TCE and TCW functions were considered separate because it allows us not to consider any skew between the products cost and evaluate each cost product in terms of the unit in which they are quantified, rather than combined into one function if it used the unit product per exergy unit.

The TCE and TCW are calculated following Eq. 4.4 and Eq. 4.5, in \$/MWh and \$/m^3, respectively. Conversely, the $Suf_{e\&w}$ is calculated by Eq. 4.6 that considers the same weight for the electric and water capacity factors (CF_{el} and CF_w). The objective functions are defined as:

$$TCE = \frac{\sum_{t=1}^{8760} \dot{C}_{el,t}}{\sum_{t=1}^{8760} Elec_{i,t}} \quad (4.4)$$

$$TCW = \frac{\sum_{t=1}^{8760} \dot{C}_{w,t}}{\sum_{t=1}^{8760} Water_{i,t}} \quad (4.5)$$

$$Suf_{e\&w} = \frac{CF_{el}+CF_w}{2} \quad (4.6)$$

where $\dot{C}_{el,t}$ and $\dot{C}_{w,t}$ are the hourly thermoeconomic cost of the products in \$, $Elec_{i,t}$ is the net electricity production in MWh and $Water_{i,t}$ is the water production in m^3. The CF_{el} is calculated by the ratio between the total net electricity production and the nominal power of the plant (P_{net} = 100 MW$_e$) multiplied by the number of hours in a year (Eq. 4.7). At the same time, the CF_w (Eq. 4.8) is calculated by the ratio between the total net water production and the desalination unit capacity (W_{nom} = 10,000 m^3/day) multiplied by the days of the year and the maximum number of units allowable in both integrations (Units = 8).

$$CF_{el} = \frac{\sum_{t=1}^{8760} Elec_t}{8760 \cdot P_{net}} \quad (4.7)$$

$$CF_w = \frac{\sum_{t=1}^{8760} Water_t}{365 \cdot Units \cdot W_{nom}} \quad (4.8)$$

4.4.3 Surrogate model and validation

Solving GA optimization of the analyzed systems requires a large number of simulations of complex thermal systems to meet the convergence criteria, implying a very high computational time. To avoid that, a surrogate model was created for each objective function following the methodology developed in (Starke et al., 2018), which allows decreasing the computational time drastically from months to hours. The aim relies on performing the fitness evaluations with a process that approximates the objective function results obtained from the simulations.

The surrogate model was developed using the griddedInterpolant function of MATLAB with linear interpolation. A performance map of four-dimensions (4-D) is built, in which the axes are the sizing parameters, and the values of the multidimensional matrix are the objective function results for each combination. The model works interpolating within the values according to the sizing parameters evaluated. To do this, a parametric analysis of the plant was performed considering the four sizing parameters (PV size, SM, TES hours, and MED/RO units) with the constraints and steps described in Table 4-3. The parameters limits were adjusted with preliminary simulations (11,232 runs for each case) but maintaining a sufficiently discretized solution space. Finally, the objective function values obtained from the parametric analysis were used to build the performance maps. It should be noted that the parameter corresponding to the number of units of the MED/RO plants is rounded in the surrogate model since this variable must be an integral.

Table 4-3: Design parameter constrains for the parametric analysis.

Parameter	Unit	Range	Step
PV size	[MW]	0-120	10
SM	[-]	1.8-4	0.2
TES hours	[h]	10-18	1

MED/RO units	[-]	1-8	1

The surrogate models were validated against a random sample of 20% of the number of parametric runs within the sizing parameters' range. The Normalized Root-Mean-Square Deviation (NRMSD) was used to evaluate the errors between the simulated and the surrogate model results, obtaining a good agreement with NRMSDs under 1%.

4.4.4 Multi-objective optimization

The multi-objective optimization was performed using the *gamultiobj* algorithm of MATLAB (Mathworks, 2020), which uses a controlled, elitist GA (a variant of NSGA-II – Non-dominated Sorting Genetic Algorithm) to find the Pareto front. This algorithm favors individuals with better fitness values and helps to increase the diversity of the population. The setting parameters that were modified from the default value are presented in Table 4-4. Additionally, it was defined an initial population matrix composed of the optimal solutions of each objective function, and the decision variable boundaries were in terms of the sizing parameter constraints (Table 4-3). Hence, the optimization problem was formulated as follows:

Minimize: $f_1(\vec{x}) = TCE(\vec{x})$

Minimize: $f_2(\vec{x}) = TCW(\vec{x})$

Maximize: $f_3(\vec{x}) = Suf_{e\&w}(\vec{x})$

To find $\vec{x} = [PV_{size}, SM, TES_{hours}, MED/RO_{unit}]$

Subject to: $x_j^L \leq x_j \leq x_j^U$

Table 4-4: Setting parameters of the multi-objective GA.

Parameter set	Value
Solver	*gamultiobj*
Population size	600 (2-obj) - 1000 (3-obj)
Crossover fraction	0.8
Pareto fraction	1

Function tolerance	$1x10^{-5}$
Convergent tolerance	$1x10^{-5}$
Maximum generations	1600
Maximum stall generations	200

Two approaches were analyzed. First, the optimization with only two objective functions (*TCE* and *TCW*) was performed, in which the trade-off between both product costs is obtained. The second approach considers three objective functions, in which the $Suf_{e\&w}$ is included to assess the plant productivity with respect to the cost of the products. At last, the LINMAP algorithm was implemented to select an optimum solution and analyze its cost formation regarding other cases (Boyaghchi & Safari, 2017; Starke et al., 2018). This method computes the Euclidian distance of each point on the Pareto frontier from the ideal solution and selects the point with the minimum distance from the ideal solution, composed by the lowest TCE and TCW and highest $Suf_{e\&w}$ values (Arora, Kaushik, Kumar, & Arora, 2016). Figure 4-2 illustrates the process, showing the parametric analysis, the Pareto-solutions from the optimization, and the LINMAP solutions for one of the cases studied.

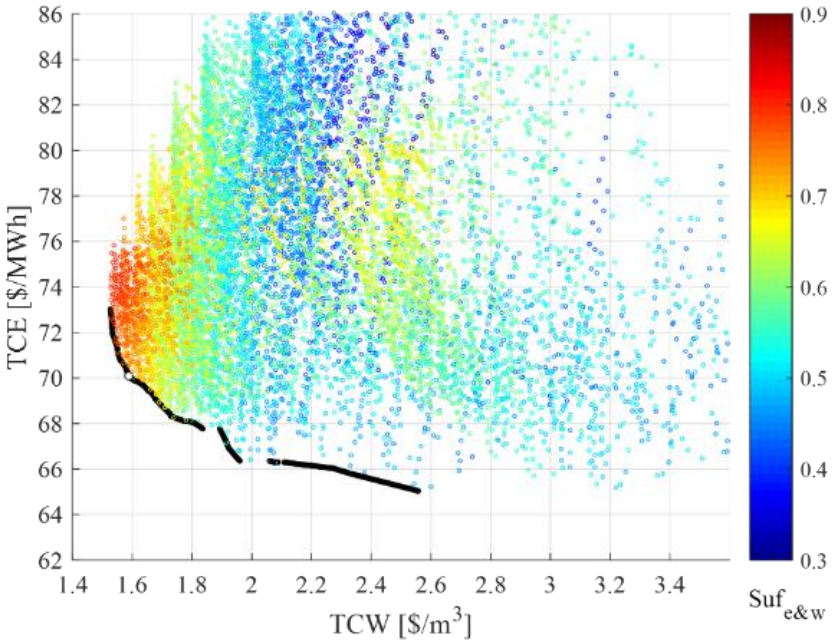

Figure 4-2: Parametric analysis and Pareto frontier of the 2-objective optimization, where the scattered point are the parametric analysis results, the black point are the Pareto-frontier and the white circle point is the optimal solution selected by LINMAP

4.5 Geographical and meteorological parameters of the plants

The study was performed considering three demand locations in northern Chile. The first is a city at the coast (Antofagasta), the second is an inland mine at high altitude (Atacama Mine), and the last is an inland city at a valley (Copiapó). However, the MED and RO plants integration into the hybrid CSP+PV plant imply different geographical locations of the systems that are explained below (Figure 4-3):

- CSP+PV+RO: the RO is powered by electricity only, so it is not required to be at the same location as the CSP+PV plant. Therefore, the RO plant is located 1 km far from the coast (Distance 1), in which the P/R system transports the seawater and returns the brine through the pumping and discharge pipelines (blue and orange lines), while the CSP+PV plant is at a close location (5-7 km far from the coast). The DIST system transports the produced water from the RO plant to the demand site through the distribution pipeline (purple line) with a length equal to Distance 2.
- CSP+PV+MED: in this case, the MED process requires to be co-located with the CSP+PV plant to use the exhaust turbine steam of the power block. Thus, the MED is located at the same location as the CSP+PV plant, and the P/R system transports the seawater from the coast to the desalination plant through the pumping pipeline (blue line), and the brine is returned to sea through the discharge pipeline (orange line). Both pipelines have a length equal to Distance 1. Then, the water is transported from the plant location to the demand site through the distribution pipeline (DIST system), with a length equal to Distance 2. For this system, three different CSP+PV plant locations were analyzed for the Atacama Mine and Copiapó case.

Table 4-5 presents the cases considered in the study showing the values of Distance 1 and Distance 2 for each case and the altitude of the desalination plant and demand locations that are taken into account to assess the power consumption of the P/R and DIST systems. The

annual GHI (global horizontal irradiation) and DNI of each plant location are also presented. The data were extracted from the Explorador Solar de Chile (Departamento de Geofísica - Facultad de Ciencias Físicas y Matemáticas - Universidad de Chile, 2017). Additionally, the seawater temperature profile throughout the year is considered in terms of intake location. The profile considers a daily/monthly variation, being the maximum temperature in summer and the lowest one in winter (Olwig et al., 2012). For the Antofagasta and Atacama Mine cases, the temperature profile throughout the year varies between 15-21 °C, while for the Copiapó case, it varies between 12-18 °C. The temperature data were extracted from (Global Sea Temperature, 2019).

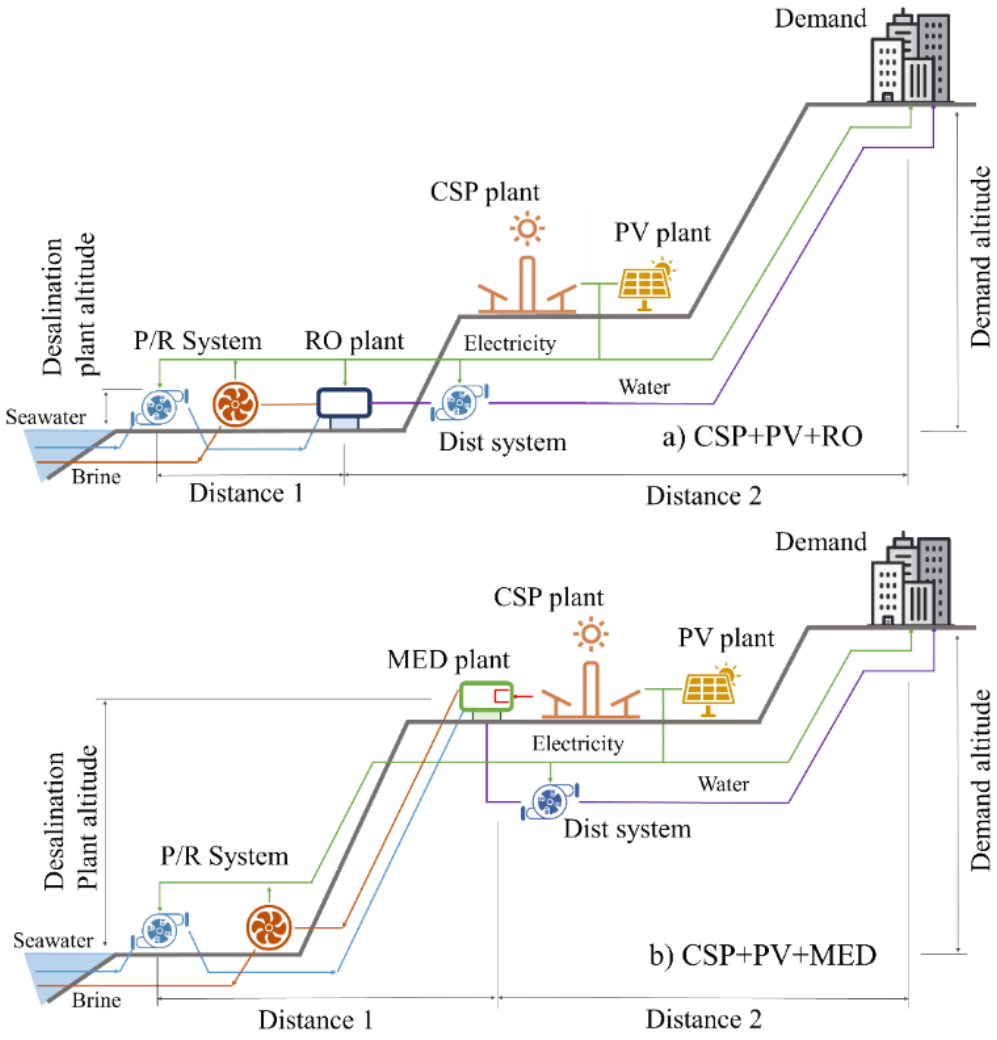

Figure 4-3: Geographical locations of the hybrid CSP+PV plant, the desalination plants, and the demand for the case of RO (a) and MED (b).

Table 4-5: Distance and altitude of the desalination plant and demand location; DNI and GHI for each location.

Demand case	Plant case	Distance 1 [km]	Desalination plant altitude [m]	Distance 2 [km]	Demand altitude [m]	GHI [kWh/m^2-yr]	DNI [kWh/m^2-yr]
A: Antofagasta (coast)	RO-1	1	30	51	100	2325	3142
	MED-1	7	75	45	100	2325	3142
B: Atacama Mine (mountain)	RO-1	1	30	154	1650	2325	3142
	MED-1	7	75	153	1650	2325	3142
	MED-2	40	680	115	1650	2492	3409
	MED-3	86	1550	69	1650	2585	3765
C: Copiapó (valley)	RO-1	1	30	67	390	1878	2506
	MED-1	3	75	65	390	1878	2506
	MED-2	35	360	37	390	2037	2763
	MED-3	55	700	17	390	2281	3207

4.5.1 Antofagasta (coast)

The demand was located at Antofagasta city, but the solar power plant was located 45 km from the city. The RO and MED seawater intake were located at 52 km from Antofagasta city due to the unavailability at Antofagasta coast for the RO (international port, large fishing industry, local natural monuments, among others), and aiming to be the nearest distance from the CSP+PV plant for the MED unit. One RO and one MED case were evaluated (RO-1 and MED-1). Figure 4-4 shows a map of the location of the plant, the RO plant, the demand location, and the layout of the pipelines from the sea to the demand.

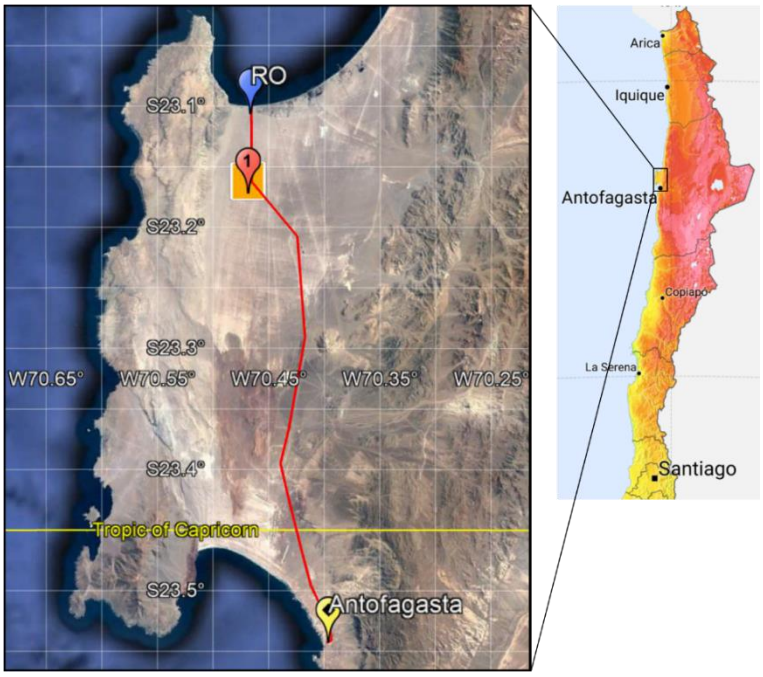

Figure 4-4: The geographical location of the plants and the pipelines for the Antofagasta case (colors means level of DNI, map data: Google and (The World Bank & SolarGIS, 2019)).

4.5.2 Atacama Desert Mine (mountain)

The demand was located 155 km from the coast and 1650 m above the sea level. In this scenario, three CSP+PV plant locations were evaluated. In Figure 4-5, a map of the proposed

sites for the CSP+PV plants, the RO plant, and the demand locations are shown, as well as the layout of the pipeline from the sea to the demand location passing the plants. The CSP+PV+RO plant was evaluated with the RO plant at the coast and the CSP+PV plant at location 1 (RO-1), while the CSP+PV+MED was evaluated at locations 1, 2, and 3 (MED-1, MED-2, MED-3). Notice that for the MED cases, the pipeline distance of the P/R system and the DIST system changes according to the plant location. It is important to note that the second and third plant locations have a better DNI compared to the first location, 9% and 20% higher, respectively.

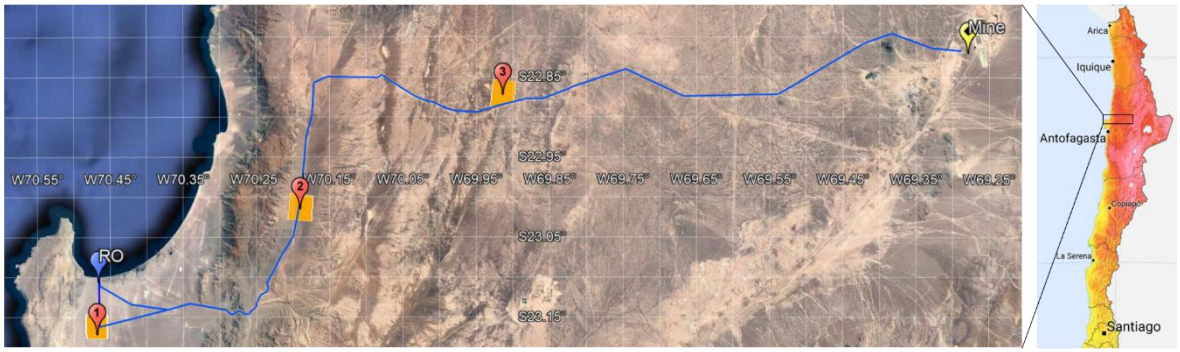

Figure 4-5: The geographical location of the plants and the pipelines for the Atacama Mine case (colors means level of DNI, map data: Google and (The World Bank & SolarGIS, 2019)).

4.5.3 Copiapó (valley)

The demand was located 70 km from the coast and 390 m above sea level. Figure 4-6 shows the locations of the CSP+PV plants, the RO plant, the demand, and two pipeline layouts from the sea to the demand location. The CSP+PV+RO plant was evaluated with the RO plant at the coast and the CSP+PV plant at location 1 (RO-1), while the CSP+PV+MED was assessed at locations 1, 2, and 3 (MED-1, MED-2, MED-3). Moreover, the RO-1 and MED-1 cases were analyzed using the red pipeline layout, which has the benefit that crosses the valley, increasing the altitude progressively until reaching the maximum at the final demand location. The second and third locations (cases MED-2 and MED-3) were analyzed using the blue pipeline layout. The pipeline passes through a mountain at 870 m of altitude before

reaching the demand location. These locations are considered of interest because they have higher DNI compared to the first location (10% and 28%, respectively).

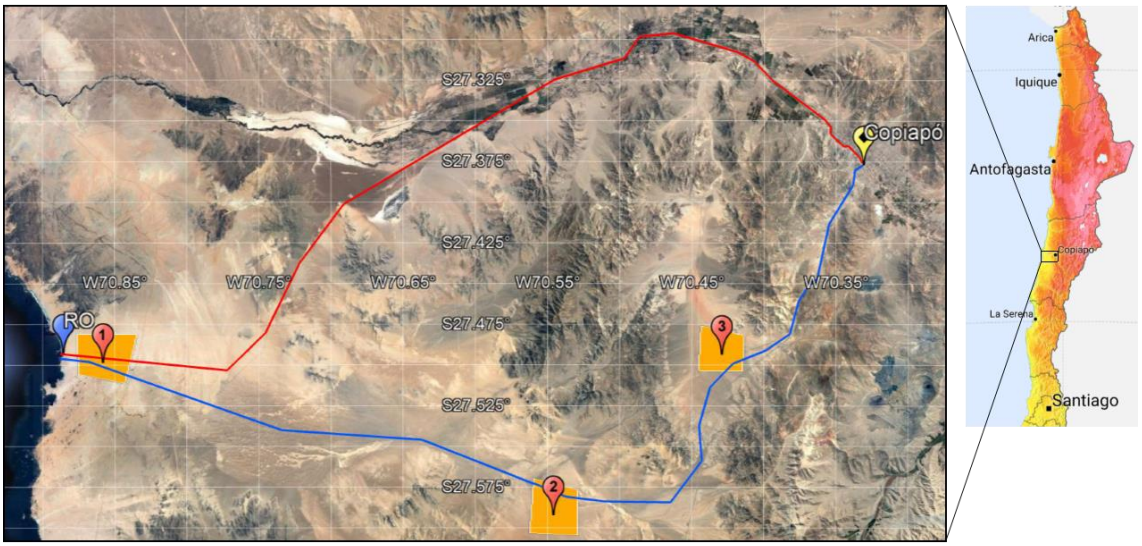

Figure 4-6: The geographical location of the plants and the pipelines assessed for the Copiapó case (colors means level of DNI, map data: Google and (The World Bank & SolarGIS, 2019)).

4.6 Results

In this section, the multi-objective optimization results for the three demand locations selected are presented. The LINMAP solutions for the two-objective and three-objective optimizations are analyzed, as well as their products cost formation. A sensitivity analysis of the CSP, MED, and pipeline costs is performed to determine the reduction required for the MED integration be competitive.

4.6.1 Case A: Antofagasta (coast)

Figure 4-7 shows the Pareto-front for the RO and MED integration into the CSP+PV plant in the coastal city of Antofagasta. Two Pareto-fronts for the CSP+PV+RO plant, considering different PV plant sizes (50 MW_e for RO-1a and 100 MW_e for RO-1b), are shown since the Pareto front depends on the PV plant size. It is observed that the RO fronts exhibit the lowest

TCW, which is at least 35% lower than the TCW of the MED Pareto-front. Conversely, the TCE of the MED front achieves competitive values up to 66 $/MWh, between 2 to 10% lower than RO fronts. Also, it can be observed that the three-objective Pareto-fronts reach values with a higher TCE trying to increase the $Suf_{e\&w}$. The LINMAP solutions are also presented by the circle points, evidencing that the chosen solution tends to have lower TCW at the expense of having a higher TCE. This is caused because the TCW is a more sensitive function since it depends significantly on the water productivity to amortize the MED CAPEX. The higher TCW values vary between 30 to 100% respect to the minimum TCW. In comparison, the higher TCEs values only vary between 10-15% respect to the minimum TCE. This trend is more evident in the three-objective optimization, where the higher $Suf_{e\&w}$ values are located at the end of the front with the lower TCW values. Therefore, the two functions ($Suf_{e\&w}$ and TWC) are prioritized over the TCE.

The optimum sizing of the cogeneration plant from the LINMAP solutions is presented in Table 4-6. In the RO cases, the optimum sizing tends to have medium/large CSP plants with 13-14h of TES and the maximum number of the RO units (8 units). It is observed that the RO-1a case tends to a larger CSP plant than the RO-1b that has a larger PV plant. Moreover, this has a moderate impact in the TCE (5 $/MWh lower), and a marginal effect in the TCW. Therefore, the PV and CSP plant sizes compensate each other so that they can generate electricity for more hours, allowing the continuous operation of the RO plant. In the case of the MED-1, the optimum sizing consists of a small PV plant, with a large CSP plant with 15-16h of TES and 7 MED units. This optimum sizing focuses on maintaining the power block and the MED plant operating as many hours as possible, while the PV plant only covers the parasitic consumptions and a fraction of the nominal power during the day, without forcing the power block to operate at low part-load conditions (under 70%). This operation of the power block allows the seven MED units to work close to the nominal point during the year, maximizing the water production.

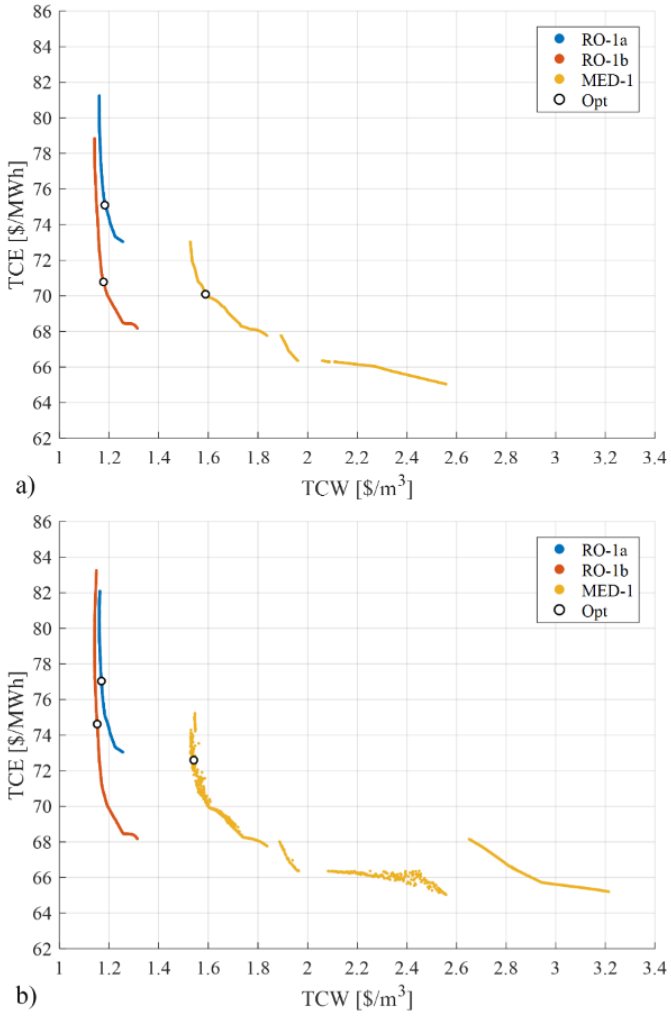

Figure 4-7: Two-objective (a) and three-objective (b) optimization Pareto-fronts and LINMAP solutions for the Antofagasta case.

Additionally, it is observed that the three-objective solutions present respect to the two-objective solutions a larger CSP plant (around +0.5 SM), which decreases the TCW in 0.05 $/m^3 (less than 3%) and increases the $Suf_{e\&w}$ in 3-8%. However, the TCE only raises in 4 $/MWh (<5%). In that way, different optimum sizing of the plant could achieve similar performances and costs, so the inclusion of $Suf_{e\&w}$ as an objective function can give relevant information to help to make a final decision about the most suitable optimum sizing.

Table 4-6: LINMAP solutions for the Antofagasta case for the two and three objectives optimization

Cases	PV [MW]	SM [-]	TES [h]	DES [Units]	TCE [$/MWh]	TCW [$/m^3]	$Suf_{e\&w}$ [%]
Two objectives							
RO-1a	50	3.2	14.0	8	75.06	1.19	81.29
RO-1b	100	2.6	13.0	8	70.75	1.18	79.20
MED-1	31	3.2	15.0	7	70.06	1.59	72.67
Three objectives							
RO-1a	50	3.5	14.0	8	77.00	1.17	84.13
RO-1b	100	3.1	14.0	8	74.59	1.15	84.28
MED-1	22	3.8	16.2	7	72.56	1.54	78.85

Figure 4-8 shows the contribution of each of the components (PV, CSP, PB, MED, RO, P/R, and DIST system) to the TCE and TCW. In general, the TCE is mainly affected by the CSP and PB costs, with approximately 90% of the total cost. The PV plant has a small contribution to the TCE of 6-12% due to its low cost. In the MED case, a small contribution of the P/R system of 4% can be observed. Moreover, the TCW allocation shows relevant differences between the RO and MED integration. The RO cases show a combined contribution of 0.45 $/m^3 from the PV, CSP, and PB components, which represents the energy cost of the water. The RO cost contribution (composed of 70% CAPEX and 30% OPEX) is around 0.6 $/m^3, while the distribution system contributes with 0.15 $/m^3. In the MED case, the main difference is the energy cost (heat and electric consumption) from the PV, CSP, and PB components, which is around 0.73 $/m^3, although the PV system has a marginal contribution (1%) due to small PV plant are selected. The MED plant contributes with 0.65 $/m^3, and the conveyance systems add 0.18 $/m^3. Therefore, the competitiveness of the MED plant is mainly affected by the cost of the energy, which is 0.25 $/m^3 higher than the RO case and moderately affected by the desalination plant and the costs of the conveyance system.

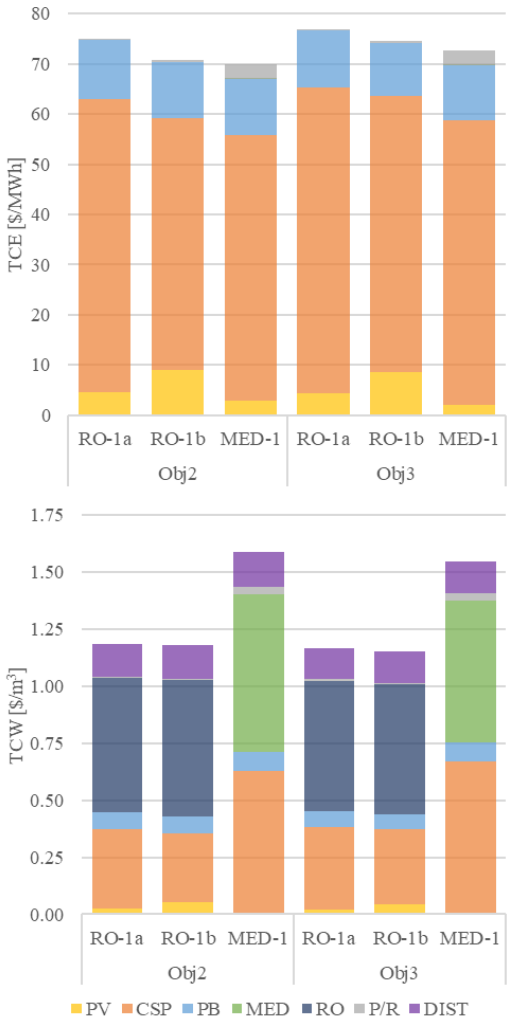

Figure 4-8: Contribution of the PV, CSP, PB, MED, RO, P/R, and DIST system costs to the TCE (a) and TCW (b) for the optimum values of the Antofagasta case.

To understand in detail the cost formation of the products in both integrations, a thermoeconomic flow diagram illustration of the annual balance of the plant for RO-1a and MED-1 cases is presented in Figure 4-9 and Figure 4-10, respectively.

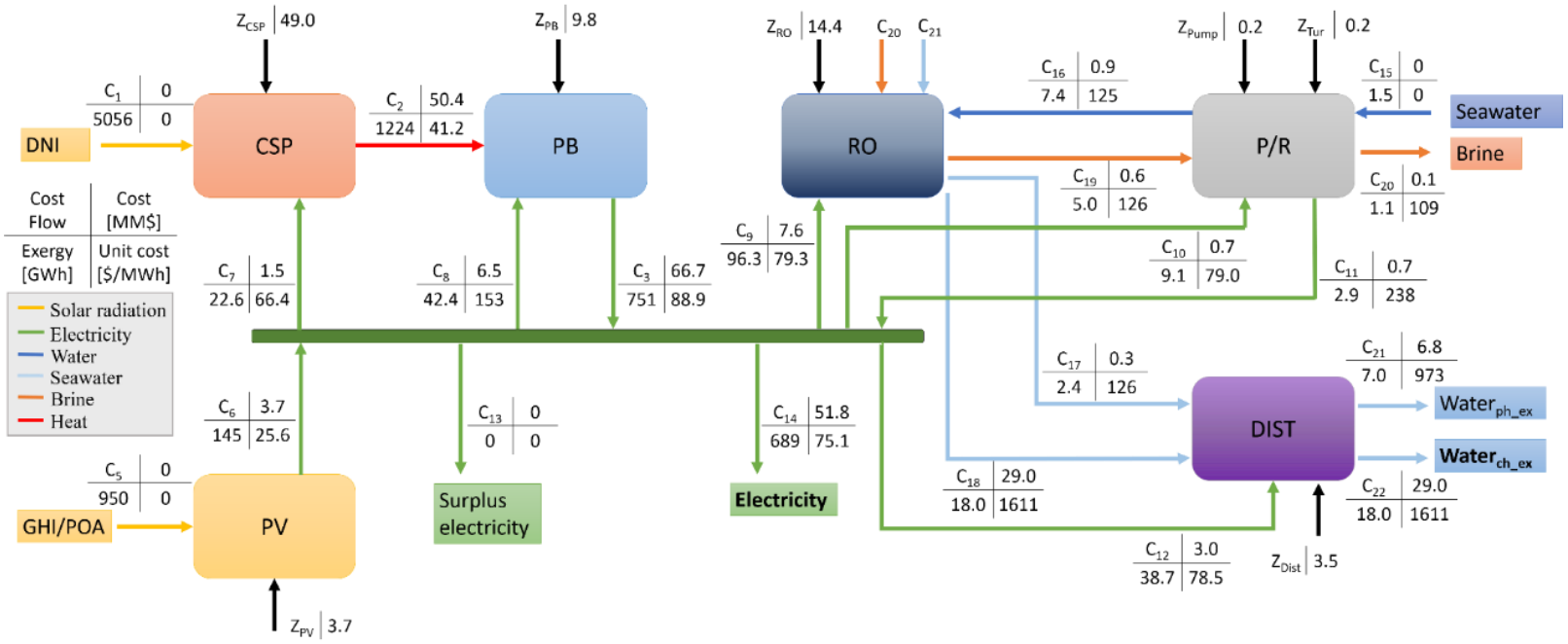

Figure 4-9: Plant thermoeconomic flux map of the RO-1a (Antofagasta case)

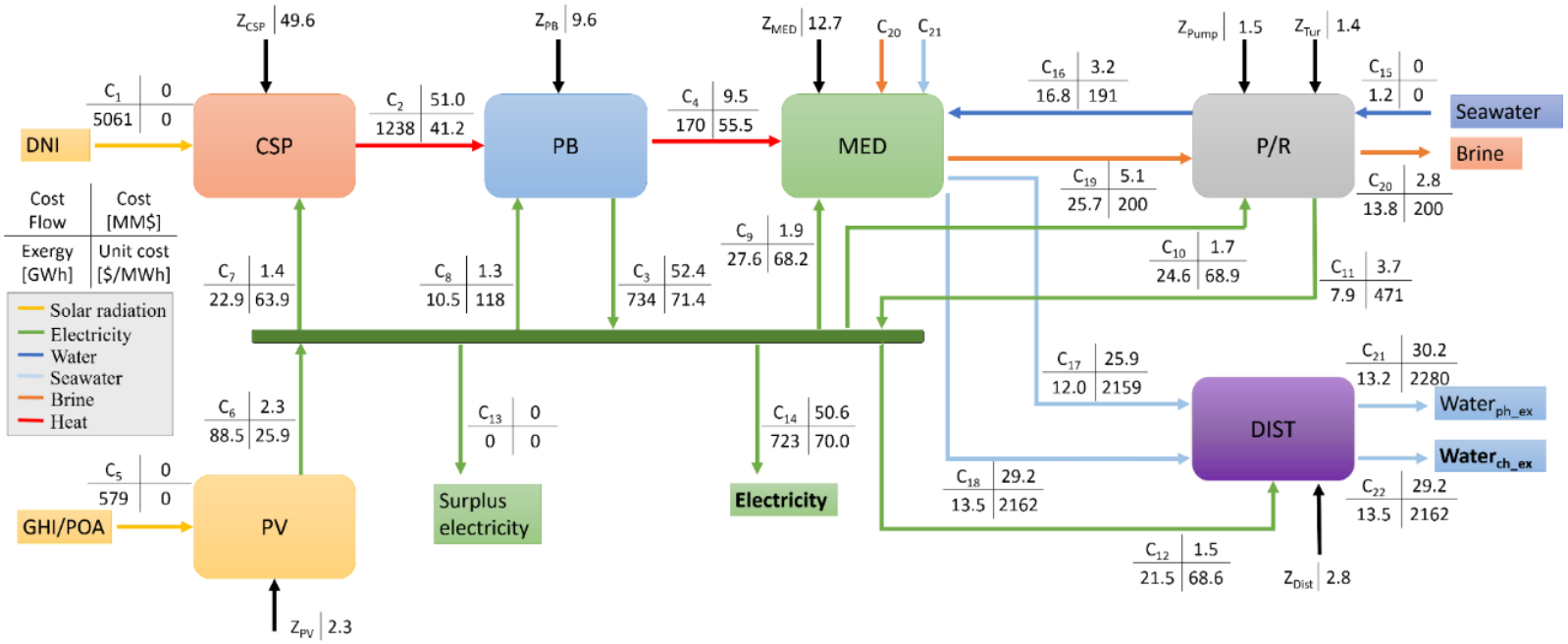

Figure 4-10: Plant thermoeconomic flux map of the MED-1 (Antofagasta case)

They show the sum, on an annual basis, of the exergy, the cost, and the unit thermoeconomic cost of the representative streams of the plant, in which it can be observed the resource/products relation in each system and could be calculated the destroyed exergy during the year. In the RO case, the sum of the costs allocated to the water through the electricity is 11.3 M$. However, the water chemical exergy is 18 GWh (which represents 24.5 hm^3). On the contrary, the MED case shows that the heat cost input of the MED plant is 9.5 M$, while the sum of the electricity related to the water production is 5.1 M$, giving a total of 14.6 M$ (65% from heat and 35% from electricity), while the water chemical exergy is 13.5 GWh (18.4 hm^3). Therefore, the cost of the energy in the MED case is relatively higher, while the water production is lower compared to the RO plant integration. Thus, the low competitiveness of the MED plant is related to the high cost of the heat and the efficiency of the MED plant, even though the MED integration allows decreasing the cost of the electricity by sharing the allocation cost in the power block.

4.6.2 Caso B: Atacama Desert Mine (mountain)

Figure 4-11 shows the Pareto-front for the demand at the inland location, Atacama Mine. In this case, two Pareto-fronts are shown for the CSP+PV+RO plant and three for the CSP+PV+MED plant (different plant locations). Both RO-1 fronts follow a similar trend to the observed for the Antofagasta case, achieving the lowest TCEs and TCWs. The TCW is considerably higher compared to the Antofagasta case due to the conveyance of water to the inland location, reaching values around 2.1 $\$/m^3$. The CSP+PV+MED cases show three different Pareto-fronts, which are influenced by the available solar resource and the geographical parameters. Pareto-fronts with higher costs are obtained as the location moves away from the coast, despite the improvement of the solar resource. Nonetheless, some MED-2 Pareto-solutions can achieve a lower TCW compared to the MED-1, but with a significant increase of the TCE.

Table 4-7 presents the optimal LINMAP solutions in the Atacama Mine case. It is observed that similar optimum sizing is selected for RO-1a, RO-1b and MED-1 cases compared to the Antofagasta scenario, which has the same DNI. Although the $Suf_{e\&w}$ is considerably lower

due to a higher electric consumption required by the conveyance systems, the TCE is slightly reduced, and the TCW is dramatically increased. Thus, the sizing parameters of the cogeneration plant are marginally affected when the demand location is different.

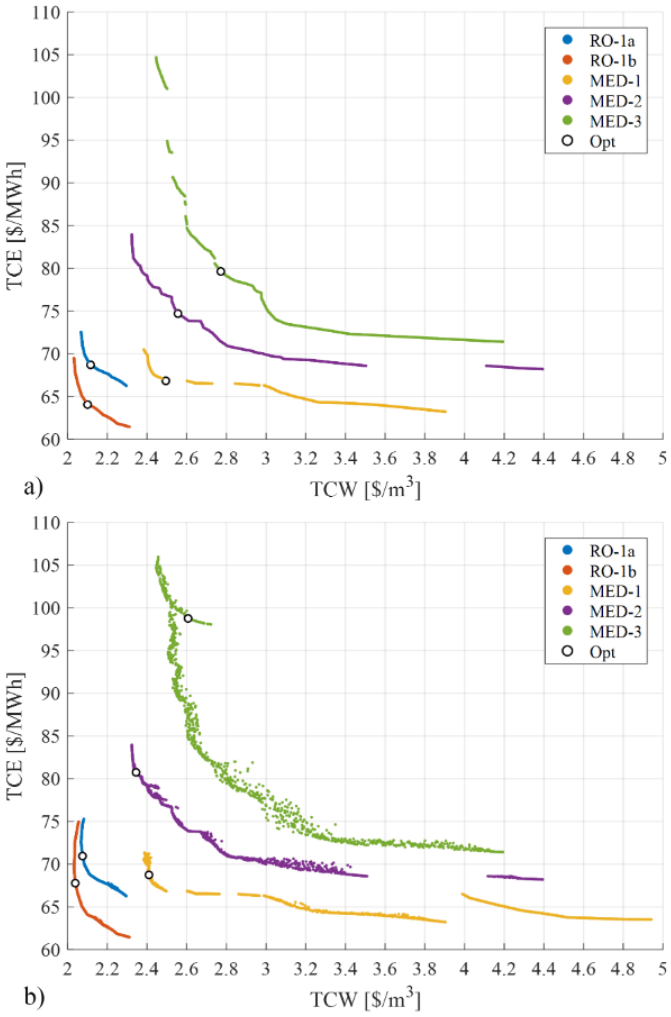

Figure 4-11: Two-objective (a) and three-objective (b) optimization Pareto-fronts, and LINMAP solutions for Atacama Mine case.

The MED-2 and MED-3 cases present optimal sizing that are affected by the conditions of the locations. For the two-objective solution, the MED-2 case selects a medium PV plant with a medium CSP plant and four MED units, while the MED-3 case has a smaller CSP plant with two MED units. These results show that it is preferred to select a fewer number of MED units when the plant is placed at an inland location to reduce the parasitic

consumption and the P/R system costs (smaller pipeline diameters lead to reduced pipeline costs). However, water production and $Suf_{e\&w}$ are drastically reduced in these cases. In contrast, medium PV plants with oversized CSP plants and eight MED units result for the three-objective solutions, obtaining high water production and high $Suf_{e\&w}$ values but with the drawback of a significant increase on the TCE despite the higher solar radiation. The locations of MED-2 and MED-3 have a DNI 9% and 20% higher with respect to the MED-1 location (3142 kWh/m^2-yr). However, this DNI is already high, and the CSP plant already achieves high capacity factors. Thus, radiation levels over 3100 kWh/m^2-yr do not have a significant impact on the cogeneration plant's performance.

Table 4-7: LINMAP solutions for the Atacama Mine case for the two and three objectives optimization

Cases	PV [MW]	SM [-]	TES [h]	DES [Units]	TCE [$/MWh]	TCW [$/m^3]	$Suf_{e\&w}$ [%]
Two objectives							
RO-1a	50	3.2	13.0	8	68.64	2.12	71.67
RO-1b	100	2.6	13.0	8	63.99	2.10	70.76
MED-1	50	3.2	15.0	7	66.76	2.50	67.64
MED-2	80	2.8	15.0	4	74.63	2.56	61.15
MED-3	100	2.4	14.0	2	79.56	2.78	53.34
Three objectives							
RO-1a	50	3.6	14.0	8	70.88	2.08	75.88
RO-1b	100	3.2	14.0	8	67.71	2.04	76.94
MED-1	40	3.8	16.3	7	68.67	2.41	73.51
MED-2	40	3.7	16.0	8	80.68	2.35	78.38
MED-3	60	3.4	16.1	8	98.70	2.61	75.20

The contribution of the plant's components in the TCE and TCW for the LINMAP solutions are presented in Figure 4-12. Regarding the TCE, the contribution of the PV, CSP, and PB components is similar for all the cases ranging between 63 and 70 $/MWh, in which the CSP

plant is the principal contributor. However, for the MED cases, the contribution of the P/R system becomes more relevant the more distant the location of the plant is and the higher the number of MED units is (up to 34 $/MWh for the MED-3), increasing the TCE significantly. In terms of the TCW, for the RO cases, the energy (PV, CSP, and PB systems) and distribution costs present a contribution of 1.03 $/m^3 and 0.45 $/m^3, respectively; while the RO cost achieved a contribution of 0.6 $/m^3.

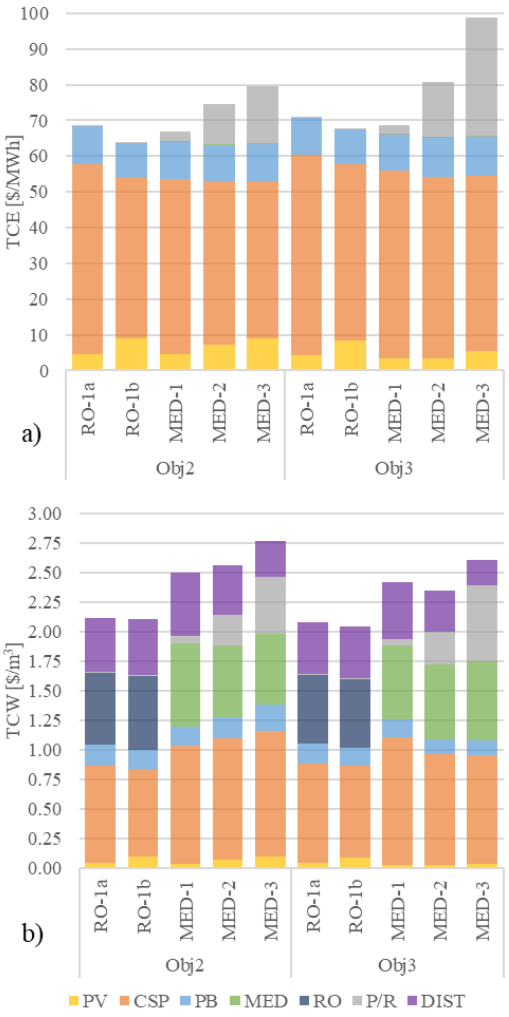

Figure 4-12: Contribution of the PV, CSP, PB, MED, RO, P/R, and DIST system costs in the TCE (a) and TCW (b) for the optimum values of the Atacama Mine case.

For the MED case, the energy cost for the two-objective solutions tends to increase with fewer number of MED units (up to 1.39 $/m^3), while for the three-objective solutions, it

reaches 1.09 $/m^3 for the configuration with eight MED units. This could happen because the MED plants with a higher number of units work a larger number of hours in a year at part-load conditions, and the MED unit slightly increases their GOR on those conditions. Moreover, it has been found that the energy cost (roughly composed of 44% from heat and 56% from electricity) is between 6% and 35% higher than the RO case. Besides, the MED plant contributes between 0.6 and 0.7 $/m^3, while the conveyance systems increase their contribution from 0.55 to 0.85 $/m^3 as further the plant location is. Therefore, it is proven that locating the plant inland with better solar resource conditions (over 3100 kWh/m^2-yr) to have higher performance does not compensate due to the increase in the conveyance cost and parasitic consumption.

4.6.3 Case C: Copiapó (valley)

Figure 4-13 depicts the Pareto-front for the inland valley location, Copiapó. It is observed that the CSP+PV+RO plant achieves the lowest TCWs between 1.5 and 1.8 $/m^3, while the lowest TCE is reached by the CSP+PV+MED solutions, with values lower than 80 $/MWh. Moreover, the Pareto-fronts of the MED cases present different trade-offs, resulting the MED-1 case with lower TCEs compared to the RO-1 fronts but with higher TCWs. The MED-2 case has slightly lower TCWs than the MED-1 case, while the TCE is higher. Finally, the MED-3 case front presents the best trade-off of the MED cases, in which the lowest TCW of the MED-3 front is only 16% higher than the lowest TCW corresponding to the RO-1a front. Notice that the MED-2 and MED-3 locations have an annual DNI 10% and 28% higher than the MED-1 location (2506 kWh/m^2-yr) and are situated at 35 and 55 km far from the coast. Therefore, there are some specific conditions in which the CSP+PV+MED plant could take advantage of a better solar resource and it could compensate the increase of the electric consumption and cost of the P/R system to improve the cogeneration plant performance and cost.

The optimal solutions obtained by the LINMAP algorithm are presented in Table 4-8. It is observed that the CSP+PV+RO plants tend to present a large/oversized CSP with 15-17h of TES, being larger than the previous cases. This happens mainly because the lower solar

resource levels of the location 1 forces to oversize the CSP plant to increase the RO operation hours. Concerning the MED solutions, in general, they present a large/oversized CSP plant with 16-18h of TES, especially for the three-objective solutions, with a medium PV plant between 50-80 MW_e. Moreover, the MED units tend to decrease the far the plant location for the two-objective solutions (similar to the Atacama Mine case) from the coast is, also decreasing the $Suf_{e\&w}$. For the three-objective solutions, seven MED units are obtained for the three cases.

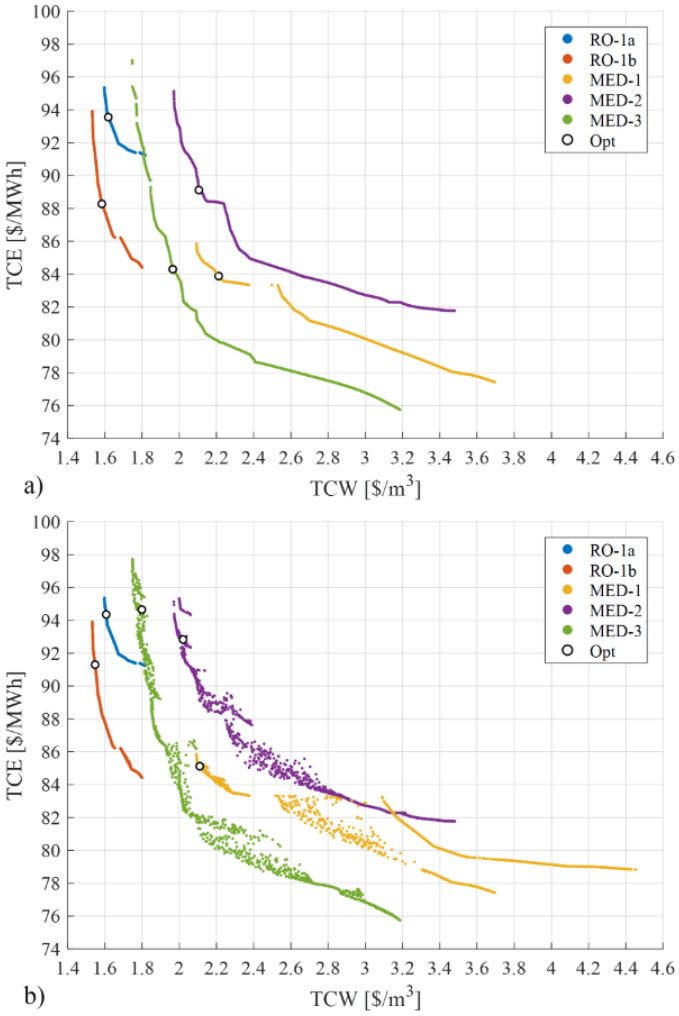

Figure 4-13: Two-objective (a) and three-objective (b) optimization Pareto-fronts and LINMAP solutions for Copiapó case.

Furthermore, Figure 4-14 shows the cost breakdown of the TCE and TCW. Regarding the TCE, it is observed that the contribution of the CSP, PV, and PB components varies depending on the case. The RO cases show values between 88 $/MWh and 94 $/MWh, while the MED cases present a trend in which the contribution of these three systems decreases as the plant location is further away from the coast, from 83 $/MWh to 70 $/MWh. The main reason for this behavior is because better solar resource conditions are found at inland locations, which significantly improves the performance of the cogeneration plant. Although the P/R system contribution increases with the distance of the plant to the sea, reaching almost 21 $/MWh for the MED-3 case, the TCE remains competitive, compensating the effects of both factors.

Table 4-8: LINMAP solutions for the Copiapó case for the two and three objectives optimization

Cases	PV [MW]	SM [-]	TES [h]	DES [Units]	TCE [$/MWh]	TCW [$/m^3]	$Suf_{e\&w}$ [%]
Two objectives							
RO-1a	50	3.8	15.2	8	93.52	1.62	69.57
RO-1b	100	3.2	15.0	8	88.24	1.59	69.51
MED-1	50	3.5	16.1	6	83.85	2.21	58.80
MED-2	70	3.4	17.0	4	89.08	2.11	59.03
MED-3	80	2.8	14.0	3	84.26	1.97	55.95
Three objectives							
RO-1a	50	3.9	17.0	8	94.32	1.61	70.81
RO-1b	100	3.7	16.0	8	91.26	1.55	73.75
MED-1	41	3.9	18.0	7	85.08	2.11	65.07
MED-2	50	3.9	17.2	7	92.80	2.02	70.27
MED-3	50	3.8	17.2	7	94.61	1.80	76.33

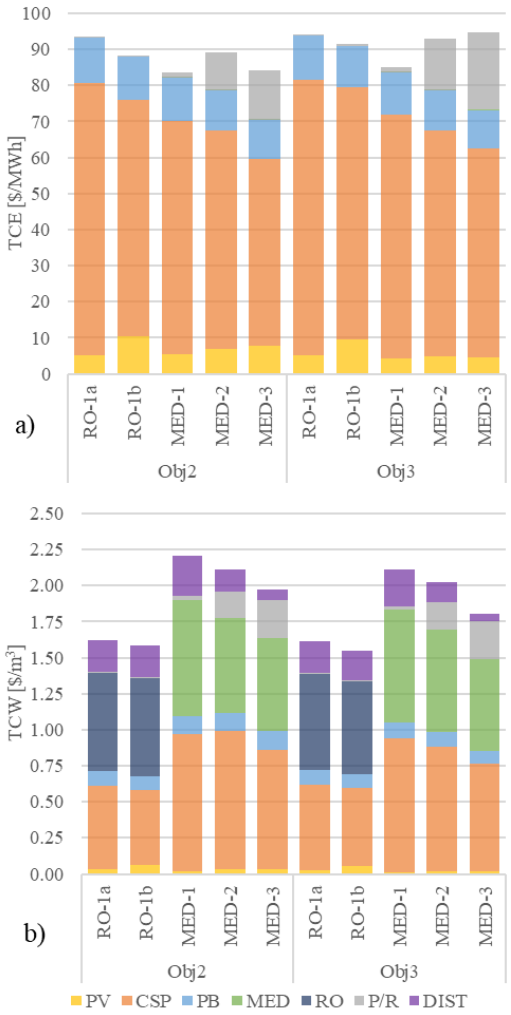

Figure 4-14: Contribution of the PV, CSP, PB, MED, RO, P/R, and DIST system costs in the TCE (a) and TCW (b) for the optimum values of the Copiapó case.

The TCW of the RO cases presents an energy cost (from the CSP, PV, and PB system) of 0.7 $/m^3, while the RO plant and the distribution system contributes with 0.67 $/m^3 and 0.23 $/m^3, respectively. For the MED cases, it is observed that the energy cost contribution tends to decrease from 1.1 $/m^3 to 0.86 $/m^3 as the location presents a higher solar resource. This trend is more pronounced for the three-objective solutions in which the CSP plant is oversized. However, these energy costs are 25-50% higher than for the RO cases. Meanwhile, the conveyance systems contribute with 0.31 $ /m^3 for the MED cases, and the MED plant decreases its contribution from 0.8 $/m^3 to 0.64 $/m^3 as the solar resource is higher because the water production is increased. In summary, these factors reduce the TCW

for the MED-3 location. Therefore, a location with a DNI over 3100 kWh/m^2-yr (at least 25% better than the coast radiation) and 60 km or less distance from the coast can have an improvement of the performance, compensating the increase in the conveyance cost and the parasitic consumption.

4.6.4 Analysis of the Pareto-frontiers

In this section, an analysis of the sizing along the Pareto-front solutions is carried out for the two-objective optimization in order to analyze the different optimal solutions and determine which of them are the most suitable solutions for the cogeneration plant. For that, the 600 solutions of each Pareto-front were sorted in terms of the TWC to evaluate the progressive change of the variables. Figure 4-15 presents the four sizing parameters (PV size, SM, TES hours, MED/RO units) as well as the TCE, TCW, and $Suf_{e\&w}$ values of each Pareto-front (CSP+PV+RO and CSP+PV+MED cases) for the three cases (Antofagasta, Atacama Mine, and Copiapó). The LINMAP solutions are depicted as black outlined circles. Each graph has the solutions sorted in the same order, so the sizing of a specific solution can be assessed. Also, a red area representing the limit of 70% and 60% of $Suf_{e\&w}$ is shown, in which the CSP+PV+MED solutions that are into these areas have a representative productivity.

It is observed that the CSP+PV+RO plants achieve higher $Suf_{e\&w}$ than CSP+PV+MED plants in all the cases, with the exception of a few solutions of the MED-2 and MED-3 cases in Atacama Mine and Copiapó that reaches the same productivity of the RO-1 cases. In the case of the CSP+PV+RO plants, it is observed that they present similar trends for the three cases, always giving the maximum number of RO units. This means that it is preferred to build the largest RO plant possible with the lower specific desalination cost, despite the higher conveyance costs. Also, it is seen that the $Suf_{e\&w}$ values tend to increase as the SM and TES hours raise until it reaches a maximum, where larger CSP plants present a marginal contribution. In that way, a CSP+PV+RO plant with a SM of 2.8 and 13h of TES is required to achieve $Suf_{e\&w}$ values over 80% and 70%, for the Antofagasta and Atacama Mine cases, respectively. For the Copiapó case, larger CSP plants (3.2 and 3.6 SM and 15 TES hours) are needed to achieve a value of 70% for $Suf_{e\&w}$. Therefore, it is demonstrated that high

sufficiency factors are obtained if large hybrid CSP+PV plants are selected in order to ensure the continuous operation of the RO plant and a significant water production.

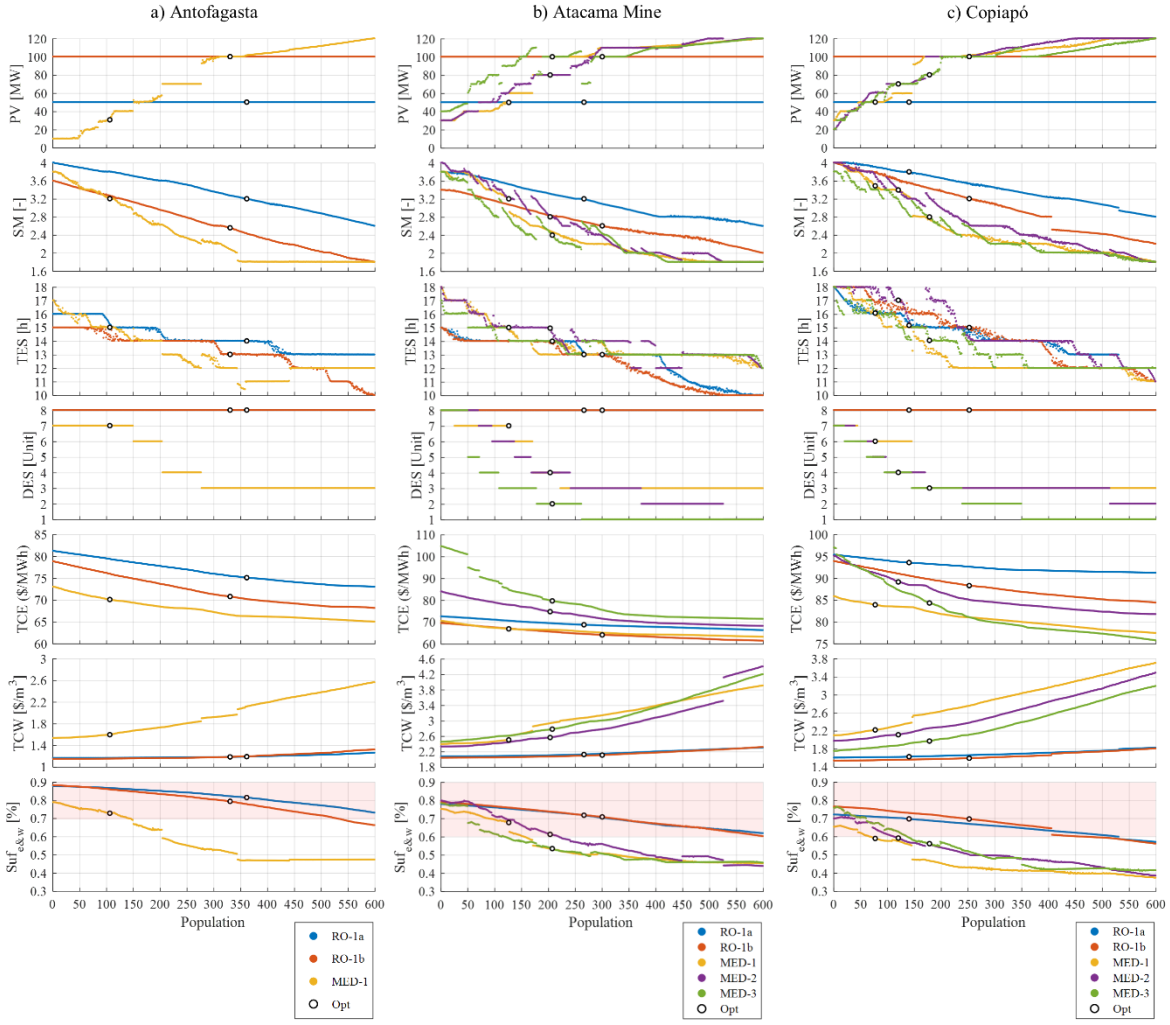

Figure 4-15: Design configurations across the Pareto-front for the three cases.

In the case of the CSP+PV+MED plants, different trends are perceived. It is observed that the number of MED units changes according to the TCW, resulting in the lowest costs for seven or eight MED units. For the TCE, the lower values are obtained for configurations with 1-3 MED units. It is important to notice that the number of MED units affects the $Suf_{e\&w}$ considerably, since the capacity of the plant changes, limiting the water production. In general, the highest sufficiencies and lower TCW values are obtained with small PV plants, oversized CSP plants, and 7-8 MED units, while the lowest TCE values are obtained for

large PV plants, medium CSP plants, and 1-3 MED units. Nevertheless, for those last solutions (300 to 600), the TCW results significantly increase due to the fact that the water production significantly decreases, so these solutions may not be suitable for the cogeneration plant.

Furthermore, it has been proven that it is difficult to achieve similar $Suf_{e\&w}$ for the MED cases compared with the RO cases. As a matter of fact, it is required a CSP+PV+MED plant with a 40 MW_e PV plant, 2.9 of SM, 14h of TES, and 7 MED units to achieve a $Suf_{e\&w}$ value over 70% for the Antofagasta coast case. In contrast, to achieve a value of 60% in $Suf_{e\&w}$ for the Atacama Mine and Copiapó cases, it is required a plant with 50 MW_e PV plant, 3.3 of SM, 15h of TES, and 6-8 MED units. Moreover, in these two last cases, the location with a better solar resource (MED-3) can achieve the same $Suf_{e\&w}$ with smaller CSP plants (3 SM and 14h TES) and larger PV plants (80 MW_e). Therefore, the most suitable sizing for the CSP+PV+MED plant may be the one that allows to have a significant sufficiency (>60-70%) since that solution has a high productivity with lower TCW, despite having a moderately higher TCE. For that, a MED plant with 7-8 units (which use more than 80% of the residual heat) is required together with an oversized CSP plant whose design is focused on maintaining the MED plant operation continuously, and a medium PV plant that contributes with the electric parasitic consumptions needs.

4.6.5 Cost sensitivity analysis

As shown in previous sections, the CSP+PV+MED plant is not competitive with respect to the CSP+PV+RO plant in terms of the TCW. In general, the MED integration develops a TCW between 18% and 40% higher than the RO cases, showing a lower percentage difference in the case of the three-objective solutions. Furthermore, it has been demonstrated that the main contributor of the TCW in the MED cases is the energy cost (heat and electricity) that is mainly composed by the CSP components, followed by the MED capital cost, and lastly, the conveyance systems (P/R and DIST systems), which is more than 90% dependent on the pipeline specific cost. Therefore, in order to assess the impact of the cost of these components, a sensitivity analysis was performed for the three-objective solutions

obtained by the LINMAP method. It was done by varying the CAPEX of the CSP, MED and pipelines (P/R and DIST systems) from 0% to 50%.

The TCE and TCW obtained with the cost reduction for the three cases scenarios (Antofagasta, Atacama Mine and Copiapó) are presented in Figure 4-16.. The figures illustrate the cost reduction effect of the CSP system (CSP), the MED plant (MED), the conveyance systems (pipeline), and finally, the combined impact of the CSP and MED components (CSP+MED). The colored-area represents the feasible TCE and TCW that could be obtained. The shape of this area is determined similarly from the area with the four lines of the components cost reduction. Additionally, the solution for the RO-1a plant is added since it is the RO case that has a similar PV plant size to the MED plants and the CSP+PV+RO power & water costs are also affected by the cost reduction of the CSP, PB, and conveyance systems. The colored-area (blue) represents the reduction of the cost that could be achieved in the CSP+PV+RO plant.

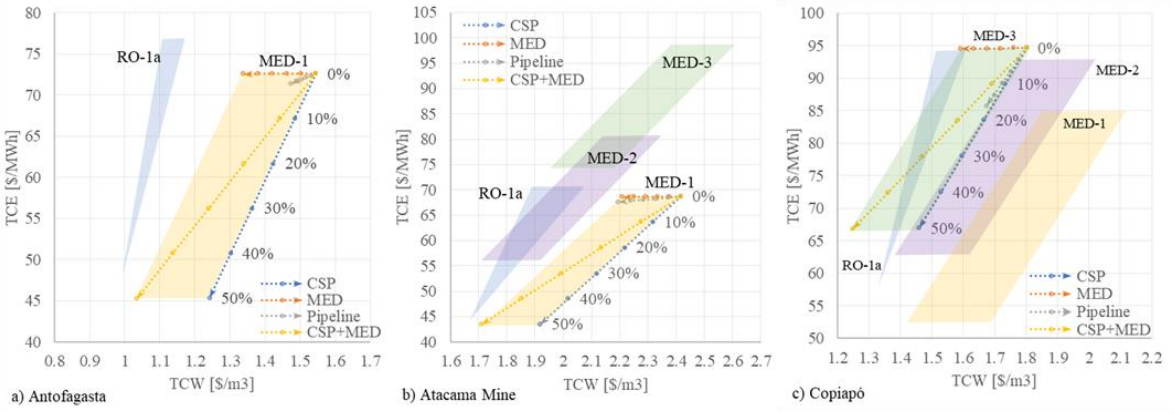

Figure 4-16: TCE and TCW with the reduction of the CSP, MED, and Pipeline cost for the three cases.

Firstly, it is observed that the cost reduction of the CSP system has the most significant effect on the TCW among the other components for the CSP+PV+MED cases analyzed, reducing the TCW around 20% for a 50% of CSP cost reduction. In the case of the TCE, it is reduced between 30-38%. Secondly, the MED cost reduction only affects the TCW, decreasing it in 9-13% for a 50% of MED cost reduction. Thirdly, the pipeline cost reduction affects the

costs depending on the plant and the demand location. For the Antofagasta case, the TCW is reduced by 5% for a 50% pipeline cost reduction, while the TCE is marginally affected. For the Atacama Mine case (MED-1 location), the TCW is reduced by 9%. Finally, for the Copiapó case (MED-3 location), the TCW is reduced by 9% while the TCE is reduced by 7%. Thus, the impact on the TCW of the pipeline cost could be significant if the distance from the sea to the demand location is representative (more than 30 km). Also, it could have a considerable effect on the TCE if the plant location is far from the sea. Lastly, the 50% of the CSP+MED cost reduction could decrease the TCW in 25-33%. Moreover, with a reduction of 30%, competitive TCW and TCE against the CSP+PV+RO plant can be achieved. Therefore, for the competitiveness of the CSP+PV+MED plant, the priority must be to reduce the energy cost of water production (CSP cost), while the MED specific cost could help reach lower TCW values.

Another alternative to close the cost gap with the RO integration is by improving the CSP+PV+MED plant performance and increasing water production through some design modifications. Among them, the following development could be considered:

- Include a hybridization of a low or medium-temperature solar thermal system (parabolic-trough, linear Fresnel, collectors) used to maintain the heat supply of the MED plant and thus enlarge its operational hours.
- Re-design the MED plant to increase the GOR or the recovery ratio (RR) by raising the number of effects of the MED plant. This can be achieved either with a rise in top brine temperature (TBT) or a decrease in the last effect temperature. The integration of the nanofiltration pretreatment could eliminate the divalent ions allowing to raise the TBT to 120°C, while integrating the absorption/adsorption systems at the condenser could decrease the last effect temperature under 10°C. In this second option, there is a barrier to achieving vacuum conditions at industrial-scale plants that are important to consider. Additionally, the RR could be improved by defining the freshwater quality, allowing the MED to operate at the brine operation limit, and blending for remineralization purposes.

- Assessment of other MED integration schemes that avoid the penalty in the electricity production due to the large amount of high-temperature waste heat that can be exploited by the MED technology. The integration of MED-TVC units into high-temperature power cycles (Brayton Cycle, supercritical CO_2 power cycle) is an example of these schemes.
- Consider alternative MED designs focused on reducing the extra seawater flow rate, like the use of ACC for the cooling system of the MED plant or other brine disposal processes (evaporation ponds and zero liquid discharge).

All these concepts should be analyzed considering the impact on whole plant performance in order to assess their technical and thermoeconomic viability, define their benefits and drawbacks, and determine the best technology integration option.

4.7 Conclusions

The present work describes a thermoeconomic comparison between MED and RO processes when they are proposed for integration into a hybrid CSP+PV plant. The analysis focuses on assessing the technical and economic factors that impact the costs of both integrations. The study considers three locations for the demand (coast, mountain, and valley) and different locations regarding the distance from the sea for the solar power plants. Moreover, a multi-objective optimization was performed for each case considering three-objective functions (TCE, TCW, and $Suf_{e\&w}$) to assess the optimum sizing and product cost formation. Additionally, a sensitivity analysis of the CSP, MED, and pipeline costs was carried out. The main conclusions and suggestions are presented as follows:

- The CSP+PV+RO plant obtains the most competitive trade-off of TCE and TCW for the three cases evaluated. In contrast, the CSP+PV+MED plant shows competitive TCE, while the TCW is 15% to 35% higher than the RO integration. In that way, the main contributor to the higher TCWs is the energy cost (PV, CSP, and PB components), which is significantly influenced by the cost of the heat that drives the MED plant, while the MED capital cost affects moderately the TCW.

- The MED plant performance and its capital costs, and the P/R pipeline costs are the other important factors in the TCW. High water capacity factors are required to amortize the MED and P/R pipeline capital cost and obtain competitive TCW. A re-design of the MED plant focused on increasing the GOR and RR and reducing the design seawater flow rate is recommended.
- The sizing optimization of the CSP+PV+MED has to consider the $Suf_{e\&w}$ as an objective function since different configurations could achieve similar costs but with significant differences in terms of electric and water capacity factors. This could give a more in-depth insight into which is the best optimum sizing for a decision-maker, where the market conditions and the rentability of the project can influence the decision.
- The optimum configurations for the CSP+PV+MED plant consist of a medium PV plant (PV=50 MW_e) and a large/oversized CSP plant (SM=3.6 and TES=16h) integrated with 7 or 8 MED units, achieving low TCW with high $Suf_{e\&w}$ (>75%) in detriment of slightly higher TCE.
- The solar resource and the distance respect to the sea of the CSP+PV+MED plant location significantly influence the costs of the CSP+PV+MED plant. In general, it is better to produce water on the coast and then transport it. However, some specific inland conditions can take advantage of the better solar resource over the conveyance cost and electric consumption increase. Specifically, a location at 60 km from the coast with a DNI 25% higher than the coast levels (2500 kWh/m^2-yr or less) could have a better performance.
- The cost sensitivity analysis shows that the priority must be to decrease the energy cost by reducing the CSP specific cost, following by a MED cost reduction to lowering the TCW. A combined reduction of CSP, PB, and MED components over 30% could enable us to reach the competitive TCE and TCW of the CSP+PV+MED plant respect to the RO integration.

5. MULTI-OBJECTIVE OPTIMIZATION OF A CONCENTRATING SOLAR POWER + PHOTOVOLTAIC + MULTI-EFFECT DISTILLATION PLANT: UNDERSTANDING THE IMPACT OF THE SOLAR IRRADIATION AND THE PLANT LOCATION

5.1 Introduction

In recent years, the integration of Multi-Effect Distillation (MED) units into Concentrating Solar Power (CSP) plants to produce electricity and freshwater has been evaluated. The CSP generates high-temperature heat to produce electricity via a power cycle, in which the waste heat can be used to power thermal desalination systems in the same locations, obtaining both products from solar energy and improving the overall efficiency (Mohammadi et al., 2019). Moreover, the CSP has been particularly analyzed and developed in areas with high solar irradiation levels (Palenzuela, Alarcón-Padilla, et al., 2015b; Valenzuela et al., 2017). These areas present different topographies, with a combination of an abundant solar resource, long distance from the coast, and different altitudes above the sea level. Sites with higher solar irradiation could enhance the performance of CSP+MED plants. However, it is important to consider the additional cost of seawater pumping and pipeline deployment to assess real performance and cost-benefit. These facts emphasize the need to study the effect of the cogeneration plant's location to establish the possible areas that would have the best potential for its implementation.

Several studies and state-of-the-art reviews about the integration of CSP+MED plants can be found in the literature (Aboelmaaref et al., 2020b; Alhaj & Al-Ghamdi, 2019; Mohammadi et al., 2019; Omar, Nashed, Li, Leslie, & Taylor, 2020b) and, from all of them, it is concluded that the concept can be competitive in some specific conditions. Mohammadi et al. (Mohammadi et al., 2019) and Aboelmaaref et al. (Aboelmaaref et al., 2020b) presents extensive reviews of CSP + Desalination systems, showing that the research in this field has been focused on cogeneration of water and power, where the irradiation levels, water

salinity, and distance from shore are the main factors that impact the economics. Moreover, one of the challenges of integrating thermally-driven desalination systems with CSP is that both plants must be co-located, and coastal locations typically have lower irradiation levels, making the development less competitive at the coastline. Alhaj and Ghamdi (Alhaj & Al-Ghamdi, 2019) highlight the advantages of cogeneration of power and water in CSP+MED plants is on reducing some overall shared costs. Still, the main downside is the misalignment of the optimal location of the CSP and MED plant. Additionally, the economic feasibility relies on many factors such as the location and plant scale, thereby optimizing these factors to obtain the lowest water costs is required. Omar et al. (Omar et al., 2020b) show that the CSP+MED plant can have different economic feasibility results according to the geographical location (mostly the seawater salinity), which can make the concept more competitive against other systems integration.

Palenzuela et al. (Palenzuela, Alarcón-Padilla, et al., 2015b; Palenzuela, Zaragoza, et al., 2015; Palenzuela et al., 2013) studied the performance of CSP+MED plants and demonstrated that the geographical location had a relevant role, being more competitive for CSP+MED systems the sites with high salinities. Olwig et al. (Olwig et al., 2012) performed a techno-economic analysis of a CSP+MED in Israel and Jordan, where the CSP plant was located at less than 5 km from the coast. The study considered the solar irradiation, seawater salinity, and temperature according to the geographical location. Casimiro et al. (Casimiro et al., 2013, 2014) modeled and evaluated the performance of a CSP+MED plant in San Diego (USA) and Trapani, Sicily (Italy), considering a location close to the coast of 600 m and 4 km, respectively. Sharan et al. (Sharan et al., 2019) assessed the performance of a CSP+MED plant using a supercritical CO_2 power cycle in six coastal areas, obtaining competitive water costs in some of the selected locations with values between 1.1 $\$/m^3$ and 1.5 $\$/m^3$. Hoffmann and Dall (Hoffmann & Dall, 2018) performed a techno-economic study of a CSP+MED plant located 50 km inland in Namibia. The study showed that the seawater pumping is a primary contributor to the water cost, resulting in a high water cost (2.6 $\$/m^3$) that is not competitive against other technologies like RO (1.8 $\$/m^3$). Palenzuela et al. (Palenzuela, Ortega-Delgado, & Alarcón-Padilla, 2020) present a detailed simulation of a CSP+MED plant, considering the meteorological and geographical conditions in Almeria

(Spain) and Abu Dhabi (UAE). Mata-Torres et al. (Mata-Torres et al., 2017) carried out a CSP+MED plant simulation with fossil backup, considering a seawater pumping system to the plant's location. The analysis assumed an inland site in Chile (80 km from the coast and 1200 m of altitude) and Venezuela (30 km from the coast and 40 m of altitude). The results showed that the power consumption for the Chilean plant was significant (around 9.6 kWh/m^3), and the existence of an optimal MED size that minimized the water cost for each location (26.000 m^3/day for Venezuela and 11,000 m^3/day for Chile). Moreover, significant differences in the water cost (0.8 \$/m^3 for Venezuela and 2.0 \$/m^3 for Chile) were obtained, evidencing the influence of plant location respect to the sea.

It can also be found in the literature research works about the integration of a MED plant into a hybrid CSP + Photovoltaic (PV) plant, showing that the performance and the costs of this kind of systems can be improved due to the lower PV cost. Valenzuela et al. (Valenzuela et al., 2017) performed a study of a CSP+MED plant integrated with a PV plant, where the CSP system worked as a backup of the PV facility. The results showed different CSP and PV plant sizes that allowed minimizing both the electricity and water costs. However, in this work, the seawater pumping was not considered. Mata-Torres et al. (Mata-Torres et al., 2020) presented a thermoeconomic analysis of a CSP+PV+MED plant, considering the seawater pumping to an inland location at 100 km from the coast and 1000 m of altitude. The results showed that the pipelines and seawater pumping were relevant factors in the costs, contributing by more than 25% of the total water cost (between 2.6 and 3 \$/m^3). However, the analysis was performed for a particular location in northern Chile, and the results may be different for other sites or regions.

Therefore, from the works presented above, it is proven that the plant's location has a key role in its performance and cost feasibility. However, these studies have only considered specific locations with defined distance and altitude conditions. So, the effect of these parameters has not been analyzed, which raises the question of what should be the most relevant constraints of the location to achieve the most competitive costs. In addition, the sensitivity of one of the most important parameters, the solar irradiation, has not been considered in any of the referenced studies. Thus, the individual impact on the performance

and the costs of each parameter (solar irradiation, distance from the sea, altitude above sea level) associated with a specific geographic location has not been determined yet. Moreover, the previous studies have not considered the optimum sizing of the CSP+PV+MED plant that leads to the minimum electricity and water costs for different location conditions, which is carried out in the present work.

This study analyzes the effect of the solar irradiation, the distance from the coast, and the location's altitude for a CSP+PV+MED plant by a multi-objective optimization, aiming to determine the required conditions to minimize the product (electricity & freshwater) costs. Thus, this study allows us to have an insight into the most competitive sites or the ideal location to develop this kind of cogeneration plants. The study considers four TMY with Direct Normal Irradiation (DNI) varying from 2000-3500 kWh/m^2-yr, six distances from the sea (from 5 to 100 km), and six altitudes (from 20 to 1000 m.a.s.l.). The impact of each variable and the combined effect of the variables is also assessed, which result in cost maps of electricity and water that can be very useful to find the deployment potential of this technology in some regions of the world.

5.2 System description

The whole plant consists of a MED plant integrated into a solar hybrid CSP+PV plant (CSP+PV+MED system). Figure 5-1 illustrates the layout of this combined plant, where a detailed layout of all components is depicted: the CSP plant with the power block (PB), the PV plant, the MED plant, and the pumping and energy recovery system (P/R system). The hybrid CSP+PV plant operates synergistically to deliver a net power output of 100 MW_e. Thus, the PV plant output is prioritized to cover the parasitic and auxiliary consumption first and then to provide electricity to the grid, and the CSP plant works to complement the net output capacity (Starke et al., 2016; Valenzuela et al., 2017; Zurita, Mata-Torres, et al., 2018). The MED plant is integrated at the turbine output, in parallel to the power block condenser (air-cooled condenser - ACC), consuming part or all of the exhausted turbine steam. The MED plant has the priority regarding the steam demand, being the rest condensed

by the ACC. The conveyance system to transport the seawater and brine is also considered within the cogeneration plant.

The CSP plant consists of a central receiver tower with a direct two-tank thermal energy storage (TES) system that uses a molten salt mixture (60% NaNO3 and 40% KNO3) as heat transfer fluid. The molten slats are heated in the receiver during the day, and then they are stored in a hot tank and used when it is required to provide heat to a power block to generate electricity. The operational temperatures are 565 °C and 290 °C for the hot and cold tanks, respectively [19]. The power block consists of a steam Rankine cycle, including a high- and low-pressure turbine, a reheater, an ACC, two close feedwater heaters, and a deaerator, and has a gross electricity production of 110 MWe (typical power block size in Central Tower power plants). On the other hand, the PV plant consists of a mono-crystalline modules plant with one-axis tracking [20], which can be scalable from 0 to 100 MWe according to the number of inverters.

Regarding the desalination technology, the cogeneration system has a forward-feed Multi-Effect Distillation (MED) plant with a scalable number of units (from one to several modular units) and with an individual capacity of 10,000 m3/day per unit. Each MED unit is composed of 14 effects and 13 preheaters. The MED plant has been designed to use all exhaust steam from the turbine when it has the maximum number of units (8). Regarding the P/R system, it considers two pipelines, one for the pumped seawater and another for the brine disposal, a seawater pumping station, and a hydraulic turbine for energy recovery from the rejected stream of the desalination plant.

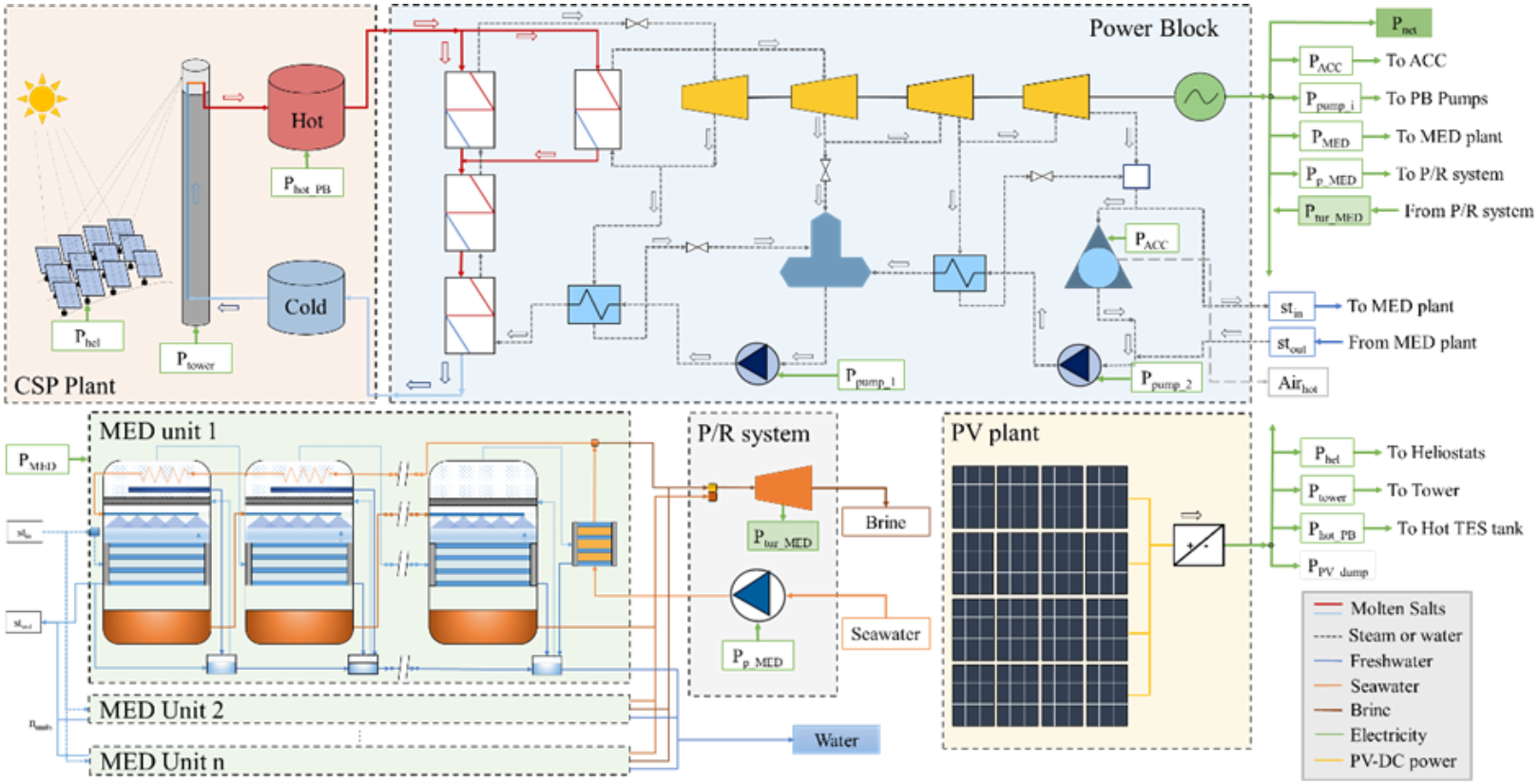

Figure 5-1: Layout of the CSP+PV+MED plant.

5.3 Methodology

The analysis was carried out for different location parameters (DNI, the distance from the coast, and the plant's altitude) of the plant. The methodology consists of performing a multi-objective optimization of the sizing of the CSP+PV+MED plant for each combination of DNI, distance, and altitude. Such optimization aims to find the configuration that minimizes the electricity and water costs and maximizes the production for each combination. Chapter 4 present the extended details.

The optimization has been carried out by the use of the genetic algorithm (GA) technique. This technique is based on biological evolution, where individuals' population is stochastically iterated to seek the Pareto-solutions. The procedure is as follows: firstly, a set of simulations of the whole plant model is performed in Transient System Simulation tool (TRNSYS) for a specific location and DNI. The simulation set consists of a parametric analysis in terms of the sizing parameters (PV size, solar multiple -SM-, TES hours, and MED units). After that, a thermoeconomic analysis (based on previous work [16]) is carried out to determine the values of the three objective functions: electricity and water cost and plant productivity. With this information, a surrogate model of the whole plant simulation and the thermoeconomic analysis is created, aiming to approximate the objective function solutions in a model with a faster fitness evaluation. Then, the multi-objective optimization with GA is performed to minimize the electricity and water costs. Finally, the optimum solution among the Pareto-solutions is selected by the decision-making process, also considering the maximization of productivity.

5.3.1 Plant modeling

The modeling of the whole plant was performed in TRNSYS software in a single file, enabling the integration of different components and considering the interconnection between them to assess the actual performance of the plant. The simulations were carried out with an hourly time step considering a Typical Meteorological Year (TMY) for each specific location. All models, assumptions, model correlations, and control procedures of

the plant were developed by the authors in previous works (Mata-Torres et al., 2020, 2019a). For the sake of brevity, only a summary of the modeling is presented in this section.

The CSP model consists of a heliostat field, a central receiver, a TES system, and the power block model. The heliostat field model includes an efficiency in terms of sun altitude and azimuth and the heliostat reflectivity to calculate the incident power. The central receiver models a cylindrical receiver composed by tubes. The molten salt mass flow rate is computed to reach a specified outlet temperature in terms of the incident power, thermal losses, and inlet molten salt temperature. The TES model considers two tanks with variable volume that works as the hot and cold tank. The steam power block model was developed in Engineering Equation Solver (EES) to perform the thermodynamic balance in nominal and part-load conditions. The model was used to build a multi-variable polynomial regression of the Rankine cycle performance in terms of the molten salt inlet mass flow rate and temperature and the power block's condensing temperature. The regression was integrated into a TRNSYS Type and incorporated into the plant model. Conversely, the PV plant was modeled using Type 190 of TRNSYS.

The MED unit model was developed in EES, based on the proposed model by Ortega-Delgado et al. (Ortega-Delgado, García-Rodríguez, et al., 2017), that evaluates the thermal performance (mass, energy, and heat transfer balance) of a 10,000 m^3/day plant in nominal and off-design conditions. The model was used to develop a multi-variable polynomial regression in terms of the thermal load (respect to the nominal steam mass flow rate), inlet steam enthalpy, and seawater temperature (Mata-Torres et al., 2020). The regression was employed in a TRNSYS type to integrate into the CSP+PV+MED plant model, where the MED plant was composed of n units. Finally, the P/R system modeling consists of computing the head losses of the seawater and brine pipeline to determine the power consumption and/or energy recovery (in the case of the hydraulic turbine). The pipeline geometry was determined by the distance between the coast and the plant (length) and the diameter computed to achieve a nominal inner velocity of 2 m/s. The head losses were calculated using the Darcy-Weisbach approach, and after that, the power consumption was

calculated considering the altitude difference. Lastly, the electric consumption or production were computed taking into account the efficiency of the pump and hydraulic turbine.

The hybrid plant operation was carried out so that the CSP plant operates complementing the PV output after covering all the parasitic, including the energy consumption of the P/R system. The MED plant was set to operate when: the power block is working, there is enough steam to run the MED start-up process, and the PV+CSP output can cover the MED and P/R system electric consumption. All the MED unit was established to operate at the same thermal load (means that the steam is equally distributed to each unit). Additionally, the MED plant determines the condensing temperature of the power block that varies from 60 and 70°C. When the MED is tuned off, the ACC covers the thermal load dissipation, and the condensing temperature is fixed to 60°C. The assumptions and control procedures of the integration are detailed in (Mata-Torres et al., 2020).

5.3.2 Thermoeconomic analysis

The thermoeconomic analysis merges thermodynamic performance based on exergy and economic analysis. Each stream's cost is computed according to the system's costs, the exergy flow, the destroyed exergy, and waste exergies. The analysis is performed in MATLAB using the results of the plant simulations obtained from TRNSYS. The thermoeconomic cost ($\dot{C}_{i,t}$) is calculated by a linear equation system composed of the cost balance of each component (Eq. 5.1) and the auxiliary equations (Eq. 5.2), which relates the unit thermoeconomic cost ($c_{i,t}$) of different streams according to the fuel-product principle (Bejan et al., 1995; Lazzaretto & Tsatsaronis, 2006). Both mathematical expressions are defined as follows:

$$\sum \dot{C}_{in,t} + \dot{Z}_{k,t} = \sum \dot{C}_{out,t} \tag{5.1}$$

$$\dot{C}_{i,t} = c_{i,t}\dot{X}_{i,t} \tag{5.2}$$

where $\dot{Z}_{k,t}$ is the component cost rate in \$/h, and $\dot{X}_{i,t}$ is the exergy rate in MWh. Firstly, the exergy analysis is carried out, calculating the physical exergy for all the streams. On one

hand, the potential exergy is only considered for the streams that have a considerable change with the altitude. On the other hand, the chemical exergy is considered only for the water and brine streams. In detail, there were considered 88 exergy flows between the solar radiation, molten salts, steam, seawater, freshwater and brine streams, and 30 components (4 for the CSP plant, 20 for the power block, 1 for the MED plant, 3 for the P/R system, and 2 for the PV plant). The net electricity output (resultant from the electric balance of the plant - Figure 5-1) and the chemical exergy of water exergy flows are considered the products of the plant. The approach is extensively detailed on previous works developed by the authors (Mata-Torres et al., 2020, 2019a).

The economic analysis consists of computing the components cost rate in Eq. 5.3: the total capital costs (${Z_k}^{Capex}$), the annual operational and maintenance costs (${Z_k}^{Opex}$) and the annual operation time ($O_{time,k}$) in hours. The amortization factor (A_f) results from considering an interest rate of 5% and a lifetime of 30 years. The total capital cost and the annual operational and maintenance costs were calculated using the mathematical correlations described in APPENDIX A5.

$$\dot{Z}_{k,t} = \frac{A_f {Z_k}^{Capex} + {Z_k}^{Opex}}{O_{time,k}} \tag{5.3}$$

Regarding the objective functions, three ones were considered: the Thermoeconomic Cost of Electricity (TCE), the Thermoeconomic Cost of Water (TCW), and the Electric and Water Sufficiency ($Suf_{e\&w}$). This latter objective function represents the actual production of electricity and water compared to the maximum production we could get for both items (average value of both the electric and water capacity factors – CF). The TCE and TCW are calculated by Eq. 5.4 and Eq. 5.5, in \$/MWh and \$/m^3, respectively. Conversely, the $Suf_{e\&w}$ is calculated by Eq. 5.6 that considers the same weight for the electric and water capacity factors.

$$TCE = \frac{\sum_{t=1}^{8760} \dot{C}_{el,t}}{\sum_{t=1}^{8760} Elec_{i,t}} \tag{5.4}$$

$$TCW = \frac{\sum_{t=1}^{8760} \dot{C}_{w,t}}{\sum_{t=1}^{8760} Water_{i,t}} \tag{5.5}$$

$$Suf_{e\&w} = \frac{\frac{\sum_{t=1}^{8760} Elec_t}{8760 \cdot P_{net}} + \frac{\sum_{t=1}^{8760} Water_t}{365 \cdot Units \cdot W_{nom}}}{2} \quad (5.6)$$

$\dot{C}_{el,t}$ and $\dot{C}_{w,t}$ are the hourly thermoeconomic cost of the products for each hour in $, where the electricity considers the net cost balance of the CSP, PV and hydraulic turbine electric output and the auxiliary consumptions, while the water considers the cost associated with the chemical exergy, $Elec_{i,t}$ is the net electricity production in MWh and $Water_{i,t}$ is the water production in m^3, P_{net} is the nominal power of the plant (established as 100 MW_e), W_{nom} is the individual MED unit capacity (established as 10,000 m^3/day), and *Units* is the maximum number of MED units allowable, which was set as 8.

5.3.3 Multi-Objective Optimization

The multi-objective optimization is performed using the GA method, which implies a large number of simulations of the plant model to meet the convergence criteria, resulting in a high computational time. Therefore, a surrogate model that approximates the results of the objective function is applied. This approach drastically reduces the computational time of the fitness evaluations. The surrogate model consists of performance maps of four-dimensions whose axes are the sizing parameters (PV size, SM, TES hours, and MED units), together with the objective function results that make up the multidimensional matrix values.

These results are obtained from a parametric analysis, being the constraints of each parameter represented in Table 5-1. The surrogate model uses MATLAB's griddedInterpolant function, which interpolates values within the matrix in terms of the sizing parameters. The validation is performed against a random sample of 20% of the parametric runs within the constrained limits. The Normalized Root-Mean-Square Deviation (NRMSD) obtained between the simulated and the surrogate model results were under 1%, which proves the validity of the model.

Table 5-1: Constrains of the sizing parameters for the parametric analysis.

Parameter	Unit	Range	Step
PV size	[MW]	0-120	10
SM	[-]	1.8-4	0.2
TES hours	[h]	10-18	1
MED/RO units	[-]	1-8	1

The multi-objective optimization is performed using the *gamultiobj* algorithm of MATLAB (Mathworks, 2020), which uses a controlled elitist GA, a variant of the NSGA-II (non-dominated Sorting Genetic Algorithm). The modified setting parameters regarding the default values provided by the MATLAB algorithm are presented in Table 5-2.

The decision variables boundaries were established in terms of the sizing parameters constraints, and the optimization problem was formulated as follows:

Minimize: $f_1(\vec{x}) = TCE(\vec{x})$

Minimize: $f_2(\vec{x}) = TCW(\vec{x})$

To find $\vec{x} = [PV_{size}, SM, TES_{hours}, MED/RO_{unit}]$

Subject to: $x_j^L \leq x_j \leq x_j^U$

Table 5-2: Setting parameters of the multi-objective GA.

Parameter set	Value
Population size	800
Crossover fraction	0.8
Pareto fraction	1
Function tolerance	$1x10^{-5}$
Convergent tolerance	$1x10^{-5}$
Maximum generations	1600
Maximum stall generations	200

Finally, the decision-making process is performed using the LINMAP method (Linear Programming Technique for Multidimensional Analysis of Preference) (Boyaghchi & Safari, 2017; Starke et al., 2018), including the maximization of the $Suf_{e\&w}$. For selecting the optimum solution, it was considered the point with the lower Euclidian distance from the ideal solution which is composed of the lowest TCE and TCW and the highest $Suf_{e\&w}$ values of the Pareto-front (Arora et al., 2016).

5.3.4 Plant location parameters: DNI, distance, and altitude

The optimization of the plant for each combination of the location parameters was performed separately. The plant location parameters are the DNI, the distance from the sea, and the altitude of the location. Figure 5-2 shows the system's location with respect to the coast, where the respective CSP+PV plant and the MED unit are co-located, and the P/R system is at the coast to transport the seawater and recover energy from the rejected brine and cooling streams from the desalination plant. The distance of the pipeline and the head pressure are considered in terms of the distance and altitude values.

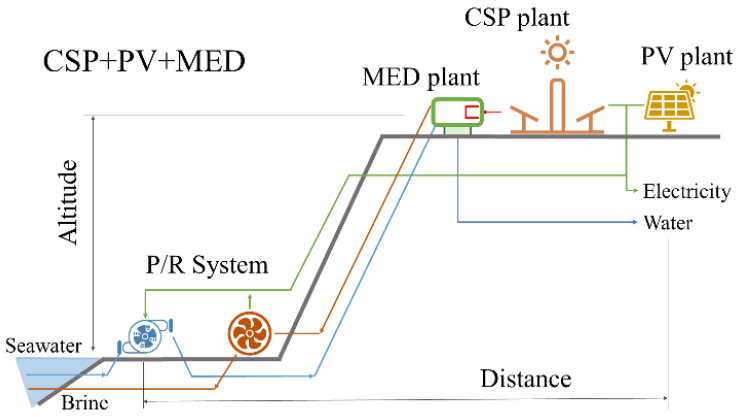

Figure 5-2: Geographic locations of the CSP+PV+MED systems.

Regarding DNI, four TMY were taken out from the Explorador Solar of Chile (Departamento de Geofísica - Facultad de Ciencias Físicas y Matemáticas - Universidad de Chile, 2017) as representative data, including the irradiation and meteorological data and the

latitude and longitude coordinates (shown in Table 5-3). The DNI data used in the analysis contemplates four DNI levels, from 2000 to 3500 kWh/m^2-yr, a range that covers most of the DNI levels of potential locations around the world where CSP implementation would be a feasible option.

Table 5-3: Solar irradiation data used for each DNI case (data extracted from Explorador Solar de Chile).

Case	GHI [kWh/m^2-yr]	DNI [kWh/m^2-yr]	DIF [kWh/m^2-yr]	Lat [°]	Lon [°]
DNI-2000	1577	2030	452	-38.852	-72.586
DNI-2500	1885	2509	377	-33.313	-71.460
DNI-3000	2219	3033	291	-26.275	-70.526
DNI-3500	2454	3501	251	-26.414	-69.980

With respect to distances and altitudes, different values of each of them were analyzed for every DNI level. The distance was changed from 5 to 100 km, while the altitude was varied from 20 to 1000 meters. Table 5-4 shows the cases evaluated with the respective DNIs, distances, and altitudes considered.

As the reference case, it was considered a plant located at the minimum distance and altitude, 5 km and 20 m, respectively, with a DNI level of 2500 kWh/m^2-yr. An optimization is performed to the reference location, and the LINMAP optimum solution is obtained. Then, a sensitivity analysis considering the optimum plant configuration of the reference location is carried out to assess the effect of each location parameter. After that, optimizations of the plant varying each location parameter are done considering the cases presented in **Error! R eference source not found.**. The Pareto-fronts and LINMAP optimum solutions are obtained and analyzed. Finally, cost maps are built with the LINMAP optimal solution of each possible combination of the location parameters. For that, four levels of DNI (2000, 2500, 3000 and 3500 kWh/m^2-yr), six distance values (5, 20, 40, 60, 80 100 km) and six altitude values (20, 100, 250, 500, 750, 1000) were considered. Each map is built with the

TCE and TCW of the LINMAP optimum solution, which is obtained by varying two location parameters, while the other is kept fixed. As a result, the following maps are presented in the next section: DNI vs. distance with an altitude of 20 m, DNI vs. altitude with a distance of 5 km, and distance vs. altitude with a DNI of 2500 and 3000 kWh/m^2-yr.

Table 5-4: Solar irradiation, distance from the sea, and altitude parameters of each case.

Case	DNI [kWh/m^2-yr]	Distance [km]	Altitude [m]
DNI 2000	2000	5	20
DNI 2500	2500	5	20
DNI 3000	3000	5	20
DNI 3500	3500	5	20
Dis-5	2500	5	20
Dis-20	2500	20	20
Dis-40	2500	40	20
Dis-60	2500	60	20
Dis-80	2500	80	20
Dis-100	2500	100	20
Alt-20	2500	5	20
Alt-100	2500	5	100
Alt-250	2500	5	250
Alt-500	2500	5	500
Alt-750	2500	5	750
Alt-1000	2500	5	1000

5.4 Results and discussion

The results of the study are presented in three sections. Firstly, the reference case results are presented. After that, the results of the sensitivity analysis of each location parameter. Finally, the cost maps for different combinations of the location parameters are presented.

5.4.1 Reference case analysis

Figure 5-3 shows the optimal solution and the optimization procedure for the reference case. The scattered points represent the parametric analysis results used to build the surrogate model, in which the values of $Suf_{e\&w}$ are illustrated with the color bar, the black points are the Pareto-frontier from the multi-objective optimization, and the white circle with the black edge is the optimal solution selected by LINMAP. It can be highlighted that the solutions with higher $Suf_{e\&w}$ are associated with the lower TCW due to the fact that the higher water production has a favorable impact on the water cost.

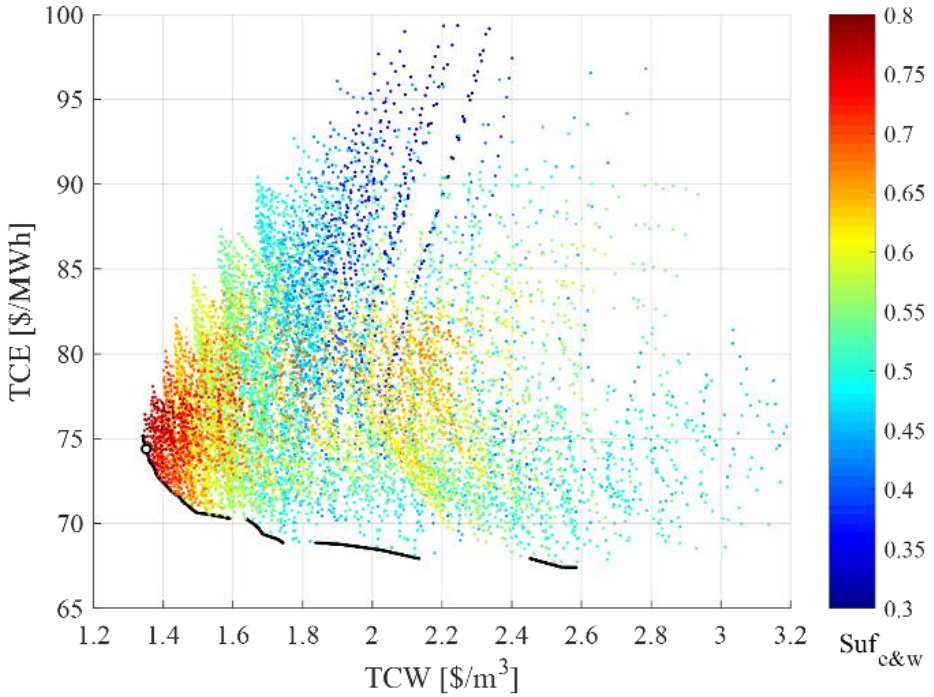

Figure 5-3: Feasible solution space from the parametric analysis, the Pareto frontier obtained from multi-objective GA, and the LINMAP solution for the reference case.

Table 5-5 shows the optimum solution selected by LINMAP. Regarding the sizing, an oversized CSP plant with a large number of MED units is obtained, integrated with a small PV plant. Due to the size obtained for the PV plant, its operation aims to cover the plant's parasitic consumption, so the continuous operation of the CSP+MED system is, in this case, prioritized to enhance their operation hours. The $Suf_{e\&w}$ achieves a value of 59%.

Table 5-5: LINMAP optimum solution for 3000 DNI, 5 km distance, and 20 m altitude.

Case	PV [MW]	SM [-]	TES [h]	MED [units]	TCE [$/MWh]	TCW [$/m^3]	Electricity [GWh]	Water [m^3]	CF_{el} [%]	CF_w [%]	$Suf_{e\&w}$ [%]
Opt1	10.4	3.75	15.9	7	74.35	1.35	740.8	19.80	84.6	77.5	76.2

5.4.2 Sensitivity analysis, Pareto frontier and optimum solutions for different location parameters

Taking the optimum plant configuration obtained from the reference case, a sensitivity analysis was performed to evaluate the change in the electric and water cost with the variation of each location parameter (solar radiation, distance, and altitude). The results are shown is Figure 5-4, where it is observed that the DNI has the main effect in the TCE and TCW, but the impact is nonlinear. For the DNI level of 2000 kWh/m^2-yr, the TCE and TCW increase 35% and 30%, respectively, comparing to the reference case. However, for DNI levels of 3000 kWh/m^2-yr and 3500 kWh/m^2-yr, the TCE and TCW decrease 22% and 28%, respectively, with respect to the reference case. It means that the increase in the cost is significant for lower DNI levels, and as the DNI is higher, the decrease in the cost is lower. Regarding the distance from the sea, it is shown that it mainly affects the TCW and has a slight impact on the TCE. The TCW increases 170% for a distance of 100 km with respect to the reference case. Finally, the altitude has a moderate impact on the costs, resulting in the TCE and TCW increases of 9% and 18%, respectively, for an altitude of 1000 meters compared to the reference case. Therefore, the DNI level and the distance from the sea have resulted in being the most critical variables.

Moreover, the variation of the location parameters changes the solutions that compose the Pareto-frontier and the LINMAP optimal solution configuration. Figure 5-5 shows the Pareto-fronts resulted from the optimization procedure for each sensitivity case of DNI, distance, and altitudes with their respective optimal solution. The non-linearity of the cost impact for the DNI variation is highlighted, showing a significant increase in the TCE and TCW tradeoff for 2000 kWh/m^2-yr. For the distance, the TCE for the different Pareto-fronts is maintained, but the TCW is considerably increased. Finally, for the altitude, it seems that its impact is linear the higher the altitude is.

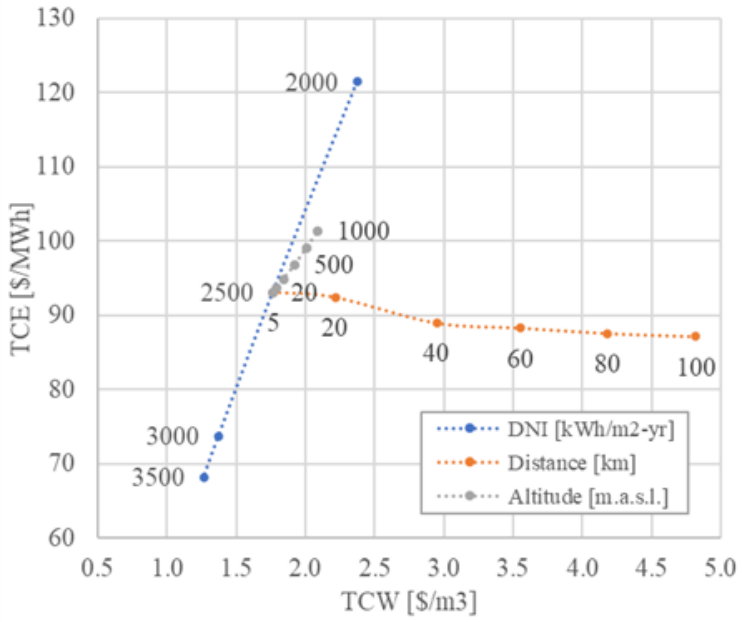

Figure 5-4: Sensitivity analysis with respect to the reference case varying the DNI, the distance, and the altitude of plant location.

The results of the LINMAP optimal solutions for each case evaluated are detailed in Table 5-6. In general, the size obtained corresponds to an oversized CSP plant with 3.6 to 3.8 of SM and 16-18 h of TES capacity. The exception was for the location with the highest DNI (3500 kWh/m^2-yr), in which a CSP plant slightly smaller (3.3 of SM and 14 h of TES) is obtained. Regarding the MED plant, seven units were found for most of the cases, which evidences that this could be the ideal size of the desalination plant. This happens because this number of units can use the largest amount of the steam available, maintaining the MED operation at a nominal load. In the case of 8 units, the MED plant would operate at 90% of the nominal load since the heat demand is higher than the exhaust steam flow rate provided by the power block. In this case, the increase in water production would not compensate since the cost addition of the MED and P/R system plus the increasing pumping consumption would lead to a rise in the TCW. Regarding the PV plant size, it is shown that a PV plant of 30 MW is the optimum one for most of the cases, with a maximum of 40 and 50 MW for the longest distance and the lower DNI, respectively. This is due to the parasitic consumption increase the higher the distance and altitude are.

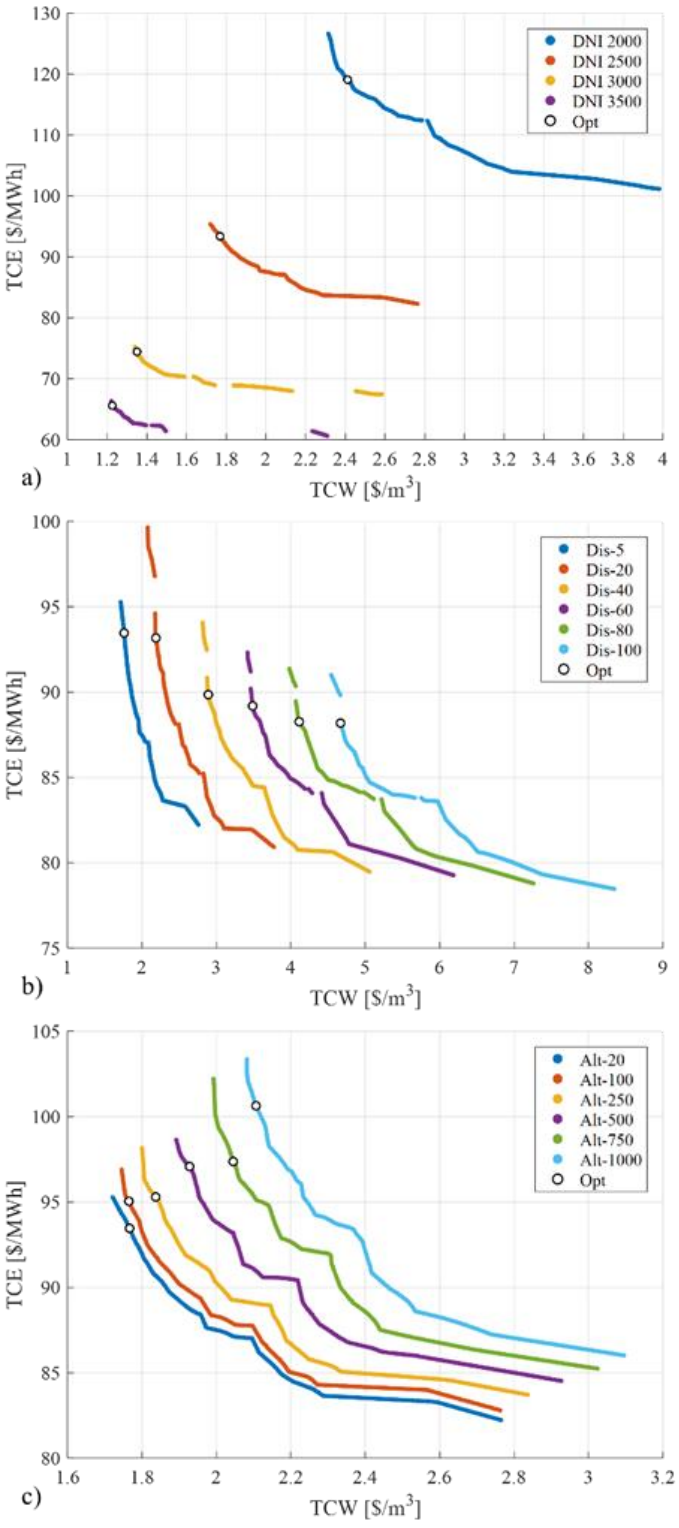

Figure 5-5: Pareto frontier and optimum solutions for different DNIs (a), distances (b), and altitudes (c).

Table 5-6: Optimum configurations and thermoeconomic results.

Case	PV [MW]	SM [-]	TES [h]	MED [units]	TCE [$/MWh]	TCW [$/m^3]	Electricity [GWh]	Water [hm^3]	CF_{el} [%]	CF_w [%]	$Suf_{e\&w}$ [%]	C_{el} [M$]	C_w [M$]
DNI 2000	50.4	3.79	17.3	6	118.92	2.40	491.1	9.99	56.1	45.6	45.1	58.40	24.03
DNI 2500	30.3	3.66	17.2	7	93.68	1.77	598.9	14.68	68.4	57.4	59.3	56.10	25.91
DNI 3000	10.1	3.72	16.1	7	74.28	1.35	738.7	19.78	84.3	77.4	76.0	54.87	26.66
DNI 3500	10.0	3.30	14.0	7	65.58	1.23	766.6	20.68	87.5	81.0	79.2	50.27	25.39
Dis-5	30.3	3.66	17.2	7	93.68	1.77	598.9	14.68	68.4	57.4	59.3	56.10	25.91
Dis-20	30.1	3.80	17.3	7	89.90	2.33	606.6	14.94	69.3	58.5	60.2	54.54	34.78
Dis-40	21.3	3.81	17.7	7	89.38	2.91	585.1	15.14	66.8	59.3	59.3	52.30	44.11
Dis-60	30.0	3.81	18.0	7	88.68	3.52	580.9	15.03	66.3	58.8	58.9	51.51	52.87
Dis-80	39.4	3.79	17.6	7	87.79	4.13	574.0	14.87	65.5	58.2	58.2	50.39	61.42
Dis-100	40.0	4.00	18.0	7	88.07	4.67	565.3	15.34	64.5	60.0	58.5	49.78	71.72
Alt-20	30.3	3.66	17.2	7	93.68	1.77	598.9	14.68	68.4	57.4	59.3	56.10	25.91
Alt-100	23.1	3.80	17.7	7	94.98	1.76	601.6	15.19	68.7	59.4	60.3	57.14	26.78
Alt-250	30.7	3.80	16.2	7	95.18	1.83	598.7	14.78	68.3	57.8	59.5	56.98	27.08
Alt-500	38.5	3.76	17.3	7	96.99	1.93	589.5	14.69	67.3	57.5	58.8	57.18	28.27
Alt-750	40.0	3.42	16.0	7	97.24	2.04	547.5	13.83	62.5	54.1	54.9	53.24	28.21
Alt-1000	40.2	3.78	16.0	7	100.59	2.11	549.5	14.67	62.7	57.4	56.5	55.28	30.93

It is also important to mention the differences in the production, the electric and water CF, the $Suf_{e\&w,}$ and the annual cost allocated to the electricity and water (C_{el} and C_w). The DNI level significantly affects the performance of the CSP and PV plants, varying the cogeneration plant production. It is observed that for 2000 kWh/m^2-yr, the electric and water CF decrease up to 56 and 34%, respectively, achieving the lowest $Suf_{e\&w}$, and causing an increase in the TCE and TCW. On the contrary, with a DNI level of 3500 kWh/m^2-yr, the highest electric and water CF are achieved, both over 70%, reaching a $Suf_{e\&w}$ of 79%, which results in lower values of TCW and TCE. In the case of the effect of the distance, it is observed no impact on the $Suf_{e\&w}$ but a significant increase in the C_w over 40 km, varying from 26 to 72 M$. This increase is due to the high capital costs of the two pipelines which are allocated entirely to the water. Concerning the altitude, a moderate decrease in the $Suf_{e\&w}$ is observed for higher altitudes, which can be referred to the increase of the P/R system electric consumption. Moreover, it is detected a change in the C_{el} and C_w, varying the C_{el} slightly, and increasing the C_w moderately for higher altitudes. This change is because of the increase in the electric consumption to transport the seawater and the rise of the pumping station and recovery turbine costs (higher power capacities).

Figure 5-6 presents the cost breakdown of the TCE and TCW for the twelve cases. It is shown that the CSP cost is the main contributor to both TCE and TCW, while the MED plant has a significant contribution only to the TCW. The P/R system cost has a substantial contribution to TCW for distances larger than 40 km. Specifically, it is shown that the higher the DNI levels, the lower the contribution of the CSP cost in both TCE and TCW is, achieving contributions under 0.6 $/m^3 to the TCW. Also, the MED contribution to the TCW depends on the water CF, achieving a contribution under 0.65 $/m^3 for higher values of DNI.

Regarding the effect of the distance, the TCE presents only a small variation for the P/R cost allocation. For 5 and 20 km, a P/R cost fraction is allocated to the electricity, while for 40 to 100 km, the entire P/R cost is assigned to the water. This happens because the recovery system for the latter cases requires power to transport the brine back to the sea (a pumping system) since the pipeline's head losses are higher than the height difference. In contrast, the CSP contribution to the TCW increases for longer distances, implying that additional cost is

allocated due to the higher pumping consumption. The MED contribution is maintained around 0.85 $/m^3, and the P/R cost significantly increases with distances over 40 km. Concerning the altitude effect, the TCE has a small increase of 7 $/MWh for higher altitudes, with contributions of the CSP and P/R costs. For altitudes over 500 m, there is a moderately lower electricity production that increases the contribution of the CSP, while the P/R cost grows its allocation to the TCE due to the rise in the recovery turbine power. Conversely, the TCW increases 0.3 $/m^3 for 1000 m due to the increase of the CSP contribution because the pumping consumption.

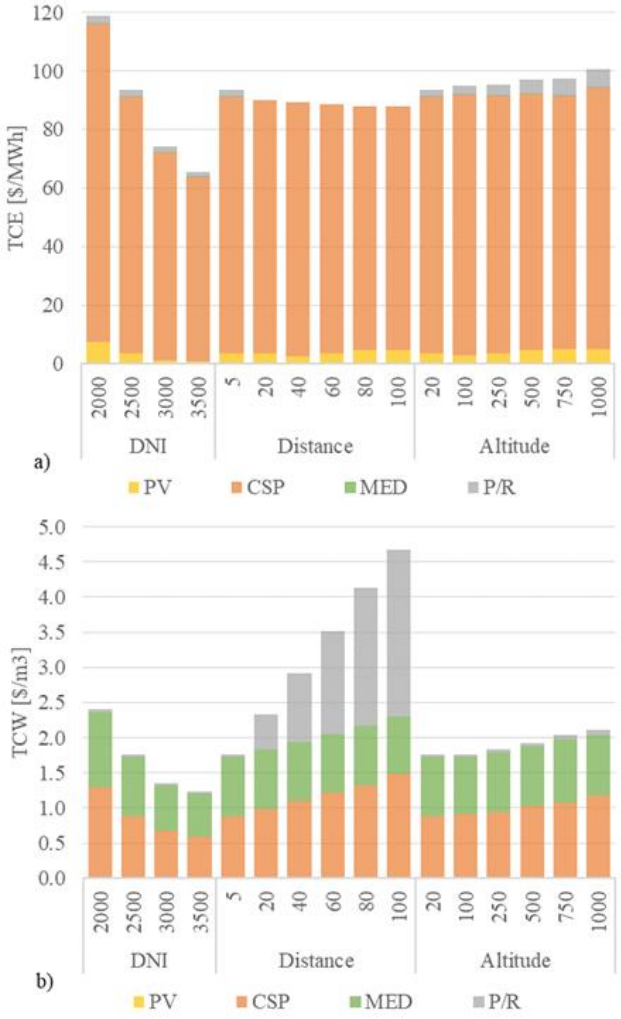

Figure 5-6: TCE (a) and TCW (b) breakdown of the LINMAP optimum solution in terms of the PV, CSP, MED, and P/R systems costs.

5.4.3 TCE and TCW maps

This section presents the results obtained from the assessment of the combined effect of the location parameters (DNI, distance from the sea, and altitude), where the resulting cost maps are presented. Figure 5-7 shows the TCE and TCW maps in terms of the DNI and the distance from the sea, maintaining an altitude of 20 m. The figure shows that a similar TCE with respect to the distance is held, and the nonlinear effect of the DNI is kept for all distances. On the contrary, the TCW is considerably affected by the distance, where the impact is more accentuated for lower DNI values. From these maps, it can be stated that locations with DNI lower than 2500 kWh/m^2-yr are less competitive for the CSP+PV+MED deployment since they achieve TCW over 2.5 \$/m^3, despite achieving TCE under 120 \$/MWh (competitive water cost should be between 1-2 \$/m^3 according to (Alhaj & Al-Ghamdi, 2019; IRENA, 2012; Omar et al., 2020a)). Those locations should not be considered as potential sites unless they are close to the coast (less than 5 km distance) or the CSP cost has a significant reduction.

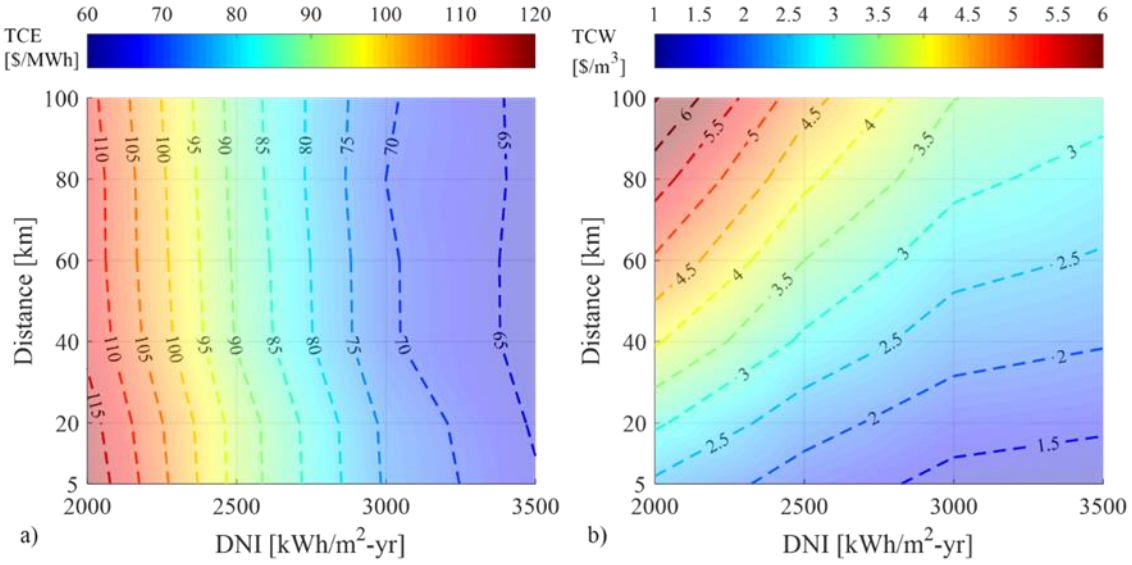

Figure 5-7: TCE (a) and TCW (b) of the LINMAP optimum solution in terms of the DNI and the distance (altitude = 20 m).

Figure 5-8 shows the TCE and TCW maps in terms of the DNI and the altitude, maintaining a distance from the sea of 5 km. It is observed the same trend as the previous figure for the TCE, with a slight increase for higher altitudes. In contrast, it is observed an increase of around 15-20% of the TCW for the highest altitude. Competitive TCE and TCW (under 100 \$/MWh and 2 \$/m^3) can be obtained for DNI values over 2500 kWh/m^2-yr and altitudes up to 1000 m.

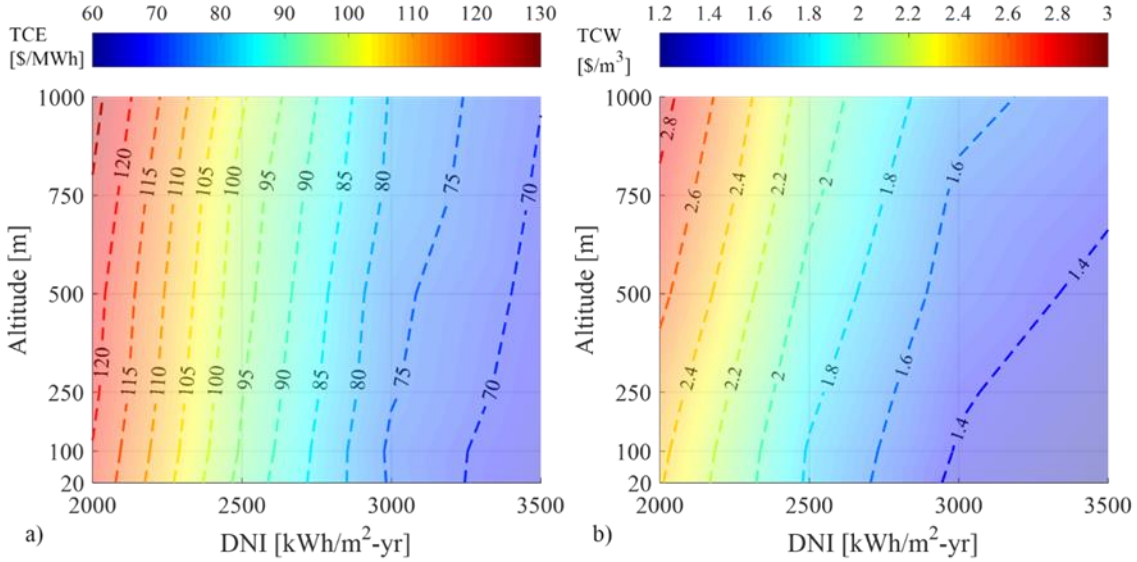

Figure 5-8: TCE (a) and TCW (b) of the LINMAP optimum solution in terms of the DNI and the altitude (distance = 5 km).

Finally, Figure 5-9 shows the TCE and TCW maps in terms of the distance from the sea and the altitude, maintaining a DNI of 2500 and 3000 kWh/m^2-yr. In this case, it is observed the combined effect of distance and altitude, where one of the most relevant factors is the allocation of the P/R cost. From both TCW maps, it can be deduced that the solution within the triangle with coordinates (Altitude, Distance): 20-40, 20-100, and 500-100 present pipeline head losses higher than the height difference, so additional power is required to transport the brine and cooling rejection, and the P/R cost is fully allocated to the TCW. However, out of this area, the pipeline head losses are lower than the height difference, so part of the resultant brine and cooling rejection potential energy can be recovered, allocating part of the P/R cost to the TCE. Evidence of this is the increase of the TCE for distances and

altitudes over 20 km and 250 m, respectively. On the other hand, we can identify some interesting areas where the cogeneration plant shows more competitive costs. In the case of a DNI of 2500 kWh/m^2-yr, TCE under 120 \$/MWh and TCW under 2.4 \$/m^3 are achieved for altitudes over 250 m and distances under 60 km. In the case of altitudes below 250 m, TCEs lower than 100 \$/MWh can be achieved, while TCW values under 2.0 \$/m^3 are only obtained for a distance below 40 km.

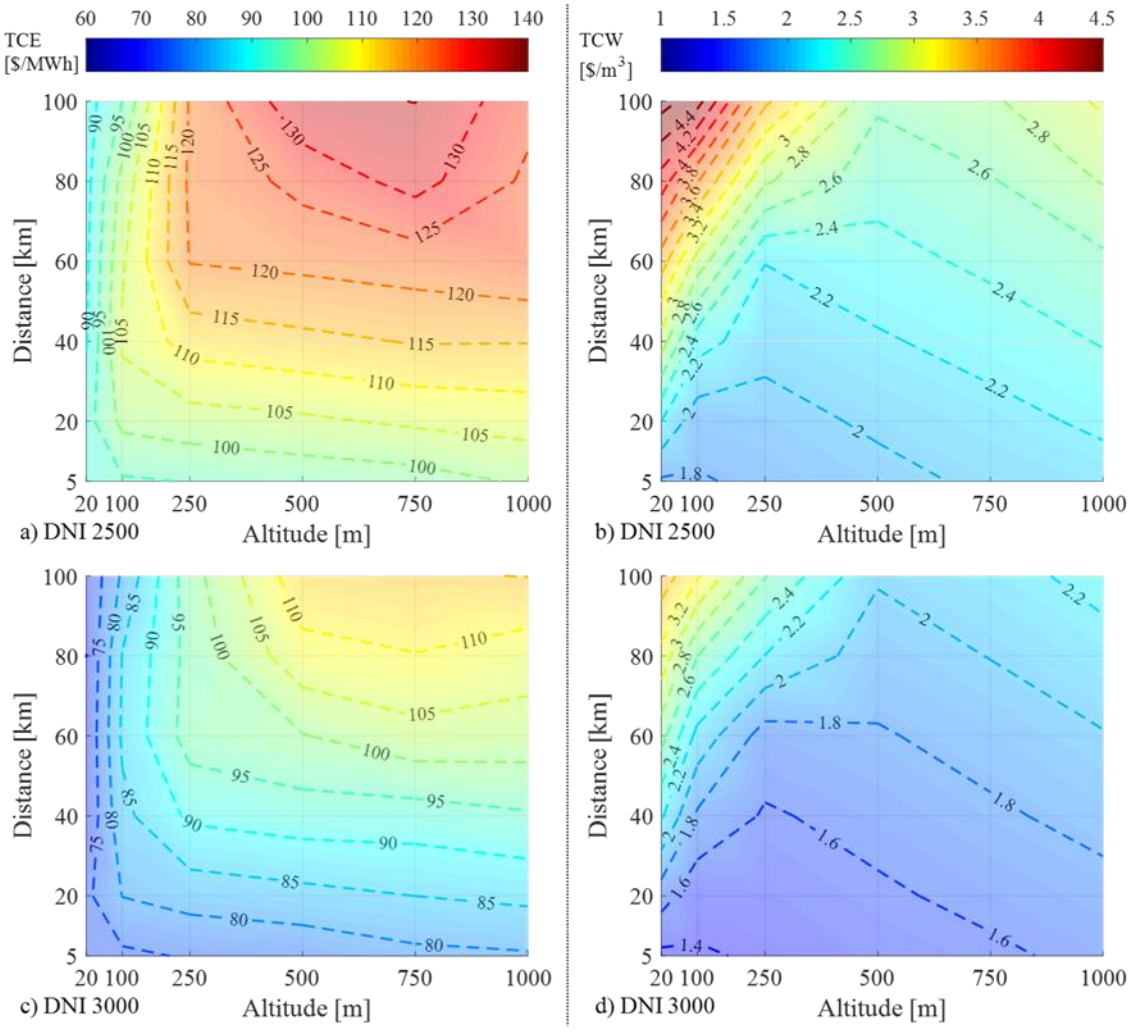

Figure 5-9: TCE (a and c) and TCW (b and d) of the LINMAP optimum solution in terms of the distance and the altitude (DNI = 2500 and 3000 kWh/m^2-yr).

With the increase of the DNI up to 3000 kWh/m^2-yr, more competitive costs can be achieved, following the same tendency of the map at 2500 kWh/m^2-yr, with approximately 15-25% of

costs difference. Comparing with the cost for a coastal location (5 km of distance and 20 m of altitude) with a DNI of 2500 kWh/m^2-yr (TCE = 93 $/MWh and TCW = 1.8 $/m^3), a location with a DNI of 3000 kWh/m^2-yr would be equivalent in terms of costs, for distances between 40-60 km and altitudes between 100-750 m. Under this threshold, more competitive costs can be achieved in an inland location. Therefore, the results show that the limit of the distance that could be considered to install a CSP+PV+MED plant at an inland location with a higher solar resource should be no more than 60 km. In the case of the altitude, altitudes up to 750 m could be taken into account, and over 750 m should be carefully considered if there is a significant increase of the DNI.

5.5 Conclusion

The present work describes a multi-objective optimization of a CSP+PV+MED plant that determines the effect of the location parameters (solar irradiation, distance from the coast, and altitude of the plant above the sea level) on the performance and the electricity and water costs to define the ideal site characteristics from an economic point of view. The study comprehends a thermoeconomic analysis of the plant that assesses the cost formation process and seek the differences in the cost allocation to both products: electricity and water. The main conclusions can be summarized as follows:

- From the optimization results, it has been obtained that the optimum sizing for a CSP+PV+MED plant for most location conditions would be an oversized CSP plant with 3.6-3.8 of SM and 16-18 h of TES capacity, 7 MED units, and a small PV plant of 30-50 MW. This sizing would lead to reduce the TCW and to maximize the water production, having a slightly higher TCE.
- The solar irradiation is the variable that has the most important effect on both costs, the TCE and TCW. Its effect is nonlinear, so a higher DNI allows lower costs, but the cost reduction becomes smaller the higher the DNI is. Locations with a DNI of 2000 kWh/m^2-yr can have an increase of over 35% on the costs compared to the reference case (2500kWh/m^2-yr), while locations with DNI levels of 3500 kWh/m^2-yr can achieve a decrease of 28% in the costs regarding the reference case. Moreover, TCE under 100 $/MWh and TCW under 2 $/m^3 are found for DNI over

2500 kWh/m^2-yr. Thus, locations with DNI above this level would have a higher potential for installing a CSP+PV+MED plant.

- The distance from the coast is the second most important variable that affects the costs, mainly the TCW, and its effect is related to the high capital pipeline cost. It is obtained that the increase in the TCW can be over 100% for a distance of 60 km compared to the reference case (5 km). Over this distance, the P/R system's cost becomes significantly higher, making the TCW less attractive. Thus, distances under this threshold are recommended for the installation of this kind of cogeneration plants.
- The altitude has a moderate impact on the costs, affecting the electric consumption of the P/R system and the plant's electric balance. The results show that for higher altitudes, the electric parasitic consumption of the conveyance system is relevant. However, the cost of the P/R system is allocated to the TCE and TCW depending on the brine pipeline's head losses with respect to the height difference. If the head losses are higher than the height difference, the cost of the P/R system is entirely allocated to the TCW, while if they are lower, part of the pipeline cost is assigned to the TCE. It is concluded that it is better to have higher solar irradiation and shorter distance to the coast instead of a lower altitude, in which potential locations can be found for altitudes up to 750 m if a significant increase of the DNI is available.
- Finally, maps of the TCE and TCW in terms of the location parameters (DNI, distance from the sea, and altitude) have been obtained. These maps give insights about which locations have a higher potential for deploying a cogeneration CSP+PV+MED plant. The information obtained can be used as a reference about the worldwide deployment potential, helping to discard certain areas and focusing on the places that meet the best cost expectations. In real locations, the DNI levels change with the distance from the coast and altitude. From the results obtained, it is concluded that it is possible to find inland locations where the increase of the DNI levels can compensate for the higher cost of the P/R system. In fact, we recommend focusing the potential for installation of these cogeneration plants on inland locations with a considerable increase of the DNI (above of 300 kWh/m^2-yr) with respect to

DNI levels at the coast, distances from the coast of no more than 60 km and altitudes up to 750-1000 m. These constraints limit the deployment of this kind of plant to a few locations around the world.

6. CONCLUSIONS

This dissertation outlines a methodology focused on determining the set of optimal design configurations of a solar power plant integrated with a desalination plant to produce electricity and water, that is based on thermoeconomic analysis. The study analyzes in detail a CSP+PV+MED plant concept, performing an exhaustive thermoeconomic analysis to determine the cost formation process of the products. For this, a model and simulation of the plant were developed considering the solar irradiation variability, the sizing of the components, different operation conditions, and the location parameters. In that way, a multi-objective optimization of the design configuration is performed in terms of costs and productivity to determine the optimal solutions under different location conditions. Additionally, a comparison between the CSP+PV+MED and the CSP+PV+RO integration is performed to determine the CSP+PV+MED concept competitiveness and identify the aspects to improve its overall performance. The research's specific conclusions are found in each journal paper in Chapter II, III, IV, and V. Moreover, a summary of the main conclusions from the appended papers and the general findings are the following:

- In the modeling of a solar power plant integrated with a desalination plant, it is relevant to consider the additional and auxiliary components and the specific part-load operation performance of each system. Systems such as seawater transportation significantly affect the plant’s performance and power balance. Thus, the plant's detailed modeling allows us to assess the performance accurately, considering the interaction between the systems, giving clear insights about the plant’s operation mode.
- The thermoeconomic analysis illustrates the relevance between the destroyed exergy, the plant operation mode, and component cost allocation into the plant products, electricity and water. The study reveals that the main factor that affects the cost allocation is the cost rate of the components. Contrarily, the impact of the plant operation and the destroyed exergy have a secondary role. Among the plant operation factors, the operation at part-load conditions shows a considerable impact. This is because the component production per hour decreases, increasing the product specific cost. Moreover, this effect is extended for the operation of all plant

components throughout the year that result in a complex combination of each system's contribution, where the cost allocation changes on an hourly basis. The analysis performed allows us to detect the hourly, daily, monthly, and seasonal impact of these factors. Therefore, it is crucial to perform the thermoeconomic analysis in hourly resolution due to it allows capturing the cost allocation variations to properly determine the actual annual cost of electricity and water.

- The sizing of a CSP+PV+MED plant has high importance on the plant operation, and the final products cost. The CSP coupling with a MED plant represents a complex problem due to each system has a different mode of operation. The CSP has a variable operation due to the nature of the solar irradiation variability. At the same time, the MED plant requires a continuous 24/7 operation near the nominal point to increase its productivity. When these systems are integrated, it is necessary to modify the CSP plant's sizing to adapt to the MED plant operation needs, oversizing the CSP plant (large SM and TES capacity). This sizing allows us to obtain the lower water cost but with the detriment of a moderate higher electricity cost.
- The inclusion of the PV plant into a CSP+MED plant can improve the electricity production and significantly decrease electricity costs. However, depending on its size, it could positively or negatively affect the performance of the desalination plant and the water cost. The PV integration implies that the power cycle would work at part-load or turn off since the PV output is prioritized, reducing the MED plant's operational hours. Therefore, small-medium PV sizes that contribute with a small share of the nameplate capacity (30%) are required, maintaining the power block and MED operating at more than 70% of its nominal capacity and covering the parasitic consumptions. This size benefits the water production and minimizes the water cost.
- The number of MED units mainly affect the water productivity and moderately impact the overall plant performance. The conveyance systems (P/R system) highly depend on the MED capacity since the pipeline cost becomes significant with large capacities. In this way, the minimum electricity costs are achieved with the minimum number of MED units. In contrast, the lower water costs can be reached with a high number of MED units and PV+CSP configurations that achieve water capacity

factors over 85%. Moreover, large MED plants configurations (between 80-100% of the maximum capacity) have a technological challenge related to its reliability. The MED must ensure the power block cooling requirements, considering that these systems have different time responses. The research concludes that it is better to select a large number of units, taking advantage of the economy of scale and compensating the higher cost of the pipeline.

- The multi-objective optimization using the surrogate model drastically reduces the computational time needed to perform a genetic algorithm analysis. This approach illustrates how a complex problem can be simplified and resolved in order to analyze different cases and scenarios without losing the accuracy of the results. The aim was to obtain the Pareto-fronts to explore the different optimum solutions and perform a decision-making analysis to select the most suitable solution. Thus, it is recommended to use this method in similar optimization problems concerning cogeneration or polygeneration systems.
- In addition to minimizing the electricity and water costs, one of the relevant factors in CSP+PV+MED plant optimization is to maximize the plant's productivity. The study has shown that different optimal solutions in the Pareto-front obtain similar costs but significant productivity differences. Therefore, the inclusion of productivity as an objective function of the optimization problem allows analyzing another dimension of the solution space. This can give a more in-depth insight into what is the best design configuration for a decision-maker, where the market conditions, the demand requirements, and the project profitability can influence the final decision.
- The optimum sizing of a CSP+PV+MED plant was assessed to obtain the lowest electricity and water costs and the highest productivity (electricity and water). The optimum sizing consists of a medium PV plant (PV=40-70 MW_e) and a large/oversized CSP plant (SM=3-3.6 and TES=14-18 h) integrated with 6 to 8 MED units (amount required to use more than 80% of the power cycle waste heat). This sizing aims to minimize the water cost and maximize productivity, considering a moderate higher electricity cost. This approach should be taken as a reference in the evaluation of solar power plants integrated with desalination plants.

- Compared to the CSP+PV+RO plant, the CSP+PV+MED plant achieves competitive electricity cost but moderately higher water cost (18-30% higher). The main reason for the difference is the high energy cost (heat and electricity) used to produce water, in which the main contributor is the CSP cost. The MED cost significantly contributes to the water cost, while the pipeline cost could be relevant if the plant is at an inland location. Moreover, the concept's economic viability can be achieved with a 30% CAPEX reduction of the CSP and MED plant. Other potential improvements should consider: integrating other solar technologies with lower heat cost, improving the performance (GOR) of the MED plant with nanofiltration pretreatment, integration of absorption or adsorption system to the condenser or use thermal vapor compressor, reduce the seawater requirement of the MED plant for the same productivity and consider hybrid MED+RO desalination system. However, these concepts can affect the power block performance and the plant’s power balance, so they must be evaluated.
- The CSP+PV+MED plant location has a key role in the performance and actual products cost. The results conclude that the DNI level is the factor with the major effect on electricity and water costs, and its impact is nonlinear. For lower DNI, the higher are the electricity and water cost, but as higher is the DNI, the lower is the decrease in the cost. Thus, for a location with DNI higher than 3000 kWh/m^2-yr, the benefit is minor. The distance respect to the sea is the second most important location variable affecting the water cost principally, where it becomes considerable from 40 km. Finally, the altitude presents a moderate effect on the costs because it only changes the plant’s power balance. From 500 m, it can change the allocation of the conveyance system between electricity and water cost. Therefore, the ideal location for the CSP+PV+MED should have a DNI higher of 2500 kWh/m^2-yr (unless the CSP cost decreases considerably), a distance less than 60 km from the coast and an altitude under 1000m.
- Finally, electric and water cost maps regarding the location conditions (DNI, distance respect to the sea, and altitude) are obtained. These maps can be used as a tool to

preliminary define the cost feasibility of the CSP+PV+MED plant for different conditions.

This dissertation presents an extensive methodology to optimize a CSP+PV+MED plant with models, results, analysis, and discussion that contributes to the field of cogeneration plants with solar power and desalination. The models and methodology serve as a basis for future studies related to the cost-benefit analysis that can improve the competitiveness of these types of plants. Moreover, the method could be used as a design tool in a case-by-case analysis for a specific project or study. Furthermore, future research studies are required for studying new technology and novel plant concepts that could enhance the understanding about the potential of the cogeneration of electricity and water with solar energy.

REFERENCES

Abdelkareem, M. A., El Haj Assad, M., Sayed, E. T., & Soudan, B. (2018). Recent progress in the use of renewable energy sources to power water desalination plants. *Desalination*, *435*(2018), 97–113. https://doi.org/10.1016/j.desal.2017.11.018

Aboelmaaref, M. M., Zayed, M. E., Zhao, J., Li, W., Askalany, A. A., Salem Ahmed, M., & Ali, E. S. (2020a). Hybrid solar desalination systems driven by parabolic trough and parabolic dish CSP technologies: Technology categorization, thermodynamic performance and economical assessment. *Energy Conversion and Management*, *220*(June), 113103. https://doi.org/10.1016/j.enconman.2020.113103

Aboelmaaref, M. M., Zayed, M. E., Zhao, J., Li, W., Askalany, A. A., Salem Ahmed, M., & Ali, E. S. (2020b). Hybrid solar desalination systems driven by parabolic trough and parabolic dish CSP technologies: Technology categorization, thermodynamic performance and economical assessment. *Energy Conversion and Management*, *220*(June), 113103. https://doi.org/10.1016/j.enconman.2020.113103

Adibhatla, S., & Kaushik, S. C. (2017). Exergy and thermoeconomic analyses of 500 MWe sub critical thermal power plant with solar aided feed water heating. *Applied Thermal Engineering*, *123*, 340–352. https://doi.org/10.1016/j.applthermaleng.2017.05.099

Ahmadi, P., Dincer, I., & Rosen, M. A. (2014). Thermoeconomic multi-objective optimization of a novel biomass-based integrated energy system. *Energy*, *68*, 958–970. https://doi.org/10.1016/j.energy.2014.01.085

Ahmed, F. E., Hashaikeh, R., & Hilal, N. (2019). Solar powered desalination – Technology, energy and future outlook. *Desalination*, *453*(November 2018), 54–76. https://doi.org/10.1016/j.desal.2018.12.002

Al-Karaghouli, A., & Kazmerski, L. L. (2013). Energy consumption and water production cost of conventional and renewable-energy-powered desalination processes. *Renewable and Sustainable Energy Reviews*, *24*, 343–356. https://doi.org/10.1016/j.rser.2012.12.064

Al-Obaidi, M. A., Filippini, G., Manenti, F., & Mujtaba, I. M. (2019). Cost evaluation and optimisation of hybrid multi effect distillation and reverse osmosis system for seawater desalination. *Desalination*, *456*(February), 136–149. https://doi.org/10.1016/j.desal.2019.01.019

Alhaj, M., & Al-Ghamdi, S. G. (2019). Why is powering thermal desalination with concentrated solar power expensive? assessing economic feasibility and market commercialization barriers. *Solar Energy*, *189*(August), 480–490. https://doi.org/10.1016/j.solener.2019.07.046

Aly, A., Bernardos, A., Fernandez-Peruchena, C. M., Solvang Jensen, S., & Pedersen, A. B. (2019). Is Concentrated Solar Power (CSP) a feasible option for Sub-Saharan Africa?: Investigating the techno-economic feasibility of CSP in Tanzania. *Renewable Energy*, *135*, 1224–1240. https://doi.org/10.1016/j.renene.2018.09.065

Ameri, M., Ahmadi, P., & Hamidi, A. (2009). Energy, exergy and exergoecnomic analysis of a steam power plant: A case study. *International Journal of Energy Research*, *33*, 499–512. https://doi.org/10.1002/er.1495

Ameri, M., & Jorjani, M. (2016). Performance assessment and multi-objective optimization of an integrated organic Rankine cycle and multi-effect desalination system. *Desalination*, *392*, 34–45. https://doi.org/10.1016/j.desal.2016.04.009

Arora, R., Kaushik, S. C., Kumar, R., & Arora, R. (2016). Soft computing based multi-objective optimization of Brayton cycle power plant with isothermal heat addition using evolutionary algorithm and decision making. *Applied Soft Computing Journal*, *46*, 267–283. https://doi.org/10.1016/j.asoc.2016.05.001

Askari, I. B., & Ameri, M. (2016). Techno economic feasibility analysis of Linear Fresnel solar field as thermal source of the MED/TVC desalination system. *Desalination*, *394*, 1–17. https://doi.org/10.1016/j.desal.2016.04.022

Askari, I. B., Ameri, M., & Calise, F. (2018). Energy, exergy and exergo-economic analysis of different water desalination technologies powered by Linear Fresnel solar field. *Desalination*, *425*(March), 37–67. https://doi.org/10.1016/j.desal.2017.10.008

Bejan, A., Tsatsaronis, G., & Moran, M. (1995). Thermal Design and Optimization.

Blair, N., Dobos, A. P., Freeman, J., Neises, T., Wagner, M., Ferguson, T., … Janzou, S. (2014). *System Advisor Model, SAM 2014.1.14: General Description*.

Blanco, J., Palenzuela, P., Alarcón-Padilla, D., Zaragoza, G., & Ibarra, M. (2013). Preliminary thermoeconomic analysis of combined parabolic trough solar power and desalination plant in port Safaga (Egypt). *Desalination and Water Treatment*, *51*(7–9), 1887–1899. https://doi.org/10.1080/19443994.2012.703388

Boretti, A. (2018). Cost and production of solar thermal and solar photovoltaics power plants in the United States. *Renewable Energy Focus*, *26*(September), 93–99. https://doi.org/10.1016/j.ref.2018.07.002

Boyaghchi, F. A., & Safari, H. (2017). Parametric study and multi-criteria optimization of total exergetic and cost rates improvement potentials of a new geothermal based quadruple energy system. *Energy Conversion and Management*, *137*, 130–141. https://doi.org/10.1016/j.enconman.2017.01.047

Carballo, J. A., Bonilla, J., Roca, L., De la Calle, A., Palenzuela, P., & Alarcón-Padilla, D. C. (2018). Optimal operating conditions analysis for a multi-effect distillation plant according to energetic and exergetic criteria. *Desalination*, *435*(August 2017), 70–76. https://doi.org/10.1016/j.desal.2017.12.013

Casimiro, S., Cardoso, J., Alarcón-Padilla, D.-C., Turchi, C., Ioakimidis, C., & Mendes, J. F. (2013). Modeling multi effect distillation powered by CSP in TRNSYS. *Energy Procedia*, *49*, 2241–2250. https://doi.org/10.1016/j.egypro.2014.03.237

Casimiro, S., Cardoso, J., Ioakimidis, C., Farinha Mendes, J., Mineo, C., & Cipollina, A. (2014). MED parallel system powered by concentrating solar power (CSP). Model and case study: Trapani, Sicily. *Desalination and Water Treatment*, *3994*(March 2015), 1–14. https://doi.org/10.1080/19443994.2014.940222

Catrini, P., Cipollina, A., Micale, G., Piacentino, A., & Tamburini, A. (2017). Exergy analysis and thermoeconomic cost accounting of a Combined Heat and Power steam cycle integrated with a Multi Effect Distillation-Thermal Vapour Compression

desalination plant. *Energy Conversion and Management, 149*, 950–965. https://doi.org/10.1016/j.enconman.2017.04.032

Chiandussi, G., Codegone, M., Ferrero, S., & Varesio, F. E. (2012). *Comparison of multi-objective optimization methodologies for engineering applications*. *Computers and Mathematics with Applications* (Vol. 63). Elsevier Ltd. https://doi.org/10.1016/j.camwa.2011.11.057

Christ, A., Regenauer-Lieb, K., & Tong Chua, H. (2015). Boosted Multi-Effect Distillation for sensible low-grade heat sources: A comparison with feed pre-heating Multi-Effect Distillation. *Desalination, 366*, 32–46. https://doi.org/10.1016/j.desal.2014.12.047

Cipollina, A., Micale, G., & Rizzuti, L. (2009). *Seawater Desalination. Conventional and Renewable Energy Processes*. Springer.

Collette, Y., & Siarry, P. (2003). *Multiobjective optimization : principles and case studies*. *Decision Engineering*. Springer-Verlag Berlin Heidelberg. https://doi.org/10.1007/978-3-662-08883-8

Comision Chilena del Cobre. (2015). *Consumo de agua en la minería del cobre al año 2014*.

Comision Chilena del Cobre. (2016a). Consumo de agua en la minería del cobre al 2016.

Comision Chilena del Cobre. (2016b). *Proyección de consumo de agua en la minería del cobre 2016-2027*. Santiago, Chile.

Comision Chilena del Cobre. (2018). *Forecast for water consumption in the copper mining industry, 2018-2029*.

Comision Chilena del Cobre. (2019a). *Consumo de agua en la minería del cobre al 2018*.

Comision Chilena del Cobre. (2019b). *Proyección de consumo de agua en la minería del cobre 2019-2030*.

Comision Nacional de Energía. (2020). Electricity - Comisión Nacional de Energía. Retrieved October 19, 2020, from https://www.cne.cl/en/estadisticas/electricidad/

Comisión Nacional de Energía. (2020). Capacidad total instalada.

Comite Solar e Innovacion Energetica de Corfo. (2019). *Reporte de relacion y magnitud de*

costos de Inversion (Capex) y Operacion y Mantenimiento (Opex) (Vol. 6). https://doi.org/10.1017/CBO9781107415324.004

Concha, F., Castro, S., & Vergara, M. (2016). Economic Evaluation of Alternatives for Using Desalinated and Non-Desalinated Seawater in Cu/Mo Flotation Plants. In *5thInternational Congress on Water Management in Mining* (pp. 1–12).

Departamento de Geofísica - Facultad de Ciencias Físicas y Matemáticas - Universidad de Chile. (2017). Explorador Solar. Retrieved from http://ernc.dgf.uchile.cl:48080/inicio

Desaldata. (2020). DesalData. Retrieved September 23, 2020, from https://www.desaldata.com/

Dieckmann, S., Dersch, J., Giuliano, S., Puppe, M., Lüpfert, E., Hennecke, K., … Ralon, P. (2017). LCOE reduction potential of parabolic trough and solar tower CSP technology until 2025. *AIP Conference Proceedings*, *1850*(June). https://doi.org/10.1063/1.4984538

Dinçer, I., & Rosen, M. (2012). *EXERGY: Energy, Environment and Sustainable Development.* Elsevier Science. Retrieved from https://books.google.cl/books/about/Exergy.html?id=3QyaMQEACAAJ&redir_esc=y&hl=en

DuPont. (2020a). *Membrane System Design Guidelines for 8" FilmTec™ Elements*. Retrieved from https://www.dupont.com/content/dam/dupont/amer/us/en/water-solutions/public/documents/en/45-D01695-en.pdf

DuPont. (2020b). WAVE Software for Water Treatment Plant Design. Retrieved August 23, 2020, from https://www.dupont.com/water/resources/design-software.html

Eke, J., Yusuf, A., Giwa, A., & Sodiq, A. (2020). The global status of desalination: An assessment of current desalination technologies, plants and capacity. *Desalination*, *495*(July), 114633. https://doi.org/10.1016/j.desal.2020.114633

El-Dessouky, H. T., & Ettouney, H. M. (2002). *Fundamentals of Salt Water Desalination*. *Fundamentals of Salt Water Desalination*. https://doi.org/10.1016/B978-044450810-2/50008-7

Elsafi, A. M. (2015). Exergy and exergoeconomic analysis of sustainable direct steam generation solar power plants. *Energy Conversion and Management*, *103*, 338–347. https://doi.org/10.1016/j.enconman.2015.06.066

Elsayed, M. L., Mesalhy, O., Mohammed, R. H., & Chow, L. C. (2018). Transient performance of MED processes with different feed configurations. *Desalination*, *438*, 37–53. https://doi.org/10.1016/j.desal.2018.03.016

Escobar, R. A., Cortés, C., Pino, A., Salgado, M., Pereira, E. B., Martins, F. R., … Cardemil, J. M. (2015). Estimating the potential for solar energy utilization in Chile by satellite-derived data and ground station measurements. *Solar Energy*, *121*, 139–151. https://doi.org/10.1016/j.solener.2015.08.034

Fu, R., Feldman, D., & Margolis, R. (2018). *U.S. Solar Photovoltaic System Cost Benchmark: Q1 2018*. *NREL*. https://doi.org/10.7799/1325002

Gabriel, K. J., Linke, P., & El-Halwagi, M. M. (2015). Optimization of multi-effect distillation process using a linear enthalpy model. *Desalination*, *365*, 261–276. https://doi.org/10.1016/j.desal.2015.03.011

Global Sea Temperature. (2019). Chile Sea Temperatures. Retrieved June 7, 2019, from https://www.seatemperature.org/south-america/chile/

Gómez-Hernández, J., González-Gómez, P. A., Briongos, J. V., & Santana, D. (2018). Influence of the steam generator on the exergetic and exergoeconomic analysis of solar tower plants. *Energy*, *145*, 313–328. https://doi.org/10.1016/j.energy.2017.12.129

Guédez, R., Topel, M., Conde, I., Ferragut, F., Callaba, I., Spelling, J., … Laumert, B. (2016). A Methodology for Determining Optimum Solar Tower Plant Configurations and Operating Strategies to Maximize Profits Based on Hourly Electricity Market Prices and Tariffs. *Journal of Solar Energy Engineering*, *138*(2), 021006. https://doi.org/10.1115/1.4032244

Herrera-León, S., Lucay, F. A., Cisternas, L. A., & Kraslawski, A. (2019). Applying a multi-objective optimization approach in designing water supply systems for mining industries. The case of Chile. *Journal of Cleaner Production*, *210*, 994–1004.

https://doi.org/10.1016/j.jclepro.2018.11.081

Hoffmann, J. E., & Dall, E. P. (2018). Integrating desalination with concentrating solar thermal power: A Namibian case study. *Renewable Energy*, *115*, 423–432. https://doi.org/10.1016/j.renene.2017.08.060

Iaquaniello, G., Salladini, A., Mari, A., Mabrouk, A. A., & Fath, H. E. S. (2014). Concentrating solar power (CSP) system integrated with MED-RO hybrid desalination. *Desalination*, *336*(1), 121–128. https://doi.org/10.1016/j.desal.2013.12.030

IRENA. (2012). *Renewable energy technologies: cost analysis series concentrating solar power* (Vol. 1).

IRENA, & IEA-ETSAP. (2012). *Water Desalination Using Renewable Energy*.

Jamil, M. A., & Zubair, S. M. (2017). Design and analysis of a forward feed multi-effect mechanical vapor compression desalination system: An exergo-economic approach. *Energy*, *140*(August), 1107–1120. https://doi.org/10.1016/j.energy.2017.08.053

Jones, E., Qadir, M., van Vliet, M. T. H., Smakhtin, V., & Kang, S. (2019). The state of desalination and brine production: A global outlook. *Science of the Total Environment*, *657*, 1343–1356. https://doi.org/10.1016/j.scitotenv.2018.12.076

Jorgenson, J., Mehos, M., & Denholm, P. (2016). Comparing the net cost of CSP-TES to PV deployed with battery storage. *AIP Conference Proceedings*, *1734*(May 2016), 08003. https://doi.org/10.1063/1.4949183

Kassem, A., Al-Haddad, K., & Komljenovic, D. (2017). Concentrated solar thermal power in Saudi Arabia: Definition and simulation of alternative scenarios. *Renewable and Sustainable Energy Reviews*, *80*(May), 75–91. https://doi.org/10.1016/j.rser.2017.05.157

Khoshgoftar Manesh, M. H., Ghalami, H., Amidpour, M., & Hamedi, M. H. (2013). Optimal coupling of site utility steam network with MED-RO desalination through total site analysis and exergoeconomic optimization. *Desalination*, *316*, 42–52. https://doi.org/10.1016/j.desal.2013.01.022

Kosmadakis, G., Papapetrou, M., Ortega-Delgado, B., Cipollina, A., & Alarcón-Padilla, D.-

C. (2018). Correlations for estimating the specific capital cost of multi-effect distillation plants considering the main design trends and operating conditions. *Desalination*, *447*(May), 74–83. https://doi.org/10.1016/J.DESAL.2018.09.011

Kouta, A., Al-Sulaiman, F., Atif, M., & Marshad, S. Bin. (2016). Entropy, exergy, and cost analyses of solar driven cogeneration systems using supercritical CO2 Brayton cycles and MEE-TVC desalination system. *Energy Conversion and Management*, *115*, 253–264. https://doi.org/10.1016/j.enconman.2016.02.021

La Cerva, M., Gurreri, L., Cipollina, A., Tamburini, A., Ciofalo, M., & Micale, G. (2019). Modelling and cost analysis of hybrid systems for seawater desalination: Electromembrane pre-treatments for Reverse Osmosis. *Desalination*, *467*(March), 175–195. https://doi.org/10.1016/j.desal.2019.06.010

Laissaoui, M., Palenzuela, P., Sharaf Eldean, M. A., Nehari, D., & Alarcón-Padilla, D.-C. (2018). Techno-economic analysis of a stand-alone solar desalination plant at variable load conditions. *Applied Thermal Engineering*, *133*(October 2017), 659–670. https://doi.org/10.1016/j.applthermaleng.2018.01.074

Lazzaretto, A., & Tsatsaronis, G. (2006). SPECO: A systematic and general methodology for calculating efficiencies and costs in thermal systems. *Energy*, *31*(8–9), 1257–1289. https://doi.org/10.1016/j.energy.2005.03.011

Leiva-Illanes, R., Escobar, R., Cardemil, J. M., & Alarcón-Padilla, D.-C. (2017). Thermoeconomic assessment of a solar polygeneration plant for electricity, water, cooling and heating in high direct normal irradiation conditions. *Energy Conversion and Management*, *151*(September), 538–552. https://doi.org/10.1016/j.enconman.2017.09.002

Leiva-Illanes, R., Escobar, R., Cardemil, J. M., & Alarcón-Padilla, D.-C. (2018). Comparison of the levelized cost and thermoeconomic methodologies – Cost allocation in a solar polygeneration plant to produce power , desalted water , cooling and process heat. *Energy Conversion and Management*, *168*(January), 215–229. https://doi.org/10.1016/j.enconman.2018.04.107

Leiva-Illanes, R., Escobar, R., Cardemil, J. M., Alarcón-Padilla, D.-C., Uche, J., & Martínez,

A. (2019). Exergy cost assessment of CSP driven multi-generation schemes: Integrating seawater desalination, refrigeration, and process heat plants. *Energy Conversion and Management*, *179*(September 2018), 249–269. https://doi.org/10.1016/j.enconman.2018.10.050

Lilliestam, J., & Pitz-Paal, R. (2018). Concentrating solar power for less than USD 0.07 per kWh: finally the breakthrough? *Renewable Energy Focus*, *26*(00), 17–21. https://doi.org/10.1016/j.ref.2018.06.002

Ma, Y., Morozyuk, T., Liu, M., Yan, J., & Liu, J. (2019). Optimal integration of recompression supercritical CO 2 Brayton cycle with main compression intercooling in solar power tower system based on exergoeconomic approach. *Applied Energy*, *242*(March), 1134–1154. https://doi.org/10.1016/j.apenergy.2019.03.155

Mata-Torres, C., Escobar, R. A., & Cardemil, J. M. (2018). Techno-Economic Analysis of CSP+MED+PV Plant: Electricity and Water Production For Mining Industry in Northern Chile. In *AIP Conference Proceedings, SolarPACES 2017* (Vol. 2033, p. 180007). https://doi.org/10.1063/1.5067179

Mata-Torres, C., Escobar, R. A., Cardemil, J. M., Simsek, Y., & Matute, J. A. (2017). Solar polygeneration for electricity production and desalination: Case studies in Venezuela and northern Chile. *Renewable Energy*, *101*, 387–398. https://doi.org/10.1016/j.renene.2016.08.068

Mata-Torres, C., Palenzuela, P., Zurita, A., Cardemil, J. M., Alarcón-Padilla, D.-C., & Escobar, R. A. (2020). Annual thermoeconomic analysis of a Concentrating Solar Power + Photovoltaic + Multi-Effect Distillation plant in northern Chile. *Energy Conversion and Management*, *213*(June). https://doi.org/10.1016/j.enconman.2020.112852

Mata-Torres, C., Zurita, A., Cardemil, J. M., & Escobar, R. A. (2018). Exergy cost analysis of a CSP-Rankine Cycle coupled with a MED plant considering time-varying conditions and part-load operation. In *Proceedings of the 31th International Conference on Efficiency, Cost, Optimization, Simulation and Environmental Impact of Energy Systems, ECOS 2018*.

Mata-Torres, C., Zurita, A., Cardemil, J. M., & Escobar, R. A. (2019a). Exergy cost and thermoeconomic analysis of a Rankine Cycle + Multi-Effect Distillation plant considering time-varying conditions. *Energy Conversion and Management*, *192*, 114–132. https://doi.org/10.1016/j.enconman.2019.04.023

Mata-Torres, C., Zurita, A., Cardemil, J. M., & Escobar, R. A. (2019b). Thermoeconomic Analysis of a CSP+PV+MED Plant in Chile: Assessing the Impact of the PV Plant Integration. In *Proceedings of the 32nd International Conference on Efficiency, Cost, Optimization, Simulation and Environmental Impact of Energy Systems, ECOS 2019*.

Mathworks. (2020). gamultiobj Algorithm.

Mayor, B. (2019). Growth patterns in mature desalination technologies and analogies with the energy field. *Desalination*, *457*(January), 75–84. https://doi.org/10.1016/j.desal.2019.01.029

Ministerio de Energía. (2014). Energía 2050 - Política Energetica De Chile. Retrieved from http://eae.mma.gob.cl/uploads/D03_Politica_Energetica_de__Chile_2050_Anteproyecto2.pdf

Mohammadi, K., Saghafifar, M., Ellingwood, K., & Powell, K. (2019). Hybrid concentrated solar power (CSP)-desalination systems: A review. *Desalination*, *468*(July), 114083. https://doi.org/10.1016/j.desal.2019.114083

Mokhtari, H., Sepahvand, M., & Fasihfar, A. (2016). Thermoeconomic and exergy analysis in using hybrid systems (GT+MED+RO) for desalination of brackish water in Persian Gulf. *Desalination*, *399*, 1–15. https://doi.org/10.1016/j.desal.2016.07.044

Moser, M., Trieb, F., & Fichter, T. (2013). Potential of Concentrating Solar Power Plants for the Combined Production of Water and Electricity in MENA Countries. *Journal of Sustainable Development of Energy, Water and Environment Systems*, *1*(2), 122–141. https://doi.org/10.13044/j.sdewes.2013.01.0009

Nassrullah, H., Anis, S. F., Hashaikeh, R., & Hilal, N. (2020). Energy for desalination: A state-of-the-art review. *Desalination*, *491*(June). https://doi.org/10.1016/j.desal.2020.114569

National Renewable Energy Laboratory. (2018). System Advisor Model (SAM). Golden, CO. Retrieved from https://sam.nrel.gov/download

Olwig, R., Hirsch, T., Sattler, C., Glade, H., Schmeken, L., Will, S., … Messalem, R. (2012). Techno-economic analysis of combined concentrating solar power and desalination plant configurations in Israel and Jordan. *Desalination and Water Treatment*, *41*(1–3), 9–25. https://doi.org/10.1080/19443994.2012.664674

Omar, A., Nashed, A., Li, Q., Leslie, G., & Taylor, R. A. (2020a). Pathways for integrated concentrated solar power - Desalination: A critical review. *Renewable and Sustainable Energy Reviews*, *119*(November 2019), 109609. https://doi.org/10.1016/j.rser.2019.109609

Omar, A., Nashed, A., Li, Q., Leslie, G., & Taylor, R. A. (2020b). Pathways for integrated concentrated solar power - Desalination: A critical review. *Renewable and Sustainable Energy Reviews*, *119*(November 2019), 109609. https://doi.org/10.1016/j.rser.2019.109609

Ortega-Delgado, B., Cornali, M., Palenzuela, P., & Alarcón-Padilla, D. C. (2017). Operational analysis of the coupling between a multi-effect distillation unit with thermal vapor compression and a Rankine cycle power block using variable nozzle thermocompressors. *Applied Energy*, *204*, 690–701. https://doi.org/10.1016/j.apenergy.2017.07.062

Ortega-Delgado, B., Garcia-Rodriguez, L., & Alarcón-Padilla, D.-C. (2016). Thermoeconomic comparison of integrating seawater desalination processes in a concentrating solar power plant of 5 MWe. *Desalination*, *392*, 102–117. https://doi.org/10.1016/j.desal.2016.03.016

Ortega-Delgado, B., García-Rodríguez, L., & Alarcón-Padilla, D.-C. (2017). Opportunities of improvement of the MED seawater desalination process by pretreatments allowing high-temperature operation. *Desalination and Water Treatment*, *97*(November 2018), 94–108. https://doi.org/10.5004/dwt.2017.21679

Ortega-Delgado, B., Palenzuela, P., & Alarcón Padilla, D.-C. (2016). Parametric study of a multi-effect distillation plant with thermal vapor compression for its integration into a

Rankine cycle power block. *Desalination*, *394*, 18–29. https://doi.org/10.1016/j.desal.2016.04.020

Oyekale, J., Petrollese, M., & Cau, G. (2019). Multi-objective thermo-economic optimization of biomass retrofit for an existing solar organic Rankine cycle power plant based on NSGA-II. *Energy Reports*, (September). https://doi.org/10.1016/j.egyr.2019.10.032

Palenzuela, P., Alarcón-Padilla, D.-C., & Zaragoza, G. (2015a). *Concentrating Solar Power and Desalination Plants: Engineering and Economics of Coupling Multi-Effect Distillation and Solar Plants*. Springer International Publishing. https://doi.org/10.1007/978-3-319-20535-9

Palenzuela, P., Alarcón-Padilla, D. C., & Zaragoza, G. (2015b). Large-scale solar desalination by combination with CSP: Techno-economic analysis of different options for the Mediterranean Sea and the Arabian Gulf. *Desalination*, *366*, 130–138. https://doi.org/10.1016/j.desal.2014.12.037

Palenzuela, P., Hassan, A. S., Zaragoza, G., & Alarcón-Padilla, D. C. (2014). Steady state model for multi-effect distillation case study: Plataforma Solar de Almería MED pilot plant. *Desalination*, *337*(1), 31–42. https://doi.org/10.1016/j.desal.2013.12.029

Palenzuela, P., Ortega-Delgado, B., & Alarcón-Padilla, D.-C. (2020). Comparative assessment of the annual electricity and water production by concentrating solar power and desalination plants: A case study. *Applied Thermal Engineering*, *177*(March), 115485. https://doi.org/10.1016/j.applthermaleng.2020.115485

Palenzuela, P., Zaragoza, G., & Alarcón-Padilla, D. C. (2015). Characterisation of the coupling of multi-effect distillation plants to concentrating solar power plants. *Energy*, *82*, 986–995. https://doi.org/10.1016/j.energy.2015.01.109

Palenzuela, P., Zaragoza, G., Alarcón-Padilla, D. C., & Blanco, J. (2013). Evaluation of cooling technologies of concentrated solar power plants and their combination with desalination in the mediterranean area. *Applied Thermal Engineering*, *50*(2), 1514–1521. https://doi.org/10.1016/j.applthermaleng.2011.11.005

Patnode, A. M. (2006). *Simulation and performance evaluation of parabolic trough solar power plants*. Retrieved from http://www.minds.wisconsin.edu/handle/1793/7590

Petela, R. (1964). Exergy of Heat Radiation. *Journal of Heat Transfer*, *86*(2), 187. https://doi.org/10.1115/1.3687092

Piacentino, A. (2015). Application of advanced thermodynamics, thermoeconomics and exergy costing to a Multiple Effect Distillation plant: In-depth analysis of cost formation process. *Desalination*, *371*, 88–103. https://doi.org/http://dx.doi.org/10.1016/j.desal.2015.06.008

Pohl, R., Kaltschmitt, M., & Holländer, R. (2009). Investigation of different operational strategies for the variable operation of a simple reverse osmosis unit. *Desalination*, *249*(3), 1280–1287. https://doi.org/10.1016/j.desal.2009.06.029

PVInsights. (2020). PVinsigths Grid the world.

Qasim, M., Badrelzaman, M., Darwish, N. N., Darwish, N. A., & Hidal, N. (2019). Reverse osmosis desalination: A state-of-the-art review. *Desalination*, *459*(March), 59–104. https://doi.org/10.1016/j.desal.2019.02.008

Qureshi, B. A., & Zubair, S. M. (2015). Exergetic analysis of a brackish water reverse osmosis desalination unit with various energy recovery systems. *Energy*, *93*, 256–265. https://doi.org/10.1016/j.energy.2015.09.003

Sadri, S., Ameri, M., & Haghighi Khoshkhoo, R. (2017). Multi-objective optimization of MED-TVC-RO hybrid desalination system based on the irreversibility concept. *Desalination*, *402*, 97–108. https://doi.org/10.1016/j.desal.2016.09.029

Schwarzbözl, P., Eiden, U., Pitz-Paal, R., Zentrum, D., & Scott, J. (2006). *A TRNSYS Model Library for Solar Thermal Electric Components (STEC) Reference Manual*. *DLR, Germany*.

Shahabi, M. P., McHugh, A., Anda, M., & Ho, G. (2015). Comparative economic and environmental assessments of centralised and decentralised seawater desalination options. *Desalination*, *376*, 25–34. https://doi.org/10.1016/j.desal.2015.08.012

Shahzad, M. W., Burhan, M., Ang, L., & Choon Ng, K. (2017). Energy-water-environment

nexus underpinning future desalination sustainability. *Desalination*, *413*, 52–64. https://doi.org/10.1016/j.desal.2017.03.009

Shakib, S. E., Amidpour, M., & Aghanajafi, C. (2012). A new approach for process optimization of a METVC desalination system. *Desalination and Water Treatment*, *37*(1–3), 84–96. https://doi.org/10.1080/19443994.2012.661258

Sharan, P., Neises, T., Mctigue, J. D., & Turchi, C. (2019). Cogeneration using multi-effect distillation and a solar-powered supercritical carbon dioxide Brayton cycle. *Desalination*, *459*, 20–33. https://doi.org/10.1016/j.desal.2019.02.007

Sharma, C., Sharma, A. K., Mullick, S. C., & Kandpal, T. C. (2018). Cost reduction potential of parabolic trough based concentrating solar power plants in India. *Energy for Sustainable Development*, *42*, 121–128. https://doi.org/10.1016/j.esd.2017.10.003

Sharqawy, M. H., Lienhard V, J. H., & Zubair, S. M. (2011a). On exergy calculations of seawater with applications in desalination systems. *International Journal of Thermal Sciences*, *50*(2), 187–196. https://doi.org/10.1016/j.ijthermalsci.2010.09.013

Sharqawy, M. H., Lienhard V, J. H., & Zubair, S. M. (2011b). Thermophysical properties of seawater: A review of existing correlations and data. *Desalination and Water Treatment*, *29*(1–3), 355–355. https://doi.org/10.5004/dwt.2011.2947

Sharqawy, M. H., Zubair, S. M., & Lienhard, J. H. (2011). Second law analysis of reverse osmosis desalination plants: An alternative design using pressure retarded osmosis. *Energy*, *36*(11), 6617–6626. https://doi.org/10.1016/j.energy.2011.08.056

Shenvi, S. S., Isloor, A. M., & Ismail, A. F. (2015). A review on RO membrane technology: Developments and challenges. *Desalination*, *368*, 10–26. https://doi.org/10.1016/j.desal.2014.12.042

Sola, I., Sánchez-Lizaso, J. L., Muñoz, P. T., García-Bartolomei, E., Sáez, C. A., & Zarzo, D. (2019). Assessment of the requirements within the environmental monitoring plans used to evaluate the environmental impacts of desalination plants in Chile. *Water*, *11*(10), 1–17. https://doi.org/10.3390/w11102085

Spyrou, I. D., & Anagnostopoulos, J. S. (2010). Design study of a stand-alone desalination

system powered by renewable energy sources and a pumped storage unit. *Desalination*, *257*(1–3), 137–149. https://doi.org/10.1016/j.desal.2010.02.033

Starke, A. R., Cardemil, J. M., Escobar, R. A., & Colle, S. (2016). Assessing the performance of hybrid CSP + PV plants in northern Chile. *Solar Energy*, *138*, 88–97. https://doi.org/10.1016/j.solener.2016.09.006

Starke, A. R., Cardemil, J. M., Escobar, R. A., & Colle, S. (2018). Multi-objective optimization of hybrid CSP+PV system using genetic algorithm. *Energy*, *147*, 490–503. https://doi.org/10.1016/j.energy.2017.12.116

The World Bank, & SolarGIS. (2019). Global Solar Atlas - Chile. Retrieved August 29, 2020, from https://globalsolaratlas.info/download/chile

Tsatsaronis, G. (1993). Thermoeconomic analysis and optimization of energy systems. *Progress in Energy and Combustion Science*, *19*(3), 227–257. https://doi.org/10.1016/0360-1285(93)90016-8

Turchi, C. S., Boyd, M., Kesseli, D., Kurup, P., Mehos, M., Neises, T., … Wendelin, T. (2019). *CSP Systems Analysis - Final Project Report CSP Systems Analysis - Final Project Report*.

Turchi, C. S., & Heath, G. A. (2013). *Molten Salt Power Tower Cost Model for the System Advisor Model (SAM)*. https://doi.org/10.2172/1067902

Uche, J., Serra, L., & Valero, A. (2001). Thermoeconomic optimization of a dual-purpose power and desalination plant. *Desalination*, *136*(1–3), 147–158. https://doi.org/10.1016/S0011-9164(01)00177-1

UNESCO, & UN-Water. (2020). *The United Nations World Water Development Report 2020: Water and Climate Change*.

Valenzuela, C., Mata-Torres, C., Cardemil, J. M., & Escobar, R. A. (2017). CSP + PV hybrid solar plants for power and water cogeneration in northern Chile. *Solar Energy*, *157*(October), 713–726. https://doi.org/10.1016/j.solener.2017.08.081

Voutchkov, N. (2019). *Desalination Project Cost Estimating and Management*. Taylor & Francis.

Wang, Y., & Lior, N. (2007). Fuel allocation in a combined steam-injected gas turbine and thermal seawater desalination system. *Desalination*, *214*, 306–326. https://doi.org/10.1016/j.desal.2007.01.001

Wellmann, J., Meyer-Kahlen, B., & Morosuk, T. (2017). Exergoeconomic evaluation of a CSP plant in combination with a desalination unit. *Renewable Energy*, *128*, 586–602. https://doi.org/10.1016/j.renene.2017.11.070

Xiong, J., Zhao, H., Zhang, C., Zheng, C., & Luh, P. B. (2012). Thermoeconomic operation optimization of a coal-fired power plant. *Energy*, *42*(1), 486–496. https://doi.org/10.1016/j.energy.2012.03.020

Zurita, A., Castillejo-Cuberos, A., García, M., Mata-Torres, C., Simsek, Y., García, R., … Escobar, R. A. (2018). State of the art and future prospects for solar PV development in Chile. *Renewable & Sustainable Energy Reviews*, *92*(September), 701–727. https://doi.org/10.1016/j.rser.2018.04.096

Zurita, A., Mata-Torres, C., Valenzuela, C., Felbol, C., Cardemil, J. M., Guzmán, A. M., & Escobar, R. A. (2018). Techno-economic evaluation of a hybrid CSP + PV plant integrated with thermal energy storage and a large-scale battery energy storage system for base generation. *Solar Energy*, *173*(August), 1262–1277. https://doi.org/10.1016/j.solener.2018.08.061

APPENDIX

APPENDIX A1: DETAILS OF THE AUXILIARY EQUATIONS OF THE EXERGETIC COST ANALYSIS

The auxiliary equations were separated into three main groups: RC equations, MED plant equations, and P/R system equations. The RC equations summary are the following:

- The input exergy of the hot MS is equal to its exergy cost (C_i).
- C_i of all MS streams are equal to 1.
- C_i of the air output from the ACC is equal to 0.
- c_{ex_i} of the turbine inlet steam is equal to the c_{ex_j} of the turbine outlet steam
- c_{ex_i} of the pump inlet stream is equal to the c_{ex_j} of the pump outlet stream
- c_{ex_i} of the hot inlet steam of the CFWH heater is equal to the c_{ex_j} of the hot outlet steam of the CFWH heater
- c_{ex_i} of all extractions of the same turbine have the same value.
- c_{ex_i} of the air inlet of the ACC is equal to the c_{ex_j} of the air outlet from the ACC.
- c_{ex_i} of the net electricity produced is equal to the c_{ex_j} of the total pump power consumed
- c_{ex_i} of the net electricity produced is equal to the c_{ex_j} of the ACC electric power consumed

For the MED plant, it was selected a disaggregation level that analyzes each effect separately (12 components). In Fig. 15 shows the first, an intermediate and the final effect of the plant, with the considered streams. For the effects 1 to 11, six outputs were defined: the physical and chemical exergy of the vapor distillate stream ($vd_{ph,i}$ and $vd_{ch,i}$), of the condensate distillate stream ($cd_{ph,i}$ and $cd_{ch,i}$), and of the brine stream ($b_{ph,i}$ and $b_{ch,i}$), and one input: the physical exergy of the feed-seawater (f_i), which are the inputs and the output of the following effect. In addition, in the first effect was considered the input steam (st_{in}) from the turbine exhaust and output condensate (st_{out}) that goes to the power cycle pump. Also, it was included a desuperheater that decreases the enthalpy of the st_{in} to the saturated vapor enthalpy, if this stream is in the superheated state, with a fraction of the condensate distillate of the last effect. Thus, it was considered the distillate desuperheater stream (dsh_1) as an

input of the first effect. For the last effect, it was considered one additional input: the physical exergy of the condenser input seawater (s_{in_2}) and seven output: the physical exergy of the cooling water seawater stream (s_{cw}) used to condensate all the distillate in the last effect, and the physical and chemical exergy of the brine ($b_{ph,12}$ and $b_{ch,12}$), the physical and chemical exergy of the condensate distillate ($cd_{ph,12}$ and $cd_{ch,12}$) and the physical and chemical exergy of the distillate used in the desuperheater ($dsh_{ph,1}$ and $dsh_{ch,1}$). In Figure A-1, the b_i, vd_i, cd_i and dsh_1 streams consider separately the physical and the chemical exergy.

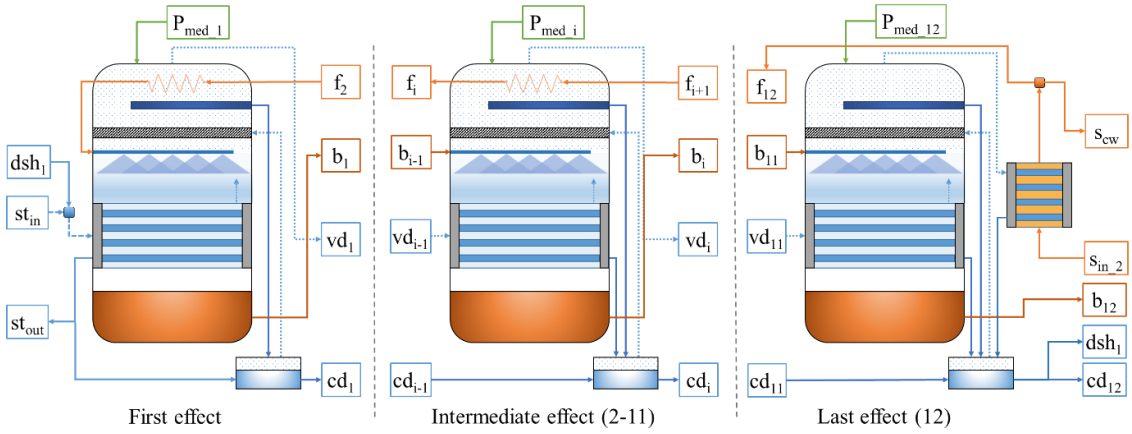

Figure A-1: Fig. 1. MED plant components (first effect, intermediate effect, and last effect) with the streams.

Finally, for the MED plant, it was defined as the electric consumption of the MED plant (P_{MED_i}), which was divided by the 12 effects as an input for each MED component. For these streams, the MED auxiliary equations are the following (Piacentino, 2015):

- C_i of the $b_{ch,i}$ of every effect is equal to 0.
- C_i of the $cd_{ph,12}$ is equal to 0.
- c_{ex_i} of the $vd_{ph,i}$ is equal to the c_{ex_j} of the $cd_{ph,i}$ for effect from 1 to 11.
- c_{ex_i} of the $vd_{ch,i}$ is equal to the c_{ex_j} of the $cd_{ch,i}$ for effects from 1 to 11.
- c_{ex_i} of the $vd_{ph,i}$ is equal to the c_{ex_j} of the $vd_{ch,i}$ for effects from 1 to 11.
- c_{ex_i} of the $b_{ph,i}$ is equal to the c_{ex_j} of the $b_{ph,i+1}$ of the following effect.
- c_{ex_i} of the $cd_{ph,1}$ of the first effect is equal to the c_{ex_j} of the $b_{ph,1}$ of the first effect.
- c_{ex_i} of the f_{12} of the last effect is equal to the c_{ex_j} of the s_{cw}.

- c_{ex_i} of the st_{in} and st_{out} that power the MED plant are equal.
- c_{ex_i} of the $dsh_{1,ch}$ is equal to the c_{ex_j} of the $cd_{ch,12}$
- c_{ex_i} of the $dsh_{1,ch}$ is equal to the c_{ex_j} of the $dsh_{1,ph}$

For the P/R system, it was considered 4 components: a brine mixer, where the output brine from the 12th effect (b_{12}) is mixed with the resultant s_{cw}, resulting in the mixed brine stream (b_{mix1}), the pumping system (includes the pipeline and the pump), the recovery system (it includes the pipeline and the turbine) and a net MED plant electric node where is calculated the required electricity for the MED plant operation. Also, it was considering the following streams: the physical exergy of pumping input seawater (s_{in_1}), the physical and chemical exergy of the mixed brine (b_{ph_mix1} and b_{ch_mix1}), the physical and chemical exergy of the mixed brine at sea level (b_{ph_mix2} and b_{ch_mix2}) after the energy recovery system, the power output of the turbine (P_{tur_MED}), the power required by the pump (P_{p_MED}) and the net electricity required by the MED plant and P/R system (P_{MED_t}). For these streams, the P/D system equations are the following:

- C_i of the s_{in_1} is equal to its exergy cost.
- C_i of the b_{ch_mix1} is equal to 0.
- C_i of the b_{ch_mix2} is equal to 0.
- c_{ex_i} of the b_{ph_mix1} is equal to the c_{ex_j} of the b_{ph_mix2}.
- c_{ex_i} of the P_{p_MED} is equal to the c_{ex_j} of the power required by the MED plant.
- c_{ex_i} of the P_{MED_t} is equal to the c_{ex_j} of the net electricity produced.

Finally, the b_{ph_mix2} is a stream that is considered waste, however, it cost is related to the unit exergy cost of some streams that are resources or products different components. For this issue, Piacentino (Piacentino, 2015) proposes to divide the exergy costs corresponding to this stream between the effect of MED plant, in order to share as an additional input cost in all the components (each effect) that have contributed to generating the residue.

APPENDIX A2: REGRESSION FOR THE POWER BLOCK

The polynomial multi-variable regression of the power block was obtained considering a second-degree polynomial according to the structure of the equation A.1 for each output (W_{net}, $\dot{m}_{cond}$, h_s and T_{outHTF}). The coefficients are presented in Table A-1. The temperatures and mass flow rate inputs were in °C and kg/s. The units of the variables (W_{net}, $\dot{m}_{cond}$, h_s and T_{outHTF}) are obtained in kW, kg/s, kJ/kg and °C, respectively.

$$Variable = a_1 T_{amb} + a_2 T_{inHTF} + a_3 T_{inHTF} T_{amb} + a_4 \dot{m}_{in\,HTF} + a_5 \dot{m}_{in\,HTF} T_{amb} + a_6 \dot{m}_{in\,HTF} T_{inHTF} + a_7 + a_8 \dot{m}_{in\,HTF}{}^2 + a_9 T_{inHTF}{}^2 + a_{10} T_{amb}{}^2 \quad \text{(A.1)}$$

Table A-1: Coefficients of the Power Block regressions

Variables	W_{net}	$\dot{m}_{cond}$	h_s	T_{outHTF}
Coefficients	*a*	*b*	*c*	*d*
1	802.260449	-0.10035345	7.89993818	-0.00254884
2	252.93949	-0.09569104	6.76346253	-0.52047855
3	-1.43221726	9.79E-05	0.00503829	2.29E-06
4	-377.049784	-0.20563778	-0.7892647	-0.10499621
5	-0.51398804	4.61E-05	-0.00022502	-1.74E-06
6	1.0358509	0.00057948	-0.00106855	0.00033949
7	-107328.177	25.1184066	734.935064	459.72985
8	0.00685085	-5.97E-06	0.00086653	-3.70E-05
9	-0.13462605	9.03E-05	-0.00644664	0.00027109
10	-0.43974145	0.00047372	-0.0184497	2.49E-05

APPENDIX A3: REGRESION FOR THE MED MODEL

The polynomial multi-variable regression of the MED plant was calculated considering a second-degree polynomial according to the structure of the equation A.2 and the design parameters mentioned in section 2.3. The variables calculated were: the freshwater mass flow rate ($\dot{m}_{water}$), the feed seawater mass flow rate ($\dot{m}_f$), the steam temperature at the inlet of the first effect (T_s), the freshwater outlet temperature (T_{water}), the brine outlet temperature (T_{br}), and the seawater temperature at the outlet of the last condenser (T_{csw}). The coefficients are presented in Table A-2 . In the equation, $\dot{m}_s$ is the thermal load (between 0.4 to 1), which represent the inlet steam mass flow rate flow fraction with respect to the design mass flow rate (11.45 kg/s), h_{steam} is steam enthalpy in kJ/kg, and T_{sw} is the seawater temperature in °C. The variables are obtained in kg/s for the mass flow rates and °C for the temperatures.

$$Variable = a_1 T_{sw} + a_2 h_{steam} + a_3 h_{steam} T_{sw} + a_4 \dot{m}_s + a_5 \dot{m}_s T_{sw} + a_6 \dot{m}_s h_{steam} + a_7 + a_8 {\dot{m}_s}^2 + a_9 {h_{steam}}^2 + a_{10} {T_{sw}}^2 \qquad (A.2)$$

For the regression of the cooling seawater mass flow rate ($\dot{m}_{csw}$), it was considered a third-degree polynomial with four inputs: $\dot{m}_s$, h_{steam}, T_s and T_{sw}, to achieve and NRMSD under 1%. The T_s is taken from the previous regression result. Table A-3 presents the exponents associated to each input and the regression coefficients.

Table A-2 : Coefficients of the MED plant regressions

Variable	$\dot{m}_{water}$	$\dot{m}_f$	T_s	T_{water}	T_{br}	T_{csw}
Coefficients	*a*	*b*	*c*	*d*	*e*	*f*
1	0.63908436	1.43791024	0.1118902	0.0152036	-2.51E-14	0.67584346
2	0.03026028	0.06808431	0.00827368	0.00029074	-7.19E-16	0.00365412
3	-0.0001026	-0.00023084	-1.75E-05	-2.28E-06	3.95E-18	-9.21E-05
4	100.126441	225.284257	28.7551129	1.08804772	-3.34E-13	14.6611841
5	-0.37237943	-0.8378414	-0.06510767	-0.00842487	3.87E-15	-0.35051739
6	0.02093228	0.0470977	0.00288226	4.02E-05	8.27E-17	-0.00390137
7	-61.079828	-137.427406	28.236119	34.3531461	34.8487	21.9652553
8	-35.8524985	-80.6682349	-10.3487037	-0.35109641	2.19E-14	-2.52450911
9	-2.95E-06	-6.64E-06	-8.07E-07	-2.29E-08	1.09E-19	-1.79E-07
10	-0.00610317	-0.0137323	-0.00113787	-0.0001722	2.74E-16	-0.0098178

Table A-3 : Input exponent and coefficients of the cooling seawater mass flow rate regression

Coefficients	a	$\dot{m}_s$	h_{steam}	T_s	T_{sw}
1	-242.968952	0	0	0	1
2	42.2092227	0	0	0	2
3	5984.59346	0	0	1	0
4	-17.9638018	0	0	1	1
5	-1.67856066	0	0	1	2
6	-279.742341	0	0	2	0
7	0.42978931	0	0	2	1
8	-34.1529419	0	1	0	0
9	0.65231287	0	1	0	1
10	0.00944732	0	1	0	2
11	2.15213348	0	1	1	0
12	-0.00873418	0	1	1	1
13	-0.0314104	0	1	2	0
14	-0.00078664	0	2	0	0
15	-8.25E-05	0	2	0	1
16	-3.85E-05	0	2	1	0
17	0	1	0	0	0
18	3258.27084	1	0	0	1
19	37.2179266	1	0	0	2
20	-316.661128	1	0	1	0
21	-85.9012176	1	0	1	1
22	9.22684737	1	0	2	0
23	113.402404	1	1	0	0
24	0.85206171	1	1	0	1
25	-3.4561388	1	1	1	0
26	0.02422076	1	2	0	0
27	0	2	0	0	0

28	629.42245	2	0	0	1
29	-559.977085	2	0	1	0
30	40.3279563	2	1	0	0
31	0	0	0	0	0
32	0	3	0	0	0
33	4.97E-07	0	3	0	0
34	3.33608596	0	0	3	0
35	0.25119342	0	0	0	3

APPENDIX A4: DESCRIPTION OF THE RO MODEL

The model consists the calculation of one pressure vessel operation, in which the performance of each membrane element is assessed. The model is solved in an iterative process for each membrane element, until the volumetric flow balance and concentrations converge. Then, the electric power computation is obtained considering the volumetric flow of the RO unit to compute the performance of the RO pumps and PX. Figure A-2 shows the layout of the RO plant with its components and Table A-4 presents the model equations.

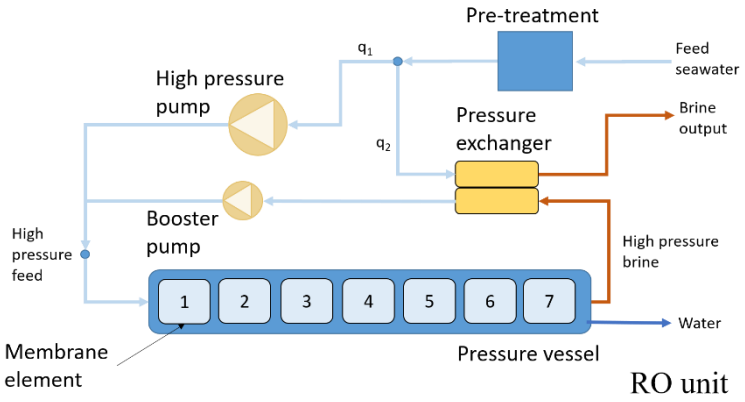

Figure A-2 : Scheme of the RO unit plant.

A5.1 RO model validation

The RO model was validated with WAVE (DuPont, 2020b), a commercial software. The feed and permeate flow rate, feed pressure, permeate flux, feed and permeate concentration are evaluated as function of the membrane elements (seven elements) of the pressure vessel. Figure A-3 shows the comparison between the model and the WAVE results. They show a good agreement with a slightly underestimation of the pressure loss in the membrane element.

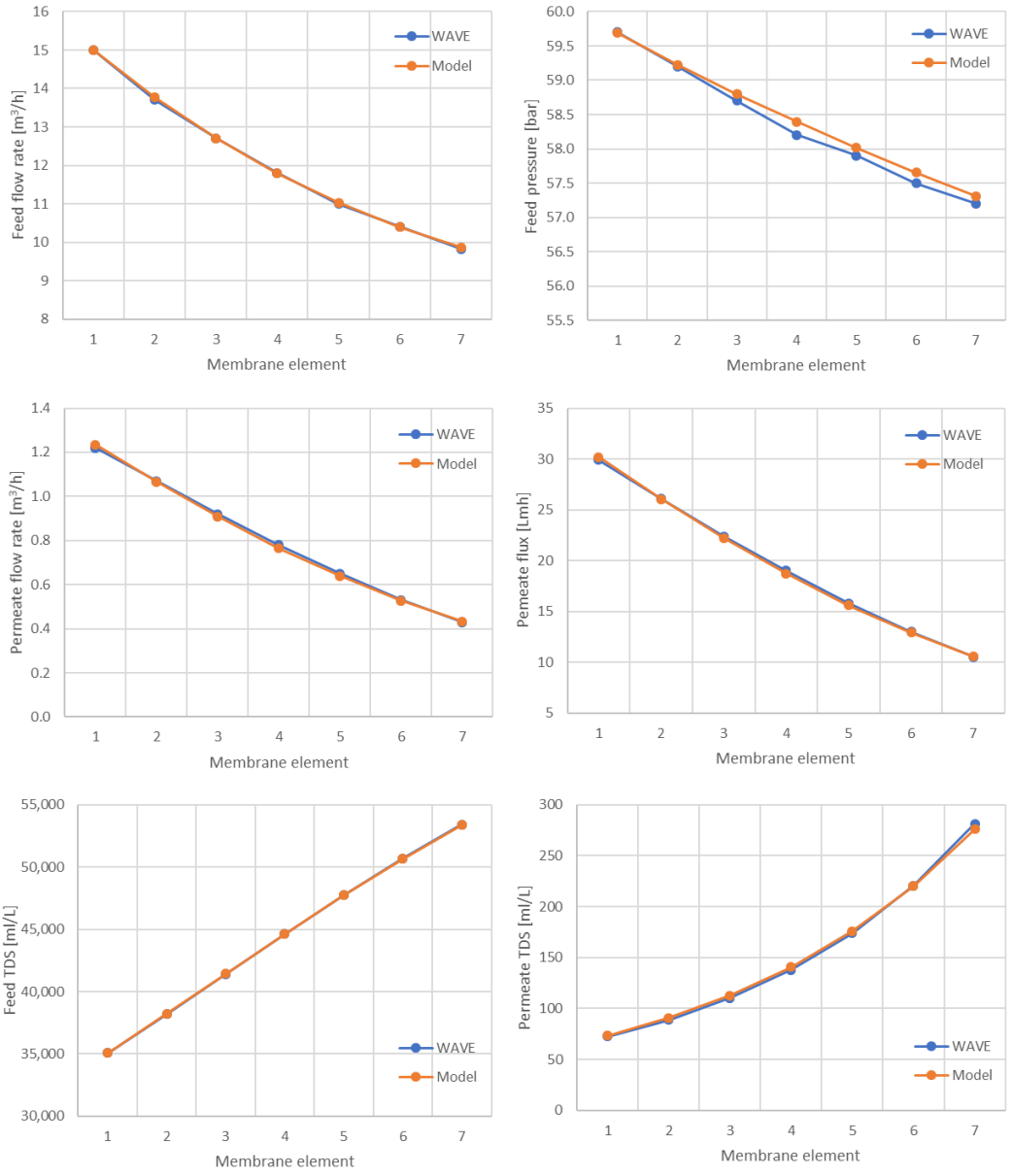

Figure A-3 : Comparison between the RO model and WAVE results considering a SW30HRLE-440, inlet flow rate of 15 m^3/h, inlet concentration of 35 g/l NaCl and feed pressure of 60 bar.

Table A-4 : RO model and electric power equations.

Component	Equation	Ref
Equations for each element in the pressure vessel		
Volumetric flow balance	$q_{f,i} = q_{p,i} + q_{b,i}$	(La Cerva et al., 2019)
Concentration balance	$q_{f,i}X_{f,i} = q_{p,i}X_{p,i} + q_{b,i}X_{b,i}$	(La Cerva et al., 2019)
Water transport	$q_{p,i} = J_{w,i}A_m$	(La Cerva et al., 2019)
Water flux	$J_{w,i} = \left(\left(\overline{Pr_i} - Pr_p\right) - \left(\bar{\pi}_i - \pi_p\right)\right) K_w T_{cf} f_f$	(La Cerva et al., 2019)
Salt transport	$q_{s,i} = \left(\bar{X}_{wall,i} - x_{p,i}\right) K_s A_m T_{cf} f_f$	(Laissaoui et al., 2018)
	$q_{s,i} = x_{p,i} q_{p,i}$	
Osmotic pressure	$\pi_{w,j,i} = \frac{1.9 R\ T\ \bar{X}_{wall,j,i}}{M_g}$	
Membrane pressure	$Pr_{f,out,i} = Pr_{f,in,i} - \Delta Pr_i$	
	$\bar{P}r_i = \frac{Pr_{f,i} + Pr_{b,i}}{2}$	
Pressure losses	$\Delta Pr_i = f_{fric,i}\ \rho_i \frac{Lv^2}{2D_h}$	
	$f_{fric,i} = 1.5 \cdot 10 \frac{96}{Re}$	

Average concentration at wall	$\bar{X}_{wall,i} = \frac{X_{wall,f,i} + X_{wall,b,i}}{2}$	
Concentration at the wall	$X_{wall,j,i} = X_{p,i} + (X_{j,i} - X_{p,i}) e^{\frac{J_{w,i}}{k_i}}$	(Al-Obaidi, Filippini, Manenti, & Mujtaba, 2019)
Mass transfer coefficient	$k_i = 0.065 {Re_i}^{0.875} {Sc_i}^{0.25} \frac{D_i}{D_h}$	(Al-Obaidi et al., 2019)
Schmidt number	$Sc_i = \frac{\mu_i}{\rho_i D_i}$	(Al-Obaidi et al., 2019)
Diffusivity	$D_i = 6.725 \cdot 10^{-6} e^{0.1546 \cdot 10^{-3} \bar{X}_{f,i} - \frac{2513}{273.15+T}}$	(Al-Obaidi et al., 2019)
Reynolds	$Re_i = \frac{\rho_i}{\mu_i} v_i D_h$ $v_i = \frac{q_{f,i}}{1000 \cdot 3600} \frac{A_m th_m}{L}$	
Temperature correction factor	$T_{cf} = e^{\left(a_1 \left(\frac{1}{298} - \frac{1}{273+T}\right)\right)}$	(Laissaoui et al., 2018)
Seawater density	$\rho_i = (a_1 + a_2 T + a_3 T^2 + a_4 T^3 + a_5 T^4) + (b_1 s_i + b_2 s_i T + b_3 s_i T^2 + b_4 s_i T^3 + b_5 {s_i}^2 T^2)$ $s_i = \frac{X_i}{1000}$;	(Sharqawy, Lienhard V, & Zubair, 2011b)

	$a_1 = 9.999 \cdot 10^2$; $a_2 = 2.034 \cdot 10^{-2}$; $a_1 = -6.616 \cdot 10^{-3}$; $a_4 = 2.261 \cdot 10^{-5}$; $a_5 = 4.657 \cdot 10^{-8}$; $b_1 = 8.020 \cdot 10^2$; $b_2 = 2.001$; $b_3 = 1.677 \cdot 10^{-2}$; $b_4 = 3.060 \cdot 10^{-5}$; $b_5 = 1.613 \cdot 10^{-5}$	
Seawater viscosity	$\mu_i = \left(4.2844 \cdot 10^{-5} + \frac{1}{(0.157(T-64.993)^2-91.296)}\right) \cdot (1 + as_i + bs_i{}^2)$ $s_i = \frac{X_i}{1000}$; $a = 1.541 + 1.998 \cdot 10^{-2}T - 9.52 \cdot 10^{-5}T^2$; $b = 7.974 - 7.561 \cdot 10^{-2}T - 4.724 \cdot 10^{-4}T^2$;	(Sharqawy, Lienhard V, et al., 2011b)
RO power equations		
Power balance	$P_{RO,total} = P_{hp1} + P_{booster} + P_{pre\_tre} + P_{p\_sea}$	
High pressure pump	$P_{hp1} = \frac{q_1}{3600}\frac{(Pr_{pump}-Pr_{in})\cdot 100}{\eta_{pump}}$	
Booster pump	$P_{booster} = \frac{q_2}{3600}\frac{(Pr_{pump}-Pr_{px\_out})\cdot 100}{\eta_{pump}}$	(Jamil & Zubair, 2017)
Pressure exchanger	$Pr_{px\_out} = Pr_{br\_out}\eta_{px}$ $q_2 = q_{br\_out}$	(Qureshi & Zubair, 2015)
Mass flow balance	$q_{f\_total} = q_1 + q_2$ $q_{f\_total} = q_{p\_out} + q_{br\_out}$ $q_{f\_total} = q_{f,1}N_{units}N_{vessel}$	

Power losses	$q_{p\_out} = q_{p,7} N_{units} N_{vessel}$ $q_{br\_out} = q_{b,7} N_{units} N_{vessel}$ $P_{pre\_tre} = \frac{q_{f\_total}}{3600} \frac{(Pr_{pre\_tre} + Pr_{control} + Pr_{losses}) \cdot 100}{\eta_{pump}}$ $P_{p\_sea} = \frac{q_{f\_total}}{3600} \frac{(Pr_{p\_sea}) \cdot 100}{\eta_{pump}}$	(Voutchkov, 2019)

APPENDIX A5: CAPEX AND OPEX COST FUNCTIONS

In Table A-5 and Table A-6 is presented the CAPEX and OPEX correlations for each of the system analyzed, while in Table A-7 is presented the parameters of the cost equations. The cost equation and parameters were actualized throughout the research. Here is presented the last update used in Paper III and Paper IV.

Table A-5 : CAPEX cost equations.

Component	Total cost of investment equations	Ref.
CSP system		
Heliostats	$C_{hel} = c_{hf} A_{ref}$	(Aly et al., 2019; Dieckmann et al., 2017; Guédez et al., 2016; Hoffmann & Dall, 2018; Jorgenson et al., 2016; Zurita, Mata-Torres, et al., 2018) Assumption[*1]
Receiver and Tower	$C_{tower} = c_{tow} \cdot (ht_{tow} - ht_{rec}) \cdot \left(\frac{ht_{tow} - ht_{rec}}{ht_{rec,ref}}\right)^{exp,tow}$	
	$C_{rec} = c_{rec} \cdot P_{rec}^{th} \cdot \left(\frac{P_{rec}^{th}}{P_{rec,ref}^{th}}\right)^{exp,rec}$	
	$C_{rec\_total} = Z_{rec} + Z_{tower}$	
TES system	$C_{TES} = c_{TES} TES_{hours} Q_{PB\_thermal}$	
Contingency and Indirect cost	$C_{CSP,direct} = \left(C_{hel} + C_{rec_{total}} + C_{TES}\right) \cdot (1 + \%Cont_{CSP})$	
	$C_{CSP,indirect} = C_{CSP,direct}\ \%EPC_{CSP}$	
	$C_{CSP,total} = C_{CSP,direct} + C_{CSP,indirect}$	
Total cost of investment	${Z_{hel}}^{Capex} = C_{CSP,total} \frac{C_{hel}}{C_{hel} + C_{rec\_total} + C_{TES}}$	
	${Z_{rec\_total}}^{Capex} = C_{CSP,total} \frac{C_{rec\_total}}{C_{hel} + C_{rec\_total} + C_{TES}}$	
	${Z_{TES}}^{Capex} = C_{CSP,total} \frac{C_{TES}}{C_{hel} + C_{rec\_total} + C_{TES}}$	
	${Z_{TES\_hot}}^{Capex} = 0.6 {Z_{TES}}^{Capex}$	

	$Z_{TES\_cold}{}^{Capex} = 0.4 Z_{TES}{}^{Capex}$	
PV system		
PV modules	$C_{PV} = c_{mod}\, P_{PV,DC} \left(\frac{P_{PV,MW}}{P_{PV,ref}}\right)^{exp,pv}$	(Fu et al., 2018) Assumption
Inverter	$C_{inverter} = c_{inv}\, P_{PV,AC} \left(\frac{P_{PV,MW}}{P_{PV,ref}}\right)^{exp,pv}$	
Installation	$C_{installation} = \left(c_{PV,BoS} + c_{PV,labor} + c_{PV,overh}\right) P_{PV,DC}$	
Contingency and Indirect cost	$C_{PV,direct} = (C_{PV} + C_{inverter} + C_{installation}) \cdot (1 + \%Cont_{PV})$ $C_{PV,indirect} = c_{PV,EPC}\, P_{PV,DC}$ $C_{PV,total} = C_{PV,direct} + C_{PV,indirect}$	
Total cost of investment	$Z_{PV}{}^{Capex} = C_{PV,total} \frac{C_{PV}}{C_{PV}+C_{inverter}}$ $Z_{inverter}{}^{Capex} = C_{PV,total} \frac{C_{inverter}}{C_{PV}+C_{inverter}}$	
Power Block		
Steam generator	$C_{boi} = 208582 \frac{\$}{kg\ s} \dot{m}_{sg}{}^{0.8} e^{\left(\frac{P_e-28}{150}\right)} F_{AN} F_{AT} F_{SHRH}$ $F_{AN} = 1 + \left(\frac{1-0.95}{1-\eta_1}\right)^7$ $F_{AT} = 1 + 5e^{\left(\frac{T_1-593}{10.42}\right)}$	(Adibhatla & Kaushik, 2017; Ameri et al., 2009; Xiong et al., 2012)

	$F_{SHRH} = 1 + \frac{T_{sg_{out}} - T_{sg_{in}}}{T_{sg_{out}}} + \left(\frac{\dot{m}_{sg}}{\dot{m}_{rh}}\right)\frac{\left(T_{rh_{out}} - T_{rh_{in}}\right)}{T_{rh_{out}}}$	Assumption
	$C_{sg} = (1 - f_{rh})C_{boi}$	
	$f_{rh} = 0.12$	
Re-heater	$C_{rh} = f_{rh}C_{boi}$	
Turbine	$C_{st,i} = 3880.5\frac{\$}{kW^{-0.7}}{P_{st}}^{0.7}\left[1 + \left(\frac{0.05}{1-\eta_{st}}\right)^3\right]\left[1 + 5e^{\left(\frac{T_a - 886}{10.42}\right)}\right]$	
PB Pump	$C_{pump,i} = 705.48\frac{\$}{kg\ s}{P_{pump}}^{0.71}\left(1 + \frac{0.2}{1-\eta_{pump}}\right)$	
Condenser	$C_{cond} = \left(\frac{1}{T_o e_1}\right)\left\{217\left[0.247 + \left(\frac{1}{3.24{V_{cw}}^{0.8}}\right)\right]\ln\left(\frac{1}{1-e_1}\right) + 138\right\}\left(\frac{1}{1-\eta_{cond}}\right)S$	
	$e_1 = \frac{T_{cw\_out} - T_{cw\_in}}{T_{in} - T_{cw\_out}};\ \eta_c = \frac{T_o(s_{in} - s_{out})}{h_{in} - h_{out}}$	
Deaerator	$C_{dea} = 145315\frac{\$}{kW^{-0.7}}{\dot{m}_{dea\_water}}^{0.7}$	
CFWH	$C_{CFWH,i} = 66\ Q_{CFWH}\left(\frac{1}{T_{TTD,i} + a}\right)^{0.1}(10\Delta P_t)^{-0.08}(10\Delta P_s)^{-0.04}$	
	$a = 6$ for high-pressure FWH and $a = 4$ for low-pressure FWH	
Generator	$C_{gen} = 60{P_{gen}}^{0.95}$	
Contingency and Indirect cost	$C_{PB,direct} = \left(C_{sg} + C_{rh} + \sum C_{st,i} + \sum C_{pump,i} + C_{cond} + C_{dea} + \sum C_{CFWH,i} + C_{gen}\right) \cdot (1 + \%Cont_{CSP} + f_a)$	

	$C_{PB,indirect} = C_{PP,direct}\ \%EPC_{CSP}$	
	$C_{PB,total} = C_{PB,direct} + C_{PB,indirect}$	
Total cost of investment	$Z_{sg}^{Capex} = C_{PB,total}\frac{C_{sg}}{C_{sg}+C_{rh}+\sum C_{st,i}+\sum C_{pump,i}+C_{cond}+C_{dea}+\sum C_{CFWH,i}+C_{gen}}$	
	$Z_{rh}^{Capex} = C_{PB,total}\frac{C_{rh}}{C_{sg}+C_{rh}+\sum C_{st,i}+\sum C_{pump,i}+C_{cond}+C_{dea}+\sum C_{CFWH,i}+C_{gen}}$	
	$Z_{st,i}^{Capex} = C_{PB,total}\frac{C_{st,i}}{C_{sg}+C_{rh}+\sum C_{st,i}+\sum C_{pump,i}+C_{cond}+C_{dea}+\sum C_{CFWH,i}+C_{gen}}$	
	$Z_{pump,i}^{Capex} = C_{PB,total}\frac{C_{pump,i}}{C_{sg}+C_{rh}+\sum C_{st,i}+\sum C_{pump,i}+C_{cond}+C_{dea}+\sum C_{CFWH,i}+C_{gen}}$	
	$Z_{cond}^{Capex} = C_{PB,total}\frac{C_{cond}}{C_{sg}+C_{rh}+\sum C_{st,i}+\sum C_{pump,i}+C_{cond}+C_{dea}+\sum C_{CFWH,i}+C_{gen}}$	
	$Z_{dea}^{Capex} = C_{PB,total}\frac{C_{dea}}{C_{sg}+C_{rh}+\sum C_{st,i}+\sum C_{pump,i}+C_{cond}+C_{dea}+\sum C_{CFWH,i}+C_{gen}}$	
	$Z_{CFWH,i}^{Capex} = C_{PB,total}\frac{C_{CFWH,i}}{C_{sg}+C_{rh}+\sum C_{st,i}+\sum C_{pump,i}+C_{cond}+C_{dea}+\sum C_{CFWH,i}+C_{gen}}$	
	$Z_{gen}^{Capex} = C_{PB,total}\frac{C_{gen}}{C_{sg}+C_{rh}+\sum C_{st,i}+\sum C_{pump,i}+C_{cond}+C_{dea}+\sum C_{CFWH,i}+C_{gen}}$	
MED system		
MED plant	$C_{MED} = c_{MED,esp}A_{MED}^{0.95}$	(Askari & Ameri, 2016; Desaldata, 2020;
	$C_{MED1} = C_{MED}N_{MED\_units}^{0.95} + Cap_{MED}\left(c_{MED,tre} + c_{MED,intake} + c_{MED,disposal} + c_{MED,others}\right)N_{MEd\_units}^{-0.1}$	

Contingency and Indirect cost	$C_{PB,direct} = C_{MED1}\,(1 + \%Cont_{MED})$ $C_{PB,indirect} = C_{MED,direct}\,\%EPC_{MED}$ $C_{MED,total} = C_{MED,direct} + C_{MED,indirect}$	Kosmadakis, Papapetrou, Ortega-Delgado, Cipollina, & Alarcón-Padilla, 2018; Mata-Torres et al., 2019a; Mokhtari et al., 2016; Piacentino, 2015)
Total cost of investment	${Z_{MED}}^{Capex} = C_{MED,total}$	
RO system		
Intake	$C_{RO,intake\_pipe} = c_{RO,ref1}(24\,q_f)^{\exp\_ro1} L_{intake}$ $C_{RO,intake\_pump} = 1000\,c_{RO,ref2}(24\,q_f)^{\exp\_ro2}$ $C_{RO,intake\_screens} = 1000\,c_{RO,ref3}(24\,q_f)^{\exp\_ro3}$ $C_{RO,intake} = C_{RO,intake\_pipe} + C_{RO,intake\_pump} + C_{RO,intake\_screens}$	(Al-Obaidi et al., 2019; Desaldata, 2020; Palenzuela, Alarcón-Padilla, et al., 2015b; Voutchkov, 2019) Assumption[*2]
Pre-treatment	$C_{RO,pretreatment1} = 1000\,c_{RO,ref4}(24\,q_f)^{\exp\_ro4}$ $C_{RO,pretreatment2} = 1000\,c_{RO,ref5}(24\,q_f)^{\exp\_ro5}$ $C_{RO,pretreatment} = C_{RO,pretreatment1} + C_{RO,pretreatment2}$	

RO equipment	$C_{RO,equip1} = 1000\ c_{RO,ref6}(24\ q_p)^{\exp\_ro6}$
	$C_{RO,piping} = c_{RO,piping} Cap_{RO}$
	$C_{RO,equip} = C_{RO,equip1} + C_{RO,piping}$
Post-treatment	$C_{RO,postreatment1} = 1000\ c_{RO,ref7}(24\ q_p)^{\exp\_ro7}$
	$C_{RO,postreatment2} = 1000\ c_{RO,ref8}(24\ q_p)^{\exp\_ro8}$
	$C_{RO,postreatment} = C_{RO,postreatment1} + C_{RO,postreatment2}$
Others	$C_{RO,others} = (c_{RO,disposal} + c_{RO,waste} + c_{RO,electrical} + c_{RO,auxiliary} +$ $c_{RO,others1})(24q_p)$
Contingency and Indirect cost	$C_{RO,direct} = (C_{RO,intake} + C_{RO,pretreatment} + C_{RO,equip} + C_{RO,posttreatment} +$ $C_{RO,others}) \cdot (1 + \%Cont_{RO})$
	$C_{RO,indirect} = c_{RO,EPC}(24q_p)$
	$C_{RO,total} = C_{RO,direct} + C_{RO,indirect}$
Total cost of investment	$Z_{RO}{}^{Capex} = C_{RO,total}$

P/R system

Seawater pump, recovery turbine and pipeline	$C_{PR,pipe} = c_{pipe}(1000\ L_{PR,pipe})2^{0.9}$ $c_{pipe} = c_{esp,pipe} Dm_{PR,pipe}^{\ exp,pipe}$ $C_{PR,pump} = 4940 P_{PR,pump}^{\ 0.7231}$ $C_{PR,rec\_tur} = 7410 P_{rec\_tur}^{\ 0.7231}$ $C_{P/R\_pump1} = C_{PR,pump} + \frac{C_{PR,pipe}}{2}$ $C_{P/R\_recovery1} = C_{PR,tur\_rec} + \frac{C_{PR,pipe}}{2}$	(Herrera-León et al., 2019; Hoffmann & Dall, 2018; Shahabi et al., 2015) Assumption[*3]
Contingency and Indirect cost	$C_{P/R\_pump,direct} = C_{P/R\_pump1}\ (1 + \%Cont_{PR})$ $C_{P/R\_pump,indirect} = C_{P/R\_pump,direct}\ \%EPC_{PR}$ $C_{P/R\_pump} = C_{P/R\_pump,direct} + C_{P/R\_pump,indirect}$ $C_{P/R\_recovery,direct} = C_{P/R\_recovery1}\ (1 + \%Cont_{PR})$ $C_{P/R\_recovery,indirect} = C_{P/R\_recovery,direct}\ \%EPC_{PR}$ $C_{P/R\_recovery} = C_{P/R\_recovery,direct} + C_{P/R\_recovery,indirect}$	
Total cost of investment	$Z_{P/R\_pump}^{\ Capex} = C_{P/R\_pump}$ $Z_{P/R\_recovery}^{\ Capex} = C_{P/R\_recovery}$	
DIST system		
Water pump and pipeline	$C_{DIST,pipe} = c_{pipe}(1000\ L_{DIST,pipe})$ $c_{pipe} = c_{esp,pipe} Dm_{DIST,pipe}^{\ exp,pipe}$	(Herrera-León et al., 2019;

	$C_{DIST,pump} = 4940 P_{PR,pump}{}^{0.7231}$	Hoffmann & Dall, 2018; Shahabi et al., 2015) Assumption[*3]
	$C_{DIST1} = C_{DIST,pump} + C_{DIST,pipe}$	
Contingency and Indirect cost	$C_{DIST,direct} = C_{DIST1}\,(1 + \%Cont_{PR})$	
	$C_{DIST,indirect} = C_{DIST,direct}\,\%EPC_{PR}$	
	$C_{DIST} = C_{DIST,direct} + C_{DIST,indirect}$	
Total cost of investment	$Z_{DIST}{}^{Capex} = C_{DIST}$	

[*1] The CSP cost data implemented is in concordance with the values reported by the CSP Association of Chile in 2019, which represent costs reported in the literature for central-receiver plants (Aly et al., 2019; Boretti, 2018; Dieckmann et al., 2017; Jorgenson et al., 2016; Kassem, Al-Haddad, & Komljenovic, 2017; Sharma, Sharma, Mullick, & Kandpal, 2018) validated by the industry in Chile.

[*2] The RO cost data is adapted to be in concordance with the Desaldata cost data and cost curve presented by Voutchkov (Voutchkov, 2019).

[*3] The pipeline cost was updated with information reported in previous works adapted to particular conditions in Chile (Herrera-León et al., 2019; Hoffmann & Dall, 2018; Shahabi et al., 2015).

Table A-6 : OPEX cost equations.

Component	Total cost of investment equations	Ref.
CSP system	$c_{CSP,mat} = 0.5\, c_{OM,CSP,Fixed}\left(\frac{SM}{SM_{ref}}\right)^{exp,mat}$ $c_{CSP,lab} = 0.4\, c_{OM,CSP,Fixed}\left(\frac{SM}{SM_{ref}}\right)^{exp,labor}$ $c_{CSP,ser} = 0.1\, c_{OM,CSP,Fixed}$ $c_{CSP,land} = 1.9\left(\frac{SM}{SM_{ref}}\right)^{exp,land}$ $C_{o\&m,CSP} = 1000 Cap_{net}\left(c_{CSP,mat} + c_{CSP,lab} + c_{CSP,ser} + c_{CSP,land}\right)$ $Z_{hel}{}^{Opex} = C_{O\&M,CSP}\frac{C_{hel}}{C_{hel}+C_{rec\_total}+C_{TES}}$ $Z_{rec\_total}{}^{Opex} = C_{O\&M,CSP}\frac{C_{rec\_total}}{C_{hel}+C_{rec\_total}+C_{TES}}$ $Z_{TES}{}^{Opex} = C_{O\&M,CSP}\frac{C_{TES}}{C_{hel}+C_{rec\_total}+C_{TES}}$ $Z_{TES\_hot}{}^{Opex} = 0.6 Z_{TES}{}^{Opex}$ $Z_{TES\_cold}{}^{Opex} = 0.4 Z_{TES}{}^{Opex}$	(Comite Solar e Innovacion Energetica de Corfo, 2019; Guédez et al., 2016; Turchi et al., 2019)
PV system	$C_{o\&m,PV} = c_{PV,esp,O\&M} P_{PV,MW} 1000$ $Z_{PV}{}^{Opex} = C_{o\&m,PV}\frac{C_{PV}}{C_{PV}+C_{inverter}}$	(Fu et al., 2018)

	$Z_{inverter}^{Opex} = C_{o\&m,PV}\frac{C_{inverter}}{C_{PV}+C_{inverter}}$	
Power Block	$C_{o\&m,PB} = c_{OM,CSP,var}Gen_{PB}$ $Z_{sg}^{Opex} = C_{o\&m,PB}\frac{C_{sg}}{C_{sg}+C_{rh}+\sum C_{st,i}+\sum C_{pump,i}+C_{cond}+C_{dea}+\sum C_{CFWH,i}+C_{gen}}$ $Z_{rh}^{Opex} = C_{o\&m,PB}\frac{C_{rh}}{C_{sg}+C_{rh}+\sum C_{st,i}+\sum C_{pump,i}+C_{cond}+C_{dea}+\sum C_{CFWH,i}+C_{gen}}$ $Z_{st,i}^{Opex} = C_{o\&m,PB}\frac{C_{st,i}}{C_{sg}+C_{rh}+\sum C_{st,i}+\sum C_{pump,i}+C_{cond}+C_{dea}+\sum C_{CFWH,i}+C_{gen}}$ $Z_{pump,i}^{Opex} = C_{o\&m,PB}\frac{C_{pump,i}}{C_{sg}+C_{rh}+\sum C_{st,i}+\sum C_{pump,i}+C_{cond}+C_{dea}+\sum C_{CFWH,i}+C_{gen}}$ $Z_{cond}^{Opex} = C_{o\&m,PB}\frac{C_{cond}}{C_{sg}+C_{rh}+\sum C_{st,i}+\sum C_{pump,i}+C_{cond}+C_{dea}+\sum C_{CFWH,i}+C_{gen}}$ $Z_{dea}^{Opex} = C_{o\&m,PB}\frac{C_{dea}}{C_{sg}+C_{rh}+\sum C_{st,i}+\sum C_{pump,i}+C_{cond}+C_{dea}+\sum C_{CFWH,i}+C_{gen}}$ $Z_{CFWH,i}^{Opex} = C_{o\&m,PB}\frac{C_{CFWH,i}}{C_{sg}+C_{rh}+\sum C_{st,i}+\sum C_{pump,i}+C_{cond}+C_{dea}+\sum C_{CFWH,i}+C_{gen}}$ $Z_{gen}^{Opex} = C_{o\&m,PB}\frac{C_{gen}}{C_{sg}+C_{rh}+\sum C_{st,i}+\sum C_{pump,i}+C_{cond}+C_{dea}+\sum C_{CFWH,i}+C_{gen}}$	(Comite Solar e Innovacion Energetica de Corfo, 2019; Guédez et al., 2016; Turchi et al., 2019)
MED system	$C_{o\&m,MED} = c_{OM,MED,Fixed}C_{MED,total} + c_{MED,chem}W_{MED} + c_{MED,lab}(365Cap_{MED})$ $Z_{MED}^{Opex} = C_{o\&m,MED}$	(Christ, Regenauer-Lieb, & Tong Chua, 2015;

		Mata-Torres et al., 2017)
RO system	$C_{RO,memb} = 0.2\ c_{memb}(N_{vessel}N_{elements})N_{RO,units}$ $C_{RO,cartridge} = \left(25 \cdot 10 \cdot 6\ N_{RO,units}\right) c_{cartridge}$ $C_{RO,other} = (c_{RO,chem} + c_{RO,disposal})W_{RO}$ $C_{RO,lab} = \left(c_{RO,lab} + c_{RO,indirect}\right)(365Cap_{RO})$ $C_{o\&m,RO} = C_{RO,memb} + C_{RO,cartridge} + C_{RO,other} + C_{RO,lab} + c_{OM,RO,Fixed}C_{RO,total}$ $Z_{RO}{}^{Opex} = C_{o\&m,RO}$	(Al-Obaidi et al., 2019; Voutchkov, 2019)
P/R System	$C_{o\&m,P/R\_pump} = c_{OM,PR,Fixed}C_{P/R\_pump}$ $C_{o\&m,P/R\_recovery} = c_{OM,PR,Fixed}C_{P/R\_recovery}$ $Z_{P/R\_pump}{}^{Opex} = C_{o\&m,P/R\_pump}$ $Z_{P/R\_recovery}{}^{Opex} = C_{o\&m,P/R\_recovery}$	Assumption
DIST system	$C_{o\&m,DIST} = c_{OM,PR,Fixed}C_{DIST}$ $Z_{DIST}{}^{Opex} = C_{o\&m,DIST}$	Assumption

Table A-7 : Parameters of the cost correlations.

Parameter	Unit	Value
c_{hf}	$/m^2	140 (Turchi et al., 2019)
c_{tow}	$/m	90,000 (Dieckmann et al., 2017; Hoffmann & Dall, 2018)
$ht_{rec,ref}$	m	200
exp,tow	-	0.3
c_{rec}	$/kW$_{th}$	125 (Dieckmann et al., 2017)
$P^{th}_{rec,ref}$	kW	550,000
exp,rec	-	-0.3
c_{TES}	$/kW$_{th}$	22 (Comite Solar e Innovacion Energetica de Corfo, 2019)
$\%Cont_{CSP}$	%	5 (Comite Solar e Innovacion Energetica de Corfo, 2019)
$\%EPC_{CSP}$	%	13 (Turchi et al., 2019)
c_{mod}	$/W$_{dc}$	0.3 (PVInsights, 2020)
$P_{PV,ref}$	MW	100
exp,pv	-	-0.05
c_{inv}	$/W$_{ac}$	0.05 (Fu et al., 2018)
$c_{PV,BoS}$	$/W$_{dc}$	0.21 (Fu et al., 2018)
$c_{PV,labor}$	$/W$_{dc}$	0.1 (Fu et al., 2018)
$c_{PV,overh}$	$/W$_{dc}$	0.05 (Fu et al., 2018)
$\%Cont_{PV}$	%	3 (Fu et al., 2018)
$c_{PV,EPC}$	$/W$_{dc}$	0.08 (Fu et al., 2018)
f_a	%	15
$c_{MED,esp}$	$/m$^{1.9}$	300
$c_{MED,tre}$	$/m^3/d	55
$c_{MED,intake}$	$/m^3/d	200
$c_{MED,disposal}$	$/m^3/d	40
$c_{MED,others}$	$/m^3/d	160
$\%Cont_{MED}$	%	5
$\%EPC_{MED}$	%	13

$c_{RO,ref1}$	-	1.45
$c_{RO,ref2}$	-	0.0213
$c_{RO,ref3}$	-	0.0042
$c_{RO,ref4}$	-	0.679
$c_{RO,ref5}$	-	0.194
$c_{RO,ref6}$	-	4
$c_{RO,ref7}$	-	2.934
$c_{RO,ref8}$	-	0.574
exp $\_ro1$	-	0.8
exp $\_ro2$	-	0.93
exp $\_ro3$	-	1.07
exp $\_ro4$	-	0.81
exp $\_ro5$	-	0.77
exp $\_ro6$	-	0.8
exp $\_ro7$	-	0.61
exp $\_ro8$	-	0.6
$c_{RO,piping}$	$/m^3/d	30 (Voutchkov, 2019)
$c_{RO,disposal}$	$/m^3/d	60 (Voutchkov, 2019)
$c_{RO,waste}$	$/m^3/d	30 (Voutchkov, 2019)
$c_{RO,electrical}$	$/m^3/d	55 (Voutchkov, 2019)
$c_{RO,auxiliary}$	$/m^3/d	25 (Voutchkov, 2019)
$c_{RO,others1}$	$/m^3/d	50 (Voutchkov, 2019)
$\%Cont_{RO}$	%	5 (Voutchkov, 2019)
$c_{RO,EPC}$	$/m^3/d	275 (Voutchkov, 2019)
$c_{esp,pipe}$	$/m	1000
$exp,pipe$	-	1.5
$\%Cont_{PR}$	%	5
$\%EPC_{PR}$	%	13
$c_{OM,CSP,Fixed}$	$/kW$_e$	60 (Comite Solar e Innovacion Energetica de Corfo, 2019)

SM_{ref}	-	2.3
exp, mat	-	1
$exp, labor$	-	0.8
$exp, land$	-	1.35
$c_{PV,esp,O\&M}$	\$/kW$_e$	10 (Fu et al., 2018)
$c_{OM,CSP,var}$	\$/MWh	3.5 (Turchi et al., 2019)
$c_{OM,MED,Fixed}$	%	1
$c_{MED,chem}$	\$/m^3	0.03 (Christ et al., 2015)
$c_{MED,lab}$	\$/m^3	0.1 (Askari & Ameri, 2016)
c_{memb}	\$/element	600 (Voutchkov, 2019)
$c_{cartridge}$	\$/unit	10 (Voutchkov, 2019)
$c_{RO,chem}$	\$/m^3	0.05 (Voutchkov, 2019)
$c_{RO,disposal}$	\$/m^3	0.01 (Voutchkov, 2019)
$c_{RO,lab}$	\$/m^3/d	0.05 (Voutchkov, 2019)
$c_{RO,ind}$	\$/m^3/d	0.03 (Voutchkov, 2019)
$c_{OM,RO,Fixed}$	%	1.5
$c_{OM,PR,Fixed}$	%	1.5

[*4] Values without reference were computed with info from the respective references in equations sections tables.